Kinetic and Thermodynamic Studies on the Effect of Amino Acids, Alcohols, Crowding Agents, and Lyotropic Salts on Proteins

A THESIS

submitted to

THAPAR UNIVERSITY, PATIALA

for the degree of

DOCTOR OF PHILOSOPHY

by

Rajesh Kumar

Regd. No. 901109011

SCHOOL OF CHEMISTRY AND BIOCHEMISTRY

THAPAR UNIVERSITY, PATIALA

PATIALA-147004, PUNJAB (INDIA)

Acknowledgement

In order to succeed, we must first believe that we can.

N. Kazantzakis

Firstly, I would like to express my sincere gratitude to my advisor **Dr. Rajesh Kumar, Associate Professor, Thapar University, Patiala** for the continuous support of my Ph.D study and related research, for his patience, motivation, and immense knowledge. His guidance helped me in all the time of research and writing of this thesis. I could not have imagined having a better advisor and mentor for my Ph.D study. Though it's not possible to thank him in words still I want to say THANK YOU for making it possible for me, thanks from deep of my heart.

I offer special thanks to **Dr. Bonamali Pal, Head, School of Chemistry and Biochemistry, Thapar University, Patiala** and other faculty members of our department for providing all the necessary lab equipments and facilities in the department. They patiently provided the vision, encouragement and advice necessary for me to move through the doctoral program and complete my dissertation.

I would like to thank all the members of my doctoral committee, **Dr. Susheel Mittal** (Senior Professor, School of Chemistry and Biochemistry), **Dr. Bonamali Pal** (Professor, School of Chemistry and Biochemistry), and **Dr. Haripada Bhunia** (Professor, Department of Chemical Engineering) for giving their valuable suggestions in the progress of research work. Also I want to extend my special thanks to **Dr. Abani K. Bhuyan** (Professor, School of Chemistry, University of Hyderabad) and **Dr. Deepak Sharma** (Scientist E, Institute of Microbial Technology, Chandigarh) for his consistent helps and supports throughout my Ph.D study.

I can never forget to acknowledge the Council of Scientific and Industrial Research (Govt. of India) and Thapar University for providing me financial assistance in the form of **JRF**, **SRF and Teaching Associateship,** respectively which supports me to perform my work comfortably.

With heart full feelings I acknowledge my lab mates Mr. **Sandeep Kumar** and Dr. Rishu Jain, Ritika Chhabra, Neha Goyal (M.Sc. project student) Mukesh Chand Agarwal and many others research scholars here at Thapar University, Patiala.

My special gratitude and love for my brothers (**Abhay** and **Ritesh**) and sisters (**Ranjana, Renuka** and **Rashmi**) and bhabhi (**Sarita**), who had always been with me and keep me motivated towards achievement of my goal. Sometimes I felt half hearted but they always kept me going throughout.

I owe a special thanks to my family, my Maa (**Smt**. **Sumitra Verma**), Papa (**Sri**. **Ram Kumar Verma**) and my wife **Prativa**, who always supported me and helped me throughout my Ph.D study. Maa and Papa, I really do not know how to thank you enough for providing me with the opportunity to be where I am today. I dedicate this all work to my parents and grandparents (**Late K.L Verma** and **Late C.M. Verma**). My sweetest acknowledgements to my little fairies **Aishani**, **Angel** and **Ijya** reason for smile under stress. You are indispensible part of my journey and it is for my complete life.

Rajesh Kumar

CONDIDATE's DECLEARATION

I hereby declared that the work presented in the thesis entitled **"Kinetic and Thermodynamic Studies on the Effect of Amino Acids, Alcohols, Crowding Agents, and Lyotropic Salts on Proteins"** being submitted partial fulfillments of requirement for the degree **Doctor of Philosophy** submitted in the **School of Chemistry and Biochemistry, Thapar University, Patiala** is an authentic record of my own work carried out under the supervision of **Dr Rajesh Kumar,** Associate Professor, School of Chemistry and Biochemistry, Thapar University, Patiala. The matter embodied in this thesis has not formed the basis for the award of any other degree of this or any other university.

Date: 17th March 2017

Place: Patiala

Rajesh kumar

Rajesh Kumar

This is certified that above statement made by student concern is correct and true to the best of my knowledge.

Dr Rajesh Kumar
(Supervisor)

Head of Department

Dean
(Research and Sponsored Project)

External Examiner

List of Abbreviations

Abbreviation	Description
Ferrocyt *c*	Ferrocytochrome *c*
Ferricyt *c*	Ferricytochrome *c*
Cyt *c*	Cytochrome *c*
NCO	Natively folded carbonmonoxycytochrome *c*
Cyt-CO	CO-liganded Ferrocytochrome *c*
Mb	Myoglobin
apoMb	Apomyoglobin
MbCO	Carbonmonoxymyoglobin
Lyz	Lysozyme
GdnHCl	Guanidium Hydrochloride
CO	Carbon monoxide
MG	Molten globule
TFE	2,2,2-Triflouroethanol
CD	Circular dichroism
UV	Ultra violet
DSC	Differential scanning calorimetric
Trp	Tryptophan
Tyr	Tyrosine
M80	Methionine-80
CAPS	3-[Cyclohexylamino]-1-propanesulfonic acid
ANS	1-anilino-8-napthalene sulfonate
Tfs	Transferrins
Apo-Tfs	Apo-transferrin
sTf	Serum transferrin
oTf	Ovotransferrin
Fe_2Tfs	Diferric transferrins
Fe_NTfs	Monoferric transferrins (N-lobe)
Fe_CTfs	Monoferric transferrins (C-lobe)
HEPES	4-(2-Hydroxyethyl)-1-piperazineethanesulfonate
MES	2-(*N*-mopholino) ethanesulfonate
NTA	Nitrilotriacetic acid
BPS	Bathophenanthroline sulfonate

Contents

	Abstract	
1	**Introduction**	1-14
2	**Materials and Methods**	15-29
2.1	Materials	15
2.2	Methods	15
2.2.1	*Measurement of CO dissociation kinetics of natively folded CO-liganded Ferrocyt c under various concentrations of crowding agents, viscogens, amino acids and denaturants*	15
2.2.2	*Measurement of CO-dissociation kinetics of NCO at different concentrations of denaturants in the absence and presence of fixed concentrations of crowding agents and amino acids*	16
2.2.3	*Measurement of kinetics of CO association with Ferrocyt c under various concentrations of crowding agents, salt and alcohol*	17
2.2.4	*Measurement of CO-replacement kinetics of carbonmonoxymyoglobin (MbCO) under various concentrations of crowding agents and amino acids*	17
2.2.5	*Measurement of urea-denaturation induced iron (Fe^{3+}) release and reduction-induced iron (Fe^{2+}) release from carbonate and oxalate bound Fe_NTfs*	17
2.2.6	*Measurement of activation parameters for kinetics of CO-dissociation from NCO, CO-association with Ferrocyt c, CO-replacement from MbCO and iron-release from Fe_NTfs*	18
2.2.7	*Measurement of thermal denaturation of Ferricyt c, Ferrocyt c, Mb and Lyz under various concentrations of crowding agents, amino acids, salts and denaturants*	19
2.2.8	*Measurement of thermal denaturation of Ferricyt c, Ferrocyt c, Mb and Lyz under various concentrations of denaturants in the absence and presence of fixed concentrations of crowding agents and amino acids*	21
2.2.9	*Measurement of denaturant-induced-unfolding of Ferricyt c, Ferrocyt c, Mb and Lyz under various concentrations of crowding agents and amino acids*	21
2.2.10	*Measurement of denaturant-induced-unfolding of diferric transferrins (Fe_2Tfs)*	22
2.2.11	*Measurement of pH- titrations of Ferricyt c, apoMb and Lyz*	23
2.2.12	*Measurement of fraction of iron released from Fe_2Tfs as a function of pH, temperature and urea*	23
2.2.13	*Measurement of the far-UV CD, near-UV CD and fluorescence emission spectra of Ferricyt c, Ferrocyt c, apoMb, Lyz and Fe_2Tfs*	25
2.2.14	*Measurement of extrinsic fluorescence emission spectra of 8-anilinona phthalene-1-sulphonic acid (ANS)-bound Ferricyt c, Mb and Lyz*	26
2.2.15	*Preparation of carbonate and oxalate bound Fe_2Tfs*	26
2.2.16	*Preparation of carbonate and oxalate Fe_NTfs*	27
2.2.17	*Differential scanning calorimetric studies of carbonate and oxalate bound Fe_2sTf*	27
2.2.18	*Differential scanning calorimetric studies of Ferrocyt c*	27

2.2.19	*Denaturants concentration corrections (in the presence of dextran 40, dextran 70 and ficoll 70)*	28
2.3	References	28
3	**Role of Macromolecular Crowding on the Stability, Folding and Internal Dynamics of Native Cytochrome *c* and Myoglobin**	30-55
3.1	Introduction	30
3.2	Results and discussion	31
3.2.1	*Thermal dissociation of CO from natively folded carbonmonoxycytochrome c (NCO) and CO replacement from carbonmonoxymyoglobin (MbCO) by hexacyanoferrate ion*	32
3.2.2	*Crowding agents dependence of log k_{diss}, log k_{off} and activation parameters (activation enthalpy ($\Delta H_{diss/off}^{\ddagger}$), activation entropy ($\Delta S_{diss/off}^{\ddagger}$) and activation free energy ($\Delta G_{diss/off}^{\ddagger}$))*	32
3.2.3	*Effect of monomers of crowding agent (sucrose and glucose) and other viscogen (glycerol) on log k_{diss}*	36
3.2.4	*Phenomenological description of viscosity dependence of the NCO $\rightarrow$ N + CO conversion rate*	38
3.2.5	*Internal friction and its role in protein folding and dynamics*	40
3.2.6	*Effect of crowding agents on the thermodynamic stability of proteins*	42
3.2.7	*Effect of crowding agents on thermal stability of native Ferrocyt c and Mb*	43
3.2.8	*Reversibility and two states folding of native Ferrocyt c*	45
3.2.9	*Effect of crowding agents on the secondary (far-UV CD) structure of Ferrocyt c and Mb*	49
3.3	Conclusion	50
3.4	References	51
4	**Factor Defining the Effect of Macromolecular Crowding on the Thermodynamic Stability and Internal Dynamics of Cytochrome *c* and Myoglobin**	56-76
4.1	Introduction	56
4.2	Results and discussion	57
4.2.1	*Effect of crowding agents on the denaturants dependent internal dynamics of NCO*	58
4.2.2	*Effect of crowding agents on the denaturant-dependent activation thermodynamic parameter of CO-dissociation reaction of NCO*	60
4.2.3	*Effect of crowding agents on the denaturant-dependent thermal unfolding of Ferrocyt c and Mb*	62
4.2.4	*Effects of crowding agents on the denaturant-dependent thermodynamic stability of Ferricyt c and Mb*	68
4.2.5	*Effect of crowding agents on the denaturant dependent-secondary structure of Ferricyt c and Mb*	71
4.3	Conclusion	72
4.4	References	73

5	**Role of Amino Acids on the Stability, Folding, and Internal Dynamics of Cytochrome *c* and Myoglobin.**	77-94
5.1	Introduction	77
5.2	Results and discussion	78
5.2.1	*Effect of amino acids on the internal dynamics of natively folded carbonmonoxycytochrome c (NCO) and carbonmonoxymyoglobin (MbCO)*	78
5.2.2	*Effect of amino acids on the activation thermodynamic parameters of CO-dissociation reaction of NCO and CO-replacement reaction of MbCO*	81
5.2.3	*Effect of amino acids on the thermodynamic stability of Ferrocyt c and Mb*	83
5.2.4	*Effects of amino acids on the thermal stability of Ferrocyt c and Mb*	84
5.2.5	*Effect of amino acids on the tertiary structure of Ferricyt c and Mb*	89
5.3	Conclusion	90
5.4	References	91
6	**Factor Defining the Effect of Amino Acids on the Thermodynamic Stability and Internal Dynamics of Cytochrome *c* and Myoglobin.**	95-116
6.1	Introduction	95
6.2	Results and Discussion	96
6.2.1	*Effect of amino acids on the denaturant-dependent internal dynamics of NCO*	96
6.2.2	*Effect of amino acids on the denaturant-dependent activation thermodynamic parameter of CO-dissociation reaction of NCO*	98
6.2.3	*Effect of amino acids on the denaturant-dependent thermal unfolding of Ferrocyt c and Mb*	102
6.2.4	*Effect of amino acids on the denaturant-dependent thermodynamic stability of Ferricyt c and Mb*	108
6.2.5	*Effect of amino acids on the denaturant dependent tertiary structure of Ferricyt c and Mb at pH 7.0*	112
6.3	Conclusion	113
6.4	References	114
7	**Structural, Kinetic and Thermodynamic Characterizations of the Macromolecular Crowding-Induced Molten Globule States of the Alkali pH-Denatured Proteins.**	117-136
7.1	Introduction	117
7.2	Results and Discussion	118
7.2.1	*pH-induced denaturation of Ferricyt c, apoMb and Lyz*	118
7.2.2	*Effect of crowding agents on the fluorescence emission spectrum of base-denatured Ferricyt c, apoMb and Lyz*	120
7.2.3	*Effect of crowding agents on the secondary structure of base-denatured Ferricyt c, apoMb and Lyz*	121
7.2.4	*Crowding agents-induced refolding in the base-denatured Ferricyt c, apoMb and Lyz*	122
7.2.5	*Effect of crowding agents on the tertiary structures of base-denatured Ferricyt c, apoMb and Lyz*	124
7.2.6	*ANS binding to different states of Ferricyt c, apoMb and Lyz*	124
7.2.7	*Effects of crowding-agents on thermal denaturations of base-denatured*	126

	proteins	
7.2.8	*Effects of dextran 70 and ficoll 70 on the internal dynamics of base-denatured Cyt c*	128
7.3	Conclusion	131
7.4	References	132
8	**Structural, Kinetic and Thermodynamic Characterizations of the Alcohol and Cation-induced Molten Globule States of the Base-Denatured Proteins.**	137-159
8.1	Introduction	137
8.2	Results and Discussion	140
8.2.1	*Effect of cations on the base-denatured Ferricyt c, apoMb and Lyz*	140
8.2.2	*Cations-induced molecular compaction of base-denatured Ferricyt c, apoMb and Lyz*	141
8.2.3	*Cations and TFE induce the native-like secondary structures in the base-denatured Ferricyt c, apoMb and Lyz*	142
8.2.4	*B–states and H_B–states of Ferricyt c, apoMb and Lyz do not acquire tertiary structure*	147
8.2.5	*ANS binding to native, base-denatured and cations and alcohol-induced MG states of Ferricyt c, apoMb and Lyz*	147
8.2.6	*Effect of cations (Cs^+, Na^+ and K^+) on thermal denaturation of base-denatured Ferricyt c, apoMb and Lyz at pH 12.9*	149
8.2.7	*Effect of cations (Cs^+, Na^+ and K^+) and alcohol (TFE) on the kinetics of CO association to alkaline* Ferrocyt *c*	151
8.2.8	*Mechanism of Cations and TFE-induced protein stabilization*	153
8.3	Conclusion	154
8.4	References	155
9	**Effect of Synergistic Anions on the Stability and Iron Release Kinetics of Transferrins**	160-179
9.1	Introduction	160
9.2	Results and Discussion	162
9.2.1	*Effect of pH, urea and temperature on the visible absorption and fluorescence emission spectra of carbonate and oxalate bound Fe_2Tfs*	162
9.2.2	*The oxalate effect on the stability of iron centers of Tfs*	163
9.2.3	*Oxalate effect on the structural stability of Fe_2Tfs*	166
9.2.4	*Oxalate effect on the dynamics of iron release from Fe_NTfs*	170
9.3	Conclusion	174
9.4	References	175

Abstract

About 10 to 40% of cytoplasm volume is generally occupied by macromolecules viz. proteins, carbohydrates, nucleic acids etc. The highly crowded conditions found in cytoplasm can affect the thermodynamic and kinetic properties of proteins. Chapter 3 investigated the role of macromolecular crowding on stability, folding, and internal dynamics of native cytochrome *c* (Cyt *c*) and myoglobin (Mb). Carbonmonoxycytochrome *c* (Cyt-CO) refolds to a native-like compact state (NCO-state), where the non-native Fe2+-CO interaction persists. Slow thermal-dissociation of CO transforms the NCO-state to native-state (N-state), where the native Fe2+-M80 bond recovers. To determine the role of macromolecular crowding on the internal dynamics of NCO and carbonmonoxymyoglobin (MbCO), the kinetic and thermodynamic parameters for CO−dissociation from NCO (NCO→N+CO) and CO-replacement from MbCO by hexacyanoferrate ion were measured at varying concentrations of crowding agents (dextran 70, dextran 40, ficoll 70) and viscogens (glycerol, sucrose, and glucose). As [crowding agent] is increased, the rate coefficients of CO−dissociation for NCO (k_{diss}) and CO-replacement for MbCO (k_{off}) decrease exponentially. The values of log k_{diss} and log k_{off} are found to be decreased more for dextran 70 than that of the ficoll 70, suggesting that the shape of crowding agent plays an important role in controlling the internal dynamics of NCO and MbCO. log k_{diss} and log k_{off} are also found to be decreased more for dextran 70 than that of dextran 40. Dextran 70 has the larger size than that of the dextran 40, so the greater decrease of log k_{diss} and log k_{off} for dextran 70 suggests that the size of crowding agent also plays a significant role in controlling the internal dynamics of NCO and MbCO. A general approach for investigating the importance of protein dynamics in a chemical reaction is to determine the role of solvent viscosity on reaction rate. log k_{diss} is found to be decreased with increasing solvent composition (glycerol, sucrose, and glucose) and viscosity, indicating that the solvent viscosity controls the internal dynamics of NCO. At a given particular concentration, dextran 70 has always higher viscosity than dextran 40 so the greater decrease of log k_{diss} for dextran 70 than that of the dextran 40 suggests that the viscosity of crowding agent also plays a vital role in controlling the internal dynamics of NCO and MbCO. The thermal or denaturant unfolding transitions measured for Ferrocyt *c* by different optical probes (CD, fluorescence and absorbance) and common optical probes with multiple wavelengths are within error nearly super imposable and cooperative. The observation of indistinct thermal or denaturant unfolding transition curves for Ferrocyt *c* do not reveal the

accumulation of any equilibrium structural intermediate to a detectable level, which suggests that the thermal and denaturant-induced unfolding of Ferrocyt *c* occur in two-state manner. Two-state thermodynamic analysis of chemical (GdnHCl or urea) and thermal unfolding transitions of native Ferrocyt *c* (N-state) and Mb carried out in the absence and presence of 200 mg/ml dextran 40, dextran 70 and ficoll 70 reveals that the smaller size crowder (dextran 40) has a greater impact on the thermodynamic stability of native Ferrocyt *c*.

The free amino acids and their derivatives are the naturally occurring osmolytes. The free amino acids in cytoplasm can influence the functional properties of protein. Chapter 5 investigated the role of amino acids on stability, folding, and internal dynamics of native cytochrome *c* (Cyt *c*) and myoglobin (Mb). To determine the role of amino acids on the internal dynamics of native-like compact state (NCO) and carbonmonoxymyoglobin (MbCO), the kinetic and thermodynamic parameters for CO-dissociation from NCO (NCO→N+CO) and CO-replacement from MbCO by hexacyanoferrate ion were measured at varying concentrations of L-amino acids (alanine, arginine, glycine, proline, serine, and threonine) at pH 7.0. As [amino acids] is increased, the CO−dissociation reaction of NCO and CO−replacement reaction of MbCO are decelerated, indicating that the amino acids presence in the reaction medium reduce the structural fluctuations responsible for CO dissociation from NCO and CO replacement from MbCO. The amino acid−mediated reduction in structural fluctuations of NCO and MbCO typically follow the order: arginine> serine> proline> glycine> alanine >threonine. Two-state thermodynamic analysis of chemical (GdnHCl or urea) and thermal unfolding transitions of native Ferrocyt *c* (N-state) and Mb carried out in the presence of various concentrations of amino acids (alanine, arginine, glycine, proline, serine, and threonine) reveals that alanine, glycine, proline, serine, and threonine presence in reaction medium increase the thermodynamic stability of Ferrocyt *c* and Mb but in the presence of arginine decreases the thermodynamic stability of these proteins. The amino acid-mediated increase in thermodynamic stability for Ferrocyt *c* and Mb typically follow the order: serine> glycine> alanine >threonine>proline. The decrease in thermodynamic stability of Ferrocyt *c* and Mb in the presence of arginine is presumably because of the presence of guanidium group (Gdn^+) in the arginine.

While the effects of denaturants (urea and GdnHCl) on the internal dynamics of native Cyt *c* and Mb have been extensively investigated, but the effect of crowding agents and amino acids on the internal dynamics of natively folded carbonmonoxycytochrome *c* (NCO) in the

presence of varying concentration denaturants, across the folding-unfolding transition are not explored so far. Chapter 4 and Chapter 6 investigated the effect of crowding agents and amino acids, respectively, on the denaturant-dependent internal dynamics of NCO and thermodynamic stability of native Cyt c and Mb at pH 7.0.

Analysis of kinetic and thermodynamic parameters measured for CO-dissociation reaction of NCO at different concentrations of GdnHCl or urea in the absence and presence of fixed concentrations of crowding agents (dextran 40, dextran 70 and ficoll 70) and L-amino acids (alanine, arginine, glycine, proline, serine, and threonine) at pH 7.0 provides three important information: (i) in subdenaturing region, crowding agents or L-amino acids presence in reaction medium exhibits an additive effect on the denaturant-mediated reduction in structural fluctuations responsible for CO dissociation, which typically follow the order for amino acids as : (arginine> serine> proline> glycine> alanine >threonine) and crowding agents as: (dextran 70> dextran 40> Ficoll 70), (ii) in denaturing region, the crowding agents or amino acids presence in reaction medium counteract the structural fluctuations responsible for unfolding the protein, and (iii) the structural fluctuation that unfolds the protein are found to be more opposed by the larger sized and anisotropic geometry shaped crowding agents (dextran 70> dextran 40> Ficoll 70) and larger sized and lesser hydrophobic amino acids (arginine> serine> proline> glycine> alanine >threonine). Two-state thermodynamic analysis of thermal and urea unfolding curves of Cyt *c* and Mb measured at different concentrations of GdnHCl in the absence and presence of fixed concentrations of crowding agents (dextran 40, dextran 70 and ficoll 70) and L-amino acids (alanine, arginine, glycine, proline, serine, and threonine) at pH 7.0 provides three important information: (i) crowding agents presence in reaction medium counteracts the deleterious effect of denaturants on stability of proteins and they typically follow the order (dextran 40> dextran 70> ficoll 70), (ii) alanine, glycine, proline, serine and threonine counteract the deleterious effect of denaturants on stability of proteins and they typically follow the order: serine> glycine>alanine>threonine>proline, and (iii) at lower concentrations of GdnHCl, L-arginine show an additive effect on the deleterious effect of denaturant on stability of proteins while at higher concentrations of GdnHCl, it counteract the deleterious effect of denaturants.

The folding of protein, an important process for protein to fulfill normal functions, takes place in crowded physiological environments. Chapter 7 characterized the structural, kinetic and thermodynamic properties of the macromolecular crowding-induced molten globule states of the

alkali pH-denatured proteins. Near-UV CD, far-UV CD, tryptophan fluorescence and 1-anilino-8-napthalene sulfonate (ANS) binding experiments of base-denatured Cyt *c*, apoMb and Lyz carried out in the absence and presence of different concentrations of crowding agents (dextran 70 and ficoll 70) indicate that the crowders-induced fully populated conformations are molecular compact states containing native-like secondary structural contents but disordered tertiary interactions. Thermodynamic analysis of the far UV-CD (222 nm) monitored thermal denaturation curves of base-denatured Cyt *c*, apoMb and Lyz measured in the absence and presence of 300 mg ml^{-1} of crowding agents (dextran 70 and ficoll 70) suggests that the crowding agent presence in the reaction medium increase the thermal stability of the base-denatured proteins. Kinetic and thermodynamic experiments involving the measurement of the CO-association to the base−denatured Ferrocyt *c* (pH 12.9 (±0.1)) in the absence and presence of different concentrations of crowding agents (dextran 70 and ficoll 70) indicate that the presence crowding agents in the reaction medium constrains the internal dynamics of base−denatured Ferrocyt *c*.

While the effects of salt and alcohol on the structural and thermodynamic properties of native and acid pH-denatured proteins are extensively studied, the effects of these additives on structural, kinetics and thermodynamic properties of base-denatured proteins are not explored so far. Chapter 8 characterized the structural, kinetic and thermodynamic properties of the cations (NaCl, KCl and CsCl) and TFE (2,2,2−trifluoroethanol)-induced molten globule states of the alkali pH-denatured proteins. Near-UV CD, far-UV CD, tryptophan fluorescence and 1-anilino-8-napthalene sulfonate (ANS) binding experiments of base-denatured Cyt *c*, apoMb and Lyz carried out in the absence and presence of different concentrations of NaCl, KCl, CsCl and TFE revealed that the cations (chloride salt of Na^+, K^+ and Cs^+) and TFE-induced fully populated conformations are molecular compact states containing native-like secondary structural contents but disordered tertiary interactions. Thermodynamic analysis of the far UV-CD (222 nm) monitored thermal denaturation curves of base-denatured Cyt *c*, apoMb and Lyz measured in the absence and presence of 1.0 M NaCl, KCl and CsCl suggests that the cations (chloride salt of Na^+, K^+ and Cs^+) presence in the reaction medium increase the thermal stability of the base-denatured proteins. Kinetic and thermodynamic experiments involving the measurement of the CO-association to the base−denatured Ferrocyt *c* (pH 12.9 (±0.1)) in the absence and presence of different concentrations of TFE and salt (NaCl, KCl and CsCl) indicate that the TFE and cations

(Na^+, K^+ and Cs^+) presence in the reaction medium constrain the internal dynamics of base−denatured Ferrocyt *c*.

Transferrins (Tfs; serum transferrin (sTf), ovotransferrin (oTf), and lactoferrin (Lf)) play the major roles in the iron metabolism of vertebrates, and some invertebrates. The iron coordination is distorted octahedral with four ligands provided by amino acid residues (two residue of tyrosine, one aspartic acid, and one histidine) and the remaining coordinates is shared by a synergistic anion. Carbonate is the main synergistic anion *in-vivo* but when carbonate is absent, other small organic molecules such as oxalate, malonate, glycine *etc* can function as synergistic anion. Chapter 9 investigated the effects of substitution of oxalate anion for carbonate anion on the stability and iron release dynamics of oTf and sTf. Analysis of the pH-, urea- and thermal-denaturations profiles of iron release (based on absorbance (465 nm)) for oxalate anion bound diferric-sTf/oTf (Fe_2sTf/Fe_2oTf) reveals that the carbonate bound Fe_2Tfs binds Fe^{3+} less tightly than the oxalate bound Fe_2Tfs. Thermodynamic analysis of the near- UV CD (282nm) or far-UV CD (222 nm) monitored thermal and urea-induced unfolding curves for these two different synergistic anions bound Fe_2sTf and Fe_2oTf reveals that the carbonate bound Fe_2sTfs has relatively lesser structural stability than oxalate bound Fe_2sTfs. Differential scanning calorimetric study of these two synergistic anions bound Fe_2sTf reveals that the carbonate bound Fe_2sTfs has relatively less thermal stability than oxalate bound Fe_2sTfs. Kinetic and thermodynamic parameters involving measurement of the reductive iron release (Fe^{2+} release) and urea-denaturation induced iron release (Fe^{3+} release) reactions for carbonate and oxalate bound monoferric N-lobe of sTf and oTf (Fe_NsTf and Fe_NoTf) at pH 7.4 and 5.6 reveal that the substitution of carbonate by oxalate retards the iron release from Fe_NTfs with a increase in enthalpic barrier.

Keywords: Structural fluctuations, constrained dynamics, macromolecular crowding agents, viscosity, non-specific attractive interactions, excluded volume effect, entropy-enthalpy plots, amino acids, molten globules, synergistic anions, Fe_2Tfs, Fe_NTfs, enthalpic stabilization, differential scanning calorimetry, reductive iron release, urea-induced iron release.

Chapter 1

Introduction

Proteins are the major functional biomacromolecules of life. Proteins execute a wide variety of biological functions, depending upon their chemical and physical structures. Protein folding is the physical process by which a protein adopts its functional conformation. Although a notable evolution has been made in the area of protein folding [1-28] but the basic question how proteins fold *in vivo* and *in vitro* remains mysterious. The manner how a newly synthesized polypeptide chain adopts the native folded structure mainly depends on two factors, (i) the intrinsic properties of the linear amino acid sequence, and (ii) the contributing influences from the surrounding environment [29]. Traditionally protein folding reaction was based on the existence of a preferred route driving the denatured chain to its native conformation via a sequence of consecutive intermediate [30]. These intermediates are populated during the course of folding pathway; they can correspond both to "on-pathway" or "off-pathway" intermediate depending on, if they can achieve the native structure or remain trapped in energy minimum [31]. The conformers or intermediates having substantial secondary structure, distorted tertiary structure and increased solvent-exposed hydrophobic surface area relative to the native state are termed as "molten globule" (MG-state) state [32-35]. MG-state involves in cell signaling, protein folding and other biological processes [36]. MG-state also plays crucial roles in human diseases related to protein aggregation or via some other mechanism [37].

Cellular environments are very much crowded because of the presence of large amounts of soluble and insoluble biomolecules (*i.e.*, carbohydrates, proteins, nucleic acids, ribosomes, free amino acids, etc) [38-41]. The usual spacing between macromolecules in such crowded environment can be much smaller than the size of the macromolecules themselves [42]. Furthermore, the volume occupied by solutes is unavailable to other molecules because two molecules cannot be in the same place at the same time. As a result, any reactions that depend on available volume can be affected by macromolecular crowding effects [43-44]. The thermodynamic consequences of the unavailable volume are called excluded volume effects [44-45]. The basic properties of crowding agents for protein biophysical studies are: (i) must be water

soluble, (ii) can not affect the pH and ionic strength of reaction medium, (iii) must be inert (i.e., not interact with the proteins) [46-47]. Dextran and ficoll are the sugar-based polymers, existing in solution, as random array of rods shape or anisotropic geometry and sphere shape, respectively [48-49]. These synthetic crowding agents typically stabilize the proteins, but the mechanism by which these crowding agents stabilize the proteins is still a matter of debate. The earlier studies showed that high concentrations of crowding agents affect the conformational stability and structural properties of proteins [42, 49-58]. Beyond the excluded volume effect, the size, shape, concentration and viscosity of crowding agents also found to alter the biophysical property of proteins [50, 59]. The macromolecular crowding effect also found to influence the various biological functions, such as protein folding, binding of small molecules, enzymatic activity, protein-protein interactions, pathological protein aggregation, and extent of amyloid formation [42, 60-63]. The effects of crowding agents on the structural and thermodynamic properties of native and pH-denatured proteins are extensively studied [49,64-70], but the effects of crowding agents and their monomers on the dynamic properties of native-like compact proteins are not explored so far. In particular, the role of crowding agents and their monomers on the internal dynamics of native-like compact proteins remain unexplored. It is also the matter of discussion whether crowding agents stabilize the proteins enthalpically or entropically. This thesis work investigated the role of macromolecular crowding effect on the structural, kinetic and thermodynamic properties of native and pH-denatured Cytochrome *c* (cyt *c*) and myoglobin (Mb). By the processes of protein degradation, the free amino acids are accumulated in cytoplasm. Under very harsh or stress conditions (heat stress, salt stress, water stress or cold stress, etc.), almost all plants and micro-organisms accumulate various low molecular-mass organic compounds normally amino acids and their derivatives, commonly termed as protecting osmolytes [71]. Earlier studies revealed that these types of osmolytes typically stabilize the proteins against heat stress [71-72]. Some other previous studies revealed that the amino acids enhance the protein stability, prevents aggregation in solution and in the dried state without affecting the biological function of protein [73-90]. This thesis work investigated the effect of various L-amino acids (alanine, arginine, glycine, proline, serine and threonine) on structural, kinetic and thermodynamic properties of Cyt *c* and Mb.

pH and salt ions can modulate the structure, stability and biological functions of proteins [91-95]. Few previous studies suggested that the salt ions modulate the stability of the native and partially denatured states of proteins [95-114]. To understand the thermodynamic properties of biological systems, it is essential to know the effects of salts ions on protein stability. Increasing evidences indicate that at lower salt concentrations, the salt ions modulate the stability of proteins by varying the electrostatic (Debye-Hückel) screening of Coulombic interactions [90-91,104] while at higher salt concentrations, the Hofmeister effect influences the stability of proteins through increasing the surface tension of solvent that eventually modulates the hydrophobic interactions [102-103,115-117].

At extreme acidic or basic pH conditions, proteins can denature because of charges repulsions. The ions-induced conformational changes of acid and base-denatured proteins were extensively studied [100-101, 106-107]. Anions and cations were found to transform the acid- and base-denatured states respectively to molten globule (MG) states, presumably by a charge screening mechanism [108-113]. MG state is important for the functioning of proteins in living cells, and involves in various processes at cellular level (*i.e.,* the interactions of the proteins with chaperones and membranes). Increasing evidences indicate that low concentrations of guanidine hydrochloride (GdnHCl) can transform the pH-denatured proteins to MG-states [109-110,118-121]. Monohydric alcohols (methanol, ethanol, 2-propanol, 3°-butanol and 2,2,2 trifluoroethanol (TFE)) are chaotropic co-solvents that typically disrupt the tertiary structure of proteins, [122-123], but enhance secondary structural elements such as helical structure [124-126]. Several previous reports indicated that the monohydric alcohols also induce partially folded states in several proteins [127-131]. The alcohol-induced partially folded states are biologically significant since they are similar to partially denatured states formed near the membrane surfaces where the pH and dielectric constant are low [132-135]. To investigate the role of cations and alcohol on structural, kinetic and thermodynamic properties of base-denatured proteins, this thesis work evaluated the effect of salt of common anion (NaCl, KCl and CsCl) and fluorinated alcohol (TFE) on the structural, kinetic and thermodynamic properties of base-denatured horse heart Ferricytochrome *c* (Ferricyt *c*), horse heart apomyoglobin (apoMb) and hen egg white lysozyme (Lyz) at pH 12.9 (±0.1).

Cyt *c* is a (MW ~12.4 kD, 104 amino acids) hemeprotein and a mobile electron carrier of the respiratory chain that, in response to specific signals, can separate from the inner mitochondrial membrane and activate apoptosis in cytoplasm [136]. The biological activity of Cyt *c* as a mitochondrial electron transport shuttle critically depends on maintaining the native HIS/MET heme coordination, and binding of alternative ligands is strongly disfavored under physiological conditions [137]. Cyt *c* is exists in inter-convertible oxidized (Ferricyt *c*) and reduced (Ferrocyt *c*) forms. Due to its smaller size and heme iron, Cyt *c* is a paradigmatic in experimental protein folding studies [26-28]. Myoglobin (Mb), an extremely compact heme protein (MW ~17.8 kD, 153 amino acids), found primarily in cardiac and red skeletal muscles, functions in the storage of oxygen and facilitates the transport of oxygen to the mitochondria for oxidative phosphorylation [138]. Mb physiologically exhibits in three pertinent forms viz; deoxymyoglobin, oxymyoglobin, and metmyoglobin (Ferrimyoglobin). These three forms of Mb are very similar except at the sixth coordination position [139-140]. Lyz is a glycoside hydrolases enzyme which also known as N-acetylmuramide glycanhydrolase. Lyz (MW ~14.3 kD, 129 amino acids) hydrolyzes the glycosidic bond of peptidoglycans (found in the cell walls of bacteria, especially Gram-positive bacteria) that connects *N*-acetylmuramic acid with the fourth carbon atom of N-acetylglucosamine. Lyz has been extensively studied to assess the role of specific residues in determining the mode of substrate binding, the mechanism of catalysis and the folding behavior of the proteins [141-142].

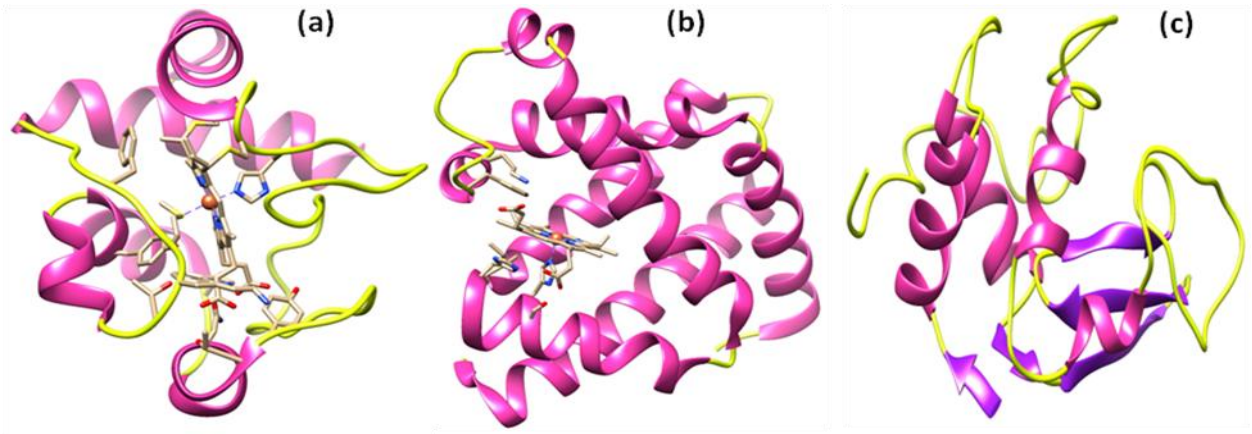

Fig.1. A ribbon model for (a) horse heart cytochrome *c* (PDB: 1HRC [143]), (b) horse myoglobin (PDB: 3YMB [144]) and (c) hen egg white lysozyme (PDB: 2LYZ [145]).

Further, for functional studies (*i.e.*, iron binding and releasing studies), this thesis work also used some metalloproteins, including serum transferrin (sTf) and egg white ovotransferrin (oTf). sTf is the protein in blood plasma that transports iron from the gut and liver to target cells to meet their metabolic needs. oTf act as bacteriostatic agent because it is able to bind iron so tightly that it is unavailable for bacterial growth. Ferritin and sTf manage essential stores of iron in our body. Inside cells, extra iron is locked safely in the protein shell of ferritin [146-147]. sTf (MW~81 kD, 760 amino acids) and oTf (MW~76 kD, 700 amino acids) are folded into two globular lobes, the *N*-lobe and the *C*-lobe, interconnected with a short peptide chain [148-152]. The iron binding sites are similar in both lobes and each lobe binds one Fe^{3+} tightly [148-150]. The iron coordination is distorted octahedral with four ligands provided by amino acid residues (two tyrosines, one aspartic acid, and one histidine) and the remaining coordinates are shared by a synergistic anion [148-150]. A defining feature of Tfs is that they do not bind Fe^{3+} at the specific binding site in the absence of synergistic anion [153-156].

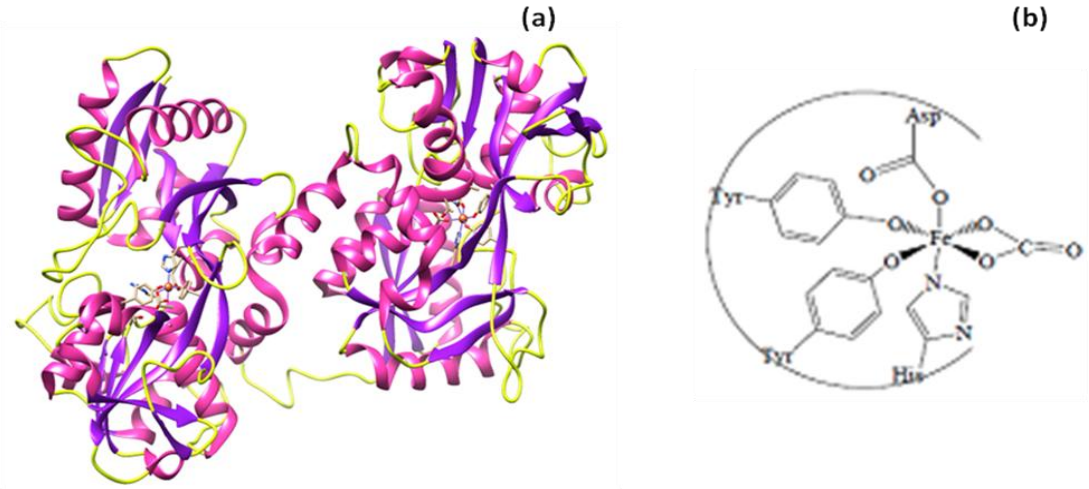

Fig.2. (a) A ribbon model for hen egg white ovotransferrin (PDB: 1OVT [157]) and (b) shows the synergistic anion carbonate or its substitute binding to transferrin.

The naturally occurring synergistic anion is carbonate but small organic molecules with adjacent electrophilic groups (oxalate, malonate, glycine, *etc*) can function as synergistic anion [154-156]. Some earlier reports revealed that the high plasma oxalate levels and iron deficiency anemia in children with autism spectrum disorders might be mediated *via* oxalate bound sTf [158-159]. The effect of non-synergistic anions (*e.g.*, SO_4^{2-}, Cl^-, NO^{3-}, ClO^{4-}, etc.) on stability and iron release kinetics of monoferric (Fe_NTfs or Fe_CTfs) and diferric Tfs (Fe_2Tfs) are extensively studied

[160-181], but the effects of synergistic anions on the stability and iron release kinetics of Fe_NTfs or Fe_CTfs and Fe_2Tfs are less explored [154-155]. Some earlier studies revealed that the substitution of carbonate by oxalate influences the stability and kinetics of iron release from Fe_NsTf and Fe_2sTf [154-155, 182-185]. However, the effects of substitution of oxalate for carbonate on the structural and thermal stability of Fe_2sTf/ Fe_2oTf (Tfs) as well as on the thermodynamics parameters (activation enthalpy ($\Delta H^{\ddagger}$), activation entropy ($\Delta S^{\ddagger}$), *etc.*) associated for iron release from Fe_NsTf/ Fe_NoTf (Fe_NTfs) are not explored so far. To understand better the manner in which substitution of oxalate for carbonate influences the structural stability of Tfs fold and stability of iron binding to Tfs, these properties for carbonate and oxalate bound Fe_2sTfs are studied by calorimetric and spectroscopic methods. To gain insight into the synergistic anion-binding linkage to protein and active site stability to the dynamics of iron release, the kinetics and thermodynamic parameters for iron release from the carbonate and oxalate bound Fe_NTfs have been studied at pH 7.4 and 5.6. My general approach is to apply a variety of spectroscopic, kinetic, thermodynamic and structural strategies to characterize the manner in which the protein environment influences the chemical and physical properties of the iron center.

References

1. S.W. Englander, L. Mayne, *Proc. Natl. Acad. Sci. USA* **111** (2014) 15873−15880.
2. A. N. Adhikari, K. F. Freed, T.R. Sosnick, *Phys. Rev. Lett.* **111** (2013) 028103.
3. V. S. Pande, *Adv. Exp. Med. Biol.* **797** (2014) 101–106.
4. K. Lindorff-Larsen, S. Piana, R.O. Dror, D.E. Shaw, *Science* **334** (2011) 517–520.
5. S. Bédard, M.M. Krishna, L. Mayne, S.W. Englander, *Proc. Natl. Acad. Sci. USA* **105** (2008) 7182–7187.
6. Y. Bai, J.J. Englande, L. Mayne, J.S. Milne, S.W. Englander, *Methods Enzymol.* **259** (1995) 344–356.
7. J. N. Onuchic, Z. Luthey-Schulten, P.G. Wolynes, *Annu. Rev. Phys. Chem.* **48** (1997) 545–600.
8. P. G. Wolynes, J.N. Onuchic, D. Thirumalai, *Science* **267** (1995) 1619–1620.
9. M. M. Krishna, S.W. Englander, *Protein Sci.* **16** (2007) 449–464.
10. C. Levinthal, *J. Chim. Phys.* **65** (1968) 44–45.

11. S. S. Plotkin, J.N. Onuchic, *Q. Rev. Biophys.* **35** (2002) 111–167.
12. S. K. Chandrayan, P. Guptasarma, *Biochim. Biophys. Acta.* **1794** (2009) 905−912.
13. S. K. Chandrayan, S. Prakash, S. Ahmed, P. Guptasarma, *PLoS One* **9** (2014) e80014.
14. B. Kundu, P. Guptasarma, *Proteins* **37** (1999) 321–324.
15. A. Shukla, P. Guptasarma, *Proteins* **55** (2004) 548–557.
16. S. K. Chandrayan, P. Guptasarma, *Proteins* **72** (2008) 539–546.
17. S. Arya, A. Kumari, V. Dalal, M. Bhattacharya, S. Mukhopadhyay, *Phys. Chem. Chem. Phys.* **17** (2015) 22862–22871.
18. M. Bhattacharya, S. Mukhopadhyay, *J. Phys. Chem. B* **116** (2012) 520–531.
19. V. Dalal, M. Bhattacharya, D. Narang, P.K. Sharma, S. Mukhopadhyay, *J. Phys. Chem. Lett.* **3** (2012)1783–1787.
20. A.K. Singh, B. Manjasetty, G.L. Balasubramani, S. Koul, A. Kaushik, M.K. Ekka, V. Singh, S. Kumaran, *PLoS One* **10** (2015) e0124333.
21. S.M. Singh, J. Cabello–Villegas, R.L. Hutchings, K.M.G. Mallela, *Proteins* **78** (2010) 2625–2637.
22. M. Assfalg, I. Bertini, A. Dolfi, P. Turano, A.G. Mauk, F.I. Rosell, H.B. Gray, *J. Am. Chem. Soc.* **125** (2003) 2913–2922.
23. L. Konermann, F.I. Rosell, A.G. Mauk, D.J. Douglas, *Biochemistry* **36** (1997) 6448–6454.
24. D. Biswas, V. Pandya, A.K. Singh, A.K. Mondal, S. Kumaran, *PLoS One* **7** (2012) e45525.
25. D. K. Rao A.K. Bhuyan, *J. Biomol. NMR* **39** (2007) 187–196.
26. A. K. Bhuyan, R. Kumar, *Biochemistry* **41** (2002) 12821–12834.
27. R. Kumar, A. K. Bhuyan, *Biochemistry* **44** (2005) 3024–3033.
28. A. K. Bhuyan, J. B. Udgaonkar, *J. Mol. Biol.* **312** (2001) 1135–1160.
29. R. J. Ellis, *Trends Biochem. Sci.* **26** (2001) 597–604.
30. Y. Ivarsson, C. Travaglini-Allocatelli, M. Brunori, S. Gianni, *Eur. Biophys. J.* **37** (2008) 721–728.
31. V. S. Pande, D. S. Rokhsar, *Proc. Natl. Acad. Sci. USA.* **96** (1999) 1273–1278.
32. K. Kuwajima, *Proteins: Struct. Funct. Genet.* **6** (1989) 87–103.
33. O.B. Ptitsyn, *Adv. Protein Chem.* **47** (1995) 83–229.
34. Y. Kumar, S. Tayyab, S. Muzammil, *Arch. Biochem. Biophy.* **426** (2004) 3–10.

35. O.B. Ptitsyn, *Protein Folding (Creighton, T.E., Eds.) Freeman*, New York, (1992) pp. 243–300.
36. R. Kumar, N.P. Prabhu, D.K. Rao, A.K. Bhuyan, *J. Mol. Biol*. **364** (2006) 483−495.
37. V.N. Uversky, A.L. Fink, Protein Misfolding, Aggregation and Conformational Diseases: II. Molecular Mechanisms of Conformational Diseases, Springer, New York (2007).
38. A. B. Fulton, *Cell* **30** (1982) 345–347.
39. S. B. Zimmerman, S.O. Trach, *J. Mol. Biol.* **222** (1991) 599–620.
40. B. van den Berg, R.J. Ellis, C.M. Dobson, *EMBO J.* **18** (1999) 6927–6933.
41. H. X. Zhou, G. N. Rivas, A. P. Minton, *Annul. Rev. Biophys.* **37** (2008) 375–397.
42. D. Homouz, M. Perham, A. Samiotakis, M. S. Cheung, P. Wittung-Stafshede, *Proc. Natl. Acad. Sci. USA* **105** (2008) 11754–11759.
43. A.P. Minton, *Biophys. J.* **88** (2005) 971–985.
44. S.B. Zimmerman, A.P. Minton, *Annu. Rev. Biophys. Biomol. Struct.* **22** (1993) 27–65.
45. A.P. Minton, *J. Biol. Chem.* **276** (2001)10577–10580.
46. J.R. Ellis, A.P. Minton, *Nature* **425** (2003) 27−28.
47. D. Hall, A.P. Minton, *Biochim. Biophys. Acta* **1649** (2003)127−139.
48. D. Venturoli, B. Rippe, *Am. J. Physiol. Renal Physiol.* **288** (2005) F605−F613.
49. A. Christiansen, Q. Wang, A. Samiotakis, M. S. Cheung, P. Wittung-Stafshede, *Biochemistry* **49** (2010) 6519–6530.
50. Y. Wang, H. He, S. Li, *Biochemistry* **75** (2010) 648–654.
51. M.S. Cheung, D. Klimov, D. Thirumalai, *Proc. Natl. Acad. Sci. USA* **102** (2005) 4753− 4758.
52. A.P. Minton, *Biophys. J.* **78** (2000) 101−109.
53. S. Mittal, L.R. Singh, *PLoS One* **8** (2013) e78936.
54. K. Sasahara, P. McPhie, A.P. Minton, *J. Mol. Biol.* **326** (2003) 1227–1237.
55. P. McPhie, Y.S. Ni, A.P. Minton, *J. Mol. Biol.* **361** (2006) 7–10.
56. D.K. Eggers, J.S. Valentine, *J. Mol. Biol.* **314** (2001) 911–922.
57. D.K. Eggers, J.S. Valentine, *Protein Sci.* **10** (2001) 250–261.
58. E. Bismuto, P.L. Martelli, A. de Maio, D.G. Mita, G. Irace, R. Casadio, *Biopolymers* **67** (2002) 85−95.
59. A.B. Goins, H. Sanabria, M.N. Waxham, Biophys *J.* **95** (2008) 5362–5373.
60. A.S. Morar, A. Olteanu, G. B. Young, G.J. Pielak, *Protein Sci.* **10** (2001) 2195–2199.

61. D.M. Hatters, A.P. Minton, G.J. Howlett, *J. Biol. Chem.* **277** (2002) 7824–7830.
62. V.N. Uversky, E.M.Cooper, K.S. Bower, J. Li, A.L. Fink, *FEBS Lett.* **515** (2002) 99–103.
63. M.D. Shtilerman, T.T. Ding, P.T. Lansbury, *Biochemistry* **41** (2002) 3855–3860.
64. L. Stagg, S. Zhang, M.S. Cheung, P. Wittung-Stafshede, *Proc. Nat. Acad. Sci. USA* **48** (2007) 18976–18981.
65. M.S. Cheung, D. Klimov, D. Thirumalai, *Proc. Nat. Acad. Sci. USA* **13** (2005) 4753–4758.
66. Y. Wang, M. Sarkar, A.E. Smith, A.S. Krois, G.J. Pielak, *J. Am. Chem. Soc.* **134** (2012) 16614−166118.
67. M. Erlkamp, S. Grobelny, R. Winter, *PhysChemChemPhys.* **16** (2014) 5965−5976.
68. M.S. Cheung, D. Thirumalai, *J. Phys. Chem. B* **111** (2007) 8250−8257.
69. Y. Zhai, R. Winter, *ChemPhysChem* **14** (2013) 386−393.
70. A. Christiansen, P. Wittung-Stafshede, *FEBS Lett.* **588** (2014) 811−814.
71. P. H. Yancey, M. E. Clark, S. C. Hand, R. D. Bowlus, G. N. Somero, *Science* **217** (1982) 1214−1222.
72. P. H. Yancey, Transport Processes, lono- and Osmoregulation (Gilles, R. and Gallen-Baillies, M., eds.), Spinger-Verlag, Berlin (1985) pp. 424436.
73. J. F. Carpenter, J. H. Crowe, *Cryobiology* **25** (1988) 244–255.
74. J. F. Carpenter, J. H. Crowe, T. Arakawa, *J. Dairy Sci*. **73** (1990) 3727–3736.
75. A. Pyne, K. Chatterjee, R. Suryanarayanan, *J. Pharmcol. Sci*. **92** (2003) 2272–2283.
76. K. Shiraki, M. Kudou, S. Fujiwara, T. Imanaha, M. Takagi, *J. Biochem.* **132** (2002) 591−595.
77. E. A. Galinski, M. Stein, M. Amendt, M. Kinder, *Comp. Biochem. Physiol*. **117** (1997) 357–365.
78. S. Taneja, F. Ahmad, *Biochem. J*. **303** (1994) 147–153.
79. T. Arakawa, S.N. Timasheff, *Arch. Biochem. Biophys.* **224** (1983) 169–177.
80. T. Arakawa, S.N. Timasheff, *J. Biol. Chem.* **259** (1984) 4979–4986.
81. T. Arakawa, S.N. Timasheff, *Biochemistry* **26** (1987) 5147–5153.
82. J.L. Milner, D.J. McClellan, J.M. Wood, *J. Gen. Microbiol.* **133** (1987) 1851–1860.
83. R.L. Foord, R.J. Leatherbarrow, *Biochemistry* **37** (1998) 2969–2978.
84. V. Vagenende, A.X. Han, M. Mueller, B. L. Trout, *ACS Chem. Biol*. **8** (2013) 416−422.
85. D. Shukla, B. L. Trout, *J. Phys. Chem. B* **114** (2010) 13426−13438.

86. C. P. Schneider, B. L. Trout, *J. Phys. Chem. B* **113** (2009) 2050−2058.
87. B.M. Baynes, D. I. C. Wang, B. L. Trout, *Biochemistry* **44** (2005) 4919−4925.
88. T. B. Eronina, N.A. Chebotareva, N. N. Sluchanko, V. V. Mikhaylova, V. F. Makeeva, S. G. Roman, S.Y. Kleymenov, B. I. Kurganov, *Int J Biol Macromol.* **68** (2014) 225−232.
89. S. Sharma, S. Sarkar, S. S. Paul, S. Roy, K. Chattopadhyay, *Sci. Rep*. **3** (2013) 3525.
90. R. Ghosh, S. Sharma, K. Chattopadhyay, *Biochemistry* **48** (2009) 1135–1143.
91. F.I. Rosell, M.R. Mauk, A.G. Mauk, *Biochemistry* **44** (2005)1872−1879.
92. M. Assfalg, I. Bertini, A. Dolfi, P. Turano, A.G. Mauk, F.I. Rosell, H.B. Gray, *J. Am. Chem. Soc.* **125** (2003) 2913−2922.
93. F.I. Rosell, T.R. Harris, D.P. Hildebrand, S. Döpner, P. Hildebrandt, A.G. Mauk, *Biochemistry* **39** (2000) 9047−9054.
94. L. Konermann, F. I. Rosell, A. G. Mauk, D. J. Douglas, *Biochemistry* **36** (1997) 6448−6454.
95. D. Nurizzo, H.M. Baker, Q.Y. He, R.T. MacGillivray, A.B. Mason, R.C. Woodworth, E.N. Baker, *Biochemistry* **40** (2001) 1616−1623.
96. S. Jayaraman, D.L. Gantz, O. Gursky, *Biochemistry* **45** (2006) 4620−4628.
97. S. N. Timasheff, *Adv. Protein Chem.* **51** (1998) 355−432.
98. F. Colonna-Cesan, C. Sander, *Biophys. J.* **57** (1990) 1103−1107.
99. P.R. Wills, D.R. Hall, D.J. Winzor, *Biophys. Chem.* **84** (2000) 217−225.
100. D.K. Rao, R. Kumar, M. Yadaiah, A.K. Bhuyan, *Biochemistry* **45** (2006) 3412−3420.
101. R. Kumar, N.P. Prabhu, D.K. Rao, A.K. Bhuyan, *J. Mol. Biol*. **364** (2006) 483−495.
102. A. K. Bhuyan, *Biochemistry* **49** (2010) 7774−7782.
103. A. K. Bhuyan, *Biochemistry* **49** (2010) 7764−7773.
104. L. M. Mayr, F. X. Schmid, *Biochemistry* **32** (1993) 7994−7998.
105. A. C. Apetri, W.K. Surewicz, *J. Biol. Chem.* **278** (2003) 22187−22192.
106. M. Arai, K. Kuwajima, *Adv. Protein Chem.* **53** (2000) 209−282.
107. Y. Goto, A. L. Fink, *Biochemistry* **28** (1989) 945−952.
108. S. Nakamura, Y. Seki, E. Katoh, S. Kidokoro, *Biochemistry* **50** (2011) 3116−3126.
109. Y. Hagihara, S. Aimoto, A.L. Fink, Y. Goto, *J. Mol. Biol.* **231** (1993) 180−184.
110. Y. Hagihara, Y. Tan, Y. Goto, *J. Mol. Biol.* **237** (1994) 336−348.
111. S. Nakamura, T. Baba, S. Kidokoro, *Biophys. Chem.* **127** (2007) 103−112.

112. D. Hamada, S. Kidokoro, H. Fukada, K. Takahashi, Y. Goto, *Proc. Natl. Acad. Sci. USA* **91** (1994) 10325–10329.
113. Y. Hagihara, Y. Tan, Y. Goto, *J. Mol. Biol.* **237** (1994) 336−348.
114. A.H. Elcock, J. A. McCammon, *J. Mol. Biol.* **280** (1998) 731−748.
115. R. Kumar, A.G. Mauk, *J. Phys. Chem. B* **113** (2009) 12400−12409.
116. R. Perez-Jimenez, R. Godoy-Ruiz, B. Ibarra−Molero, J. M. Sanchez-Ruiz, *Biophys. J.* **86** (2004) 2414−2429.
117. R.L. Baldwin, *Biophys. J.* **71** (1996) 2056−2063.
118. A.K. Bhuyan, *Biochemistry* **41** (2002) 13386–13394.
119. R. Kumar, N.P. Prabhu, M. Yadaiah, A.K. Bhuyan, *Biophys. J.* **87** (2004) 2656−2662.
120. R. Kumar, A.K. Bhuyan, *J. Biol. Inorg. Chem.* **14** (2009) 11−21.
121. R. Jain, S. Kaur, R. Kumar, *J. Biochem.* **153** (2013) 161–177.
122. J.F. Brandts, L. Hunt, *J. Am. Chem. Soc.* **89** (1967) 4826−4838.
123. T.T. Herskovits, B. Gadegbeku, H. Jaillet, *J. Biol. Chem.* **245** (1970) 2588–2598.
124. D.P. Hong, M. Hoshino, R. Kuboi, Y. Goto, *J. Am. Chem. Soc.* **121** (1999) 8427–8433.
125. N. Hirato, K. Mizuno, Y. Goto, *J. Mol. Biol.* **275** (1998) 365−378.
126. G. Conio, E. Patrone, S. Brighetti, *J. Biol. Chem.* **245** (1970) 3335–3340.
127. N. Hirato, K. Mizuno, Y. Goto, *J. Mol. Biol.* **275** (1998)365−378.
128. Y.O. Kamatari, T. Konno, M. Kataoka, K. Akasaka, *J. Mol. Biol*. **259** (1996) 512−523.
129. A. Kentsis, T. R. Sosnick, *Biochemistry* **37** (1998) 14613−14622.
130. Y.O. Kamatari, T. Konno, M. Kataoka, K. Akasaka, *Protein Sci.* **7** (1998) 681−688.
131. K. Sasahara, K. Nitta, *Proteins* **63** (2006) 127−135.
132. V. E. Bychkova, A. E. Dujsekina, S. I. Klenin, E. I. Tiktopulo, V.N. Uversky, O. B. Ptitsyn, *Biochemistry* **35** (1996) 6058−6063.
133. Y.O. Kamatari, S. Ohji, T. Konno, Y. Seki, K. Soda, M. Kataoka, K. Akasaka, *Protein Sci.* **8** (1999) 873−882.
134. P. Sashi, U.M. Yasin, A.K. Bhuyan, *Biochemistry* **51** (2012) 3273−3283.
135. G. Onori, S. Passeri, A. Cipiciani, *J. Phys. Chem.* **93** (1989) 4306−4310.
136. J. Yang, X. S. Liu, K. Bhalla, C.N. Kim, A. M. Ibrado, J. Cai, T. Peng, D.P. Jones, X. Wang, *Science* **275** (1997) 1129–1132.

137. G.R. Moore, G.W. Pettigrew, Cytochrome *c*: Evolutionary, structural and physiochemical aspects. Berlin: Springer-Verlag (1990).
138. J.C. Kendrew, G. Bodo, H.M. Dintzis, R.G. Parrish, H.W. Wyckoff, D.C. Phillips, *Nature* **181** (1958) 662−666.
139. G.B. Postnikova, Y.E. Komarov, E.M. Yumakova, *Eur. J. Biochem*. **198** (1991) 223−232.
140. G.B. Postnikova, E.M. Yumakova, *Eur. J. Biochem*. **198** (1991) 241−246.
141. I. Kumagai, S. Kojima, Y. Tamaki, K. Miura, *J. Biochem*. **102** (1987) 733−740.
142. B.A. Malcolm, S. Rosenberg, M.J. Corey, J.S. Allen, A. Baetselier, J. F. Kirsch, *Proc. Natl. Acad. Sci. USA* **86** (1989) 133−137.
143. G.W. Bushnell, G.V. Louie, G.D. Brayer, *J. Mol. Biol.* **214** (1990) 585−595.
144. S.V. Evans, G.D. Brayer, *J. Mol. Biol.* **213** (1990) 885−897.
145. R. Diamond, *J. Mol. Biol.* **82** (1974) 371−391.
146. S. Wong, J. Grigg, N. Le Brun, G. Moore, M. Murphy, G. Mauk, *J. Biol. Chem.* **290** (2015) 3732–3739.
147. A. Crow, T.L. Lawson, A. Lewin, G.R. Moore, N.E. Le Brun, *J. Am. Chem. Soc.* **131** (2009) 6808–6813.
148. P. Aisen, I. Listowsky, *Annu. Rev. Biochem.* **49** (1980)357−393.
149. E. N. Baker, *Adv. Inorg. Chem.* **41** (1994) 389–463.
150. B.F. Anderson, H.M. Baker, G.E. Norris, D.W. Rice, E.N. Baker, *J. Mol. Biol.* **209** (1989) 711−734.
151. E.N. Baker, P.F. Lindley, *J. Inorg. Biochem.* **47** (1992) 147−160.
152. M. Haridas, B.F. Anderson, E.N. Baker, *Acta Crystallogr. D. Biol. Crystallogr.* **51** (1995) 629−646.
153. O. Zak, B. Tam, R.T. MacGillivray, P. Aisen, *Biochemistry* **36** (1997) 11036−11043.
154. M. R. Schlabach, G.W. Bates, *J. Biol. Chem.* **250** (1975) 2182−2188.
155. P.J. Halbrooks, A.B. Mason, T.A. Adams, S.K. Briggs, S.J. Everse, *J. Mol. Biol.* **339** (2004) 217–226.
156. W.R. Harris, *Biochemistry* **24** (1985) 7412–7418.
157. H. Kurokawa, B. Mikami, M. Hirose, *J. Mol. Biol.* **254** (1995) 196–207
158. A.N. Luck, C.E. Bobst, I.A. Kaltashov, A.B. Mason, *Biochemistry* **52** (2013) 8333–8341.

159. J. Konstantynowicz, T. Porowski, W. Zoch-Zwierz, J. Wasilewska, H. Kadziela-Olech, W. Kulak, S.C. Owens, J.P. Jastrzebska, M. Kaczmarski, *European Journal of Paediatric Neurology* **16** (2012) 485–491.
160. Q.Y. He, A.B. Mason B.M. Tam R.T. MacGillivray, R.C. Woodworth, *Biochemistry* **38** (1999) 9704–9711.
161. D.A. Folajtar, N.D. Chasteen, *J. Am. Chem. Soc.* **104** (1982) 5775–5780.
162. J.D. Bell, J.D. Brown, G. Kubal, P.J. Sadler, *Bio. Chem. Soc. Trans.* **16** (1988) 714–715.
163. J.K. Grady, A.B. Mason, R.C. Woodworth, N.D. Chasteen, *Biochem. J.* **309** (1995) 403–410.
164. W.R. Harris, A.M. Cafferty, S. Abdollahi, K. Trankler, *Biochim. Biophys. Acta* **1383** (1998) 197–210.
165. Q.Y. He, A.B. Mason, V. Nguyen, R.T. MacGillivray, R.C. Woodworth, *Biochem. J.* **350** (2000) 909–915.
166. A. Wishnia, I. Weber, R.C. Warner, *J. Am. Chem. Soc.* **83** (1961) 2071–2080.
167. S.L. Byrne, A.N. Steere, N.D. Chasteen, A.B. Mason, *Biochemistry* **49** (2010) 4200–4207
168. T.J. Egan, D.C. Ross, L.R. Purves, P.A. Adams, *Inorg. Chem.* **31** (1992) 1994–1998.
169. H.M. Marques, D.L. Watson, T.J. Egan, *Inorg. Chem.* **30** (1991) 3758–3762.
170. S.A. Kretchmar, K.N. Raymond, *Inorg. Chem.* **27** (1988)1436–1441.
171. J. Williams, N.D. Chasteen, K. Moreton, *Biochem. J.* **201** (1982) 527–532.
172. W.R. Harris, P.K. Bali, *Inorg. Chem.* **27** (1988) 2687–2691.
173. D.A. Baldwin, T.J. Egan, H.M. Marques, *Biochim. Biophys. Acta* **1038** (1990) 1–9
174. T.J. Egan, O. Zak, P. Aisen, *Biochemistry* **32** (1993) 8162–8167.
175. H.M. Marques, T. Walton, T.J. Egan, *J. Inorg. Biochem.* **57** (1995) 11–21.
176. O. Zak, B. Tam, R.T. MacGillivray, P. Aisen, *Biochemistry* **36** (1997) 11036–11043.
177. Y. Li, W.R. Harris, *Biochim. Biophys. Acta* **1387** (1998) 89–102.
178. H.M. Marques, T.J. Egan, G. Pattrick, *S. Afr. J. Sci.* **86** (1990) 21–24
179. B.K. Muralidhara, M. Hirose, *J Biol. Chem.* **275** (2000) 12463–12469.
180. K. Mizutani, B.K. Muralidhara, H. Yamashita, S. Tabata, B. Mikami, M. Hirose, *J Biol. Chem.* **276** (2001) 35940–35946.
181. D.H. Hamilton, I. Turcot, A. Stintzi, K.N. Raymond, *J. Biol .Inorg. Chem.* **9** (2004) 936–944.
182. J.L. Zweier, *J. Biol. Chem.* **253** (1978) 7616–7621.

183. M. Sola, *Eur. J. Biochem.***194** (1990) 349–353.
184. M.S. Shongwe, C.A. Smith, E.W. Ainscough, H.M. Baker, A.M. Brodie, E.N. Baker, *Biochemistry* **31** (1992) 4451–4458.
185. A. Seidel, E. Bill, L. Häggström, P. Nordblad, F. Kilár, *Arch. Biochem. Biophys.* **308**(1994) 52–63.

Chapter 2

Materials and Methods

2.1 Materials

Horse heart cytochrome *c* (Cyt *c*) (type VI), horse heart myoglobin (Mb), bovine apo-transferrin (T0178), egg white apo-transferrin (C0755), crowding agents (dextran 40, dextran 70 and ficoll 70), viscogens (glycerol, sucrose, and glucose) various salts ($NaClO_4$, NaCl, KCl and CsCl), 2,2,2-triflouroethanol (TFE), sodium oxalate, sodium carbonate, bathophenanthroline sulfonate (BPS), nitrilotriacetic acid (NTA), ferric chloride ($FeCl_3.6H_2O$), salts of buffer (sodium phosphate, Tris-base, 4-(2-Hydroxyethyl)-1-piperazineethanesulfonate (HEPES), 2-(*N*-mopholino) ethanesulfonate (MES) and 3-[Cyclohexylamino]-1-propanesulfonic acid (CAPS)), sodium dithionite and 1-anilino-8-napthalene sulfonate (ANS) were purchased from Sigma. Hen egg white lysozyme (Lyz) was purchased from calbiochem. L-amino acids (alanine, arginine, glycine, proline, serine and threonine) were purchased from Himedia. Chemical denaturants (guanidine hydrochloride (GdnHCl) and urea) were purchased from USB (USA). All other chemicals were of analytical grade. The desired pH of the samples solutions were adjusted by using the concentrated HCl and NaOH solutions. The concentrations of GdnHCl and urea stock solutions were determined by refractive index measurements by using an Abbe's and Thermo scientific Refractometer [1]. The kinetics and thermodynamic data were analyzed by using Sigma Plot (v. 9) and origin software (MicroCal Inc.).

2.2 Methods

2.2.1. Measurement of CO dissociation kinetics of natively folded CO-liganded Ferrocyt c under various concentrations of crowding agents, viscogens, amino acids and denaturants

Unfolded Ferricytochrome *c* (Ferricyt *c*) was prepared in 6.5 M GdnHCl. Unfolded Ferricyt *c* was deaerated by passing dry N_2 gas and reduced by ~3.0 mM of sodium dithionite solution. The stock solution of sodium dithionite was prepared in a sleeved rubber stoppers glass tube by dissolving 120 mg of solid sodium dithionite in 1.0 mL of deaerated phosphate buffer, pH

7.0 under dry N_2 atmosphere. Unfolded Ferrocytochrome *c* (Ferrocyt *c*) (U) thus obtained was liganded with CO by passing the dry CO gas through the protein solution under dry N_2 atmosphere. To determine the effect of crowding agents, amino acids, viscogens and denaturants on the internal dynamics of Ferrocyt *c*, the CO-liganded unfolded Ferrocyt *c* (UCO) was diluted 101-fold into a degassed and dithionite-reduced CO-free refolding buffer containing a desired concentration of crowding agent (dextran 40, dextran 70 and ficoll 70), amino acid (alanine, arginine, glycine, proline, serine and threonine), viscogens (glucose, glycerol and sucrose) and denaturant (GdnHCl or urea) at pH 7.0. This method allows complete refolding of UCO to generate a natively folded CO-liganded Ferrocyt *c*, called NCO. The fast UCO → NCO process, measurable by stopped-flow, precedes the slow NCO → N+CO dissociation. Kinetics of CO-dissociation was monitored by 550-nm heme absorbance at pH 7, 25°C in a Shimadzu UV-visible spectrophotometer (UV-2450). Fast kinetics were measured by a Shimadzu 2450 spectrophotometer coupled with Applied Photophysics RX 2000 rapid kinetics system stopped flow mixing accessory. Final concentrations of protein and sodium dithionite were 6 µM and 3 mM respectively. The kinetic data were analyzed by nonlinear least-squares fit to a single-exponential rate expression.

2.2.2. Measurement of CO-dissociation kinetics of NCO at different concentrations of denaturants in the absence and presence of fixed concentrations of crowding agents and amino acids

Unfolded Ferrocyt *c* was prepared as mentioned in section 2.2.1.To determine the effect of crowding agents and amino acids on the denaturant-dependent internal dynamics of Ferrocyt *c*, the CO-liganded unfolded Ferrocyt *c* (UCO) was diluted 101-fold into a degassed and dithionite-reduced CO-free refolding buffer containing different concentrations of denaturants (urea and GdnHCl) at fixed concentrations of crowding agent (dextran 40, dextran 70 and ficoll 70), amino acid (alanine, arginine, glycine, proline, serine and threonine)) at pH 7. This method transforms UCO-state to NCO-state within millisecond time, measurable by stopped-flow. The slow NCO → N+CO dissociation kinetics was monitored by 550-nm heme absorbance at pH 7, 25°C. Fast kinetics were measured by a Shimadzu 2450 spectrophotometer coupled with Applied Photophysics RX 2000 rapid kinetics system stopped flow mixing accessory.

2.2.3. Measurement of kinetics of CO association with Ferrocyt c under various concentrations of crowding agents, salt and alcohol

CO-association kinetics with Ferrocyt *c* (Ferrocyt *c* + CO → Ferrocyt *c*-CO) was carried out under anaerobic conditions by using previously described methods [2-3]. Ferricyt *c* was dissolved in 50 mM phosphate buffer at pH 7.0 and reduced with sodium dithionite under dry N_2 atmosphere. About ~30 µl of the reduced protein solution was added to 2 ml of deaerated CO saturated (~1.0 mM) desired pH buffer containing sodium dithionite and varying concentrations of desired additives (crowding agents (dextran 70 and ficoll 70), salts (NaCl, KCl and CsCl), 2,2,2-triflouroethanol (TFE) at pH 7.0 and pH 12.9 (±0.1). The CO-association kinetics for Ferrocyt *c* was recorded on Shimadzu (UV- 2450) spectrophotometer by monitoring the decrease in absorbance at 550 nm, 25°C. The final concentrations of protein and sodium dithionite in CO association kinetic experiments were ~10-12 µM and ~3.0 mM, respectively.

2.2.4. Measurement of CO-replacement kinetics of carbonmonoxymyoglobin (MbCO) under various concentrations of crowding agents and amino acids

The CO replacement reaction of MbCO complex by using hexacyanoferrate ion (MbCO + CN^- → MbCN + CO) was carried out in different concentrations of crowding agents (dextran 40, dextran 70 and ficoll 70) and amino acids (alanine, arginine, glycine, proline, serine and threonine). Briefly, Mb (~1 mM) was initially dissolved in phosphate buffer at pH 7.0. It was then deaerated and reduced by the addition of sodium dithionite (final concentration ~0.5 mM). The reduced Mb was then liganded with CO under dry nitrogen atmosphere by passing a slow stream of dry CO gas. About 25 µL of this CO-liganded protein was added into 2.0 mL solution of potassium hexacyanoferrate containing a desired concentration of the crowding agents (dextran 40, dextran 70 and ficoll 70) and amino acids (alanine, arginine, glycine, proline, serine and threonine) at pH 7.0. The change in the absorbance of the reaction medium was monitored at 421 nm on Shimadzu (UV-2450) spectrophotometer at 22°C. The kinetic data were analyzed by nonlinear least-squares fit to a single-exponential rate expression.

2.2.5. Measurement of urea-denaturation induced iron (Fe^{3+}) release and reduction-induced iron (Fe^{2+}) release from carbonate and oxalate bound Fe_NTfs

The urea-induced Fe^{3+} release from carbonate and oxalate bound monoferric N-lobe of transferrins (Fe_NTfs) (Fe_NoTf (ovotransferrin) and Fe_NsTf (serum transferrin)) was measured at pH 7.4 and 5.6, 25°C by monitoring the decrease in absorbance at 465 nm [4]. Briefly, the synergistic anion (carbonate, oxalate) bound Fe_NTfs (50 μL, 11 μM, pH 7.4) was mixed rapidly to buffer (0.05 M HEPES, 0.8 mL, pH 7.4) which contained ~10 M urea and equilibrated at 25°C. At pH 5.6, the urea-induced Fe^{3+} release reaction was comparatively faster, so the kinetics of denaturant-induced Fe^{3+} release at pH 5.6 was measured by a conventional spectrophotometer configured with rapid kinetics stopped-flow mixing accessory. Fe_NTfs (pH 7.4) was taken in one stopped flow syringe and buffer (0.05 M MES, pH 5.5) that contained 5.0 M urea was taken in other syringe. Throughout the experiment, the temperature was maintained at 25 °C. pH was measured after each experiment to ensure that it remained constant. For urea-induced Fe^{3+} release experiments (pH 7.4 and pH 5.6), the final protein concentration was ~ 6 μM.

The kinetics of Fe^{2+} release from carbonate and oxalate bound Fe_NTfs by sodium dithionite was measured at pH 7.4 and 5.6, 25 °C by monitoring the increase in absorbance at 538 nm for Fe^{2+}-BPS complex formation [5-7]. Briefly, Fe_NTfs (50 μL, 11 μM, pH 7.4) was mixed rapidly to a deaerated buffer (0.1 M HEPES, 0.8 mL, pH 7.4) which already has ~10 mM sodium dithionite and 0.25 mM BPS (25 °C). At pH 5.6, Fe^{2+} release reaction was comparatively faster, so the kinetics of Fe^{2+} release at this pH was measured by a conventional spectrophotometer configured with a rapid stopped-flow mixing accessory. Fe_NTfs (pH 7.4) was taken in one stopped flow syringe and buffer (0.1 M MES, pH 5.5) that contained sodium dithionite and BPS was taken in other syringe. Throughout the experiment, the temperature was kept constant at 25 °C. The final concentrations of protein, sodium dithionite, and BPS were ~15 μM, 10 mM and 0.25 mM, respectively. Both at pH 7.4 and 5.6, the kinetics data for Fe^{3+} and Fe^{2+} release were analyzed by nonlinear least-squares fit to a single-exponential rate expression and the rates (k_{obs}) were extracted more conveniently by recording the absorbance change at 465nm (Fe^{3+} release) and 538nm (Fe^{2+} release) as a function of time.

2.2.6. Measurement of activation parameters for kinetics of CO-dissociation from NCO, CO-association with Ferrocyt c, CO-replacement from MbCO and iron-release from Fe_NTfs

The activation enthalpy (ΔH) and activation entropy (ΔS) were calculated by temperature

dependent rate profile of CO-dissociation from NCO; CO-association with Ferrocyt *c*; CO-displacement from MbCO by hexacyanoferrate ion and iron release from carbonate and oxalate bound Fe_NTfs at corresponding pH with desired buffer and additives. This is better understood from the Eyring equation [8].

$$\ln(k_{diss/ass/off/obs}h/k_B T) = (\Delta S_{diss/ass/off/obs}^{\ddagger}/R) - (\Delta H_{diss/ass/off/obs}^{\ddagger}/RT) \quad (1)$$

where 'k_B' is the Boltzmann constant, 'h' is the Planck constant, 'R' is the gas constant, $\Delta H_{diss/ass/off/obs}$ and $\Delta S_{diss/ass/off/obs}$ are changes in activation enthalpy and activation entropy. Previously, other method [9] were also used for calculating the activation entropy and activation enthalpy, by following relation

$$(\Delta H_{diss}/RT) = \ln(\nu/k_{diss}) + (\Delta S_{diss}/R) \quad (2)$$

where ν is the vibrational frequency, ΔH_{diss} and ΔS_{diss} are changes in activation enthalpy and activation entropy, respectively, between the relevant reactants and transition state. The enthalpy and entropy can be determined by using the Arrhenius equation:

$$k_{diss} = A\,exp(-E_a/RT) \quad (3)$$

where A is the frequency factor (s^{-1}) and E_a is the activation energy (kcal mol^{-1}). Comparison of equations (2) and (3) gives

$$Ea = H_{diss}$$

$$\ln(A/\nu) = (\Delta S_{diss}/R) \quad (4)$$

2.2.7. Measurement of thermal denaturation of Ferricyt c, Ferrocyt c, Mb and Lyz under various concentrations of crowding agents, amino acids, salts and denaturants

To determine the effect of crowding agents (dextran 40, dextran 70 and ficoll 70), L-amino acids (alanine, arginine, glycine, proline, serine and threonine), salts (NaCl, KCl and CsCl), denaturants (GdnHCl and urea), on thermal denaturation of Ferrocyt *c*, Ferricyt *c*, Mb and Lyz, the absorbance (550 nm (Ferrocyt *c*); 409 nm (Mb), far-UV CD (222 nm (Ferrocyt *c*, Ferricyt *c*, Mb, Lyz) and near-UV CD (282 nm (Ferricyt *c*, Mb)) monitored thermal denaturation curves of these

proteins were collected under varying concentrations of these additives at desired pH values on Shimadzu (UV-2450) spectrophotometer and JASCO-810 or 815 or Avive-430 CD-spectrophotometer. The final protein concentrations for the absorbance, far-UV CD and near-UV CD monitored thermal unfolding experiments were ~5.0 μM, ~10-15 μM and ~60-80 μM, respectively. For thermal unfolding measurements of Ferrocyt *c* the dithionite concentration was ~0.5-3 mM. For both CD and absorbance measurements, the Peltier-controlled heating rate was 1.0 or 2.0 °C/min. By assuming a two-state denaturation process, the thermal denaturation data were analyzed by using van't Hoff equation (eq. (5)) [10] or Gibbs Helmholtz equation (eq. (6)) [11],

$$y(T) = \frac{(y_F + m_F T) + (y_D + m_D T)\, exp\left[\frac{-H_m}{RT}\left(\frac{1}{T} - \frac{1}{T_m}\right)\right]}{1 + exp\left[\frac{-H_m}{RT}\left(\frac{1}{T} - \frac{1}{T_m}\right)\right]} \tag{5}$$

$$y(T) = \frac{(y_F + m_1 T) + (y_U + m_2 T)\exp\left(\frac{\Delta H_m\left(\frac{T}{T_m} - 1\right) - \Delta C_p\left(T_m - T + T\ln\left(\frac{T}{T_m}\right)\right)}{RT}\right)}{1 + \exp\left(\frac{\Delta H_m\left(\frac{T}{T_m} - 1\right) - \Delta C_p\left(T_m - T + T\ln\left(\frac{T}{T_m}\right)\right)}{RT}\right)} \tag{6}$$

where $y(T)$ is the observed variable parameter ($\varepsilon_{550\ nm}$, $\varepsilon_{409\ nm}$, $CD_{222\ nm}$, $CD_{282\ nm}$), y_F and y_U, and m_F and m_U, represent intercepts and slopes of the folded and unfolded baselines, respectively; T, absolute temperature; ΔC_p, heat capacity change; R, gas constant, and ΔH_m represent the van't Hoff enthalpy at thermal denaturation midpoint (T_m).

2.2.8. Measurement of thermal denaturation of Ferricyt c, Ferrocyt c, Mb and Lyz under various concentrations of denaturants in the absence and presence of fixed concentrations of crowding agents and amino acids

To determine the effect of crowding agents and L-amino acids on the denaturant-dependent thermal denaturation of Ferricyt *c*, Ferrocyt *c*, Mb and Lyz, the absorbance (550 nm (Ferrocyt *c*); 409 nm (Mb), far-UV CD (222 nm (Ferrocyt *c*, Ferricyt *c*, Mb, Lyz)) and near-UV CD (282 nm (Ferricyt *c*, Mb)) monitored thermal denaturation curves of these proteins were collected under varying concentrations of denaturants (urea and GdnHCl) at fixed concentrations of crowding agents (dextran 40, dextran 70 and ficoll 70) and amino acids (alanine, arginine, glycine, proline, serine and threonine) at pH 7.0 and pH 12.9 (±0.1). The final protein concentrations for the absorbance, far-UV CD and near-UV CD monitored thermal unfolding experiments were ~5 μM, ~10-15 μM and ~60-80 μM, respectively. For both CD and absorbance measurements, the Peltier-controlled heating rate was 1.0 or 2.0 °C/min. The thermal denaturation curves were analyzed by using van't Hoff equation (eq. (5)) [10] or Gibbs Helmholtz equation (eq. (6)) [11].

2.2.9. Measurement of denaturant-induced-unfolding of Ferricyt c, Ferrocyt c, Mb and Lyz under various concentrations of crowding agents and amino acids

To determine the effect of crowding agents and amino acids on the GdnHCl-induced unfolding of proteins, the samples of Ferricyt *c* (~12.0 μM) and Mb (~6.0 μM) were prepared in the 0-7.5 M range of GdnHCl in the absence and presence of fixed concentration of crowding agents (dextran 40, dextran 70 and ficoll 70) or L-amino acids (alanine, arginine, glycine, proline, serine and threonine) in 50 mM phosphate buffer at pH 7.0, 25ºC. For Ferrocyt *c* samples preparation, Ferricyt *c* samples were deaerated by passing dry N_2 gas and reduced by adding the concentrated dithionite solution to a final concentration of 2.0 mM. The samples were sealed under nitrogen and equilibrated for ~20 minutes at 25 ºC. To determine the effect of crowding agents and amino acids on urea-induced unfolding of proteins, the samples of Ferricyt *c* (~6.0 μM) and Mb (~5.0 μM) were prepared in the 0-10.5 M range of urea in the absence and presence of fixed concentration of crowding agents (dextran 40, dextran 70 and ficoll 70) or L-amino acids (alanine, arginine, glycine, proline, serine and threonine) at pH 7.0, 25ºC. To determine the effect

of crowding agents and amino acids on the GdnHCl-dependent unfolding of proteins, the samples of Ferricyt *c* (~6.0 μM) and Mb (~5.0 μM) were prepared in the 0-10.5 M range of urea at different concentrations of GdnHCl in the absence and presence of fixed concentrations of fixed concentration of crowding agents (dextran 40, dextran 70 and ficoll 70) or L-amino acids (alanine, arginine, glycine, proline, serine and threonine) at pH 7.0, 25ºC.

In aqueous solution, urea forms cyanate, which can carbamylate lysyl epsilon-amino groups and change the electrostatic properties of a protein [12-14]. The presence of cyanate in solution could lead to modification of these proteins prior to or during data collection. Therefore, the experiments that employ urea as denaturing agent were used within 12 hours of their preparation to prevent the cyanate formation. The concentrations of the urea and GdnHCl solutions before and after the experiments were determined by refractive index measurements on an Abbe or Thermo Scientific refractometer [1].

Fluorescence emission (ex: 280 nm; em: 340 nm) and far-UV (250-200nm), near-UV (300-250 nm) CD spectra of Ferricyt *c* and Mb were recorded on Perkin Elmer LS-55 fluorescence spectrophotometer and JASCO-810 or 815 spectropolarimeter, respectively. Fluorescence spectra (ex: 280 nm, ex: 340) of Ferrocyt *c* samples were collected on Cary Eclipse Agilent spectrofluorometer at 25ºC. The pH of the protein samples are those measured after the experiments. The data were fitted to a standard two-state equilibrium unfolding equation (7) [15]

$$Y_{obs} = \frac{(C_N + M_N[D]) + (C_U + M_U[D])exp\left[\frac{-\Delta G_D + m_g[D]}{RT}\right]}{1 + exp\left[\frac{-\Delta G_D + m_g[D]}{RT}\right]} \quad (7)$$

where Y_{obs} is the observed signal, C_N and C_U, and M_N and M_U represent intercepts and slopes of native and unfolded baselines, respectively, [*D*] is the concentration of denaturant in M, *R* is the gas constant, ΔG_D, the free energy associated with the transition, and m_g, the surface area of the protein exposed by the solvent. C_m, the transition midpoint of denaturant concentration, was calculated as $C_m = \Delta G_D/m_g$.

2.2.10. Measurement of denaturant-induced-unfolding of diferric transferrins (Fe_2Tfs)

To determine the effect of synergistic anion on denaturant-induced-unfolding of diferric transferrins (Fe_2Tfs), the far-UV CD (222 nm) and near-UV CD (282 nm) monitored urea-induced unfolding curves of carbonate and oxalate bound diferric ovotransferrin (Fe_2oTf) and bovine serum transferrin (Fe_2sTf) were collected at pH 7.0, 25ºC. The data were fitted to a standard two-state equilibrium unfolding equation (7) [15]. The protein samples were prepared in 0-10.5 M urea with 4 μM (far-UV CD), 8 μM (near-UV CD) of carbonate and oxalate bound Fe_2Tfs in 50 mM HEPES buffer at pH 7.0, 25ºC. The samples were sealed and equilibrated for ~6 hours at 25ºC. The data were fitted to a standard two-state equilibrium unfolding equation (7) [15].

2.2.11. Measurement of pH- titrations of Ferricyt c, apoMb and Lyz

For pH unfolding studies of Ferricyt *c*, apoMb and Lyz, the samples were prepared in 10 mM of Tris, 10 mM of disodium hydrogen phosphate and 2 mM CAPS buffers. The pH of protein samples were adjusted from 7.0-13.2 range by using the concentrated NaOH and HCl solutions. The titration did not upset the uniformity of the protein concentration. These protein samples were then incubated for ~40 minutes. Far-UV CD spectra (250-200 nm) were recorded on JASCO-810 or 815 spectropolarimeter. The pH titration curves were analyzed by using the following transformed Henderson-Hasselbalch equation (equation (8)) [11]

$$Y_{\text{obs}} = \left[\frac{C_u + C_f \left[10^{n(pH - C_m)} \right]}{1 + 10^{n(pH - C_m)}} \right] \qquad (8)$$

where, C_u and C_f are far-UV CD (222 nm) signals for the unfolded and the folded states, respectively, n is the number of OH^- ions titrated, and C_m is the pH-midpoint for the transition.

2.2.12. Measurement of fraction of iron released from Fe_2Tfs as a function of pH, temperature and urea

Fraction of iron released as a function of pH was measured for carbonate and oxalate bound Fe_2Tfs (~10 μM) at 25 °C. Aliquots of iron-saturated protein were incubated in a mixed buffer (50 mM HEPES + 50 mM MES), adjusted to pH between 3 and 8. Prior to the data collections, the

protein samples were incubated for ~5 hrs at 25 °C. The decrease in iron-phenolate charge transfer bands at 465 nm have been used the reliable indicators for iron release [16-19]. Visible absorbance (390-710 nm) for protein samples were recorded on Shimadzu 2450-UV-spectrophotometer. The percentage of iron retained by protein was estimated on the basis of absorbance maximum at 465 nm. The final pH of protein samples were those measured after experiments. And the pH unfolding curves were analyzed by nonlinear-least-squares fits of the data to the modified version of the Henderson-Hasselbalch equation (equation (9)) [20],

$$Y_{\text{obs}} = \left[\frac{C_{Fe^{3+}-Tfs} + C_{apo-Tfs}\left[10^{(C_m{}^* - pH)}\right]}{1+10^{(C_m{}^* - pH)}} \right] \qquad (9)$$

where $C_{Fe^{3+}\text{-}Tfs}$ and $C_{apo\text{-}Tfs}$ are the normalized spectroscopic signals for iron-bound and iron free states, respectively, and $C_{\text{m}}{}^*$ is the pH-midpoint where Fe_2Tfs released 50% of bound irons.

At higher urea concentrations, Fe_2Tfs can trigger iron release due to chemical denaturation of protein [4]. Fraction of iron released as a function of urea was measured for carbonate and oxalate bound Fe_2Tfs (~10 μM) at 25 °C. Aliquots of iron-saturated protein were incubated in a buffer (0.1 M HEPES with 0.1 M NaCl (pH 7.4) or 0.1M MES with 0.1 M NaCl (pH 5.7)) containing varying concentrations of urea between 0 to 10.5 M. Prior to the data collection, the protein samples were incubated for ~10 hrs at 25 °C. The fraction of iron released from the protein was estimated on the basis of absorbance maximum at 465 nm and the data were analyzed by using two-state equation (equation 7). Urea concentration was measured by Thermo-scientific refractometer. The final concentrations of urea were those measured after experiments.

At higher temperatures, Fe_2Tfs can trigger iron release due to thermal denaturation of protein [20]. Fraction of iron released as a function of temperature was measured for carbonate and oxalate bound Fe_2Tfs (~5 μM) at pH 7.4 (0.3 M HEPES with 0.1 M NaCl). The thermally-induced iron release (based on absorbance at 465 nm) profiles for Fe_2Tfs were collected on a 2450-UV-spectophotometer (Shimadzu). The temperature of protein solution was increased at a rate of 1°C/min (S-1700 thermoelectric single cell holder with *T*m analysis software, Shimadzu). The fraction of iron released from the protein was estimated on the basis of absorbance at 465 nm

and the thermal denaturation midpoint (T_m) of iron release for carbonate and oxalate bound Fe_2sTf were obtained by differentiation of the fraction of iron released versus temperature.

2.2.13. Measurement of the far-UV CD, near-UV CD and fluorescence emission spectra of Ferricyt c, Ferrocyt c, apoMb, Lyz and Fe_2Tfs

Far-UV (200-250 nm, 1.0 mm cell) CD spectra of Ferricyt *c* (12 μM), Ferrocyt *c* (15 μM), Mb (12 μM), apoMb (12 μM), Lyz (12 μM) and Fe_2Tfs (4 μM) were collected at native pH (pH 7), and at alkaline pH (pH 12.9±0.1) (except Fe_2Tfs) in the absence and presence of different additives (crowding agents/salts/alcohol/urea) on JASCO 810 or 815 spectropolarimeter at 25 °C. The near-UV CD (250-300 nm, 5.0 mm cell) spectra for Ferricyt *c* (~70 μM, pH 7), Ferrocyt *c* (~80 μM), Mb (~60 μM), apoMb (~60 μM), Lyz (~60 μM) and Fe_2Tfs (8 μM) were collected at native pH (pH 7), and at alkaline pH (pH 12.9±0.2) (except Fe_2Tfs) in the absence and presence of different additives (amino acids/salts/alcohol/urea) on a JASCO 810 or 815 spectropolarimeter at 25 °C. The far- UV CD and near-UV CD spectra of native and denatured Ferrocyt *c,* Ferricyt *c,* Mb and Fe_2Tfs were collected at pH 7.0. Neutral pH (pH 7) experiments were performed in 50 mM sodium phosphate buffer (Fe_2Tfs were in 50 mM HEPES buffer) while alkaline pH (pH 12.9±0.1) experiments were performed in 2 mM CAPS buffer.

The far-UV CD (210-250 nm) spectra of Ferricyt *c* (12 μM), apoMb (12 μM) and Lyz *(*10 μM) in the presence of different concentrations of crowding agents (dextran 70 and ficoll 70), salts (NaCl, KCl and CsCl) and TFE were collected at pH 12.9 (±0.1) on JASCO 810 or 815 spectropolarimeter in 2 mM CAPS buffer at 25 °C. All CD spectra of Ferricyt *c,* apoMb and Lyz were corrected by subtracting the CD spectra of the corresponding blank solutions of that concentrations of crowding agents (dextran 70 and ficoll 70) at pH 12.9 (±0.1) on JASCO 810 or 815 spectropolarimeter in 2 mM CAPS buffer at 25 °C.

Fluorescence emission spectra (ex: 280 nm; em: 340 nm; 10 mm path length cuvette; 5 μM protein) (310-420 nm) for different states of Ferricyt *c,* Mb and Lyz were recorded on Perkin Elmer LS-55 fluorescence spectrophotometer or Horiba Fluoromax 4 spectrofluorometer in the absence and presence of different additives viz; crowding agents (dextran 70 and ficoll 70) and salts (NaCl, KCl and CsCl) at pH 12.9 (±0.1) at 25 °C. The fluorescence emission spectra were also collected for native of Ferricyt *c,* Mb and Lyz at 25 °C. All neutral pH (pH 7) fluorescence

emission spectra were collected in 50 mM sodium phosphate buffer. All alkaline pH (pH 12.9 (±0.1)) fluorescence emission spectra were collected in 2 mM CAPS buffer.

2.2.14. Measurement of extrinsic fluorescence emission spectra of 8-anilinona phthalene-1-sulphonic acid (ANS)-bound Ferricyt c, Mb and Lyz

ANS emission spectra (ex: 380 nm, em: 400-600 nm) were collected in the absence and presence of different additives viz; crowding agents (dextran 40, dextran 70 and ficoll 70), salts (NaCl, KCl and CsCl) at pH 12.9 (±0.1) and neutral pH (pH 7) at 25 °C on Perkin Elmer LS-55 fluorescence spectrophotometer or Horiba Fluoromax 4 spectrofluorometer. For ANS fluorescence measurements, ratio of ANS (0.5mM) and protein (5μM) were 100:1.

2.2.15. Preparation of carbonate and oxalate bound Fe_2Tfs

Carbonate and oxalate bound Fe_2Tfs (Fe_2sTf and Fe_2oTf) were prepared by well established method used earlier [21-22]. Acidic deionized water (pH 3, HCl only) and preweighed amounts of solid reagents (HEPES, apo-Tfs, ferric chloride, NTA, sodium oxalate and sodium carbonate salt) were placed in a desiccator containing KOH or soda lime. Desiccator was opened under dry N_2 gas atmosphere. Buffer solution (20 mM carbonate/oxalate and 100 mM HEPES) was prepared with CO_2 free water. For preparation of carbonate and oxalate bound Fe_2Tfs, ~80 mg apotransferrins (bovine serum apo-transferrin and apo-ovotransferrin) (apo-Tfs) (1 μmol) was dissolved in 3 mL of CO_2 free buffer (100 mM HEPES, pH 7.4, 20 mM of $NaHCO_3$ sodium salt/sodium oxalate) under dry N_2 gas atmosphere and sealed with parafilm. Fe-NTA solution was prepared under dry N_2 gas atmosphere by mixing 12.2 mg of $FeCl_3.6H_2O$ and 17.2 mg of NTA in 2 ml of 6.0 M HCl and adjust the pH ~ 4.0 with concentrated NaOH and make up the final volume ~10 ml with CO_2 free water. Finally, 2.0 mL of freshly prepared Fe-NTA solution was added into the protein solution under dry N_2 gas atmosphere. After ~24 hrs incubation at ~37 °C, the protein solution was purified with 10 kDa molecular mass cut-off (Millipore, Bedford, MA, USA) with CO_2 free 50 mM HEPES buffer. The concentrations of carbonate and oxalate bound Fe_2Tfs were calculated spectrophotometrically (Fe_2Tfs; $\varepsilon_{465\ nm} = 5\times10^3$ and $3.07\times10^3\ M^{-1}\ cm^{-1}$ for carbonate and oxalate bound Fe_2Tfs) [20]. Iron saturations for carbonate and oxalate bound Fe_2sTf were confirmed by urea–polyacrylamide gel electrophoresis. The percentage of iron saturations in the carbonate and oxalate bound Fe_2Tfs were ≥ 98%.

2.2.16. Preparation of carbonate and oxalate Fe_NTfs

Carbonate and oxalate bound Fe_NTfs were prepared by well established method used earlier [23]. The carbonate or oxalate bound diferric-Tfs (Fe_2Tfs) (250 μM) was incubated at 37°C for ~3 hrs in CO_2 free 100 mM HEPES buffer which also contained ~100 mM EDTA and 2.7 M $NaClO_4$. After this, the protein solution was exchanged four times with original CO_2 free buffer (100 mM HEPES, pH 7.4) by using a Centricon filter of 10 kDa molecular mass cut-off (Millipore, Bedford, MA, USA). Iron saturations for carbonate and oxalate bound Fe_NTfs were confirmed by urea–polyacrylamide gel electrophoresis. The concentration of carbonate and oxalate bound Fe_NTfs were calculated spectrophotometrically ($\varepsilon_{465\ nm} = 2150\ M^{-1}\ cm^{-1}$) [21].

2.2.17. Differential scanning calorimetric studies of carbonate and oxalate bound Fe_2sTf

Differential scanning calorimetric studies of carbonate and oxalate bound Fe_2sTf were performed on a MicroCal VP-DSC (MicroCal, GE Healthcare). All experiments were carried out at a scan rate of 81ºC h^{-1}, scanning from 25 to 110ºC [24]. Background excess thermal power scans were obtained with buffer containing 0.5 M HEPES in both the sample and reference cells and subtracted from the scans for each sample solution containing 0.02 mM carbonate or oxalate bound Fe_2sTf. All samples were degassed for ~15 minute with gentle stirring under vacuum prior to loading into the calorimeter. Data analysis was performed using Origin software supplied by MicroCal [25].

2.2.18. Differential scanning calorimetric studies of Ferrocyt c

Differential scanning calorimetric studies of Ferrocyt *c* were performed on a MicroCal VP-DSC (MicroCal, GE Healthcare). Ferricyt *c* was reduced with a mixture of sodium dithionite (~ 4 mM) and NADH (~ 0.8 mM). Ferricyt *c* was deaerated by passing dry N_2 gas and reduced with a mixture of sodium dithionite (~ 4 mM) and nicotinamide adenine dinucleotide (NADH) (~ 0.8 mM). The protein concentration was 115 μM. The measurements were performed in 50 mM phosphate buffer (pH 7.0) and the scan rate of 65ºC h^{-1}, scanning from 25 to 110ºC [26]. Data analysis was performed using Origin software supplied by MicroCal [25].

2.2.19. Denaturants concentration corrections (in the presence of dextran 40, dextran 70 and ficoll 70)

It is assuming that the synthetic crowder does not interact with any solute molecules resulting it should be increases the concentration of any small solute by decreasing its available volume through steric repulsion [24, 27]. It was reported that there were no specific interaction between GdnHCl or urea and ficoll or dextran and partial specific volume value of macromolecular crowding was same in buffer and in denaturants [28]. According to previous report by Christiansen et al, the partial specific volume for ficoll 70 is ~0.65±0.02 ml/g, which is also same for dextrans and does not depend on the amount of crowding agent dissolved [28]. For denaturants concentration correction, we used following equation [28-29].

$$[Denaturants]_{corr} = (1/f_{av})[Denatrants] \qquad (10)$$

where f_{av} is the volume fraction available to the solvent [29]. For example, for 200 mg ml^{-1} of macromolecular solution, the value of f_{av} is ~ 0.87 (*i.e,* 1-0.65ml/g×0.2g/mL). All denaturants concentrations used in kinetic and stability experiments were corrected in this way on the basis of the amount of crowding agent present.

2.3 References:

1. C.N. Pace, B.A. Shirley, J.A. Thomson, in Protein Structure: A Practical Approach (Creighton, T.E., Ed.) IRL Press, Oxford, UK, (1989) pp. 311–330.
2. R. Kumar, N.P. Prabhu, M. Yadaiah, A.K. Bhuyan, *Biophys. J.* **87** (2004) 2656–2662.
3. D.K. Rao, R. Kumar, M. Yadaiah, A.K. Bhuyan, *Biochemistry* **45** (2006) 3412–3420.
4. K. Nakazato, T. Yamamura, K. Satake, *J. Biochem.* **103** (1988) 823–828.
5. D. A. Baldwin, T. J. Egan, H. M. Marques, *Biochim. Biophys. Acta* **1038** (1990) 1–9.
6. N. Kojima, G. W. Bates, *J. Biol. Chem.* **254** (1979) 8847–8854.
7. S. Kumar, D. Sharma, R. Kumar, R. Kumar, *J. Biol. Inorg. Chem.* **19** (2014) 1009–1024.
8. J. Mikšovská, J.H. Day, R.W. Larsen, *J. Biol. Inorg. Chem.* **8** (2003) 621─625.
9. A. K. Bhuyan, *Biochemistry* **41** (2002) 13386–13394.
10. M.M. Santoro, D.W. Bolen, *Biochemistry* **31** (1992) 4901─ 4907.
11. R. Kumar, N.P. Prabhu, D.K. Rao, A.K. Bhuyan, *J. Mol. Biol.* **364** (2006) 483–495.

12. P. Hagel, J.J. Gerding, W. Fieggen, H. Bloemendal, *Biochim. Biophys. Acta* **243** (1971) 366–373.
13. G.R. Stark, *Methods Enzymol.* **25** (1972) 103–120.
14. M.F. Lin, C.Williams, M.V.Murray, G. Conn, P.A. Ropp, *J. Chromatogr. B Analyt. Technol. Biomed. Life Sci.***803** (2004) 353–362.
15. M.M. Santoro, D.W. Bolen, *Biochemistry* **27** (1988) 8063–8068.
16. P. J. Halbrooks, A. B. Mason, T. A. Adams, S. K. Briggs, S. J. Everse, *J. Mol. Biol.* **339** (2004) 217–226.
17. N. G. James, C. L. Berger, S. L. Byrne, V. C. Smith, R.T. A. MacGillivray, A. B. Mason, *Biochemistry* **46** (2007) 10603–10611.
18. S. S. Lehrer, *J. Biol. Chem*. **244** (1969) 3613–3617.
19. P. K. Bali, W. R. Harris, *J. Am. Chem. Soc*. **111** (1989) 4457–4461.
20. R. Kumar, A. G. Mauk, *J. Phys. Chem. B* **113** (2009) 12400–12409.
21. P. K. Bali, W. R. Harris, *Arch. Biochem. Biophys* **281** (1990) 251–256.
22. I. Turcot, A. Stintzi, J. Xu, K. N. Raymond, *J. Biol. Inorg. Chem.* **5** (2000) 634–641.
23. A.H.T Hissen, M.M. Moore, *J. Biol. Inorg. Chem*. **10** (2005) 211–220.
24. M. T. Jr. Record, E. S. Courtenay, S. Cayley, H. J. Guttman, *Trends Biochem. Sci.* **23** (1998) 190–194.
25. L. N. Lin, A. B. Mason, R. C. Woodworth, J. F. Brandts, *Biochemistry* **33** (1994) 1881–1888.
26. R. Varhac, M. Antalik, M. Bano, *J. Biol. Inorg. Chem.* **9** (2004)12–22.
27. S. Cayley, B. A. Lewis, H. J. Guttman, M. T. Record, *J. Mol. Biol.* **222** (1991) 281–300.
28. A. Christiansen, Q. Wang, A. Samiotakis, M. S. Cheung, P. Wittung-Stafshede, *Biochemistry* **49** (2010) 6519−6530.
29. D. Hall, A. P. Minton, *Biochim. Biophys. Acta* **1649** (2003) 127−139.

Chapter 3

Role of Macromolecular Crowding on the Stability, Folding and Internal Dynamics of Native Cytochrome *c* and Myoglobin

3.1 Introduction

The cellular environments are very much crowded with different kinds of biomolecules with varying sizes, shapes and compositions. These crowding agents are proteins, nucleic acids, ribosomes, carbohydrates and other cytoplasmic granules. The total concentration of these crowding agents ranges from 80-400 mg ml^{-1} [1-4]. Such a cellular condition has been termed as macromolecular crowding [5]. Usually most of the *in vitro* experiments for the protein folding-unfolding have been performed in the dilute buffer solutions which actually do not mimic the *in vivo* milieu. While the understanding of protein folding has been increased dramatically but little of this work directly focuses on the environment of proteins as they fold in cytoplasmic milieu [6]. In fact, misfolding of protein linked to many diseases reveals the importance of investigating the crowded environmental effects [7-10].

Both experimental and theoretical studies suggest that the protein folding dynamics are significantly influenced by crowded conditions similar to those which are likely to exist *in vivo* [11-15]. Folding results in compaction of the polypeptide chain, so the presence of crowders near a protein could alter its folding energy landscape through the excluded volume effect [15]. While the effects of crowding agents on the structural and thermodynamic properties of native and pH-denatured proteins are extensively studied [16-24], the effect of crowding agents on internal dynamics of heme proteins remains unexplored. This chapter investigates the effect of macromolecular crowding (size, shape, concentration and viscosity of crowding agent) on folding and internal dynamics of natively folded carbonmonoxycytochrome *c* (NCO-state) and myoglobin-CO complex (MbCO). Cyt *c* is a heme protein that exists in inter-convertible oxidized (Ferricyt *c*) and reduced (Ferrocyt *c*) forms. Cyt *c* is released into the cytosol and triggers programmed cell death through apoptosis [25]. Cyt *c* is one of the essential elements of the electron-transport chain. It accepts electrons from Complex III and diffuses to Complex IV (cytochrome oxidase), where it donates the electrons to O_2, converting O_2 to H_2O. Cyt *c* is a

single domain fast folder protein, widely used as a model protein for folding and dynamics studies [26-32]. Mb, an extremely compact heme protein (MW ~17.8 kD, 153 amino acids), found primarily in cardiac and red skeletal muscles, functions in the storage of oxygen and facilitates the transport of oxygen to the mitochondria for oxidative phosphorylation [33]. Mb physiologically exhibits in three pertinent forms viz; deoxymyoglobin, oxymyoglobin, and metmyoglobin (Ferrimyoglobin). These three forms of Mb are very similar except at the sixth coordination position [34-35].

The synthetic crowding agents are inert, space occupying, noncharged polymers of defined sizes and shapes without any interaction with other biomolecules [36-37]. Ficoll is a sucrose-based polymer acquiring sphere shape in solution. Dextran is a glucose-based polymer existing random array of rods shape or anisotropic geometry in solution [24]. Both Ficoll and dextran are available in various sizes.

The effect of macromolecular crowding on internal dynamics of Cyt *c* and Mb was studied by measuring the kinetic and thermodynamic parameters for CO dissociation from NCO-state and CO replacement of MbCO by hexacyanoferrate ion under variable concentrations of synthetic crowding agents (dextran 40, dextran 70 and ficoll 70) at pH 7.0. The NCO state used here resembles the molten globule (MG)-like state which has native-like secondary structure but disordered or dynamic tertiary structure [36]. The CO dissociation process (NCO → N+CO) is essentially a Fe^{2+}-CO+M80 → Fe^{2+}-M80+CO displacement reaction [38]. The M80-contaning Ω-loop of Cyt *c* that includes residues 70 to 85 (Fig.1a, Chapter 1) [39] has been identified as a partially unfolded subglobal part of the protein [38-39] which provide the reaction site for this process. The collective motion of the Ω-loop is expected to be the main determinant of the CO dissociation process. This is presumably because the nearby residues of M80 have higher thermal factors [40-42], and the local mobility of the heme ring is suppressed by the intrinsic size and the rigidity of the ring system [43]. Protein stability characterizations are very much important for a number of applications such as protein-based pharmaceutical formulation to protein misfolding diseases. This chapter also investigates the effect of crowding agents (dextran 70, dextran 40 and ficoll 70) on thermal unfolding of native Cyt *c* and Mb.

3.2 Results and discussion

3.2.1 Thermal dissociation of CO from natively folded carbonmonoxycytochrome c (NCO) and CO replacement from carbonmonoxymyoglobin (MbCO) by hexacyanoferrate ion

Electronic absorption spectrum of Ferrocyt *c* in visible region provides three main characteristic peaks at ~416 (Soret band), 550 (α-band), and 520 (β-band) nm [38]. These values correspond to native HIS18/MET80 axial coordination of the heme [38]. CO binding to Ferrocyt *c* broadens the α-band and β-band with a significant decrease in the extinction coefficient of α-band at 25 ºC, pH 7.0 [38, 43-48]. The intensity of the α-band increases by the process of CO-dissociation from NCO, which is typically a displacement reaction Fe^{2+}–CO→Fe^{2+}–M80 [38, 44-45] (Fig. 1a, b). Fig. 1b represents the kinetics of the NCO → N+CO dissociation in the absence of any additive. The increase in absorbance at the heme π→π* α-band (550 nm) in a single exponential is due to slow dissociation of CO (τ=26.4 min; Fig. 1b).

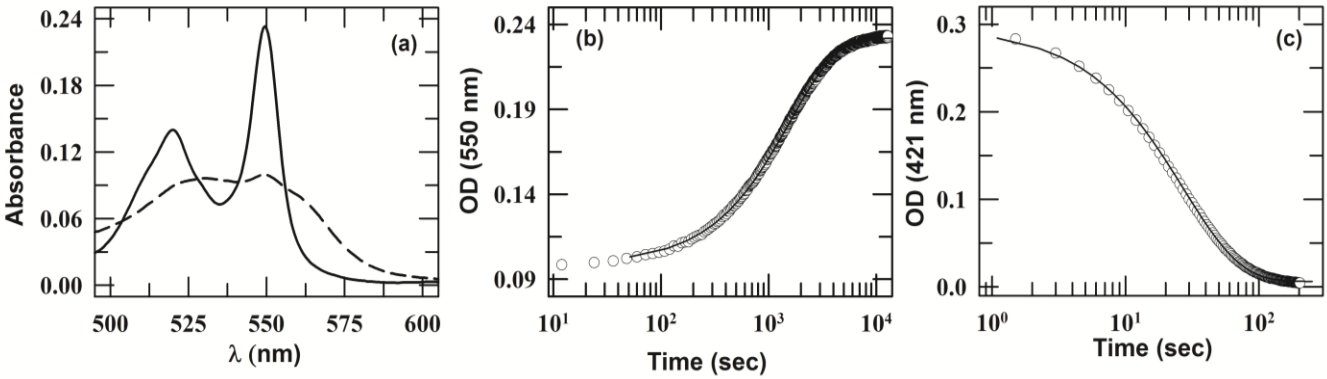

Fig.1. Steady-state visible absorption spectra of NCO (dashed line) and N (solid line) states (a). The spectra were recorded in 50mM phosphate buffer at 25°C, pH 7. (b) The slow single-phase dissociation of CO from NCO, NCO → N+CO (τ =26 min., 25°C). The NCO → N+CO reaction was probed at 550 nm. (c) The single–phase replacement of CO from the myoglobin–CO (MbCO) complex by hexacyanoferrate (III) (τ=0.45 min., 22ºC). The MbCO + CN→ MbCN + CO reaction was probed at 421 nm.

The CO replacement reaction of MbCO by hexacyanoferrate ions was performed as described earlier [49]. The representative CO-replacement kinetic profile of MbCO is shown in Fig. 1c at pH 7, 22 °C (k_{off} = 0.037 s^{-1}) in the absence of additives.

3.2.2 Crowding agents dependence of log k_{diss}, log k_{off} and activation parameters (activation enthalpy ($\Delta H_{diss/off}^{\ddagger}$), activation entropy ($\Delta S_{diss/off}^{\ddagger}$) and activation free energy ($\Delta G_{diss/off}^{\ddagger}$))

Fig. 2a and Fig. 2b show the variation of log k_{diss} and log k_{off} with varying concentrations of crowding agents (dextran 40, dextran 70 and ficoll 70) for NCO and MbCO, respectively. As [Crowding agents] (dextran 40, dextran 70 and ficoll 70) is increased from 0 to 300 mg ml^{-1}, the values of log k_{diss} (for NCO) and log k_{off} (for MbCO) decrease monoexponentially, suggesting that crowding agents restrict the internal dynamics of Cyt *c* and Mb at pH 7.0. Table 1 summarized the values of k_{diss} and k_{off} estimated at various concentrations of dextran 40, dextran 70 and ficoll 70, pH 7,25 °C (for NCO) 22 °C (for MbCO).

Table 1 The effect of crowding agent on k_{diss} of NCO and k_{off} of MbCO at pH 7.

Crowding agent	Conc.(mg ml^{-1})	k_{diss} (sec^{-1})	Std. error (k_{diss})	k_{off} (sec^{-1})	Std. error (k_{off})
Control	0.0	7.8×10^{-4}	1.8×10^{-5}	3.7×10^{-2}	1.3×10^{-4}
Dextran 40	100	6.2×10^{-4}	1.6×10^{-6}	2.5×10^{-2}	2.5×10^{-5}
	200	5.9×10^{-4}	6.7×10^{-6}	2.2×10^{-2}	6.2×10^{-5}
	300	5.7×10^{-4}	1.4×10^{-6}	2.1×10^{-2}	5.0×10^{-5}
Dextran 70	100	5.8×10^{-4}	3.3×10^{-6}	2.4×10^{-2}	1.4×10^{-4}
	200	5.3×10^{-4}	6.1×10^{-6}	1.9×10^{-2}	1.3×10^{-4}
	300	5.2×10^{-4}	8.0×10^{-6}	1.7×10^{-2}	7.8×10^{-5}
Ficoll 70	100	6.3×10^{-4}	1.0×10^{-6}	2.7×10^{-2}	2.3×10^{-5}
	200	6.0×10^{-4}	6.9×10^{-6}	2.3×10^{-2}	5.5×10^{-5}
	300	5.9×10^{-4}	1.2×10^{-6}	2.2×10^{-2}	4.6×10^{-5}

Since, under solution conditions, the dextran is regarded as a rod-shaped crowding agent while ficoll is considered as a spherical crowding agent [24]. At particular concentration of crowding agent, the k_{diss}/k_{off} values for dextran 70 and ficoll 70 are not greatly seen different in Table 1 but this slight difference is clearly in seen in Figs. 2a and 2b, which suggests that the shape of crowding agent may controls the the CO dissociation process of NCO and MbCO.

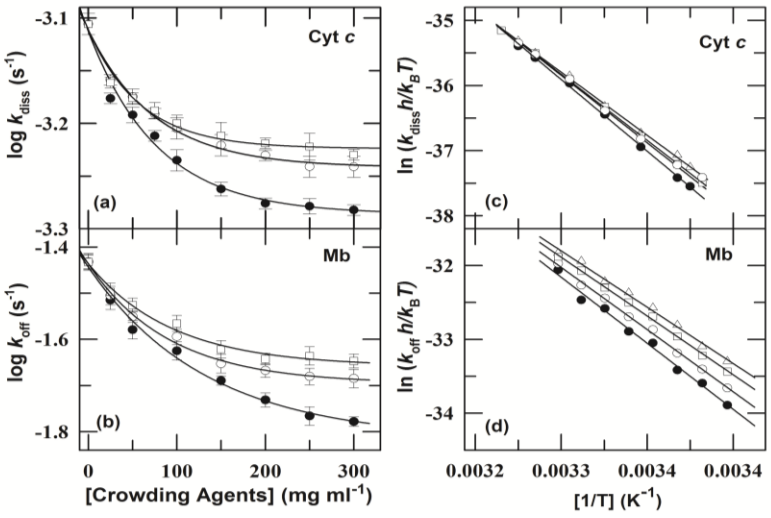

Fig.2. Panels (a) and (b) show the crowding effects of crowding agents (dextran 40 (○), dextran 70 (●) and ficoll 70 (□)) on the rate of the CO-dissociation reaction from NCO and CO-replacement reaction, from MbCO, respectively, at pH 7.0. The line through data has been drawn to guide the eye only. Panels (c) and (d) present the Eyring plots for the CO-dissociation reaction and CO-replacement reaction, respectively, pH 7.0, with no additives (Δ), and in the presence of 200 mg ml^{-1} crowding agents(dextran 40 (○), dextran 70 (●) and ficoll 70 (□)).The solid lines in panel (c) and (d) are fitted according to Eyring equation [32, 50].

The k_{diss} is also found to decrease more for dextran 70 than that for dextran 40. Dextran 70 has larger size than that of dextran 40 [24], so the greater decrease of k_{diss} for dextran 70 suggests that the size of crowding agent also plays a vital role in controlling the CO dissociation process. At a given particular concentration, dextran 70 is more viscous than dextran 40 [51,52]. The greater decrease of k_{diss} for dextran 70 then dextran 40 suggests that the viscosity of crowding agent also plays an important role in controlling the CO dissociation from NCO.

To further investigate the effect of crowding agents on the internal dynamics of these proteins, the crowding agents dependence of the activation enthalpy ($\Delta H_{diss/off}^{\ddagger}$), activation entropy ($\Delta S_{diss/off}^{\ddagger}$) and activation free energy ($\Delta G_{diss/off}^{\ddagger}$) for the CO-dissociation and CO-replacement reactions of NCO and MbCO, respectively were determined at pH 7.0. The logic is that if the internal dynamics of these proteins are restricted at some concentration of crowding agents, then the activation enthalpies for these reactions will be relatively higher.

Fig. 2c and Fig. 2d show the Eyring plots for the CO-dissociation and CO-replacement reactions of NCO and MbCO, respectively, in the absence and presence of 200 mg ml^{-1} of dextran 40, dextran 70 and ficoll 70 at pH 7.0. To estimate the crowding effect on the activation enthalpies and activation entropies for the CO dissociation and CO replacement reactions of NCO and MbCO, the Eyring plots in Fig 2c and Fig. 2d were analyzed by using the Eyring equation (Equation (2) chapter 2) [32, 50],

$$\ln(k_{diss/off} h/k_B T) = (\Delta S_{diss/off}^{\ddagger}/R) - (\Delta H_{diss/off}^{\ddagger}/RT) \qquad (1)$$

The estimated values of $\Delta H_{diss/off}^{\ddagger}$ and $\Delta S_{diss/off}^{\ddagger}$ are summarized in Table 2. By using the $\Delta H_{diss/off}^{\ddagger}$ and $\Delta S_{diss/off}^{\ddagger}$ values and Gibbs free energy equation ($\Delta G_{diss/off}^{\ddagger} = \Delta H_{diss/off}^{\ddagger} - T\Delta S_{diss/off}^{\ddagger}$), the corresponding $\Delta G_{diss/off}^{\ddagger}$ and $-T\Delta S_{diss/off}^{\ddagger}$, values were also estimated at 25°C for NCO and 22°C for MbCO (Table 2). The data in Table 2 provide some important information, (i) the increase in $\Delta H_{diss/off}^{\ddagger}$ due to crowding agent is accompanied by a decrease in the entropy change $-T\Delta S_{diss/off}^{\ddagger}$, (ii) the enthalpic effect is more dominated than the entropic effect, (iii) the extent of increase in $\Delta H_{diss/off}^{\ddagger}$ and decrease in $-T\Delta S_{diss/off}^{\ddagger}$, are higher for the larger sized crowder (dextran 70) than that for smaller sized crowder (dextran 40), (iv) relative to the spherical shaped crowding agent

(ficoll 70), the extent of increase in $\Delta H_{diss/off}^{\ddagger}$ and decrease in $-T\Delta S_{diss/off}^{\ddagger}$, are higher for the rod shaped crowding agent (dextran 70).

Table 2 The effect of crowding agent on activation parameters for CO-dissociation of NCO and CO-replacement of MbCO at pH 7.*

Crowding agent	Concentration (mg ml^{-1})	$\Delta G_{diss}^{a\ddagger}$ (kcal mol^{-1})	$\Delta H_{diss}^{\ddagger}$ (kcal mol^{-1})	$\Delta S_{diss}^{\ddagger}$ (cal mol^{-1} K^{-1})	$-T\Delta S_{diss}^{a\ddagger}$ (kcal mol^{-1} K^{-1})
Control	0.0	21.8 (0.06)	23.7 (0.3)	6.4 (0.8)	−1.9 (0.2)
Dextran 40	200	21.9 (0.04)	25.9 (0.4)	13.3 (1.2)	−4.0 (0.4)
Dextran 70	200	22.0 (0.02)	27.5 (0.4)	18.4 (1.4)	−5.5 (0.4)
Ficoll 70	200	21.9 (0.02)	25.3 (0.3)	11.5 (1.1)	−3.4 (0.3)
Crowding agent	Concentration (mg ml^{-1})	$\Delta G_{off}^{b\ddagger}$ (kcal mol^{-1})	$\Delta H_{off}^{\ddagger}$ (kcal mol^{-1})	$\Delta S_{off}^{\ddagger}$ (cal mol^{-1} K^{-1})	$-T\Delta S_{off}^{b\ddagger}$ (kcal mol^{-1} K^{-1})
Control	0.0	19.4 (0.06)	19.1 (0.6)	−1.04 (1.7)	0.3 (0.2)
Dextran 40	200	19.6 (0.04)	21.1 (0.4)	5.0 (1.5)	−1.5 (0.4)
Dextran 70	200	19.7 (0.09)	22.4 (0.9)	9.0 (2.8)	−2.7 (0.8)
Ficoll 70	200	19.5 (0.03)	19.9 (0.3)	1.5 (1.1)	−0.4 (0.2)

Activation free energy ($\Delta G_{diss/off}^{\ddagger}$) and entropy changes ($-T\Delta S_{diss/off}^{\ddagger}$) are at 25ºC [a] and 22ºC [b].
*The uncertainties (std. error) in $\Delta G_{diss/off}^{\ddagger}$, $\Delta H_{diss/off}^{\ddagger}$, $\Delta S_{diss/off}^{\ddagger}$ and $-T\Delta S_{diss/off}^{\ddagger}$ are indicated in parenthesis.

The increase in $\Delta H_{diss/off}^{\ddagger}$ by crowding agents suggests that the some crowding agents form attractive interactions with NCO-state and thus block the CO dissociation from NCO-state. Some previous reports revealed that the crowding agent forms the attractive interaction with Cyt *c* and ubiquitin [53-54]. Furthermore, the entropy-enthalpy plots could be also used to describe the entropic and enthalpic contributions of crowders on stability and folding of proteins [55]. In entropy-enthalpy plots, sector 1 and sector 2 correspond to stabilizing cosolutes while sector 3 and sector 4 correspond to destabilizing cosolutes.

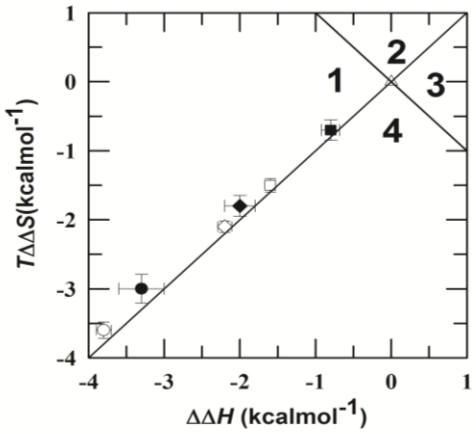

Fig.3. The $T\Delta\Delta S$ and $\Delta\Delta H$ plot for different crowders. Data points correspond to in the absence (Δ) and presence of 200 mg ml^{-1} of dextran 40(for NCO (◊), for MbCO (♦)) dextran 70(for NCO (○), for MbCO (●)) and ficoll 70(for NCO (□), for MbCO (■)) at pH 7.0.

Furthermore, sector 1 and sector 3 represent the enthalpically dominated effect while sector 2 and sector 4 represent entropically dominated effect [55]. Fig. 3 presents the $T\Delta\Delta S$ *vs* $\Delta\Delta H$ plots for NCO and MbCO in the presence of dextran 40, dextran 70 and ficoll 70 at pH 7.0.

Clearly, the data points for crowders lie in sector 1 (Fig. 3), which is in general agreement with the models that describe enthalpically dominated stabilization [55-56].

3.2.3 Effect of monomers of crowding agent (sucrose and glucose) and other viscogen (glycerol) on k_{diss}

The stability and dynamics of a protein in solution are intimately coupled to the dynamics of the solvent. A general approach for investigating the importance of protein dynamics in a chemical reaction is to determine the role of solvent viscosity on reaction rate. At a given particular concentration, dextran 70 has always higher viscosity than dextran 40 [52], so the greater decrease of log k_{diss}/k_{off} for dextran 70 than that of the dextran 40 (Table 2 and Fig. 2a, 2b) is likely due to its higher viscosity. To investigate how solvent viscosity affect the structural-fluctuations of the M80 containing Ω-loop of Cyt *c*, the rate of thermally-driven CO dissociation from NCO-state was measured at different compositions of monomers of crowding agents (sucrose and glucose are the monomers of ficoll and dextran, respectively) and other viscogens (like glycerol) at 25 °C. The CO dissociation rate of NCO is found to decrease with increasing composition of the monomers of crowding agents (sucrose and glucose are the monomers of ficoll and dextran, respectively) and other viscogen (like glycerol) (Fig. 4a).

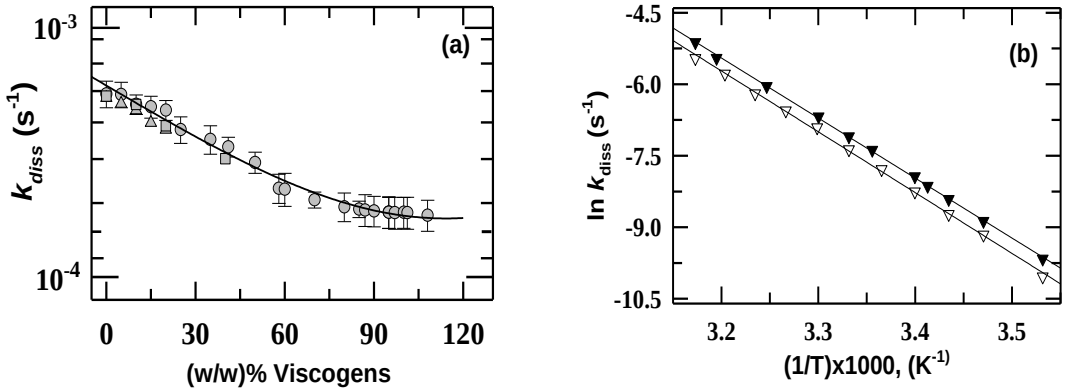

Fig.4. The [Viscogens] dependence of rate coefficients, k_{diss} for CO-dissociation of NCO (glycerol (○), sucrose (Δ), and glucose (□)) at 25°C, pH ~7. The error bars represent the standard deviations from the k_{diss} values. (b) Arrhenius plots in the absence (▼) and presence (∇, 90 % (w/w)) of glycerol (chapter 2 equation (3)). The activation energies (E_a) derived from the linear least-squares fitting of the data are ~24.5 (± 0.5) and ~24.9 (± 0.3) kcal mol^{-1} for 0.0 and 90 % of glycerol, respectively.

The solvent composition modulation of k_{diss} (Fig. 4a) reveals the way the collective motion of the loop or of a part of it responds to solvent content in the reaction medium. Since atomic fluctuations or high-frequency local motions involve only small spatial displacements, the thermal

motion viewed here must be of collective character in which groups of atoms in a part or in the entire Ω-loop move in a correlated manner or as a unit. The observation that it responds to increments of solvent composition implies that it is a local motion, and hence is a low-frequency (τ, millisecond or longer) large-amplitude mode (several Å) [57].

Fig. 5a shows the plot of k_{diss} as a function of solvent viscosity of three different viscogens (glycerol, sucrose, and glucose). The k_{diss} values below viscosity 1.01 cP (Fig. 5a, b) were eventually measured at different temperatures (*i.e.*, 30, 35, and 40°C) in the absence of viscogen and finally corrected to 25°C by Arrhenius equation (Equation (3), chapter 2) using activation energy of ~24.5 kcal/mol (Fig. 4b). Each of the three different viscogens used here had a similar slowing effect on the CO dissociation kinetics, causing the equal decrease in k_{diss} with increasing solvent viscosity (Fig. 5 a, b). The rate-viscosity data in Fig. 5a illustrates that spatial displacement of thermal fluctuations of a subglobal structural unit is reduced at low viscosity (≤ 8 cP), but saturates at high viscosity. The finding that the rate of thermally-driven CO dissociation from the NCO state decreases up to ~8 cP imply that the motional response of the M80 containing Ω-loop at lower viscosities (≤ 8 cP) is different from what is seen at higher viscosities (> 8 cP) (Fig. 5a).

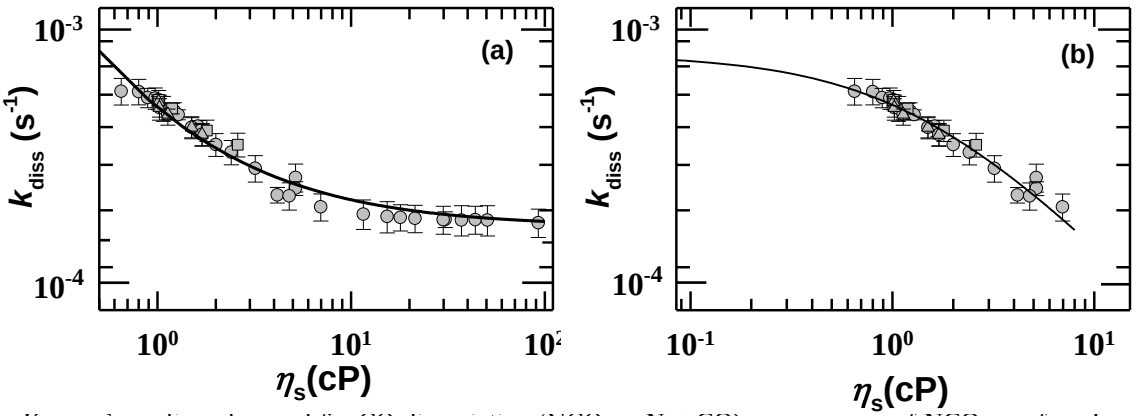

Fig.5. Non-Kramer's scaling observed for CO dissociation (NCO → N + CO) rate constant of NCO as a function of viscogen (glycerol (○), sucrose (Δ), and glucose (□)) viscosity in 15 mM phosphate buffer, 0.3 M GdnHCl, pH 7, 25°C. The k_{diss} values below viscosity 1.01 cP (Fig. 5a, b) were eventually measured at different temperatures (*i.e.*, 30, 35, and 40°C) in the absence of viscogen and by Arrhenius equation using activation energy of ~24.5 kcal/mol these were corrected to 25°C (Fig. 4b). The k_{diss} values below viscosity 1.01 cP were the temperature corrected values at 25°C. The viscosities of water below 1.01 cP (*i.e.*, η_s = 0.65, 0.80, and 0.89 cP are the viscosity of water at temperature ~40, 30, and 25 °C, respectively) were taken from the literature [58]. Fit of the data according to equation (3) in Fig. 5a yields, n ~0. 75(±0.02), A ~6.5×10^{15} s^{-1}, and ΔG = 26.5 kcal mol^{-1}. The fit to the experimentally observed rates using equation (5) is shown in Fig. 5b with a value of σ = 1.35 (±0.88) cP.

3.2.4. Phenomenological description of viscosity dependence of the NCO → N + CO conversion rate

Kramer's theory for unimolecular reactions asserts that the rate k for a barrier-crossing process subject to strong damping friction will vary as [59-60]:

$$k = \left(\frac{A'}{\gamma}\right) exp\left(\frac{-\Delta G}{RT}\right) \qquad (2)$$

where A' is a constant (that depends on m, ω_A, ω_B etc, here, ω_A and ω_B denote the frequencies of motion in the starting well and on top of the barrier, respectively, and m is the effective molecular mass of the particle that is crossing the barrier) and ΔG is the barrier height. If the friction in the NCO → N + CO conversion arises from η_s (the dynamic viscosity of the solvent) then the CO-dissociation rate should scale as $k_{diss} \alpha \gamma^{-1} \alpha \eta_s^{-1}$. Fig. 5a shows the plot of k_{diss} as a function of solvent viscosity, η_s. The value of k_{diss} varies inversely with viscosity when the solvent viscosity is low (≤ 8 cP), but saturates at higher viscosity, indicating a deviation from the $k \propto \eta_s^{-1}$ relation. In general, for protein reactions, the functional dependence of the reaction rate constant, k for the rate limiting step on solvent viscosity, η_s has the form [61-62],

$$k = \left(\frac{A'}{\eta_s^n}\right) exp\left(\frac{-\Delta G}{RT}\right) \qquad (3)$$

Several groups have tested solvent viscosity effects on protein reactions [61-67], and in most of the cases the observed rate constant has been found to be inversely proportional to the fractional power of the viscosity, $k \alpha \eta_s^{-n}$ ($0 < n < 1$). A number of efforts have been devoted to explain the fractional viscosity dependence in protein reactions, but so far there is no general agreement about the origin of the fractional n value [65]. In the consequence of protein dynamics, reactions with n close to 1 are tightly coupled to surface motion while reactions with n close to zero are well shielded by rigid protein structure [68]. It has been suggested that fractional exponent, n is the degree with which solvent viscosity is coupled with (frequency dependent friction) [68-70] or penetrates into (position dependent friction) [61-72] the protein interior. Any of these variants results in the modification of the Stokes law. Yedgar et al [65] revealed that the fractional index of a power n is a function of cosolvent's molecular weight. If one varies the solvent viscosity through large cosolvents molecules with high molecular weight that do not penetrate into protein

then one can obtain, $n \rightarrow 0$, *i.e.,* the reaction rate constant does not depend on solvent viscosity. With the decrease of cosolvent's molecular weight, the value of *n* increases [65].

To describe the deviation at high viscosities for protein reactions, Beece et al [73] added a viscosity-independent term, *A* to equation (4),

$$k_{diss} = \left(A + \frac{A'}{\eta_s^n} \right) exp\left(\frac{-\Delta G}{RT} \right) \qquad (4)$$

Fits of the rate-viscosity data according to equation (3) finally yields, *n* ~0.75 (±0.02) and *A* ~6.5×10^{15} s^{-1}. Equation (4) predicts the decoupling of structural motion from the solvent at high viscosity [73]. In an early work, to explain why the molecular oxygen rebinding rates in myoglobin decreases at low viscosity but saturates at high viscosity, Doster (1983) derived a dynamic friction model assuming that the fluctuation spectrum at the reaction site involves two components: solvent independent diffusion of local structural defects in the protein matrix and global fluctuations coupled to the solvent [68]. In general, global fluctuations involve a large part of the protein and are therefore coupled to the solvent. Here in our case, the global fluctuations of a subglobal structural unit (the M80 containing Ω-loop) of the protein coupled to the solvent at low solvent viscosity and thus the rate coefficient for CO-dissociation from the NCO decreased significantly (Fig.5).

The diffusion of local structural defects with a diffusion coefficient results in the exchange of thermal energy between internal degrees of freedom in a protein, and is independent of the solvent viscosity [68]. When the protein is suspended in a solid surrounding like poly vinyl alcohol, frozen solvents or dry films etc. the diffusion of local structural defects can explain the reason of finite reaction rates at infinite external viscosities [73-74]. For protein reactions, the propagation of the defects (*i.e.,* a hole, or a volume, or a chain fluctuation) to the reaction site speeds up the necessary motions of the relevant structural element. The physical nature of defects may differ from one system to another, and we suggest the operative defect for the NCO→N+CO dissociation step in Cyt *c* is the void created by the departing CO ligand by thermal fluctuations. Because of the availability of an increased volume in the proximity due to loss of CO, the movement of the void to the site of the M80 side-chain can allow a rapid reconfiguration of the latter. Since at high viscosity, the structural motions of reactive mode are faster than the global fluctuation [68, 75] therefore the rate coefficient for CO-dissociation varies only slightly (Fig.

5a). The defect diffusion dominates at high solvent viscosity, therefore, to facilitate structural element motions, the distance migrated by a defect should depend on the diffusion coefficient. The actual value of diffusion coefficient in a protein interior is independent of the solvent viscosity and depends only on the internal friction. The misorganized side-chain of M80 can add on to the internal frictional effect for the slow folding of NCO (NCO→N+CO) by producing additional drag forces. Thus, at high solvent viscosity, the thermally-induced slow CO-dissociation process or slow folding of a compact native-like intermediate will depend on the size, the configurational nature, and the collapsed state of the protein.

3.2.5 Internal friction and its role in protein folding and dynamics

For simple chemical reactions, solvent friction generally need to be taken into account, however in proteins, where the amino acid residues are only partially exposed to solvent, other dissipative, "internal friction" mechanisms are possible and result in a slowdown of the conformational dynamics. Internal friction, which reflects the "roughness" of the energy landscape, plays a crucial role for proteins through modulating the dynamics of their folding and other conformational changes. However, the experimental quantification of internal friction and its role to protein folding and dynamics has remained elusive.

The microscopic barrier hopping due to long-range inter-residue interactions [76] and backbone rotations [72, 77] generally results into internal friction in polymers and proteins. Further, the geometric frustrations of varying degrees in the late folding structures can also contribute to the internal friction. Portman et al. [78] presented both theory and simulations regarding the effect of internal friction in barrier crossing by a folding protein. They observed that the higher frequency modes of the protein mainly depend on large-amplitude local reconfigurations of the backbone, and are controlled by internal friction from dihedral isomerizations, whereas lower frequency modes involve large scale motions that are more influenced by solvent friction. They also found that for a partially-ordered molecule or a compact state, barrier crossing on a multidimensional free energy surface may depend sensitively on the higher frequency modes. In this case, even a small contribution of internal friction may have large number of consequences for the dynamics.

Eaton and coworkers [79-80] proposed an empirical equation to describe the viscosity dependence of the conformational relaxation rate of myoglobin, by taking into consideration both the solvent friction (η_s) and internal friction (σ),

$$k_{diss} = \left(\frac{A'}{\eta_s + \sigma} \right) exp\left(\frac{-\Delta G}{RT} \right) \qquad (5)$$

Ansari et al. [79] studied nanosecond conformational dynamics in folded myoglobin and suggested a positive value of σ (σ ~ 4.1(± 1.3) cP) for native myoglobin. Pabit et al. [81] studied laser induced microsecond folding kinetics of NCO-state (*i.e.*, NCO → N + CO) and suggested a positive value for σ (σ ~ 2.1(± 0.3) cP). For the NCO → N + CO folding, the data clearly extrapolate toward an x-intercept (–σ) that is significantly different from zero, *i.e.*, σ ~ 2.1(± 0.3) cP [81]. Jacob et al. [82] studied millisecond folding kinetics of CspB and also suggested a positive value for σ. However, for several proteins that even fold through compact transition states, the protein folding data from equation (3) has showed no clear evidence for σ > 0. Plaxco et al. [83] studied millisecond folding kinetics of protein L and calculated a small negative value for σ (σ = –0.1(± 0.2) cP) from equation (3), a result that suggests no internal friction in folding [83]. Cellmer et al. [84] studied folding/unfolding kinetics of an ultra-fast folding villin headpiece subdomain and also observed a negative value for σ (*i.e.*, σ < 0). In this very special case, the σ < 0 is attributed to the increase of the effective viscosity, which is probably associated with a shift of the transition state along the reaction coordinate toward the native state [71]. Pradeep et al. [85] studied millisecond unfolding kinetics of barstar [85], and suggested a negative value for σ (*i.e.*, σ < 0). One of the possible reasons for σ < 0 is that the local viscosity at the protein–solvent interface is lower than the bulk solvent viscosity [70]. In the millisecond unfolding kinetic experiments of barstar, the change in the folding barrier by viscogen is compensated by addition of denaturant; therefore, the variation of folding rates is solely defined by the viscosity. Based on this, it was also concluded that the violation of Kramer's theory with σ > 0 is mainly because of internal friction [83, 85]. This nature of internal friction is most likely related to the fact that only small parts of a polypeptide chain are participating in the rate-limiting step of folding.

For the present work, activation free energy barrier for the NCO → N + CO conversion is not greatly affected by viscogen; therefore, this study does not require any chemical denaturant to obtain isostability conditions in the presence of viscogen. For the NCO → N + CO case

considered here, for example, the misorganized side-chain of M80 can add on to the internal frictional effect producing additional drag forces. If the rate-limiting step in a folding reaction involves internal rearrangement, then the reaction rate is expected to be strongly influenced by the internal friction as compared to the solvent friction [86]. Provided that both internal and solvent frictions are frequency-dependent, an empirical formula was proposed by Wallace et al [87]:

$$k_{\text{diss}} = \left(\frac{A'}{\left(\eta_s + \sigma\right)^n} \right) exp\left(\frac{-\Delta G}{RT} \right) \qquad (6)$$

The data in Fig.5 indicate that for viscosities between 0.65 and 8.0 cP, the CO dissociation rate, k_{diss} is inversely proportional to an effective viscosity, $(\sigma + \eta_s)^n$. Fits of the data according to equation (6) finally yields ΔG = 25.9 (±0.5) kcal mol^{-1} and σ =1.35 (±0.88) cP. Thus, in low viscosity regime, the speed of CO dissociation from a native-like folded intermediate, NCO is controlled by internal friction.

3.2.6 Effect of crowding agents on the thermodynamic stability of proteins

To evaluate the macromolecular crowding effect on thermodynamic stability of native Ferrocyt *c* and Mb, the tryptophan fluorescence (excitation: 280 nm, emission: 360 nm) monitored GdnHCl-induced equilibrium unfolding transitions of proteins were measured in the absence and presence of crowding agents (dextran 40, dextran 70 and ficoll 70). Figs. 6a and 6b present the GdnHCl-induced denaturation curves of Ferrocyt *c* and Mb at pH 7 and 25 ºC in the absence and presence of 200 mg ml^{-1} of dextran 40, dextran 70 and ficoll 70. The denaturant-induced equilibrium unfolding transitions were analyzed by using standard two-state equation (Equation (7), chapter 2) [88]. The unfolding free energy (*i.e.*, the difference of free energies of unfolded and native states (ΔG_D)), denaturants midpoints (C_m) and surface area exposed by the solvent (m_g) of Ferrocyt *c* and Mb are listed in Table 3. Data in Table 3 and Fig. 6b clearly suggest that crowding agents increase the thermodynamic stability of Ferrocyt *c*. However, in case of Mb, dextran 40 and dextran 70 do not greatly change the thermodynamic stability of protein but ficoll 70 decrease the thermodynamic stability of Mb at pH 7 (Table 3 and Fig. 6b).

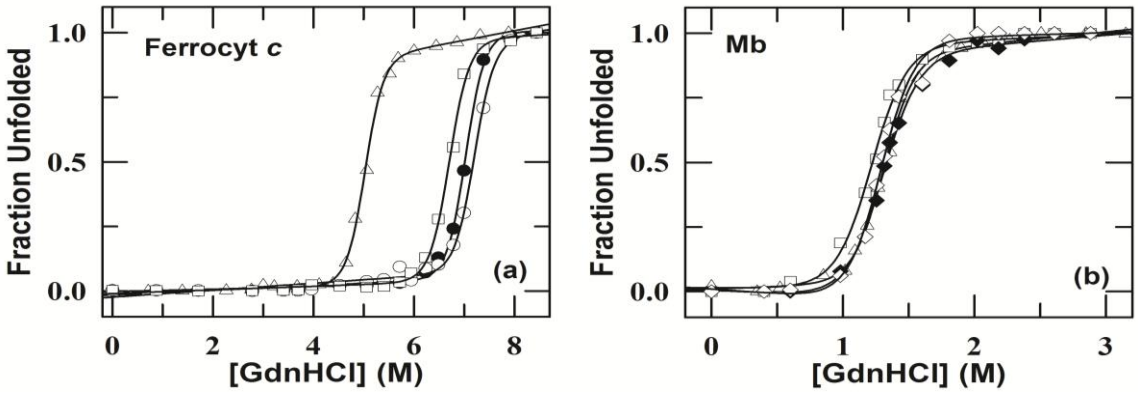

Fig.6. Panels (a) and (b) shows the GdnHCl–induced equilibrium unfolding curves of Ferrocyt *c* and Mb in the presence of 0 (Δ) and 200mg ml^{-1} of crowding agents (dextran 40 (○), dextran70 (●), and ficoll 70 (□)), respectively at 25°C, pH~ 7. The solid lines are fit to the data using two-state equilibrium equation (chapter 2 equation (7)) [88] and the results are listed in table 3.

Table 3 The effect of crowding agent on ΔG_D, m_g , and C_m value of Ferrocyt *c* and Mb at pH 7 as monitored by Trp Fluorescence (excitation at 280 and emission at 360 nm).*

	Ferrocyt *c*			Mb		
Crowding agent	C_m (M)	ΔG_D (kcal mol^{-1})	m_g (kcal $mol^{-1}M^{-1}$)	C_m (M)	ΔG_D (kcal mol^{-1})	m_g (kcal $mol^{-1}M^{-1}$)
Control	5.0	16.2	3.2	1.3	6.6	5.0
Dextran 40	7.2	23.0	3.2	1.3	6.5	5.2
Dextran 70	7.0	22.3	3.2	1.3	6.1	4.8
Ficoll 70	6.7	20.1	3.0	1.2	5.9	4.9

* The uncertainties associated with ΔG_D, m_g, and C_m are ±0.4 kcal mol^{-1}, ±0.1 kcal mol^{-1} M^{-1}, and ± 0.2 M, respectively

3.2.7 Effect of crowding agents on thermal stability of native Ferrocyt c and Mb

To determine the effect of crowding agents on thermal stability of native proteins, thermal denaturations of native Ferrocyt *c* and Mb were studied in presence of different concentrations of crowding agents (dextran 40, dextran 70 and ficoll 70) at pH 7. Figs.7a and 7b present the steady-state visible absorption spectra of Ferrocyt *c* and Mb at 25ºC (solid line), and 110ºC (dotted line), respectively. Figs. 7c and 7d present the representative heme absorption (Ferrocyt *c* at 550 nm and Mb 409 nm) monitored thermal denaturation curves as the change in excitation coefficient in the absence and presence of 100 mg ml^{-1} crowding agents (dextran 40, dextran 70 and ficoll 70) for native Ferrocyt *c* and Mb, respectively at pH 7.0. Figs.7e and 7f present the extent of protein denaturation as fraction of unfolded Ferrocyt *c* (550 nm) and Mb (409 nm), respectively. These thermal denaturation curves were analyzed for thermal denaturation midpoint (T_m), and van't Hoff enthalpy (ΔH_m) by using a nonlinear least squares method according to the Van't Hoff equation [89] (chapter 2, equation (5)). The resulting values of T_m and are provided in Table 4. It is clear

from Fig.7 and Table 4 that the crowding agents (dextran 40, dextran 70, and ficoll 70) presence in reaction medium increase the values of T_m for Ferrocyt *c* while these crowding agents decreases the values of T_m of the native Mb.

Table 4. Values of T_m and ΔH_m for thermal unfolding of Ferrocyt *c* and Mb monitored by absorbance at 550nm and 409 nm, respectively at pH 7.5 (±0.3).[a]

Crowding agents	Ferrocyt *c*		Mb	
	T_m (K)	ΔH_m (kcal mol^{-1})	T_m (K)	ΔH_m (kcal mol^{-1})
Control	372.7	122.0	355.9	119.7
Dextran 40 (100mg ml^{-1})	375.4	133.4	355.1	109.8
Dextran 70 (100mg ml^{-1})	374.6	129.6	353.0	105.0
Ficoll 70 (100mg ml^{-1})	373.5	120.9	351.0	96.0

[a] The uncertainties of T_m and ΔH_m, values reported here are ±0.5 K and ± 5.0 kcal mol^{-1}, respectively.

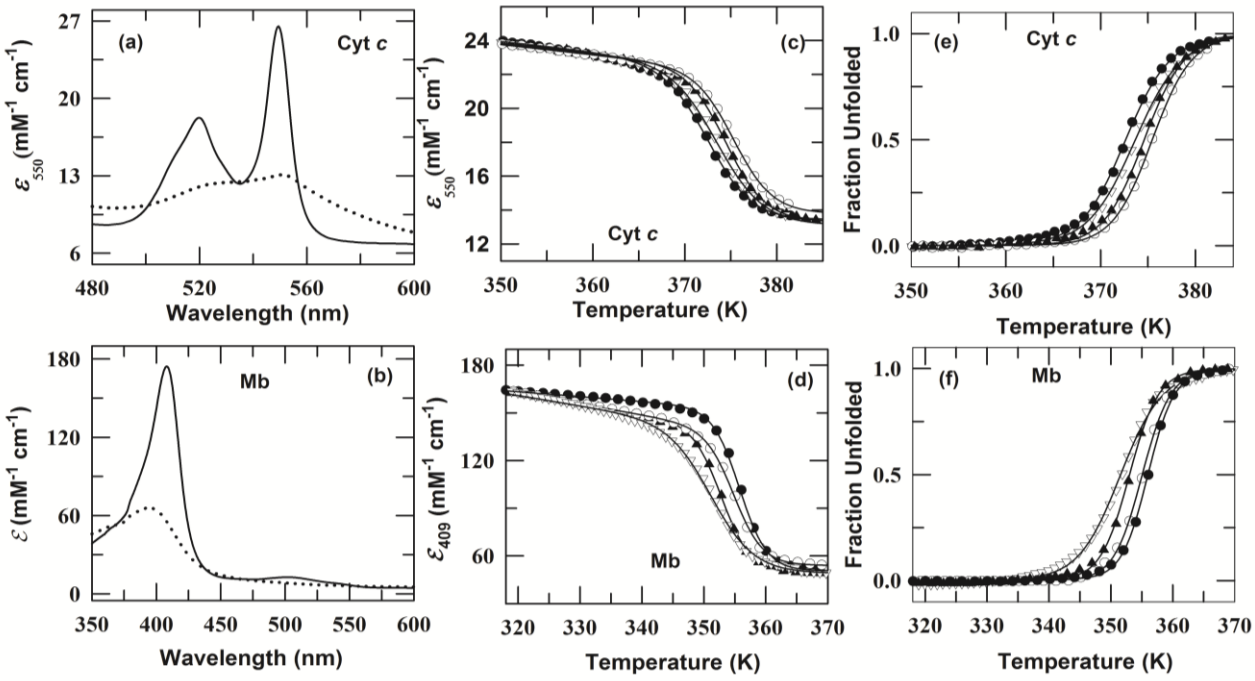

Fig.7. Panel (a) and (b) shows the steady-state visible absorption spectra of Ferrocyt *c* and Mb at 25ºC (solid line), and 110ºC (dotted line), respectively. Panel (c) and (d) thermally induced unfolding of Ferrocyt *c* monitored at 550 nm and Mb monitored at 409 nm as the change in excitation coefficient in the presence of 0 mg/ml crowding agent (●), 100mg dextran 40 (○), 100mg dextran 70 (▲) and 100mg ficoll 70 (▽), respectively. To simplify the comparison of various thermal transitions, the extent of protein denaturation is presented as a fraction of unfolded protein (550 nm) panel (e) (Ferrocyt *c*) and 409 nm panel (f) (Mb); The solid lines in panel (c), (d), (e) and (f) represents nonlinear least-squares fits to Van't Hoff equation (chapter 2, equation (5)) [89].

For native Ferrocyt *c*, the T_m value is more for dextran 40 and least for ficoll 70 (dextran 40 > dextran 70 > ficoll 70). However, in case of Mb, the T_m value is decreased more for ficoll 70 and least for dextran 40 (ficoll 70 < dextran 70 < dextran 40) at pH 7.0.

3.2.8 Reversibility and two states folding of native Ferrocyt c

In order to determine the effect of crowding agents on thermodynamic parameter of native Ferrocyt *c*, both in the absence and presence of crowding, the denaturant and thermal unfolding curves of Ferrocyt *c* were analyzed by the two state equation [88-89] (chapter 2, equations (5) and (7)). For the validity of two-state analysis, it is necessary to test the reversibility and two state behavior of Ferrocyt *c*. To verify whether the thermal or denaturant-induced unfolding of Ferrocyt *c*, occur in two state manner, the denaturant-induced unfolding transitions for Ferrocyt *c* were measured by monitoring the changes in far-UV CD at 222 nm (Fig. 8a) and 210 nm (Fig. 8b), and tryptophan fluorescence emission at 374 nm (Fig. 8c). In addition, the denaturant unfolding transitions for Ferrocyt *c* were also recorded by monitoring the changes in heme absorption at 550 nm (Fig. 8d) and 527 nm (Fig. 8e). These denaturants induced unfolding curves of Ferrocyt *c* were analyzed by two-state equation [88-89] (chapter 2, equations (7)) and the resulting ΔG_D, C_m and m_g values for Ferrocyt *c* are listed in Table 5. The denaturant unfolding transitions thus measured for Ferrocyt *c* by different optical probes (CD, fluorescence and absorbance) and common optical probes with multiple wavelengths (CD at 210 and 222 nm; absorbance at 527 and 550 nm) are within error nearly superimposable and cooperative (Fig. 8f).

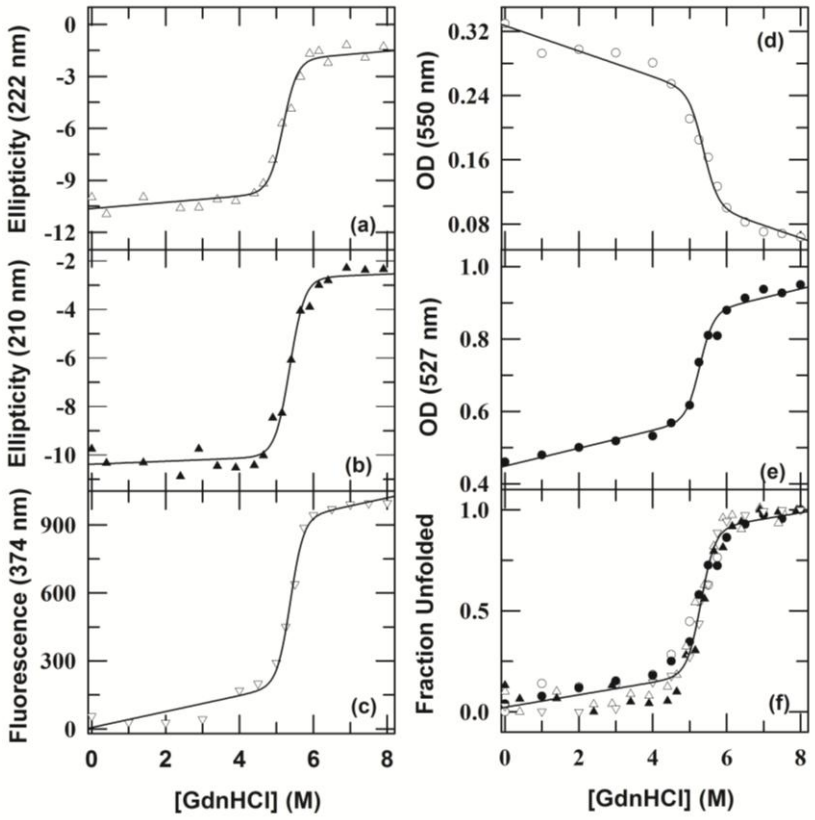

Fig.8. Panels (a), (b), (c), (d) and (e) shows the GdnHCl-induced equilibrium unfolding curves of Ferrocyt *c* monitored by far-UV CD at 222 (a) and 210 nm (b), Trp emission fluorescence at 374 nm (c) and heme absorption at 550 nm (d) and 527 nm (e). The solid lines represent the non-linear least-squares fit of the data to a two-state unfolding transition (Equation (7), chapter 2) [88]. The fit yields GdnHCl unfolding free energy, ΔG_D and surface area exposed by solvent, m_g for Ferrocyt *c*, which are provided in Table 5. Panel (f) present the plots of fraction of Ferrocyt *c* unfolded as a function

of GdnHCl probed by far-UV CD at 222 (Δ) and 210 nm (▲), Trp emission fluorescence at 374 nm (∇) and heme absorption at 550 (○) and nm 527 nm (●).The solid line represent the non-linear least-squares fit of the data to a two-state unfolding transition (Equation (7), chapter 2), which finally yields, $\Delta G_D \approx$ 16.5 kcal mol^{-1} and $m_g \approx$ 3.1 kcal mol^{-1} M^{-1}. All transitions were measured at 25°C, 0.1 M phosphate, pH 7.0.

Table 5. Values of ΔG_D, m_g, and C_m for Ferrocyt *c*, as monitored by different spectroscopic probes at pH 7.0.[a]

Wavelength (nm)	ΔG_D (kcal mol^{-1})	m_g (kcal mol^{-1} M^{-1})	C_m (M)
550	16.1	3.0	5.4
427	16.9	3.2	5.3
222	16.1	3.1	5.2
212	16.2	3.0	5.4
375	16.7	3.1	5.4
550	16.1	3.0	5.4

[a] The uncertainties associated with ΔG_D, m_g and C_m are ± 0.5 (kcal mol^{-1}), ±0.2 (kcal mol^{-1} M^{-1}) and ±0.2 (M), respectively.

To test whether temperature-induced changes in heme absorption signals are reversible, the solutions of Ferrocyt *c* were heated up gradually from 313 K to 378 K (Ferrocyt *c*) (Fig. 9 a, and b) and cooled down gradually to 313 K from or 378 K (Ferrocyt *c*) (Fig. 9a, & Fig.9b). The forward-scan and reverse-scan of panel (a) and (b) in Fig. 9 are not perfectly superimposable and same, indicating that the thermal denaturation of Ferrocyt *c* (based on absorbance at 550 and 520 nm) at pH 7.0 are not showing the high reversibility. Varhac et al. also showed that the thermal denaturation of Ferrocyt *c* at pH 7.0 does not exhibit the high reversibility [48]. It is likely that the partial interactions of Cyt *c* molecules occur at neutral pH and that may play an important role for not showing the high reversibility in thermal denaturations of Ferrocyt *c* at pH 7.0.

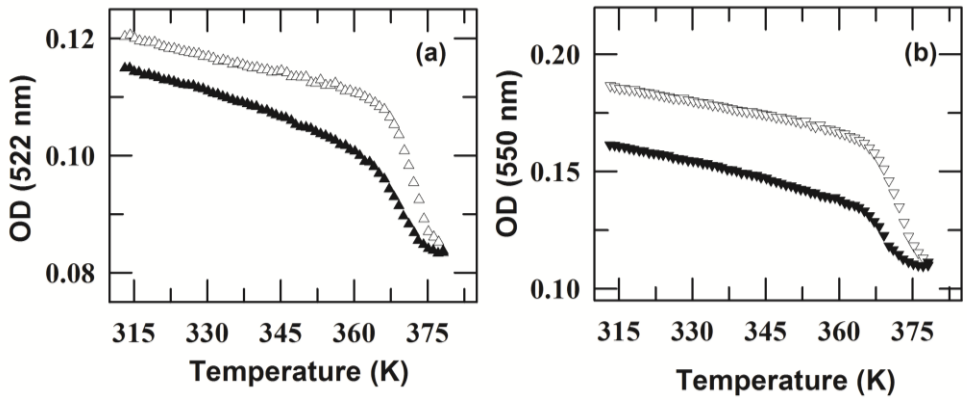

Fig.9. Panels (a), and (b) show the reversibility of thermal transitions of Ferrocyt *c* monitored by heme absorbance at 550 nm and 522 nm, respectively, heating from 313 K to 378 K (Δ or ∇) and cooling from 378 K to 313 K (▲ or▼).

The observed irreversibility in thermal denaturation of Cyt *c* may depend on pH and which can affect the thermodynamic parameters associated with the pH dependent thermal denaturation of Ferrocyt *c*. A few earlier spectroscopic and calorimetric studies have revealed that at low ionic strength, the thermal denaturation of Ferricyt *c* at low pH (2.2-3.6) and high pH (12.8-13.0) is reversible and two-state [90-92]. At low pH (2.2-3.6), a high number of positive charges may prevent the intermolecular interactions of Cyt *c* molecules [93] and that may play a key role for the reversible two-state behavior in the thermal denaturation of Ferricyt *c* at low pH (2.2-3.6) [93]. To verify whether the thermal unfolding of Ferrocyt *c* occur in two state manner, the thermal unfolding transitions for Ferrocyt *c* were recorded by monitoring the changes in far-UV CD at 222 nm (Fig. 10d) and 210 nm (Fig. 10e) and near-UV CD at 282 nm (Fig. 10f) and 290 nm (Fig. 10g). In addition, the thermal unfolding transitions for Ferrocyt *c* were also measured by monitoring the changes in heme absorption at 550 nm (Fig. 10a), 522 nm (Fig. 10b) and 416 nm (Fig. 10c). The thermal unfolding transitions thus measured for Ferrocyt *c* by different optical probes and common optical probes with multiple wavelengths, are within error nearly superimposable and cooperative (Fig. 10h). These thermal unfolding curves for Ferrocyt *c* were analyzed by Van't Hoff equation [87] (chapter 2, equations (5)) and the resulting T_m and ΔH_m values for Ferrocyt *c* are listed in Table 6.

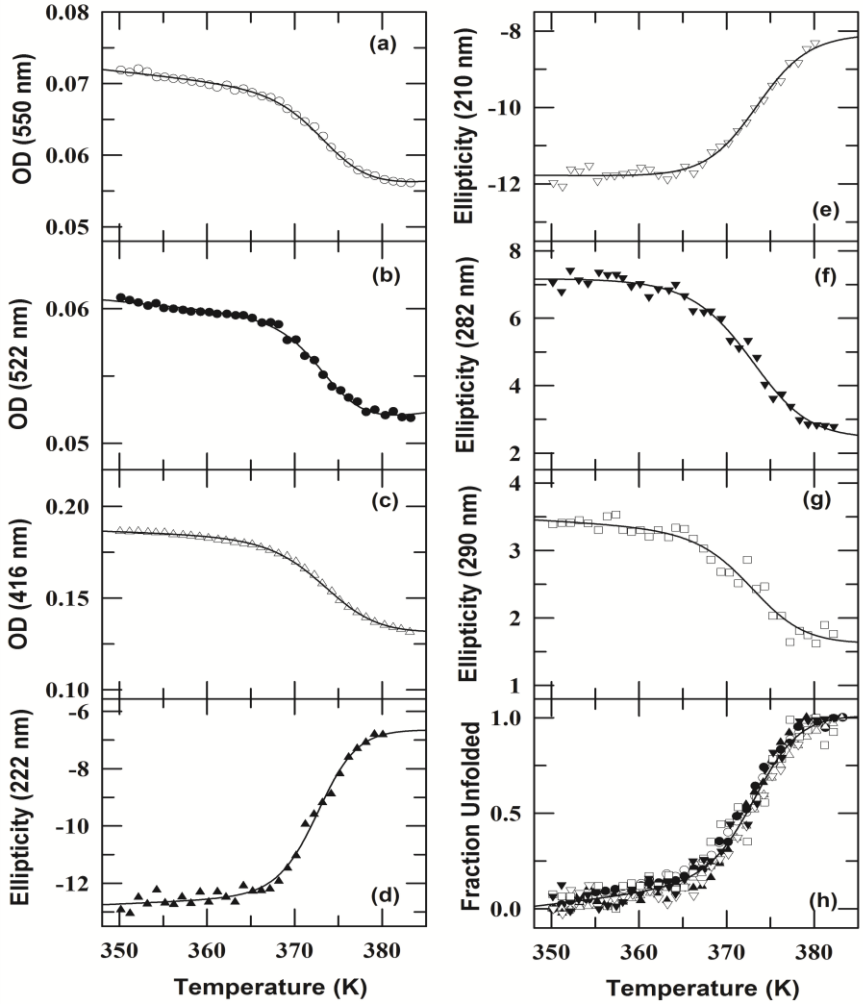

Fig.10. Panel(a),(b),(c),(d),(e),(f) and (g) shows the thermal-denaturation curves of Ferrocyt *c* monitored by heme absorption at 550 (a), 522 (b)

and 416 nm (c), far-UV CD at 222 (d) and 210 nm (e) and near-UV CD at 282 (f) and 290 nm (g). The solid lines represent the non-linear least-squares fit of the data to a Van't Hoff equation (Equation (5), chapter 2). The fit yields thermal denaturation midpoint, T_m, and enthalpy change, ΔH_m for Ferrocyt *c*, which are provided in Table 6. Panel (h) presents the plots of fraction of Ferrocyt *c* denatured as a function of temperature probed by heme absorption at 550 nm (○), 522 nm (●) and 416 nm (Δ), far-UV CD at 220 nm (▲) 210 nm (∇) and near-UV CD at 282 nm (▼) and 290 nm (□). The solid line represent the non-linear least-squares fit of the data to a Van't Hoff equation (Equation (5), chapter 2) [89] which finally yields, $T_m \approx 373.0$ K, and $\Delta H_m \approx 125$ kcal mol^{-1}. All transitions were measured in 0.1 M phosphate at pH 7.5.

Table 6. Values of T_m and ΔH_m for thermal unfolding of Ferrocyt *c* as monitored by different spectroscopic probes at pH 7.5 (±0.5).[b]

Ferrocyt *c*		
Wavelength (nm)	T_m (K)	ΔH_m (kcal mol^{-1})
282	372.4	138.0
210	373.7	132.0
222	372.7	129.5
416	372.8	134.0
522	372.4	140.1
550	373.4	130.0
290	373.0	129.0

[b] The uncertainties of T_m and ΔH_m, values reported here are ±0.5 K and ± 5.0 kcal mol^{-1}, respectively.

The finding of indistinct thermal unfolding transition curves for Ferrocyt *c* (Fig. 10h) fails the basic test for accumulation of equilibrium structural intermediate to a detectable level. A few earlier spectroscopic and calorimetric studies have revealed that at low ionic strength, the ratio between van't Hoff and calorimetric enthalpy for thermal denaturation of Ferricyt *c* under conditions of low pH (pH 2.2-3.6), neutral pH (pH ~ 7.0) and high pH (pH 12.5-13.0) is close to one [90-92, 94], indicating that the thermal denaturation of Ferricyt *c* under these conditions of pH is two state [95-98]. An earlier spectroscopic and calorimetric study has shown that at pH 7.0, the ratio between Van't Hoff and calorimetric enthalpy for thermal denaturation of Ferrocyt *c* is close to one [48], indicating that the thermal denaturation of Ferrocyt *c* at neutral pH is also two state. The current spectroscopic and calorimetric study has also revealed that at pH 7.0, the ratio between Van't Hoff and calorimetric enthalpy for thermal denaturation of Ferricyt *c* and Ferrocyt *c* is close to one (Fig. 11 and Table 7), indicating that the thermal denaturation of Ferricyt *c* and Ferrocyt *c* at neutral pH is two state.

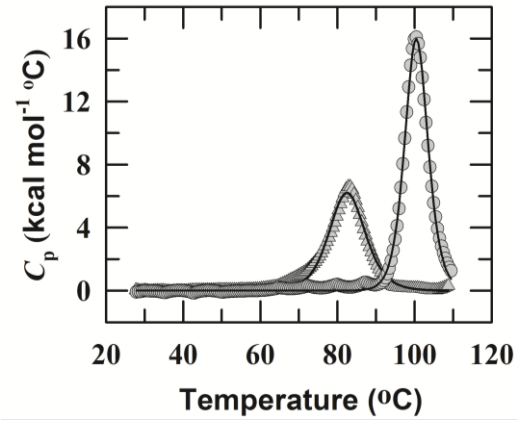

Fig.11. DSC scans for Ferrocyt *c* (○) and Ferricyt *c* (Δ) in 50 mM sodium phosphate, pH 7.0. The dashed lines resulted from fitting the data to the non two-state model (Table 7). In DSC experiments, protein

concentration was ~115 μM, and the scan rate was 60ºC h^{-1}. The DSC scans were carried out on MicroCal VP-Capillary DSC instrument.

According to few previous studies [48, 99-104], the use of the Van't Hoff formalism which is implied in (Eq. (5) from chapter 2) is valid for the analysis of the temperature-dependent spectroscopic changes exhibited by proteins even in the cases where the thermal denaturation is only partially reversible. The thermal unfolding curves for Ferricyt *c* and Ferrocyt *c* measured at different pH were analyzed for thermal denaturation midpoint (T_m) and enthalpy change, (ΔH_m) by two-state model N$\rightleftharpoons$U using Van't Hoff equation [89] (chapter 2, equation (5)).

Table 7. Thermodynamic parameters from differential scanning calorimetry for Ferricyt *c* and Ferrocyt *c* unfolding; pH 7.0.[c]

	T_m (ºC)	ΔH_{cal}(kJ mol^{-1})	ΔH_{vH} (kJ mol^{-1})	$\Delta H_{vH}/\Delta H_{cal}$
Ferricyt *c*	82.6±0.06	324.7±3.3	336.4±4.6	1.03
Ferrocyt *c*	100.5±0.07	534.0±10.8	581.2±5.8	1.08

[c] The standard errors in T_m, ΔH_{cal} and ΔH_{vH} are shown in parenthesis.

The thermal or denaturant unfolding transitions measured for Ferrocyt *c* by different optical probes (CD, fluorescence and absorbance) and common optical probes with multiple wavelengths are within error nearly super imposable and cooperative. The observation of indistinct thermal or denaturant unfolding transition curves for Ferrocyt *c* do not reveal the accumulation of any equilibrium structural intermediate to a detectable level, which suggests that the thermal and denaturant-induced unfolding of Ferrocyt *c* occur in two-state manner.

3.2.9 Effect of crowding agents on the secondary (far-UV CD) structure of Ferrocyt c and Mb

To test the effect of crowding agents on the secondary structures of native Ferrocyt *c* and Mb, the far-UV CD spectra of native Ferrocyt *c* and Mb were collected in the absence and presence of dextran 70 at pH 7.0, 25 ºC. Fig. 12a and Fig. 12b present the far-UV CD spectra of Ferrocyt *c* and Mb, respectively, collected in the absence and presence of 200 mg ml^{-1} of dextran 70 at pH 7.0, 25 ºC. Fig. 12a and Fig. 12b clearly show that crowding agent presence in reaction medium not greatly affect the secondary structures of native Ferrocyt *c* and Mb at pH 7, 25 ºC.

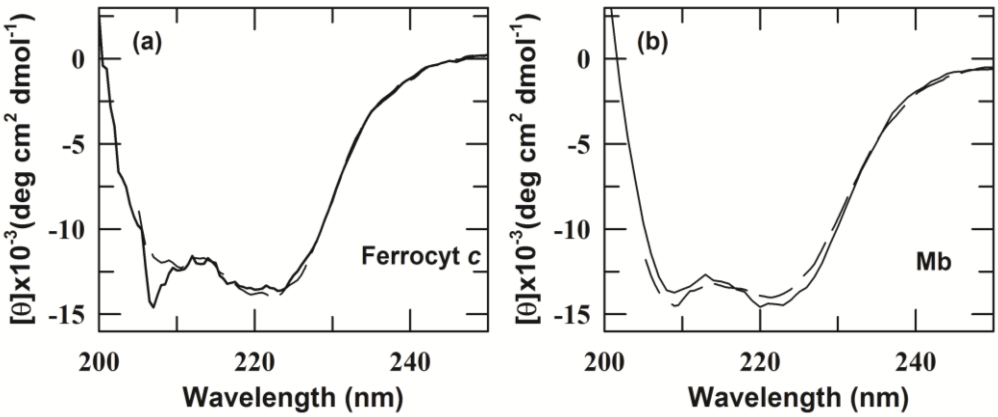

Fig.12. Panel (a) and (b) shows the equilibrium far-UV CD spectra of Ferrocyt *c* and Mb, respectively in sodium phosphate buffer native protein (solid line) and with 200 mg ml^{-1} dextran 70 (long dash line) at pH 7.0 25ºC.

3.3 Conclusion

Upto 40% of cytoplasm volume is generally occupied by macromolecules viz. proteins, carbohydrates, nucleic acids etc. The highly crowded conditions found in cytoplasm can affect the thermodynamic and kinetic properties of proteins. The kinetic and thermodynamic parameters for CO−dissociation from NCO (NCO→N+CO) and CO-replacement from MbCO by hexacyanoferrate ion were measured at varying concentrations of crowding agents (dextran 70, dextran 40, and ficoll 70) and viscogens (glycerol, sucrose, and glucose). It was found that as [Crowding agent] is increased, the rate coefficients of CO−dissociation for NCO (k_{diss}) and CO-replacement for MbCO (k_{off}) decrease exponentially. The values of log k_{diss} and log k_{off} are found to be slighltly decreased more for dextran 70 than that for ficoll 70, suggesting that the shape of crowding agent may play an important role in controlling the internal dynamics of NCO and MbCO. log k_{diss} and log k_{off} are also found to be decreased more for dextran 70 than that of dextran 40. Dextran 70 has the larger size than that of the dextran 40, so the greater decrease of log k_{diss} and log k_{off} for dextran 70 suggests that the size of crowding agent also plays a significant role in controlling the internal dynamics of NCO and MbCO. A general approach for investigating the importance of protein dynamics in a chemical reaction is to determine the role of solvent viscosity on reaction rate. log k_{diss} is found to be decreased with increasing solvent composition (glycerol, sucrose, and glucose) and viscosity, indicating that the solvent viscosity controls the internal dynamics of NCO. At a given particular concentration, dextran 70 has always higher viscosity than dextran 40 and ficoll 70, so the greater decrease of log k_{diss} for dextran 70

than that of the dextran 40 suggests that the viscosity of crowding agent also plays a vital role in controlling the internal dynamics of NCO and MbCO.

The thermal or denaturant unfolding transitions measured for Ferrocyt *c* by different optical probes (CD, fluorescence and absorbance) and common optical probes with multiple wavelengths are within error nearly superimposable and cooperative. The observation of indistinct thermal or denaturant unfolding transition curves for Ferrocyt *c* do not reveal the accumulation of any equilibrium structural intermediate to a detectable level, which suggests that the thermal and denaturant-induced unfolding of Ferrocyt *c* occur in two-state manner. Two-state thermodynamic analysis of chemical (GdnHCl or urea) and thermal unfolding transitions of native Ferrocyt *c* (N-state) and Mb carried out in the absence and presence of 200 mg ml^{-1} dextran 40, dextran 70 and ficoll 70 reveals that (i) crowding agents increase the thermodynamic stability of Ferrocyt *c* but in case of Mb, dextran 40 and dextran 70 do not greatly change the thermodynamic stability of protein but ficoll 70 decrease the thermodynamic stability of Mb at pH 7, and (ii) crowding agents also increase the thermal stability of Ferrocyt *c* while they decrease the thermal stability of native Mb. For native Ferrocyt *c*, the thermal stability is more increased for dextran 40 and least for ficoll 70 (dextran 40 >dextran 70 >ficoll 70). However, in case of Mb, the thermal stability is more decreased for ficoll 70 and least for dextran 40 (ficoll 70 < dextran 70< dextran 40). These results thus reveal that the macromolecular crowding effect influences the stability, folding and dynamics of native Ferrocyt *c* and Mb.

3.4 References:

1. S. B. Zimmerman, S.O. Trach, *J. Mol. Biol.* **222** (1991) 599–620.
2. A. B. Fulton, *Cell* **30** (1982) 345–347.
3. G. Rivas, F. Ferrone, J. Herzfeld, *EMBO Rep.* **5** (2004) 23–27.
4. B. van den Berg, R.J. Ellis, C.M. Dobson, *EMBO J.* **18** (1999) 6927–6933.
5. A. P. Minton, J. Wilf, *Biochemistry* **20** (1981) 4821–4826.
6. J. R. Ellis, *TRENDS in Biochem. Sciences* **26** (2001) 597–604.
7. D. Voet, J. Voet, C.W. Pratt, *Fundamentals of Biochemistry*. Wiley: New York, 1999.
8. L. A. Munishkina, A. L. Fink, V. N. Uversky, *Curr. Alzheimer Res.* **6** (2009) 252–260.
9. D. Homouz, L. Stagg, P. Wittung-Stafshede, M. S. Cheung, *Biophys. J.* **96** (2009) 671–680.

10. H. X. Zhou, G. N. Rivas, A. P. Minton, *Annu. Rev. Biophys.* **37** (2008) 375–397.
11. D. Hall, A. P. Minton, *Biophys. Chem.* **98** (2002) 93–104.
12. L. Stagg, A. Christiansen, P. Wittung-Stafshede, *J. Am. Chem. Soc.* **133** (2011) 646–648.
13. J. R. Ellis, A. P. Minton, *Biol. Chem.* **387** (2006) 485–497.
14. J. Adén, P. Wittung-Stafshede, *Biochemistry* **53** (2014) 2271–2277.
15. S. Mukherjee, M. M. Waegele, P. Chowdhury, L. Guo, F. Gai, *J. Mol. Biol.* **393** (2009) 227–236.
16. K. Sasahara, P. McPhie, A. P. Minton, *J. Mol. Biol.* **326** (2003) 1227–1237.
17. L. Stagg, S. Zhang, M. S. Cheung, P. Wittung-Stafshede, *Proc. Nat. Acad. Sci. USA* **48** (2007) 18976–18981.
18. M. S. Cheung, D. Klimov, D. Thirumalai, *Proc. Nat. Acad. Sci. USA* **13** (2005) 4753–4758.
19. Y. Wang, M. Sarkar, A. E. Smith, A. S. Krois, G. J. Pielak, *J. Am. Chem. Soc.* **134** (2012) 16614–166118.
20. M. Erlkamp, S. Grobelny, R. Winter, *Phys. Chem. Chem. Phys.* **16** (2014) 5965–5976.
21. M. S. Cheung, D. Thirumalai, *J. Phys. Chem. B* **111** (2007) 8250–8257.
22. Y. Zhai, R. Winter, *Chem. Phys. Chem.* **14** (2013) 386–393.
23. A. Christiansen, P. Wittung-Stafshede, *FEBS Lett.* **588** (2014) 811–814.
24. A. Christiansen, Q. Wang, A. Samiotakis, M. S. Cheung, P. Wittung-Stafshede, *Biochemistry* **49** (2010) 6519–6530.
25. Y.P. Ow, D. R. Green, Z. Hao, T. W. Mak, *Nature Reviews molecular cell biology* **9** (2008) 532−542.
26. A. K. Bhuyan, R. Kumar, *Biochemistry* **41**(2002)12821−12834.
27. A. K. Bhuyan, J. B. Udgaonkar, *J. Mol. Biol.* **312** (2001) 1135−1160.
28. N. P. Prabhu, R. Kumar, A. K. Bhuyan, *J. Mol. Biol.* **337** (2004) 195−208.
29. R. Kumar, A. K. Bhuyan, *Biochemistry* **44** (2005) 3024−3033.
30. A. K. Bhuyan, D. K. Rao, N. P. Prabhu, *Biochemistry* **44** (2005) 3034−3040.
31. S. A. Pabit, H. Roder, S. J. Hagen, *Biochemistry* **43** (2004) 12532−12538.
32. R. Jain, D. Sharma, S. Kumar, R. Kumar, *Biochemistry* **53** (2014) 5221−5235.
33. J. C. Kendrew, G. Bodo, H.M. Dintzis, R.G. Parrish, H.W. Wyckoff, D.C. Phillips, *Nature* **181** (1958) 662−666.

34. G. B. Postnikova, Y.E. Komarov, E.M. Yumakova, *Eur. J. Biochem*. **198** (1991) 223−232.
35. G. B. Postnikova, E.M. Yumakova, *Eur. J. Biochem*. **198** (1991) 241−246.
36. M. P. Bohrer, G. D. Patterson, P. J. Carroll, *Macromolecules* **17** (1984)1170−1173.
37. I. M. Kuznetsova, K. K. Turoverov, V. N. Uversky, *Int. J. Mol. Sci.* **15** (2014) 23090−23140.
38. A. K. Bhuyan, *Biochemistry* **41** (2002) 13386–13394.
39. J. F. Leszczynski, G. D. Rose, *Science* **234** (1986) 849–855.
40. L. Hoang, H. Maity, M.M.G. Krishna, Y. Lin, S.W. Englander, *J. Mol. Biol.* **331** (2003) 37–43.
41. Y. Xu, L.C. Mayne, S.W. Englander, *Nature Struct. Biol.* **5** (1998) 774–778.
42. A. M. Berghuis, G. D. Brayer, *J. Mol. Biol.* **223** (1992) 959–976.
43. J. D. Morgan, J. A. McCammon, *Biopolymers* **22** (1983)1579–1593.
44. R. Kumar, R. Jain, R. Kumar, *Chemical Physics* **418** (2013) 57–64.
45. R. Kumar, N. P. Prabhu, M. Yadaiah, A. K. Bhuyan, *Biophys J.* **87** (2004) 2656–2662.
46. D. K. Rao, R. Kumar, M. Yadaiah, A. K Bhuyan, *Biochemistry* **45** (2006) 3412–3420.
47. E. Margoliash, N. Frohwirt, *Biochem. J.* **71** (1959) 570–572.
48. R. Varhac, M. Antalik, M. Bano, *J. Biol. Inorg. Chem.* **9** (2004) 12–22.
49. J. S. Olson, *Methods Enzymol* **76** (1981) 631–651.
50. J. Miksovská, J.H. Day, R.W. Larsen, *J. Biol. Inorg. Chem.* **8** (2003) 621–625.
51. A. B. Goins, H. Sanabria, M. N. Waxham, *Biophys J.* **95** (2008) 5362–5373.
52. P.J. Flory, *Principles of Polymer Chemistry*, Cornell University Press, Ithaca, 1953.
53. P. B. Crowley, K. Brett, J. Muldoon, *ChemBioChem* **9** (2008) 685–688.
54. Y. C. Kim, J. Mittal, *Phys. Rev. lett.* **110** (2013) 208102–208105.
55. S. Sukenik, L. Sapir, D. Harries, *Colloid Interface Sci.* **18** (2013) 495–501.
56. L. Sapir, D. Harries, *Curr. Opin. Colloid Interface Sci.* **20** (2015) 3–10.
57. G. A. Petsko, D. Ringe, *Ann. Rev. Biophys. Bioeng.* **13** (1984) 331–371.
58. J. Kestin, M. Sokolov, W.A. Wakeham, *J. Phys. Chem. Ref. Data* **7** (1978) 941–1004.
59. H. A. Kramers, *Physica* **7** (1940) 284–360.
60. P. Hanggi, P. Talkner, M. Borkovec, *Rev. Mod. Phys.* **62** (1990) 251–332.
61. D. Beece, L. Eisenstein, H. Frauenfelder, D. Good, M. C. Marden, L. Reinisch, A. H. Reynolds, L. B. Sorensen, K.T. Yue, *Biochemistry* **19** (1980) 5147–5157.

62. B. Gavish, M.M. Werber, *Biochemistry* **18** (1979) 1269–1275.
63. D. Lavalette, C. Tetreau, *Eur. J. Biochem.* **177** (1988) 97–108.
64. K. Ng, A. Rosenberg, *Biophys. Chem.* **39** (1991) 57–68.
65. S. Yedgar, C. Tetreau, B. Gavish, D. Lavalette, *Biophys. J.* **68** (1995) 665–670.
66. W. Doster, T. Kleinert, F. Post, M. Settles, in: R.B. Gregory (Ed.), *Protein–solvent interactions*, Marcel Dekker Inc., New York (1995) p. 375–385.
67. A. Rosenberg, K. Ng, M. Punyiczki, *J. Mol. Liq*. **42** (1989) 31–43.
68. W. Doster, *Biophys. Chem.* **17** (1983) 97–103.
69. J. Schlitter, *Chem. Phys.* **120** (1988) 187–197.
70. C. L. Brooks, M. Karplus, *J. Mol. Biol*. **208** (1989) 159–181.
71. B. Gavish, *Phys. Rev. Lett.* **44** (1980) 1160–1163.
72. M. Fixman, *Faraday Discuss. Chem. Soc.* **83** (1987) 199–211.
73. D. Beece, L. Eisenstein, H. Frauenfelder, D. Good, M. C. Marden, L. Reinisch, A. H. Reynolds, L. B. Sorensen, K.T. Yue, *Biochemistry* **19** (1980) 5147–5157.
74. R. Korenstein, B. Hess, *Nature* **270** (1977) 184–186.
75. R. Kumar, A. K. Bhuyan, *J. Phys. Chem. B* **112** (2008) 12549–12554.
76. P. G. de-Gennes, *Scaling concepts in polymer physics*, Cornell University Press, New York, (1979) p.113–144.
77. M. Fixman, *J. Chem. Phys.* **89** (1988) 2442–2462.
78. J. J. Portman, S. Takada, P. G. Wolynes, *J. Chem. Phys.* **114** (2001) 5082–5096.
79. A. Ansari, C. M. Jones, E. R. Henry, J. Hofrichter, W. A. Eaton, *Science* **256** (1992)1796–1798.
80. S. J. Hagen, J. Hofrichter, W. A. Eaton, *Science* **269** (1995) 959–962.
81. S. A. Pabit, H. Roder, S. J. Hagen, *Biochemistry* **43** (2004) 12532–12538.
82. M. Jacob, M. Geeves, G. Holtermann, F. X. Schmid, *Nat. Struct. Biol.* **6** (1999) 923–926.
83. K.W. Plaxco, D. Baker, *Proc. Natl. Acad. Sci. USA* **95** (1998) 13591–13596.
84. T. Cellmer, E.R. Henry, J. Hofricheter, W.A. Eaton, *Proc. Natl. Acad. Sci. USA* **105** (2008) 18320–18325.
85. L. Pradeep, J. B. Udgaonkar, *J. Mol. Biol.* **366** (2007) 1016–1028.
86. R. P. Bhattacharyya, T. R. Sosnick, *Biochemistry* **38** (1999) 2601–2609.

87. M. I. Wallace, L. M. Ying, S. Balasubramanian, D. Klenerman, *Proc. Natl. Acad. Sci. USA* **98** (2001) 5584–5589.
88. M. M. Santoro, D. W. Bolen, *Biochemistry* **27** (1988) 8063−8068.
89. M. M. Santoro, D.W. Bolen, *Biochemistry* **31** (1992) 4901–4907.
90. R. Kumar, N. P. Prabhu, D. K. Rao, A. K. Bhuyan, *J. Mol. Biol.* **364** (2006) 483–495.
91. P. L. Prívalov, N. N. A. Khechínashvili, *J. Mol. Biol.* **86** (1974) 665–684.
92. Y. Kuroda, S. Kidokoro, A. Wada, *J. Mol. Biol.* **223** (1992) 1139–1153.
93. M. Antalík, J. Bágeĺová, *Gen. Physiol. Biophys.* **14** (1995) 19–37.
94. J. Bageĺova, M. Antalik, M. Bona, *Biochem. J.* **297** (1994) 99–101.
95. A. K. Bhuyan, J. B. Udgaonkar, *J. Mol. Biol.* **312** (2001) 1135–1160.
96. J. J. Osterhout, T. K. Muthukrishnan Jr., B.T. Nall, *Biochemistry* **24** (1985) 6680–6684.
97. S. T. Whitten, J. O. Wooll, R. Razeghifard, E. B. G. Moreno, V. J. Hilser, *J. Mol. Biol.* **309** (2001) 1165–1175.
98. S. Uchiyama, A. Oshima, S. Nakamura, J. Hasegawa, N. Terui, S. J. Takayama, Y. Yamamoto, Y. Sambongi, Y. Kobayashi, *J. Am. Chem. Soc.* **126** (2004) 14684–14685.
99. M. T. Fisher, *Biochemistry* **30** (1991) 10012–10018.
100. S. P. Manly, K. S. Matthews, J. M. Sturtevant, *Biochemistry* **24** (1985) 3842–3846.
101. V. Edge, N. M. Allewell, J. M. Sturtevant, *Biochemistry* **24** (1985) 5899–5906.
102. C. Q. Hu, J. M. Sturtevant, *Biochemistry* **26** (1987) 178–182.
103. M. L. Wu, W. T. Morgan, *Proteins* **20** (1994) 185–190.
104. F. I. Rosell, M. R. Mauk, A. G. Mauk, *Biochemistry* **44** (2005) 1872–1879.

Chapter 4

Factor Defining the Effect of Macromolecular Crowding on Thermodynamic Stability and Internal Dynamics of Heme Proteins

4.1. Introduction

Biophysical and structural properties of proteins are mostly characterized in dilute aqueous condition. However, protein are synthesized on endoplasmic reticulum and its biological processes including protein folding, enzyme activity, structural allostery etc. were performed under highly crowded intracellular environment [1-2]. The interior of cells contains several kinds of macromolecules like lipids, sugars, nucleic acids, proteins, along with large organized cytoskeleton fibers [3]. Thus the significant fraction of the intracellular space is not available to other macromolecular species. It has been estimated that the concentration of macromolecules in the cytoplasm ranges from 80 to 400 mg ml^{-1}[4-5]. About 10 to 40% of cellular volume is occupied by different macromolecules [6-7]. How much of the intracellular volume is available to other macromolecules depends on the concentration, size and shape of all the molecules present in each compartment. The crowded environment results in excluded volume effects, risk of nonspecific intermolecular interactions, and increased viscosity of the solvent. Earlier reports revealed that the crowding effects arise by two different phenomenon, hardcore repulsions and soft (i.e., chemical) interactions [8]. Due to hard core repulsion, crowder reduces the space available to the protein and induces the compactness of protein being studied. The hardcore repulsive effect involves only the arrangement of molecules, not their interaction with proteins and enhancing protein stability by decreasing the entropy of unfolding [9-12]. The soft or chemical interactions may be attractive or repulsive. In case of attractive interaction, the nonspecific binding with protein backbone and the cosolutes leads to a preferential exclusion of the osmolytes or crowders from the protein surface and a preferential hydration of protein [13]. As the solvent accessible surface area of the unfolded state is increased, the folding equilibrium is shifted towards the native state [12, 14-15]. Experimental studies have demonstrated that the crowding agents can affect protein structure and function [16-36]. Some previous results show that the acid-denatured cytochrome *c* (Cyt *c*) adopts a near-native molten globule state under the

high concentration of smaller crowder dextran 40 [16]. Crowders are also influence the functional properties of proteins or enzymes [37-47]. Crowder enhance the activity of phosphoglycerate kinase (PGK) more than ten folds [17], regulate the phosphorylation of ERK kinase in cells [18], alters the diffusional behavior of intracellular proteins [19-20] and molecular properties of motor proteins, kinesins [21]. Some previous studies suggested that crowding plays a key role in human diseases that are related to protein aggregation and fibril formation [22-25] which is linked with numerous neurodegenerative disorders [26-29]. Earlier reports showed that the crowding agents also increase the stability and structural content of folded [3, 30-32] and unfolded proteins [33-36].

While the effects of crowding agents on the stability of proteins have been studied extensively [3, 31, 48-50], the effects of crowding agents on the denaturant-dependent thermodynamic stability of proteins are less explored [48]. This chapter investigates the effect of macromolecular crowding (size, shape, concentration) on the denaturant dependent thermodynamic stability of native cytochrome *c* (Cyt c) and myoglobin (Mb) by analyzing the thermal unfolding transitions of Cyt *c* and Mb collected at fixed concentrations of crowding agents (dextran 40, dextran 70, ficoll 70) under variable concentrations of denaturants (urea and GdnHCl) at pH 7.0. By probing the changes in thermal fluctuations at the atomic and large-scale collective level, one can determine the possible roles of structural dynamics in folding [51]. The effects of crowding agents on the fast protein dynamics have been studied extensively [50, 53-55], but the effects of crowding agents on the slow changes in the internal dynamics of proteins are less explored [56]. In particular, the effects of crowding agents on the denaturant-dependent low frequency local motions that control the relatively slow changes in structural dynamics of proteins are not explored so far. This chapter investigates the effect of macromolecular crowding (size, shape, concentration, viscosity) on the denaturant-dependent structural-fluctuations of Cyt *c* by measuring the rate of thermally driven CO dissociation from natively-folded carbonmonoxycytochrome *c* (NCO-state) at fixed concentrations of crowding agents (dextran 40, dextran 70 and ficoll 70) under variable concentrations of denaturants (urea and GdnHCl).

4.2 Results and discussion

4.2.1 Effect of crowding agents on the denaturants dependent internal dynamics of NCO

Thermal dissociation of CO from NCO leads a significantly increase in the absorbance of α-band (550 nm) [57-58]. The representative CO-dissociation kinetic profile of NCO recorded in the presence of 0.05 M GdnHCl at 22°C, pH 7 is shown in Fig. 1a. To examine the effect of crowding agents on the denaturant dependent internal dynamics of NCO, the rate coefficient of CO-dissociation (k_{diss}) form NCO was measured at fixed concentrations of crowding agents (dextran 40, dextran 70 and ficoll 70) under variable concentrations of denaturants (urea and GdnHCl) at pH 7.0. Fig. 1b presents the denaturant-dependence of log k_{diss} measured in the absence and presence of ~50, 100, 200 mg ml^{-1} dextran 70 at pH 7.0, 22 °C. Fig. 1c shows the denaturant-dependence of log k_{diss} measured in the absence and presence of ~50, 100, 200 mg ml^{-1} ficoll 70 at pH 7.0, 22 °C. In the absence of crowding agents, when the concentration of denaturant in the reaction medium is raised from 0.0 to 4.0 M GdnHCl or 9.0 M urea, log k_{diss} initially decreases and then increases, displaying inflections centered at ~2.3 M GdnHCl or ~5.5 M urea (Fig. 1b and Fig. 1c). This finding indicates that the subdenaturing concentrations of denaturants constrain the internal dynamics of NCO.

Since both crowding agent and subdenaturing concentrations of denaturant (<2.3 M GdnHCl or <5.5 M urea) individually decrease the rate of CO dissociation reaction (Fig. 2a (chapter 3), Fig. 1b and Fig. 1c), the coexistence of the two in the reaction medium is expected to produce a cumulative effect on the rate of CO dissociation. As [crowding agent] is increased from 0 to 200 mg ml^{-1}, the rate-denaturant profile is shifted vertically down to lower k_{diss} (Fig. 1b and Fig. 1c). A slight horizontal shift toward higher concentration of denaturant is also apparent (Fig. 1b and Fig. 1c). The crowding mediated vertical and slight horizontal shifts in the rate-denaturant profile thus reveal that the crowding agent and subdenaturing concentrations of denaturants produce a cumulative effect on the restricted internal dynamics of NCO.

In the denaturing region, the increase in logarithm of k_{diss} (Fig. 1b and Fig. 1c) can be interpreted to arise from protein destabilization and structural unfolding action of denaturant that would facilitate the CO dissociation from NCO. In the denaturing region, the log k_{diss} increases to a lesser extent in the presence of crowding agent than in the absence (Fig. 1b and Fig.1c), which indicates that the inclusion of crowding agent opposes the structural fluctuation that cause unfolding of the protein.

Fig. 1d presents the denaturant-dependence of log k_{diss} measured in the presence of ~ 100 mg ml^{-1} dextran 40, dextran 70 and ficoll 70 at pH 7.0, 22 °C. Under solution conditions, ficoll is considered as spherical-shaped crowder [48, 59] while dextran 40 and dextran 70 are regarded as rod-shaped crowder [48, 59]. Within the subdenaturing region, the extent of decrease in log k_{diss} typically follows the order, dextran 70> dextran 40> ficoll 70 (Fig. 1d), which suggests that in the presence of crowding agents, the size and shape of crowding agents affect the denaturant-mediated constrained dynamics of NCO. Previous simulation studies have also shown that the shape of crowding agents affect the stability and dynamics of proteins [3, 48, 60]. At a given particular concentration, dextran is more viscous than ficoll [61] and the larger sized dextran has always higher viscosity then the smaller sized dextran [62], therefore, the greater decrease of log k_{diss} for dextran 70 than that of the dextran 40 suggests that the viscosity of crowding agents also affects the denaturant-mediated constrained dynamics of NCO.

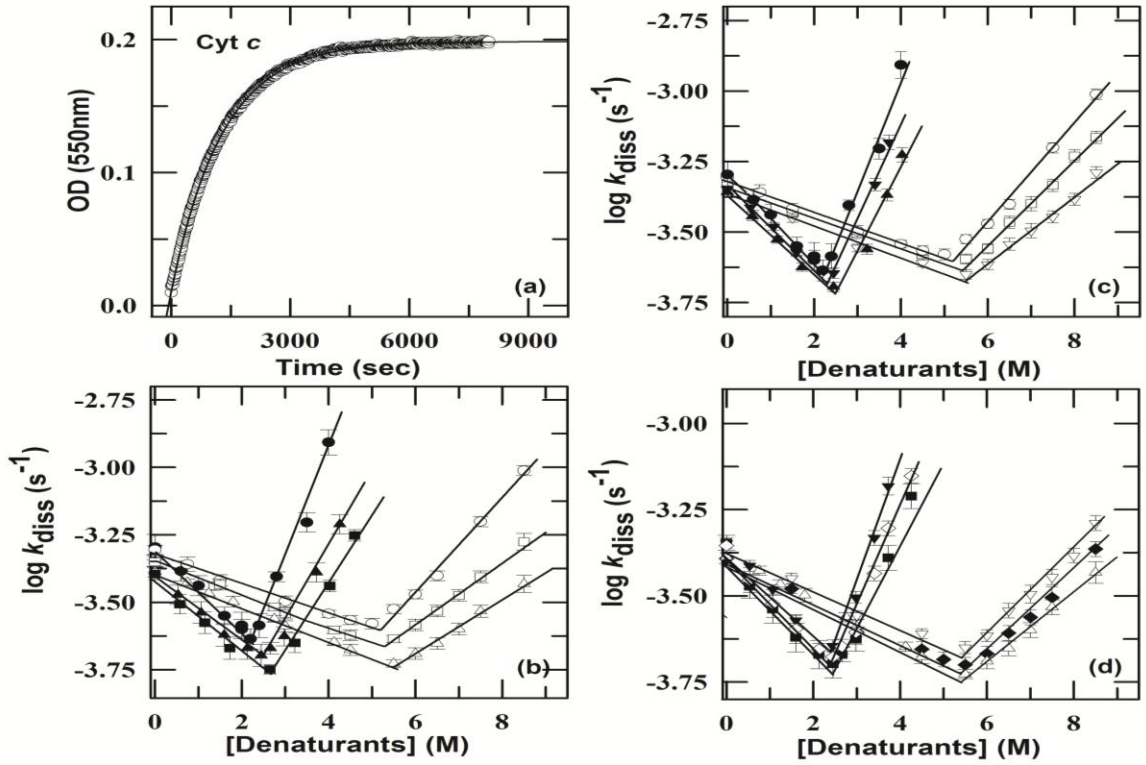

Fig.1. Effect of crowding agents on the denaturants-dependent internal dynamics of NCO. Panel (a) shows the slow single-phase dissociation of CO from NCO, NCO → N+CO (τ =32 min., 22°C). The NCO → N+CO reaction was probed at 550 nm in the presence of 0.05M GdnHCl. Panel (b) presents the denaturant-dependence of log k_{diss} in the absence (GdnHCl (●), urea (○)) and presence of 50 mg ml^{-1} (urea(□)), 100 mg ml^{-1} (GdnHCl (▲), urea (Δ)) and 200 mg ml^{-1} (GdnHCl (■)) of dextran 70 at pH 7.0, 22 °C. Panel (c) presents the denaturant-dependence of log k_{diss} in the

absence (GdnHCl (●), urea (○)) and presence of 50 mg ml^{-1} (urea (□)), 100 mg ml^{-1} (GdnHCl (▼), urea (▽)), and 200 mg ml^{-1} (GdnHCl (▲)) of ficoll 70 at pH 7.0, 22 °C. Panel (d) presents the denaturant-dependence of log k_{diss} in the presence of 100 mg ml^{-1} of dextran 40 (urea (◆), GdnHCl (◊)), dextran 70 (GdnHCl (■), urea (Δ)), and ficoll 70 (GdnHCl (▼), urea (▽))at pH 7.0, 22°C. The solid lines are just guide the eye. All the experiments are carried out in 50 mM phosphate buffer. `

A recent report revealed that the larger sized dextran forms caging or confinement environment, which indicates that caging or confinement effect may also play a vital role in controlling the dynamics of protein [63]. Within the denaturing region, the extent of increase in log k_{diss} typically follows the order, dextran 70< dextran 40< ficoll 70 (Fig. 1d), which suggests that in the presence of crowding agents, the size and shape of crowding agents also affect the denaturant-mediated structural fluctuation that cause unfolding of the protein.

4.2.2 Effect of crowding agents on the denaturant-dependent activation thermodynamic parameter of CO-dissociation reaction of NCO

To further examine the effects of crowding agents on the denaturant-dependent internal dynamics of NCO, the temperature dependent CO dissociation kinetics profiles of NCO were measured at various concentrations of denaturants (urea and GdnHCl) in the absence and presence of crowding agents (dextran 40, dextran 70 and ficoll 70) at pH 7.0. Fig. 2a presents the Eyring plots for CO-dissociation reaction of NCO in the absence of additive and at 2.3 and 4.0 M GdnHCl in the absence and presence of 100 mg ml^{-1} dextran 40, dextran 70 and ficoll 70. The Eyring plots for CO-dissociation reaction of NCO in the absence of additive and at 5.5 and 8.5 M urea in the absence and presence of ~100 mg ml^{-1} dextran 40, dextran 70 and ficoll 70 are shown Fig. 2b. Thermodynamic parameters *viz*; activation enthalpy (ΔH_{diss}) and activation entropy (ΔS_{diss}) for CO dissociation reaction of NCO in the absence of additive and at 2.3 and 4.0 M GdnHCl or 5.5 and 8.5 M urea in the absence and presence of ~100 mg ml^{-1} dextran 40, dextran 70 and ficoll 70 at pH 7.0 were calculated by Eyring equation (Equation (1), chapter 2) [64]. The calculated values of $\Delta H_{diss}^{\ddagger}$ and $\Delta S_{diss}^{\ddagger}$ are listed in Table 1. The corresponding free energy of activation ($\Delta G_{diss}^{\ddagger}$), entropy change ($-T\Delta S_{diss}^{\ddagger}$), were also calculated from Gibb free energy equation ($\Delta G_{diss}^{\ddagger} = \Delta H_{diss}^{\ddagger} - T\Delta S_{diss}^{\ddagger}$) at 25 °C and are summarized in Table 1.

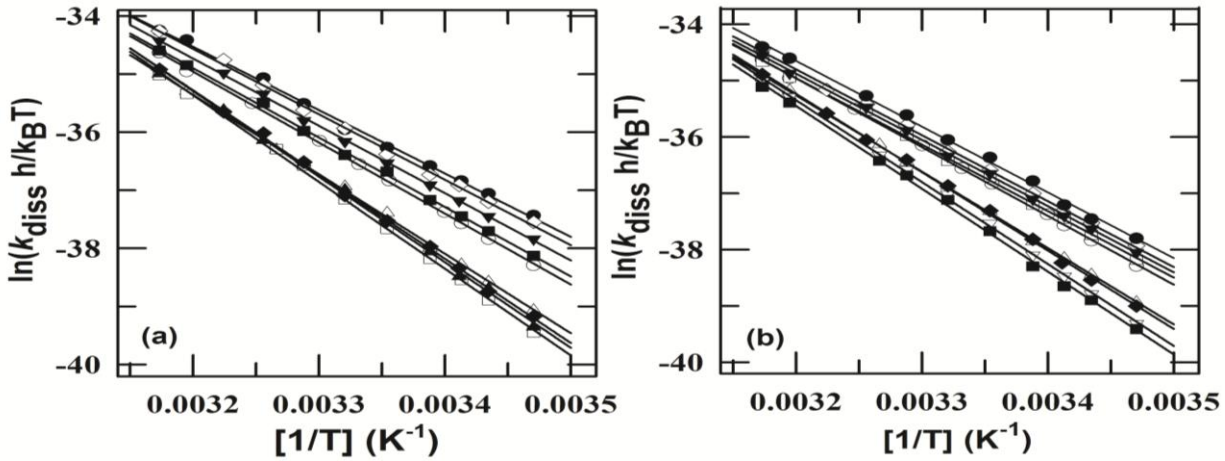

Fig.2. Effect of crowding agents on denaturant-dependent activation thermodynamic parameters of CO dissociation reaction of NCO at pH 7.0. Panel (a) shows Eyring plots for the CO dissociation reaction of NCO in the absence of additive (○) and at 2.3 M GdnHCl (Δ), 4 M GdnHCl (●), 2.3 M GdnHCl with 100 mg ml^{-1}crowding agent (dextran 70 (□), dextran 40 (▲) and ficoll 70 (◆)) and 4 M GdnHCl with 100 mg ml^{-1}crowding agent (dextran 70 (■), dextran 40 (▼) and ficoll 70 (◊)). Panel (b) shows Eyring plots for the CO dissociation reaction of NCO in the absence of additive (○) and at 5.5 M urea (Δ), 8.5 M urea (●)), 5.5 M urea with 100 mg ml^{-1} crowding agents (dextran 70 (■), dextran 40 (▽) and ficoll 70 (◆)) and 8.5 M urea with 100 mg ml^{-1}crowding agents (dextran 70 (□), dextran 40 (▼) and ficoll 70 (◊)). The solid lines are fitted according to Eyring equation (Equation (1), chapter 2).

Table 1. Effect of macromolecular crowding on denaturant-dependent $\Delta H_{diss}^{\ddagger}$, $\Delta G_{diss}^{\ddagger}$, $\Delta S_{diss}^{\ddagger}$ and $-T\Delta S_{diss}^{\ddagger}$ for CO dissociation reaction of NCO at pH 7.0*.

	Without crowding agents				dextran 40 (100 mg ml^{-1})			
[GdnHCl] (M)	$\Delta G_{diss}^{a\ddagger}$	$\Delta H_{diss}^{\ddagger}$	$\Delta S_{diss}^{\ddagger}$	$-T\Delta S_{diss}^{a\ddagger}$	$\Delta G_{diss}^{a\ddagger}$	$\Delta H_{diss}^{\ddagger}$	$\Delta S_{diss}^{\ddagger}$	$-T\Delta S_{diss}^{a\ddagger}$
control	22.0	24.4	8.3	−2.5	22.1	25.4	11.0	−3.3
2.3	22.3	27.3	16.8	−5.0	22.4	29.4	23.7	−7.0
4.0	21.6	21.8	0.7	−0.2	21.8	23.2	4.6	−1.4
[Urea] (M)								
5.5	22.3	27.1	16.3	−4.8	22.4	29.1	22.4	−6.7
8.5	21.7	23.3	5.0	−1.6	21.9	23.5	5.5	−1.6
	dextran 70 (100 mg ml^{-1})				ficoll 70 (100 mg ml^{-1})			
[GdnHCl] (M)	$\Delta G_{diss}^{a\ddagger}$	$\Delta H_{diss}^{\ddagger}$	$\Delta S_{diss}^{\ddagger}$	$-T\Delta S_{diss}^{a\ddagger}$	$\Delta G_{diss}^{a\ddagger}$	$\Delta H_{diss}^{\ddagger}$	$\Delta S_{diss}^{\ddagger}$	$-T\Delta S_{diss}^{a\ddagger}$
control	22.2	26.3	13.6	−4.0	22.0	24.8	10.5	−2.8
2.3	22.5	29.9	24.8	−7.4	22.4	29.0	22.2	−6.6
4.0	21.9	23.9	6.7	−2.0	21.6	22.5	2.9	−0.9
[Urea] (M)								
5.5 M	22.5	29.4	23.2	−6.9	22.3	27.8	18.6	−5.5
8.5 M	21.9	23.6	5.6	−1.7	21.8	23.4	5.3	−1.6

*$\Delta G_{diss}^{\ddagger}$, $\Delta H^{\ddagger}_{diss}$, $\Delta S_{diss}^{\ddagger}$ and $-T\Delta S_{diss}^{\ddagger}$ are reported as kcal mol^{-1}, kcal mol^{-1}, cal mol^{-1} K^{-1} and kcal mol^{-1} K^{-1}, respectively. The uncertainties associated with $\Delta G_{diss}^{\ddagger}$, $\Delta H^{\ddagger}_{diss}$, $\Delta S_{diss}^{\ddagger}$ and $-T\Delta S_{diss}^{\ddagger}$ are 0.5 kcal mol^{-1}, ±0.5 kcal mol^{-1}, 2.5 cal mol^{-1} and ±0.4 kcal mol^{-1} K^{-1}, respectively.

[a] Activation free energy ($\Delta G_{diss}^{\ddagger}$) and entropy changes ($-T\Delta S_{diss}^{\ddagger}$) are given at 25 °C.

The data in Table 1 provides several important information, (i) subdenaturing concentrations of denaturants increase the $\Delta H_{diss}^{\ddagger}$ and which is found to be increased more in the presence of crowding agents then in its absence, (ii) within subdenaturing region, the crowding-mediated increase in $\Delta H_{diss}^{\ddagger}$ typically follows the order, dextran 70> dextran 40> ficoll 70 (Fig. 2a and Fig.

2b), which reveals that the size, shape and viscosity of crowding agents affect the denaturant-mediated constrained dynamics of NCO, (iii) high concentrations of denaturants decrease the $\Delta H_{diss}^{\ddagger}$ and which is found to be less decreased in the presence of crowding agents then in its absence, which suggests that the crowding agent produces the counteraction effect on the denaturant-mediated structural fluctuation that unfolds the protein, (iv) the crowding-mediated counteraction effect on the denaturant-mediated structural fluctuation that cause unfolding of the protein typically follows the order, dextran 70> dextran 40> ficoll 70 (Fig. 2a and Fig. 2b), which suggests that the size, shape and viscosity of crowding agents affect the denaturant-mediated structural fluctuation that cause unfolding of the protein, and (v) the crowding-mediated increase in $\Delta H_{diss}^{\ddagger}$ is accompanied by a decrease in the entropy change, $-T\Delta S_{diss}^{\ddagger}$.

4.2.3 Effect of crowding agents on the denaturant-dependent thermal unfolding of Ferrocyt c and Mb

Fig. 3a presents the effect of temperature on α-band (550 nm) of Ferrocyt *c* at pH 7.0. When temperature is increased from 25 to 110 °C, the intensity of α-band is decreased significantly (Fig. 3a). This allows us to evaluate the effect of crowding agents on the denaturant-dependent thermal unfolding of Ferrocyt *c* at pH 7.0. Fig. 3b shows the representative absorbance (550 nm)-monitored thermal denaturation curves of Ferrocyt *c* measured at 0.5 and 2.3 M GdnHCl in the absence and presence of 100 mg ml^{-1} dextran 40 and dextran 70 at pH 7.0. Fig. 3c presents the far-UV CD spectrum of Ferrocyt *c* at 25°C, which exhibits a negative cotton effect at 222 nm that reflects the secondary structure of the native protein. When temperature is increased from 25 to 110°C, the negative cotton effect is eliminated significantly, which reveals that the secondary structure of the protein is disrupted significantly. Fig. 3d represents the far-UV CD-(222 nm) monitored normalized thermal unfolding curves of Ferrocyt *c* measured at 3.0 and 8.0 M urea in the absence and presence of 200 mg ml^{-1} dextran 40, dextran 70 and ficoll 70 at pH 7.0. Data in Fig. 3b and Fig. 3d clearly indicate that the denaturant-dependent thermal transition curve gets shifted to higher temperatures in the presence of crowding agents. Fig. 4a presents the effect of temperature on the soret-band (409 nm) of Mb at pH 7.0 When temperature is increased from 25 to 90°C, the intensity of soret-band is decreased significantly, which indicates thermal denaturation of Mb at 95 C. Fig. 4b shows the representative absorbance-monitored thermal

denaturation curves of Mb measured in the absence additives and at 0.5 M GdnHCl in the absence and presence of 200 mg ml^{-1} of crowding agent (dextran 40, dextran 70 and ficoll 70) at pH 7.0.

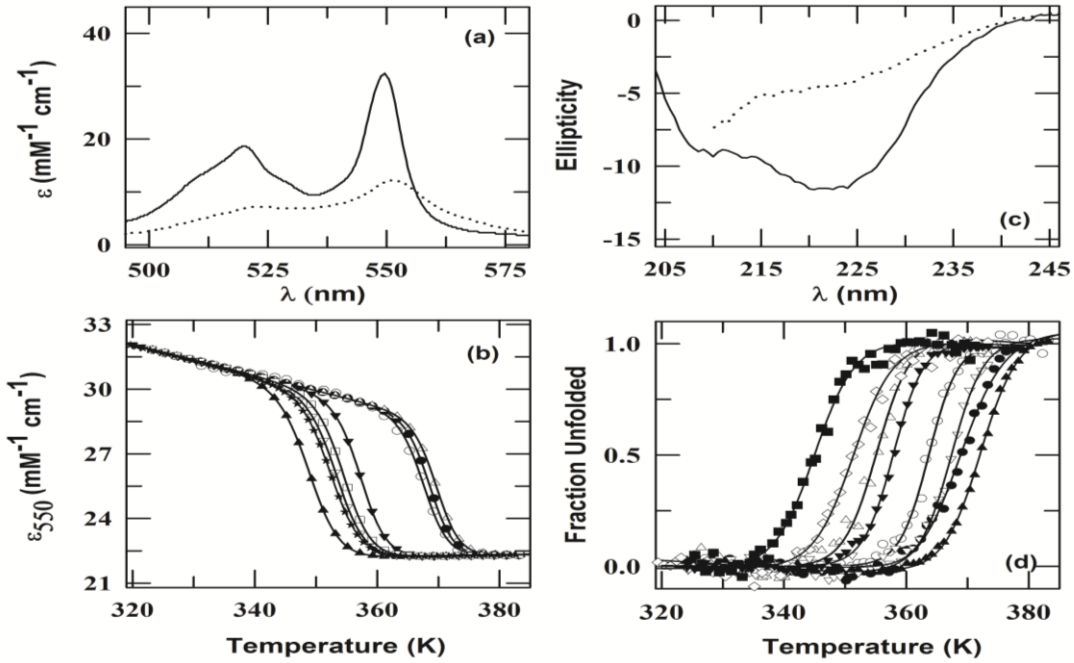

Fig.3. Effect of crowding agents on the denaturant-dependent thermal unfolding of Ferrocyt *c* at pH 7.0. Panel (a) shows the visible absorption spectra of Ferrocyt *c* collected at 25°C (solid line) and 110°C (dotted line), pH 7.0. Panel (b) represents the thermal denaturation curves of Ferrocyt *c* monitored at 550 nm as the change in excitation coefficient at 0.5 M GdnHCl (○), 2.3 M GdnHCl (▲), 0.5 M GdnHCl with 100 mg ml^{-1} dextran 40 (Δ), 0.5 M GdnHCl with 100 mg ml^{-1} dextran 70 (●), 2.3 M GdnHCl with 100 mg ml^{-1} dextran 40 (□), 0.5 M GdnHCl with 100 mg ml^{-1} dextran 70 (▽), 2.3 M GdnHCl with 100 mg ml^{-1} ficoll 70 (★), 2.3 M GdnHCl with 200 mg $ml^{-1}$of dextran 70 (▼). Panel (c) represents far-UV CD spectra of Ferrocyt *c* collected at 25°C (solid line) and 110°C (dotted line) at pH 7.0. (d) Normalized thermally-induced unfolding curves of Ferrocyt *c* monitored at CD-222 nm at 3 M urea (○), 8M urea (■), 8M urea with 200 mg ml^{-1} dextran 70 (Δ), 3 M urea with 200 mg ml^{-1} dextran 70 (●), 8M urea with 200 mg ml^{-1} dextran 40 (▼), 3 M urea with 200 mg ml^{-1} dextran 40 (▲), 8M urea with 200 mg ml^{-1} ficoll 70 (◊), 3 M urea with 200 mg ml^{-1} ficoll 70 (▽). The solid curves in panels (b) and (d) represent nonlinear least-squares fits to two-state van't Hoff equation (Equation (5), chapter 2)[65].

Fig. 4c shows the far-UV CD spectrum of Mb at 25°C, pH 7.0, which exhibits a negative Cotton effect at 222 nm that is the signature of secondary structure of the native protein. As the temperature is increased from 25 to 90°C, the negative Cotton effect is eliminated, which reveals that the secondary structure of protein is disrupted significantly at 90°C. Fig. 4d presents the far-UV CD-(222 nm) monitored normalized thermal denaturation curves of Mb measured in the absence of additives and at 1.0 and 4.5 M urea in the absence and presence of 100 mg ml^{-1} dextran

40, dextran 70 and ficoll 70 at pH 7.0. Fig. 4b and Fig. 4d suggest that the denaturant dependent thermal transition curve gets shifted to lower temperatures in the presence of crowding agents.

The absorbance and CD-monitored thermal unfolding curves of Ferrocyt *c* and Mb were analyzed for thermal denaturation midpoint (T_m) and enthalpy change (ΔH_m) by two-state model N⇌U using van't Hoff equation (Equation (5), chapter 2) [64]. The T_m and ΔH_m values for Ferrocyt *c* at various [GdnHCl] (Table 2) and [urea] (Table 3) both in the absence and presence of crowding agent are provided in Table 2 and Table 3.

Table 2. Effect of crowding agents on [GdnHCl]-dependent T_m and ΔH_m of Ferrocyt *c* at pH 7 as monitored by visible absorbance at 550 nm*.

	without crowding agents		100 mg ml^{-1} ficoll 70		100 mg ml^{-1} dextran 40	
[GdnHCl](M)	T_m	ΔH_m	T_m	ΔH_m	T_m	ΔH_m
control	373.9	119.5	374.4	122	-	-
0.25	372.2	115.0	371.7	118	371.3	127.0
0.5	367.3	109.7	369.8	116	370.2	122.4
1.0	362.6	102.0	365.0	110	365.5	115.0
1.5	356.6	98.0	360.1	105	361.9	109.0
2.3	349.0	85.0	353.7	95	354.7	100.0
2.8	346.7	78.0	349.2	88	350.3	96.0
	100 mg ml^{-1} dextran 70		200 mg ml^{-1} dextran 70		300 mg ml^{-1} dextran 70	
[GdnHCl](M)	T_m	ΔH_m	T_m	ΔH_m	T_m	ΔH_m
0.25	374.2	126.0	-	-	-	-
0.5	368.2	120.0	371.1	125.0	373.0	127.0
1.0	367.3	115.0	368.9	118.7	367.1	120.0
1.5	358.6	105.0	364.4	113.0	364.1	115.0
2.3	353.4	97.0	357.4	104.0	359.9	109.0
2.8	349.6	90.0	353.6	99.0	356.0	105.0

*ΔH_m and T_m are reported as kcal mol^{-1} and K, respectively. The uncertainties associated with ΔH_m and T_m are ±1.0 kcal mol^{-1} and ±0.5 K, respectively. GdnHCl concentrations are uncorrected for crowding agents (for each crowding agent concentration, the correct concentrations of GdnHCl were calculated by using equation 10 of chapter 2.

Table 3. Effect of crowding agents on [urea]-dependent T_m and ΔH_m of Ferrocyt *c* (CD at 222 nm) at pH 7.0 in the absence and presence of 200 mg ml^{-1} of crowding agents*.

	without crowding agents		dextran 40		dextran 70	
[Urea] (M)	T_m	ΔH_m	T_m	ΔH_m	T_m	ΔH_m
control	370.5	120.0	377.5	127	372.3	123
3.0	363.6	109.6	372.0	120	367.8	115
4.5	358.4	98.8	369.3	113	364.3	110
6.5	351.4	90.0	361.0	105	358.6	103
8.0	344.9	83.0	357.8	102	355.0	99.1
	ficoll 70					
[Urea] (M)	T_m	ΔH_m				
control	372.1	121				
3.0	367.4	113				
4.5	362.0	105				

6.5	356.9	98
8.0	351.3	90

*ΔH_m and T_m are reported as kcal mol^{-1} and K, respectively. The uncertainties of T_m and ΔH_m values reported here are ±0.5 K and ± 2.0kcal mol^{-1}, respectively. Urea concentrations are uncorrected for crowding agents counter ion experiments and correct urea concentrations were calculated by using equation 10 of chapter 2.

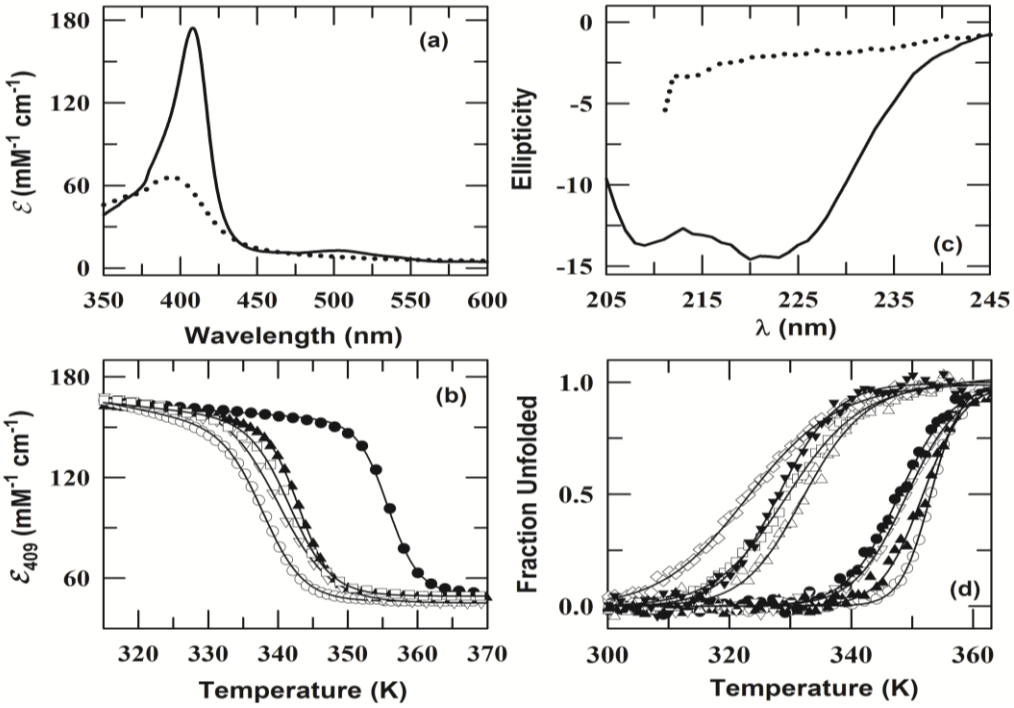

Fig.4. Effect of crowding agents on the denaturant-dependent thermal unfolding of Mb at pH 7.0. Panel (a) shows the visible absorption spectra of Mb collected at 25ºC (solid line) and 90 ºC (dotted line), pH 7.0. Panel (b) represents the thermal denaturation curves of Mb monitored at 409 nm as change in excitation coefficient in absence of additives (●) and in the presence of 0.5 M GdnHCl (▲), 0.5 M GdnHCl with 200 mg ml^{-1} of crowding agent (dextran 40 (▲), dextran 70 (▽) and ficoll 70 (○)). Panel (c) represents far-UV CD spectra of Mb collected at 25ºC (solid line) and 90 ºC (dotted line), pH 7.0. (d) Normalized thermally induced unfolding curves of Mb monitored at CD-222 nm in the presence of 1 M urea (○), 4.5 M urea (Δ) and 1 M urea with 100 mg ml^{-1} dextran 70 (▽), 4.5 M urea with 100 mg ml^{-1} dextran 70 (▼), 1 M urea with 100 mg ml^{-1} dextran 40 (▲), 4.5 M urea with 100 mg ml^{-1} dextran 40 (□), 1M urea with 100 mg ml^{-1} ficoll 70 (●), 4.5 M urea with 100 mg ml^{-1} ficoll 70 (◊), at pH 7.0. The solid curves in panels (b) and (d) represent nonlinear least-squares fits to two-state van't Hoff equation(Equation (5), chapter 2) [65].

The T_m and ΔH_m values for Mb at various [GdnHCl] (Table 4) and [urea] (Table 5) both in the absence and presence of crowding agent are provided in Table 4 and Table 5. Fig. 5a and 5b present the variations in T_m and ΔH_m for Ferrocyt *c* (at 550 nm), respectively as a function of [GdnHCl] in the absence and presence of 100 and 200 mg ml^{-1} of dextran 70, 100 mg ml^{-1} of ficoll 70, and 100 mg ml^{-1} of dextran 40 at pH 7.0. Fig. 5c and Fig. 5d show the variations in T_m and ΔH_m for Ferrocyt *c* (CD at 222nm), respectively as a function of [Urea] in the absence and presence of 200 mg ml^{-1} of dextran 70, ficoll 70 and dextran 40 at pH 7.0. Fig. 6a and Fig. 6b show the variations in T_m and ΔH_m for Mb (absorbance at 409 nm), respectively as the function of

[GdnHCl] in the absence and presence of 200 mg ml^{-1} of dextran 70, ficoll 70 and dextran 40 at pH 7.0. Fig. 6c and Fig. 6d show the variations in T_m and ΔH_m for Mb (CD (at 222nm)), respectively as a function of [Urea] in the absence and presence of 100 mg ml^{-1} of dextran 70, ficoll 70 and dextran 40 at pH 7.0.

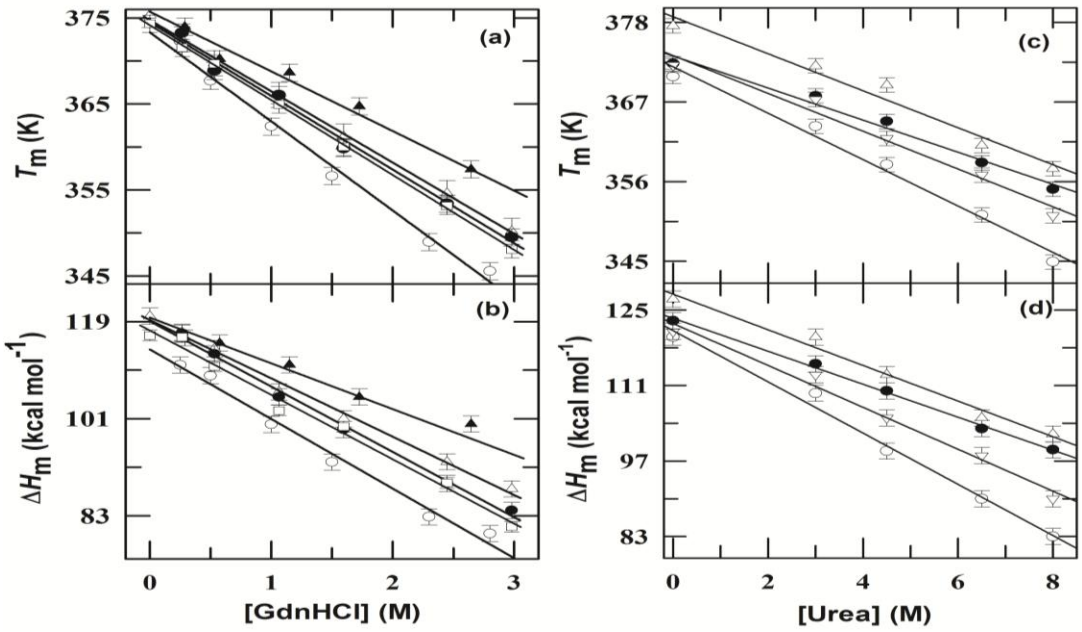

Fig.5. Effect of crowding agents on the denaturant-dependent T_m and ΔH_m of Ferrocyt *c* at pH 7.0. Panels (a) and (b) shows the variations in T_m and ΔH_m, respectively for Ferrocyt *c* (absorbance 550 nm) as the function of [GdnHCl] in the absence (○) and presence of 100 mg ml^{-1} (dextran 40 (Δ), dextran70 (●), ficoll70 (□)) and 200 mg ml^{-1} of dextran 70 (▲) at pH 7.0. Panels (c) and (d) shows the variations in T_m and ΔH_m, respectively for Ferrocyt *c* (CD 222 nm) as the function of [urea], in the absence (○), and presence of 200 mg ml^{-1} crowding agent (dextran 40 (Δ), dextran70 (●) and ficoll 70 (▽)) at pH 7.0. The parameters are summarized in Table 2 (Absorbance 550 nm) and Table 3 (CD 222 nm). The solid lines in panels (a) to (d) represent linear least-squares fit of the data.

Table 4. Effect of crowding agents on [GdnHCl]-dependent T_m and ΔH_m of Mb at pH 7 as monitored by visible absorbance at 409 nm*.

	without crowding agents		200 mg ml^{-1} ficoll 70		200 mg ml^{-1} dextran 40	
[GdnHCl](M)	T_m	ΔH_m	T_m	ΔH_m	T_m	ΔH_m
0.0	355.4	121.8	349.7	108.5	353.1	113.0
0.1	352.8	117.6	346.5	98.5	347.6	106.7
0.25	348.9	108.2	343.5	92.5	345.3	96.9
0.5	343.2	95.7	340.2	82.6	343.0	87.9
0.75	339.0	82.1	334.6	69.0	335.1	75.0
1.0	333.4	72.0	330.0	63.0	333.1	67.0
	200 mg ml^{-1} dextran 70					
[GdnHCl](M)	T_m	ΔH_m				
0.0	352.2	111.0				
0.1	347.3	100.0				

0.25	344.7	94.7
0.5	341.8	85.4
0.75	334.8	71.8
1.0	332.6	65.9

*ΔH_m and T_m are reported as kcal mol^{-1} and K, respectively. The uncertainties associated with ΔH_m, T_m and ΔG_T are ±1.0 kcal mol^{-1} and ±0.5 K, respectively. GdnHCl concentrations are uncorrected for crowding agents (for each crowding agent concentration, the correct concentration of GdnHCl were calculated by using equation 10 of chapter 2.

Table 5. Effect of crowding agents on [Urea]-dependent T_m and ΔH_m of Mb (CD at 222 nm) at pH 7.0, in the absence of presence of 100 mg ml^{-1} crowding agents*.

	without crowding agents		dextran 40		dextran 70	
[Urea](M)	T_m	ΔH_m	T_m	ΔH_m	T_m	ΔH_m
0.0	356.0	118.3	354.8	114.1	354.0	110.6
1.0	353.0	110.3	351.8	104.9	350.0	101.1
2.0	347.3	97.7	345.6	92.9	344.0	89.6
3.0	342.0	86.1	340.9	80.6	340.0	77.9
4.5	336.6	72.9	335.0	67.4	333.4	62.5

	ficoll 70	
[Urea](M)	T_m	ΔH_m
0.0	351.9	107.0
1.0	348.2	98.0
2.0	343.1	87.7
3.0	338.6	74.7
4.5	332.3	60.6

*ΔH_m and T_m are reported as kcal mol^{-1} and K, respectively. The uncertainties of T_m and ΔH_m reported here are ±0.5 °K and ± 2.0kcal mol^{-1}, respectively. Urea concentrations are uncorrected for crowding agents counter ion experiments and correct urea concentrations, were calculated by using equation 10 of chapter 2.

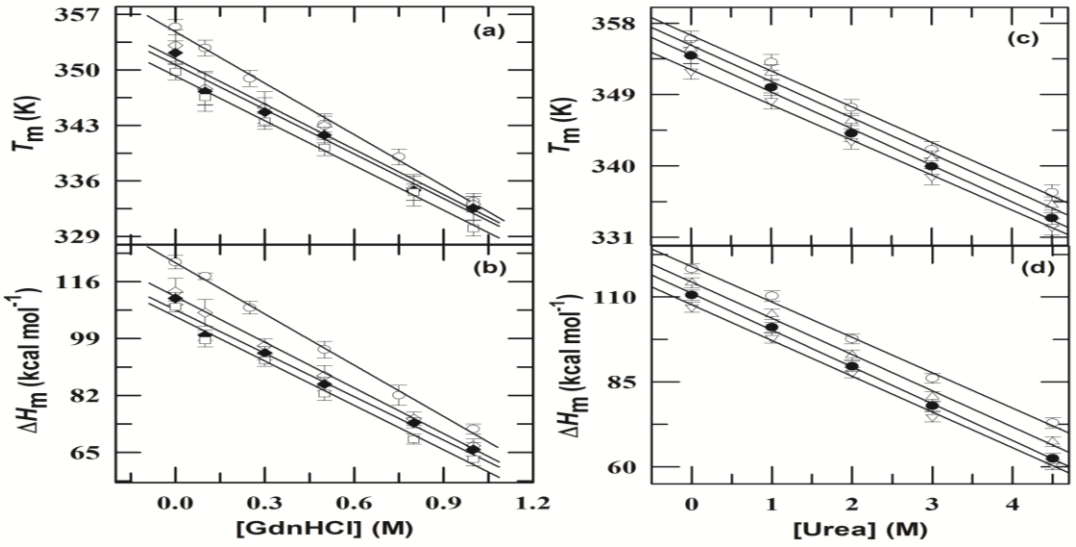

Fig.6. Effect of crowding agents on the denaturant-dependent T_m and ΔH_m of Mb at pH 7.0. Panels (a) and (b) show the variations in T_m and ΔH_m, respectively for Mb (absorbance 409 nm) as the function of [GdnHCl] in the absence (○), and presence of 200 mg ml^{-1} crowding agent (dextran 40 (Δ), dextran70 (●), ficoll70 (□)) at pH 7.0. Panels (c) and (d) show the variation in T_m and ΔH_m, respectively for Mb (CD 222 nm) as the function of [urea] in the absence (○), and presence of 100 mg ml^{-1} crowding agent (dextran 40 (Δ), dextran70 (●), ficoll70 (▽)) at pH 7.0. The

parameters are summarized in Table 4 (absorbance 409 nm) and Table 5 (CD 222 nm). The solid lines in panels (a) to (d) represent linear least-squares fit of the data.

The T_m and ΔH_m values for Ferrocyt *c* decrease linearly with [Denaturant], however in the presence of crowding agent, the T_m and ΔH_m values decrease to a lesser extent (Figs.5a, 5b, 5c, 5d, Table 2 and Table 3) then in its absence, indicating that the crowding agents counteract the destabilizing action of the denaturant on the thermal stability of Ferrocyt *c* at pH 7.0. The counteraction effect of crowding agent on the destabilizing action of the denaturant on the thermal stability of Ferrocyt *c* typically follows the order, dextran 40 > dextran 70 > ficoll 70 (Figs.5a, 5b, 5c, 5d, Table 2 and Table 3), which reveals that the size and shape of crowding are the key factors that modulate the effect of macromolecular crowding on thermal stability of Ferrocyt *c*.

The effect of crowding on protein stability can be protein specific and generally depends on the crowder-to protein size ratio and geometry of crowders [48]. The T_m and ΔH_m values for Mb decrease linearly with [denaturant], however in the presence of crowding agent. The T_m and ΔH_m values decrease to a larger extent (Figs.6a, 6b, 6c, 6d, Table 4, Table 5). This finding indicates that the crowding agent shows an additive effect with the destabilizing action of the denaturant on the thermal stability of Mb at pH 7.0. The additive effect of crowding agent on the destabilizing action of the denaturant on the thermal stability of Mb typically follows the order, ficoll 70 > dextran 70 > dextran 40 (Figs.6a, 6b, 6c, 6d, Table 4, Table 5), which reveals that the size and shape of crowding are the key factors that influences the effect of macromolecular crowding on thermal stability of Mb. The probable explanation for decrease in stability of Mb in the presence of crowding agent is the change in accessible surface area (ASA) of Mb while unfolding [66].

4.2.4 Effects of crowding agents on the denaturant-dependent thermodynamic stability of Ferricyt c and Mb

Fig.7a shows the representative normalized urea-induced unfolding curves of Ferricyt *c* measured in the absence of additives and at 1.0 M GdnHCl in the absence and presence of ~100 mg ml^{-1} of crowding agents (dextran 40, dextran 70 and ficoll 70) at pH 7.0, 25 ºC. Fig. 7b shows the representative the normalized urea-induced unfolding curves of Mb measured in the absence of additives and at 0.5 M GdnHCl in the absence and presence of 100 mg ml^{-1} of crowding agents (dextran 40, dextran 70 and ficoll 70) at pH 7.0, 25 ºC. Fig. 7a and 7b show that the inclusion of

GdnHCl shifts the urea induced unfolding curves of Ferricyt *c* and Mb to lower urea concentrations. However, in the presence of 100 mg ml^{-1} of crowding agents (dextran 40, dextran 70 and ficoll 70), the GdnHCl-triggered shift in the urea-induced unfolding curve is less pronounced for Ferricyt *c* (Fig. 7a) but more pronounced for Mb (Fig. 7b). The urea-induced unfolding curves of Ferricyt *c* and Mb were analyzed by assuming a two state transition between the folded (N) and unfolded (U) conformations by using the procedure of Santoro and Bolen (Equation (7), chapter 2) [67]. The urea-unfolding midpoint, C_m (=$\Delta G_D/m_g$), for different GdnHCl concentrations was also calculated in the absence and presence of 100 mg ml^{-1} dextran 40, dextran 70 and ficoll 70 at pH 7.0, 25ºC. The resulting values of ΔG_D, m_g and C_m are given in Table 6 and Table 7 for Ferricyt *c* and Mb, respectively. ΔG_D and C_m decrease linearly with GdnHCl concentration (Fig. 7c, 7d, 7e and 7f). However, in the presence of crowding agent (dextran 40, dextran 70 and ficoll 70), the decrease in ΔG_D and C_m with [GdnHCl] is less pronounced for Ferricyt *c* (Fig. 7c and 7e) and more pronounced for Mb (Figs. 7d and 7f). These results suggest that the presence of crowding agent in reaction medium counteracts the denaturing action of GdnHCl in case of Ferricyt *c* while it shows an additive effect on the denaturing action of GdnHCl in case of Mb. The counteracting ability of crowding agent towards the denaturing action of GdnHCl for Ferricyt *c* typically follows the order, dextran 40 > dextran 70 > ficoll 70 (Fig. 7c and 7e), which suggests that the size and shape of crowding agents are the key factors that modulate the counteracting ability of crowding agent towards the denaturing action of GdnHCl on thermodynamic stability of Ferricyt *c*. The additive effect of crowding agent with the denaturing action of GdnHCl for Mb typically follows the order, ficoll 70 > dextran 70 > dextran 40 (Figs. 7d and 7f), which reveals that size and shape of crowding are the key factors that influences the additive effect of crowding agent towards the denaturing action of GdnHCl on thermodynamic stability of Mb.

Table 6. Dependence of the ΔG_D, m_g and C_m of Ferricyt *c* on [GdnHCl] in the absence and presence of 100 mg ml^{-1} crowding agents at pH 7.0 as monitored by Trp fluorescence (ex: 280; em: 365nm)*.

	without crowding agents			100 mg ml^{-1} dextran 40		
[GdnHCl] (M)	C_m (M)	ΔG_D (kcal mol^{-1})	m_g (kcal$mol^{-1}M^{-1}$)	C_m (M)	ΔG_D (kcal mol^{-1})	m_g (kcalmol^{-1} M^{-1})
0.0	7.6	8.6	1.1	8.6	11.8	1.4
0.25	6.3	7.9	1.2	7.4	9.5	1.3
0.5	5.6	6.9	1.2	6.5	8.0	1.2
1.0	4.3	5.7	1.3	5.3	6.9	1.3

2.0	2.0	3.1	1.5	2.8	4.7	1.7
	100 mg ml^{-1} dextran 70			100 mg ml^{-1} ficoll 70		
[GdnHCl] (M)	C_m (M)	ΔG_D (kcal mol^{-1})	m_g (kcalmol^{-1} M^{-1})	C_m (M)	ΔG_D (kcal mol^{-1})	m_g (kcalmol^{-1} M^{-1})
0.0	8.4	11.1	1.3	8.3	10.3	1.2
0.25	7.2	9.1	1.3	7.2	8.6	1.2
0.5	6.4	7.4	1.2	6.3	7.3	1.2
1.0	5.2	6.5	1.2	5.1	6.0	1.2
2.0	2.7	4.5	1.6	2.6	4.0	1.6

*The uncertainties associated with ΔG_D, m_g, and C_m are ±0.5 (kcal mol^{-1}), ±0.2 (kcal mol^{-1} M^{-1}) and ±0.2 (M), respectively.

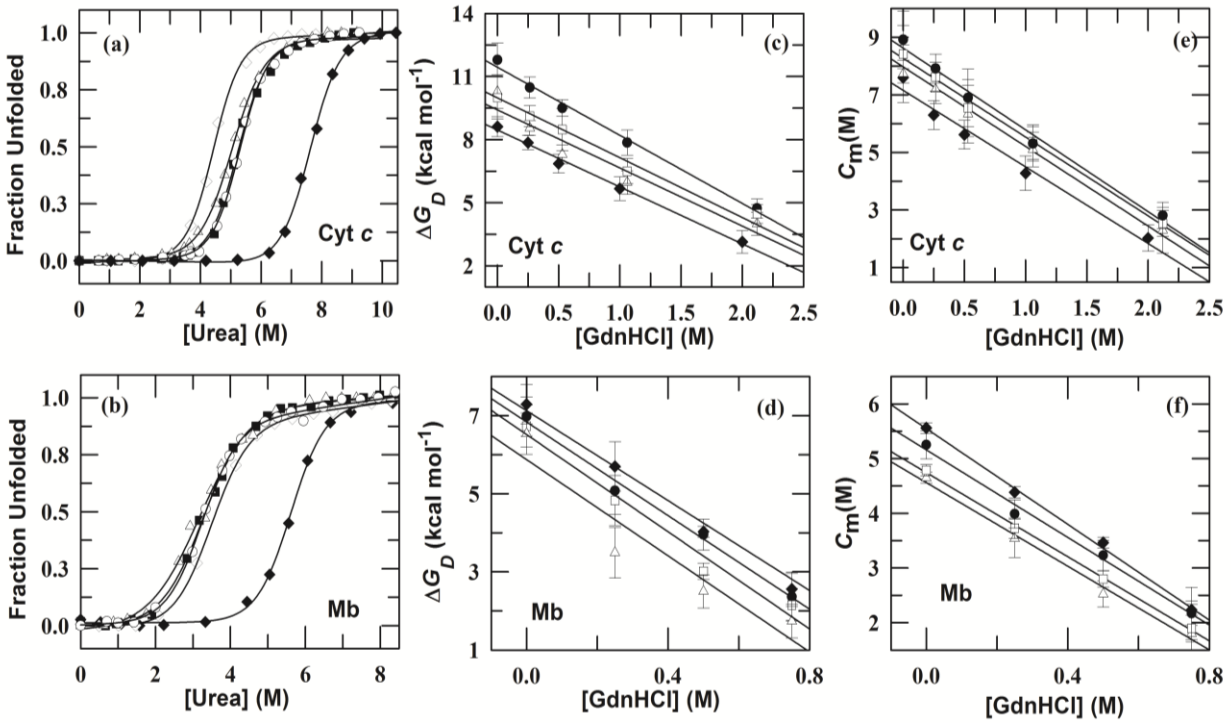

Fig.7. Effects of crowding agents on the denaturant-dependent thermodynamic stability of Ferricyt *c* and Mb at pH 7.0. Panel (a) show the fluorescence-monitored normalized urea-induced unfolding curves of Ferricyt *c* measured in the absence (◆), presence of 1 M GdnHCl (◇) and 1 M GdnHCl with 100 mg ml^{-1} of dextran 70 (□), dextran 40 (●), ficoll 70 (Δ) at pH 7.0 and 25°C. Panel (b) shows the fluorescence-monitored normalized urea-induced unfolding curves of Mb in the absence (◆) and presence of 0.5 M GdnHCl (◇) and 0.5 M GdnHCl with 100 mg ml^{-1} of dextran 70 (□), dextran 40 (●), ficoll 70 (Δ) at pH 7.0 and 25°C. The solid curves represent nonlinear least-squares fits according to the standard two-state equation (Equation (7), chapter 2) [67]. Panel (c) and (d) show the GdnHCl-dependence variation of the change in unfolding free energy, ΔG_D, for Ferricyt *c* and Mb, respectively in the absence of crowder (◆) and in the presence of 100 mg ml^{-1} of dextran 40 (●), dextran 70 (□) and ficoll 70 (Δ) at pH 7.0 and 25 °C. Panel (e) and (f) show the GdnHCl-dependence variation of the urea unfolding midpoint, C_m, of Ferricyt *c* and Mb, respectively in the absence of crowder (◆) and in the presence of 100mg ml^{-1} of dextran 40(●), dextran 70 (□) and ficoll 70 (Δ) at pH 7.0 and 25 °C. The thermodynamic parameters are listed in Table 6 (Ferricyt *c*) and Table 7 (Mb). The solid lines in panel (c), (d), (e) and (f) represent linear least-squares fit of the data.

Table 7. Dependence of the ΔG_D, m_g and C_m of Mb on [GdnHCl] in the absence and presence of 100 mg ml^{-1} crowding agents at pH 7.0 as monitored by fluorescence (ex: 280; em: 365nm)*.

	without crowding agents			100 mg ml^{-1} dextran 40		
[GdnHCl] (M)	C_m (M)	ΔG_D (kcal mol^{-1})	m_g ($kcalmol^{-1}M^{-1}$)	C_m (M)	ΔG_D (kcal mol^{-1})	m_g ($kcalmol^{-1}$ M^{-1})
0.0	5.6	7.3	1.3	5.3	7.0	1.3
0.25	4.5	5.7	1.3	3.8	5.1	1.3
0.5	3.5	4.0	1.2	3.2	4.0	1.2
0.75	3.1	2.6	1.1	2.3	2.4	1.1
	100 mg ml^{-1} dextran 70			100 mg ml^{-1} ficoll 70		
[GdnHCl] (M)	C_m (M)	ΔG_D (kcal mol^{-1})	m_g ($kcalmol^{-1}$ M^{-1})	C_m (M)	ΔG_D (kcal mol^{-1})	m_g ($kcalmol^{-1}$ M^{-1})
0.0	4.8	6.7	1.4	4.7	6.5	1.4
0.25	3.7	4.8	1.3	3.5	3.5	1.0
0.5	3.1	3.0	1.0	2.9	2.5	0.9
0.75	1.9	2.2	1.1	1.8	1.7	1.0

*The uncertainties associated with ΔG_D, m_g, and C_m are ±0.8 (kcal mol^{-1}), ±0.1 (kcal mol^{-1} M^{-1}) and ±0.3 (M), respectively.

Briefly, the thermodynamic stability of protein depends on the type of protein, geometry of crowders or size and shape of crowders, as the key factors defining the net effect of excluded volume on protein biophysics [48].

4.2.5 Effect of crowding agents on the denaturant dependent-secondary structure of Ferricyt c and Mb

In the far-UV region (200-250 nm), the CD spectrum of native protein is characterized by negative Cotton effects at ~210 nm and 222 nm, typical of proteins with α-helix structure. Fig. 8a presents the far-UV CD spectra of Ferricyt *c* collected in the absence and presence of 200mg ml^{-1} of dextran 40, dextran 70 and ficoll 70 with 2 and 10 M of urea at pH 7.0, 25 °C. Fig. 8b presents the far-UV CD spectra of Mb collected in the absence and presence of 200mg ml^{-1} of dextran 40, dextran 70 and ficoll 70 with 2 and 10 M of urea at pH 7.0, 25 °C. Figs. 8a and 8b demonstrate that the crowding agents presence not greatly alter the secondary structures of native and denatured states of Ferricyt *c* and Mb at pH 7, 25 ºC.

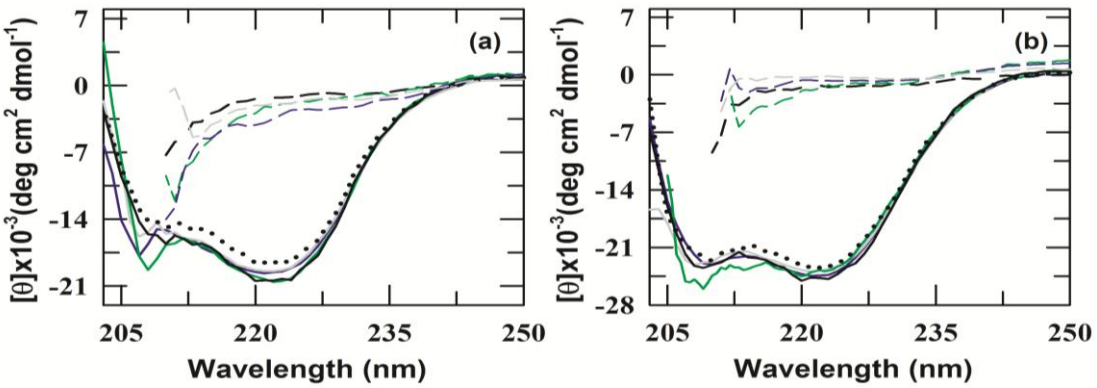

Fig.8. Effect of crowding agents on the denaturant dependent-secondary structure of Ferricyt *c* and Mb at pH 7.0. Panel (a) shows the far-UV CD spectra of Ferricyt *c* collected in the absence of crowding agents (solid black line) and in presence of ~ 2M urea (dotted black line), 10 M urea (black short line) and with 200mg ml^{-1} of dextran 40 (2M urea (blue solid line), 10 M urea (blue short line)), dextran 70 (2M urea (green solid line), 10 M urea (green short line)) and ficoll 70 (2M urea (gray solid line), 10 M urea (gray short line)) at pH 7, 25 °C. Panel (b) shows the far-UV CD spectra of Mb collected in the absence of additives (solid black line) and in presence of ~ 2M urea (dotted black line), 10 M urea (black short line) and with 200mg ml^{-1} of dextran 40 (2M urea (blue solid line), 10 M urea (blue short line)), dextran 70 (2M urea (green solid line), 10 M urea (green short line)) and ficoll 70 (2M urea (gray solid line), 10 M urea (gray short line)) at pH 7, 25 °C.

4.3 Conclusion

Analysis of kinetic and thermodynamic parameters measured for CO dissociation reaction of NCO under various concentrations of GdnHCl and urea at fixed concentrations of crowding agents (dextran 40, dextran 70 and ficoll 70) at pH 7.0 reveals that (i) subdenaturing concentrations of denaturants constrain the internal dynamics of NCO while higher concentrations of denaturants increase the level of structural fluctuations that cause unfolding of the protein (ii) within subdenaturing region, crowding agent produce a cumulative effect on the denaturant mediated restricted internal dynamics of NCO (iii) size, shape and viscosity of crowding agents are the key factors that modulate the denaturant-mediated restricted internal dynamics of NCO (iv) in the denaturing region, the inclusion of crowding agent opposes the structural fluctuation that cause unfolding of the protein, (v) the size, shape and viscosity of crowding agents are the key factors that modulate the denaturant-mediated structural fluctuation that cause unfolding of the protein (vi) subdenaturing concentrations of denaturants increase the $\Delta H_{diss}^{\ddagger}$ and which is found to be increased more in the presence of crowding agents then in its absence, (vi) high concentrations of denaturants decrease the $\Delta H_{diss}^{\ddagger}$ and which is found to be less decreased in the presence of crowding agents then in its absence, which suggests that the crowding agent produces the counteraction effect on the denaturant-mediated structural fluctuation that unfolds the protein,

and (vii) the crowding-mediated increase in $\Delta H_{diss}^{\ddagger}$ is accompanied by a decrease in the entropy change, $-T\Delta S_{diss}^{\ddagger}$.

Thermodynamic analysis of thermal and urea-induced unfolding curves of Ferrocyt *c* and Mb measured at varying concentrations of GdnHCl in the absence and presence of fixed concentrations of crowding agents (dextran 40, dextran70 and ficoll 70) reveals that: (i) the presence of crowding agent in reaction medium counteracts the denaturing action of GdnHCl in case of Ferricyt *c* while it shows an additive effect on the denaturing action of GdnHCl in case of Mb (ii) the counteracting ability of crowding agent towards the denaturing action of GdnHCl for Ferricyt *c* typically follows the order, dextran 40 > dextran 70 > ficoll 70, which reveals that the size and shape of crowding agents are the main factors that modulate the counteracting ability of crowding agent towards the denaturing action of GdnHCl on thermodynamic stability of Ferricyt *c*, and (iii) The additive effect of crowding agent with the denaturing action of GdnHCl for Mb typically follows the order, ficoll 70 > dextran 70 > dextran 40 (Figs. 7d and 7f), which reveals that size and shape of crowding are the main factors that influences the additive effect of crowding agent towards the denaturing action of GdnHCl on thermodynamic stability of Mb.

4.4 References:

1. A.B. Fulton, *Cell* **30** (1982) 345–347.
2. D.S. Goodsell, *Trends Biochem. Sci.* **16** (1991) 203–220.
3. M.S. Cheung, D. Klimov, D. Thirumalai, *Proc. Nat. Acad. Sci. USA* **13** (2005) 4753–4758.
4. S.B. Zimmerman, S.O. Trach, *J. Mol. Biol.* **222** (1991) 599−620.
5. G. Rivas, F. Ferrone, J. Herzfeld, *EMBO Rep.* **5** (2004) 23−27.
6. R. J. Ellis, A. P. Minton, *Nature* **425** (2003) 27−28.
7. A. P. Minton, *Biopolymers* **20** (1981) 2093−2120.
8. Y. Wang, M. Sarkar, A.E. Smith, A.S. Krois, G.J. Pielak, *J. Am. Chem. Soc.***134** (2012) 16614−16618.
9. S. B. Zimmerman, A.P. Minton, *Annu. Rev. Biophys. Biomol. Struct.* **22** (1993) 27–65.
10. A. P. Minton, *J. Cell Sci.***119** (2006) 2863-2869.
11. R. J. Ellis, *TIBS* **26** (2001) 597–604.
12. L. A. Benton, A.E. Smith, G.B. Young, G.J. Pielak, *Biochemistry* **51** (2012) 9773−9775.

13. S. N. Timasheff, *Annu. Rev. Biophys. Biomol. Struct.* **22** (1993) 67−97.
14. M. Senske, L. Törk, B. Born, M. Havenith, C. Herrmann, S. Ebbinghaus, *J. Am. Chem. Soc.* **136** (2014) 9036−9041.
15. G. I. Makhatadze, P. L. Privalov, *J. Mol. Biol.* **226** (1992) 491−505.
16. K. Sasahara, P. McPhie, A.P. Minton, *J Mol Biol* **326** (2003)1227–1237.
17. A. Dhar, A. Samiotakis, S. Ebbinghaus, L. Nienhaus, D. Homouz, M. Gruebele, M.S. Cheung, *Proc. Natl. Acad. Sci. U S A* **107** (2010) 17586-17591.
18. K. Aoki, M. Yamada, K. Kunida, S. Yasuda, M. Matsuda, *Proc. Natl. Acad. Sci. U S A* **108** (2011) 12675–12680.
19. Y. Wang, C. Li, G. J. Pielak, *J Am. Chem. Soc.* **132** (2010) 9392–9397.
20. S.R. McGuffee, A. H. Elcock, *PLoS Comput Biol* **6** (2010) e1000694.
21. C. Leduc, K. Padberg-Gehle, V. Varga, D. Helbing, S. Diez, J. Howard, *Proc. Natl. Acad. Sci. USA* **109** (2012) 6100–6105.
22. J. Batra, K. Xu, S. Qin, H. X. Zhou, *Biophys. J.* **97** (2009) 906–911.
23. L. Huang, R. Jin, J. Li, K. Luo, T. Huang, D. Wu, W. Wang, R. Chen, G. Xiao, *FASEB J.* **24** (2010) 3536–3543.
24. Z. Zhou, X. Yan, K. Pan, J. Chen, Z. S. Xie, G. F. Xiao, F. Q. Yang, Y. Liang, *Biophys. J.* **101** (2011) 1483–1492.
25. B.V. Berg, R. J. Ellis, C.M. Dobson, *EMBO J.* **18** (1999) 6927–6933.
26. K. X. X. Yong, T. J. Shakespeare, D. Cash, S. M. D. Henley, J. M. Nicholas, G. R. Ridgway, H. L. Golden, E. K. Warrington, A. M. Carton, D. Kaski, J. M. Schott, J. D. Warren, S. J. Crutch, *Brain* **137** (2014) 3284–3299.
27. E. Rivera, J. Straub, D. Thirumalai, *Biophys. J.* **96** (2009) 4552–4560.
28. E. E. Wanker, *Mol. Med. Today.* **6** (2000) 387–391.
29. Q. Ma, J. Hu, J. Chen, Y. Liang, *Int. J. Mol. Sci.***14** (2013) 21414–21427.
30. M. Perham, L. Stagg, P. Wittung-Stafshede, *FEBS Letters* **581**(2007) 5065–5069.
31. L. Stagg, S. Zhang, M.S. Cheung, P. Wittung-Stafshede, *Proc. Nat. Acad. Sci. USA* **48** (2007) 18976–18981.
32. A. Kudlay, M. S. Cheung, D. Thirumalai, *Phys. Rev. Lett.* **102** (2009) 118101-118104.
33. A. P. Minton, *Biophys. J.* **88** (2005) 971−985.

34. A. P. Minton, *Biophys. J.* **78** (2000) 101−109.
35. A. P. Minton, *Methods Enzymol.* **295** (1998) 127−149.
36. J. Ådén, P. Wittung-Stafshede, *Biochemistry* **53** (2014) 2271−2277.
37. G. B. Ralston, *J. Chem. Edu.* **67** (2005) 857–860.
38. S. B. Zimmerman, S.O. Trach, *Biochim. Biophys. Acta* **949** (1988) 297–304.
39. P. E. Lavery, S. C. Kowalczykowski, *J. Biol. Chem.* **267** (1992) 9307–9314.
40. B. R. Somalinga, R. P. Roy, *J. Biol. Chem.* **277** (2002) 43253–43261.
41. J. M. Liao, Z. Y. Mo, L. J. Wu, J. Chen, Y. Liang, *Biochim. Biophys. Acta* **1784** (2008) 1560–1569.
42. I. Pozdnyakova, P. Wittung-Stafshede, *Biochim. Biophys. Acta* **1804** (2010) 740–744.
43. I. Pastor, E. Vilaseca, S. Madurga, J. L. Garces, M. Cascante, F. Mas, *J. Phys. Chem. B* **115** (2011) 1115–1121.
44. M. K. Suthar, P. K. Doharey, A. Verma, J. K. Saxena, *Int. J. Biol. Macromol.***62** (2013) 657–662.
45. M. Jiang, Z. Guo, *J. Am. Chem. Soc.* **129** (2007)730–731.
46. S. R. Akabayov, B. Akabayov, C. C. Richardson, G. Wagner, *J. Am. Chem. Soc.* **135** (2013) 10040–10047.
47. K. Aoki, K. Takahashi, K. Kaizu, M. Matsuda, *Sci. Rep.* **3** (2013) 1541.
48. A. Christiansen, Q. Wang, A. Samiotakis, M. S. Cheung, P. Wittung-Stafshede, *Biochemistry* **49** (2010) 6519−6530.
49. M. M. Waegele, F. Gai, *J. Chem. Phys.* **134** (2011) 095104.
50. L. Stagg, A. Christiansen, P. Wittung-Stafshede, *J. Am. Chem. Soc.* **133** (2011) 646−648.
51. M. Karplus, J. A. McCammon, *Ann. Rev. Biochem.* **53** (1983) 263−300.
52. I. Bahar, T. R. Lezon, L.W. Yang, E. Eyal, *Annu Rev Biophys.* **39** (2010) 23–42.
53. H. Neuweiler, M. Lollmann, S. Doose, M. Sauer, *J. Mol. Biol.* **365** (2007) 856−869.
54. S. Mukherjee, M. M. Waegele, P. Chowdhury, L. Guo, F. Gai, *J. Mol. Biol.* **393** (2009) 227−236.
55. E. Chen, A. Christiansen, Q. Wang, M. S. Cheung, D.S. Kliger, P. Wittung-Stafshede, *Biochemistry* **51** (2012) 9836−9845.
56. R. Kumar, D. Sharma, R. Jain, S. Kumar, R. Kumar, *Biophys Chem.* **207** (2015) 61−73.

57. R. Kumar, N. P. Prabhu, M. Yadaiah, A. K. Bhuyan, *Biophys. J.* **87** (2004) 2656−2662.
58. R. Jain, D. Sharma, R. Kumar, *J. Biochem.* **154** (2013) 341-354.
59. K. A. Granath, *J. Colloid Sci.* **13** (1958) 308–328.
60. J. Shin, A.G. Cherstvya, R. Metzler, *Soft Matter* **11** (2015) 472–488.
61. S. Mukherjee, M. M. Waegele, P. Chowdhury, L. Guo, F. Gai, *J. Mol. Biol.* **393** (2009) 227–236.
62. A. B. Goins, H. Sanabria, M. N. Waxham, *Biophysical J.* **95** (2008) 5362–5373.
63. J. Shin, A.G. Cherstvy, R. Metzler, *Soft Matter*. **11 (**2015) 472−488.
64. J. Mikšovská, J.H. Day, R.W. Larsen, *J. Biol. Inorg. Chem.* **8** (2003) 621−625.
65. M.M. Santoro, D.W. Bolen, *Biochemistry* **31** (1992) 4901–4907.
66. A. Malik, J. Kundu, S. K. Mukherjee, P. K. Chowdhury, *J. Phys. Chem. B* **116** (2012) 12895−12904.
67. M. M. Santoro, D. W. Bolen, *Biochemistry* **27**(1988) 8063−8068.

Chapter 5

Role of Amino Acids on the Stability, Folding, and Internal Dynamics of Cytochrome *c* and Myoglobin

5.1 Introduction

In living organisms, proteins are surrounded by a variety of micro- and macro-biomolecules, including free amino acids, carbohydrates, lipids, cytoskeletons, and ribosomes [1].These exceeding macromolecules (*e.g.,* 300–400 mg/ml in *Escherichia coli*) [2] can influence the various biochemical and biophysical properties of protein molecules [3-6]. In general, the living organisms carry out their biological function in favorable physiological conditions. However, the significant deviations in any environmental condition will immediately prompt to adaptive response mechanisms [7]. Due to the adaptive response mechanisms, the living organism, like plants and micro-organisms accumulate various types of low molecular-mass organic compounds. Protective osmolytes generally accumulate under very harsh or stress conditions, like heat stress, salt stress, water stress or cold stress [8]. The naturally occurring osmolytes are polyhydric alcohols, free amino acids and their derivatives, and combinations of urea and methylamines [8-9]. Previous *in vitro* studies on the structure and function of different enzymes and proteins suggest that these osmolytes stabilize protein against harsh or stress conditions [8, 10-20]. Protecting osmolytes are compatible to the macromolecular structure and function (particularly proteins) in the cells. These osmolytes generally do not interfere with enzyme activities or functional structures of the proteins [8]. Compatible osmolytes also enhance the stability of macromolecules, mainly proteins [21-24]. Amino acids and other compatible osmolytes protect and stabilize the proteins during freezing and freeze-drying and in the dried state [25-37]. Thus amino acids can be used as a stabilizer and protector of proteins, during stringent conditions without affecting their function.

Polyols and certain amino acids are generally used to enhance protein stability for biochemical and biophysical analysis [10, 21-24, 38-42]. In pharmaceutical industries, the proteins are the major therapeutic agents and are also the major targets of drugs. The excipients (solvent additives) generally play a vital role in purification, processing and storage of the

therapeutic proteins. Therapeutic proteins require more stringent environment to ensure long term storage stability [43-44]. Amino acids, like arginine, glycine, proline, alanine, and lysine are generally used as excipients in pharmaceutical industries. Sugars (glycerol, sucrose, and xylitol), salts, buffers (phosphates, and citrates), surfactants (polysorbate 20), etc., are also used as excipients [45]. The use of excipients or solvents on proteins were depends on its concentration, effects, and functioning mechanism [45-46]. Under different stringent environmental conditions, the amino acids as excipients preferably enhance the stability of proteins [8]. Amino acids prevent the biomacromolecules (i.e., proteins and enzymes) from salt stress, water stress, cold stress and heat stress [8, 47-48]. There are several reports available on the effect of amino acids on protein stability and as osmolytes [10, 21, 24, 49-53]. Most of these reports discussed the effects of amino acids in terms of the biotechnological applications, such as protein purification, refolding of expressed proteins, and prevention of aggregate formation of newly expressed protein [54-67].

While the effects of amino acid on thermodynamic stability of proteins have been studied [10, 49], the effects of amino acids on the internal dynamics of proteins are not explored so far. This chapter investigates the effects of amino acids on the thermodynamic stability and internal dynamics of heme proteins (cytochrome *c* (Cyt *c*) and myoglobin (Mb)) at pH 7.0. The effects of amino acids on thermodynamic stability of heme proteins were investigated by analyzing the thermal and chemical denaturation curves of Ferrocyt *c* and Mb measured under various concentrations of L-amino acids (alanine, arginine, glycine, proline, serine and threonine) at pH 7.0. The effects of amino acids on the internal dynamics of heme proteins were investigated by analyzing the kinetic and thermodynamic parameters measured for CO dissociation reaction of natively folded carbonmonoxycytochrome *c* (NCO) and CO replacement reaction of carbonmonoxymyoglobin (MbCO) by hexacyanoferrate ion under various concentrations of L-amino acids (alanine, arginine, glycine, proline, serine and threonine) at pH 7.0.

5.2 Results and discussion

5.2.1 Effect of amino acids on the internal dynamics of natively folded carbonmonoxycytochrome c (NCO) and carbonmonoxymyoglobin (MbCO)

Fig. 1a shows the CO-dissociation kinetic trace of natively folded carbonmonoxy cytochrome *c* (NCO) at 25ºC, pH 7.0. The intensity of the α-band (550 nm) raises with time as the CO-dissociates from NCO (Fe^{2+}-CO + M80→Fe^{2+}-M80 + CO) occurs (Fig. 1a). The increase in absorbance at the heme π→π* α-band (550 nm) in a single exponential is due to slow dissociation of CO (τ=22.0 min; Fig. 1a). The CO replacement reaction of MbCO by hexacyanoferrate ions was performed as described earlier [68]. Fig. 1b shows the CO-replacement kinetic trace of carbonmonoxymyoglobin (MbCO) by hexacyanoferrate ion at 22ºC, pH 7.0. The soret band at 421 nm disappears with time and the intensity of soret band decreases in single exponential manner (τ = 0.40 min; Fig. 1b).

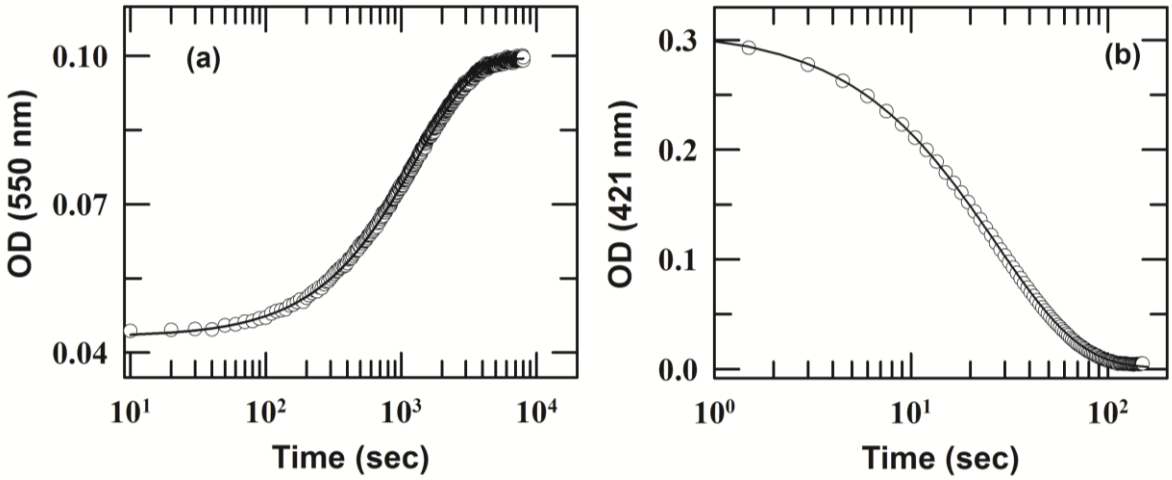

Fig.1. Kinetic profiles for thermal dissociation of CO dissociation from NCO and CO replacement of MbCO by hexacyanoferrate ion at pH 7. Panel (a) shows the slow single-phase dissociation of CO from NCO, NCO → N+CO (τ = 22 min., 25°C). The NCO→N+CO reaction was probed at 550 nm. (b) The single–phase CO-replacement from MbCO by hexacyanoferrate ion (τ=0.40 min., 22ºC). MbCO + CN^-→ MbCN + CO reaction was probed at 421 nm.

Fig. 2a and Fig. 2b show the effects of L-amino acids (alanine, arginine, glycine, proline, serine and threonine) on rates of thermal dissociation of CO from NCO (k_{diss}) and CO replacement of MbCO (k_{off}) by hexacyanoferrate ions, respectively at pH 7.0. As the [Amino acids] is increased, the values of log k_{diss} and log k_{off} decrease exponentially (Fig. 2a and Fig. 2b) (Table 1), which suggest that the amino acids retard the CO dissociation and replacement processes of NCO and MbCO, respectively at pH 7.0. This finding thus reveals that amino acid presence in reaction medium restricts the internal dynamics of NCO and MbCO at pH 7.0. The amino acids-mediated decrease in logk_{diss} and logk_{off} typically follows the order: arginine> proline> serine> glycine> alanine >threonine, which reveals that the amino acids-mediated

restricted dynamics of NCO and MbCO are more pronounced for arginine and least for threonine. It is also observed that with increase in size (stokes radii: arginine (5.32 Å) > serine (3.12 Å) > glycine (2.56 Å) > alanine (2.28 Å) [69] and hydrophobicity effect (Kyte-Doolittle scale of amino acids hydrophobicity index: arginine (-4.5) > serine (-0.8) > glycine (-0.4) > alanine (1.8) [70] of amino acids at neutral pH, the extent of amino acids-mediated constrain in the internal dynamics of NCO and MbCO increase (Fig. 2a and Fig. 2b). How could the increase in size and hydrophobic effect of amino acids increase the extent of amino acid-mediated constrained dynamics of NCO and MbCO? The fact that, the presence of three charged groups on arginine reveals a noticeable tendency to come together with head to tail hydrogen bonding [71]. At relatively high concentrations of arginine, these clusters associate with other monomeric arginine molecules to form large clusters [71]. Some previous reports revealed that the hydrogen bonds between arginine and water molecules are far weaker than the intra-hydrogen bonds formed between arginine molecules [71].

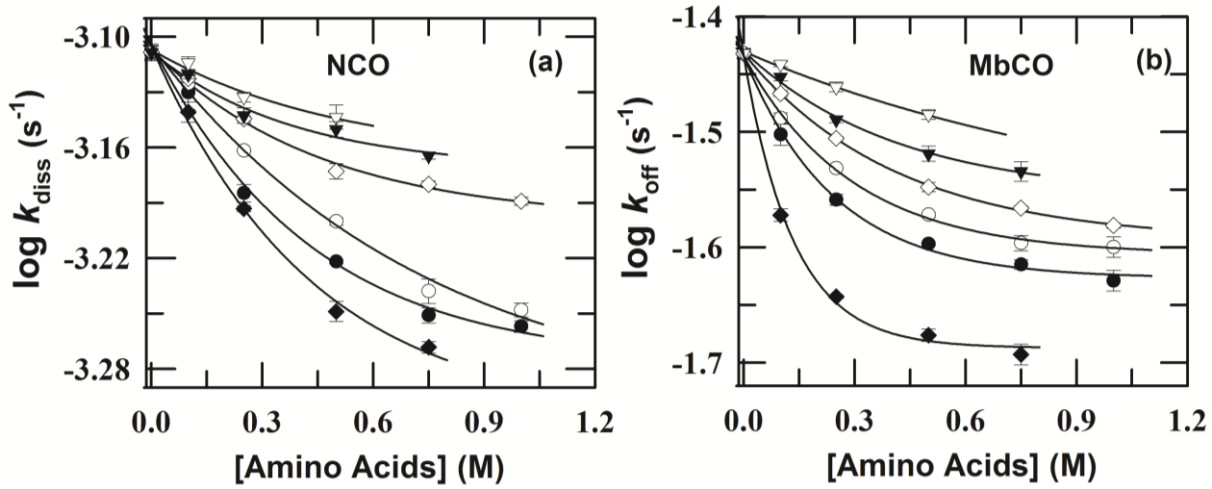

Fig.2. Effects of [amino acids] on the log k_{diss} and log k_{off} of NCO and MbCO, respectively at pH 7.0. Panels (a) and (b) show the [Amino acids] (alanine (▼), arginine (◆), glycine (◊), proline (●), serine (○) and threonine (▽)) dependence of log k_{diss} and log k_{off} of NCO (25ºC) and MbCO (22ºC), respectively at pH 7.0. The line through data has been drawn to guide the eye only. The [amino acids] dependent k_{diss} and k_{off} are listed in Table 1 at pH 7.0.

This process makes the self-association of arginine molecule enthalpically favorable [71]. The self association tendencies to form larger clusters and larger size of arginine than water in aqueous solution are likely to affect the dynamics of other macromolecules presents in the reaction medium. Some earlier reports revealed that the arginine cluster exclude out the other macromolecule present in the reaction medium and thus behaves as a "neutral crowder", an

additive that is larger than water molecules [66, 72]. This results in an increase of steric hindrance in the reaction medium and by excluding itself from the inter protein gap in reaction medium i.e. "gap effect" of arginine [66, 72]. It can be speculated that the increase of steric hindrance as well as the "gap effect" of arginine are primarily responsible for the more increased of amino acid-mediated restricted dynamics of NCO and MbCO than other amino acids.

Table 1 The effect of amino acids on k_{diss} of NCO and k_{off} of MbCO at pH 7.

Crowding agent	Conc.(M)	k_{diss} (sec^{-1})	Std. error (k_{diss})	k_{off} (sec^{-1})	Std. error (k_{off})
Control	0.0	7.79×10^{-4}	1.2×10^{-6}	3.70×10^{-2}	4.6×10^{-4}
Alanine	0.1	7.57×10^{-4}	9.8×10^{-7}	3.62×10^{-2}	9.1×10^{-5}
	0.25	7.19×10^{-4}	1.5×10^{-7}	3.46×10^{-2}	4.7×10^{-5}
	0.50	7.07×10^{-4}	4.8×10^{-7}	3.28×10^{-2}	7.0×10^{-5}
	0.75	6.84×10^{-4}	6.6×10^{-6}	3.10×10^{-2}	6.6×10^{-5}
Arginine	0.1	7.23×10^{-4}	3.4×10^{-7}	2.68×10^{-2}	8.7×10^{-5}
	0.25	6.40×10^{-4}	4.0×10^{-7}	2.28×10^{-2}	2.5×10^{-4}
	0.50	5.63×10^{-4}	7.7×10^{-7}	2.11×10^{-2}	4.0×10^{-4}
	0.75	5.39×10^{-4}	9.1×10^{-7}	2.03×10^{-2}	5.6×10^{-5}
Glycine	0.1	7.53×10^{-4}	6.2×10^{-7}	3.41×10^{-2}	1.8×10^{-4}
	0.25	7.16×10^{-4}	1.3×10^{-6}	3.12×10^{-2}	9.9×10^{-5}
	0.50	6.71×10^{-4}	7.6×10^{-7}	2.83×10^{-2}	5.8×10^{-5}
	0.75	6.60×10^{-4}	6.0×10^{-7}	2.72×10^{-2}	5.4×10^{-5}
	1.0	6.46×10^{-4}	4.7×10^{-7}	2.62×10^{-2}	1.6×10^{-4}
Proline	0.1	7.40×10^{-4}	1.1×10^{-6}	3.14×10^{-2}	1.7×10^{-4}
	0.25	6.53×10^{-4}	1.3×10^{-6}	2.76×10^{-2}	4.3×10^{-5}
	0.50	5.99×10^{-4}	2.6×10^{-6}	2.53×10^{-2}	2.2×10^{-5}
	0.75	5.61×10^{-4}	6.1×10^{-7}	2.42×10^{-2}	3.3×10^{-5}
	1.0	5.53×10^{-4}	5.3×10^{-7}	2.35×10^{-2}	6.4×10^{-5}
Serine	0.1	7.49×10^{-4}	5.9×10^{-7}	3.25×10^{-2}	1.8×10^{-5}
	0.25	6.89×10^{-4}	6.3×10^{-7}	2.94×10^{-2}	8.1×10^{-5}
	0.50	6.30×10^{-4}	5.9×10^{-7}	2.68×10^{-2}	9.2×10^{-5}
	0.75	5.78×10^{-4}	5.9×10^{-7}	2.53×10^{-2}	5.9×10^{-5}
	1.0	5.64×10^{-4}	4.8×10^{-7}	2.51×10^{-2}	2.6×10^{-4}
Threonine	0.1	7.69×10^{-4}	5.4×10^{-7}	3.62×10^{-2}	2.9×10^{-4}
	0.25	7.36×10^{-4}	7.0×10^{-7}	3.46×10^{-2}	2.4×10^{-4}
	0.50	7.18×10^{-4}	7.1×10^{-7}	3.27×10^{-2}	1.7×10^{-4}

5.2.2 Effect of amino acids on the activation thermodynamic parameters of CO-dissociation reaction of NCO and CO-replacement reaction of MbCO

Fig.3a presents the Eyring plots for CO-dissociation reaction of NCO in the absence and presence of 0.5 M amino acid (alanine, arginine, glycine, proline, serine and threonine) at pH 7.0. Fig. 3b presents the Eyring plots for CO-replacement reaction of MbCO in the absence and presence of 0.5 M amino acids (alanine, arginine, glycine, proline, serine and threonine) at pH 7.0. The activation enthalpy ($\Delta H_{diss/off}^{\ddagger}$) and activation entropy ($\Delta S_{diss/off}^{\ddagger}$) associated with CO

dissociation reaction of NCO and CO-replacement reaction of MbCO were calculated by using Eyring equation (Equation (1), chapter 2) [73]. $\Delta H_{diss/off}^{\ddagger}$ and $\Delta S_{diss/off}^{\ddagger}$ calculated in the absence and presence of 0.5 M amino acids (alanine, arginine, glycine, proline, serine and threonine) are summarized in Table 2 and Table 3. Corresponding Gibb free energy ($G_{diss/off}^{\ddagger} = \Delta H_{diss/off}^{\ddagger} - T\Delta S_{diss/off}^{\ddagger}$) and entropy change ($-T\Delta S_{diss/off}^{\ddagger}$) were also calculated and are also summarized in Table 2 and Table 3.

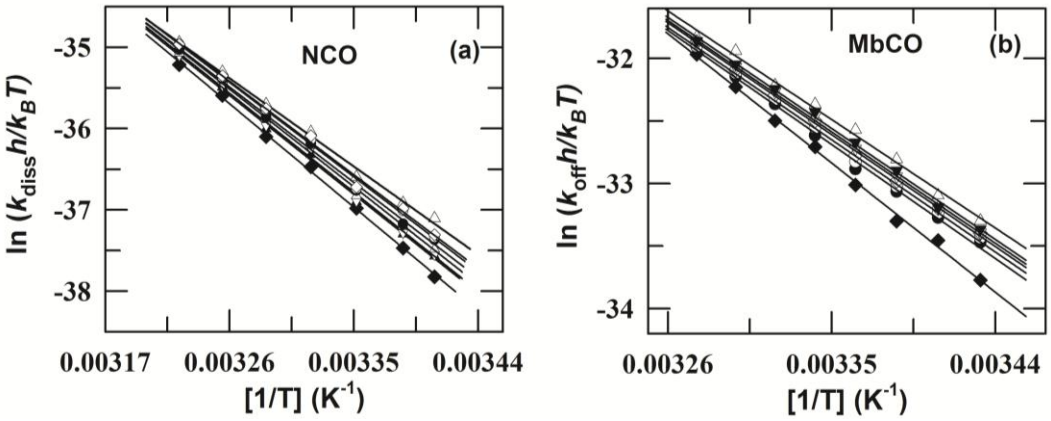

Fig.3. Effect of amino acids on the activation thermodynamic parameters of CO-dissociation reaction of NCO and CO-replacement reaction of MbCO at pH 7.0. Panel (a) shows the Eyring plots for the CO dissociation reaction of NCO in the absence (Δ) and presence of 0.5 M amino acids (alanine (▼), arginine (◆), glycine (◊), proline (●), serine (○) and threonine (▽)) at pH 7.0. Panel (b) shows the Eyring plots for the CO-replacement reaction of MbCO in the absence (Δ) and presence of 0.5 M amino acids (alanine (▼), arginine (◆), glycine (◊), proline (●), serine (○) and threonine (▽)) at pH 7.0. Respective thermodynamic parameters are listed in Table 2 (NCO) and Table 3 (MbCO).

Table 2. The effects of L-amino acids on the activation thermodynamic parameters for CO-dissociation reaction of NCO at pH 7.0.*

L-Amino acids	[Amino acids] (M)	$\Delta G_{diss}^{a\ddagger}$ (kcal mol^{-1})	$\Delta H_{diss}^{\ddagger}$ (kcal mol^{-1})	$\Delta S_{diss}^{\ddagger}$ (cal mol^{-1} K^{-1})	$-T\Delta S_{diss}^{a\ddagger}$ (kcal mol^{-1} K^{-1})
Control	0.0	21.8(0.05)	23.8(0.7)	6.9(0.2)	−2.1(0.2)
Alanine	0.5	22.1(0.08)	25.5(0.4)	12.4(1.0)	−3.4(0.2)
Arginine	0.5	22.5(0.06)	27.9(0.5)	19.7(1.6)	−5.5(0.8)
Glycine	0.5	22.1(0.04)	25.8(0.6)	13.1(1.2)	−3.6(0.5)
Proline	0.5	22.3(0.09)	26.7(0.7)	16.0(1.2)	−4.5(0.6)
Serine	0.5	22.2(0.04)	26.4(0.3)	15.0(1.1)	−4.2(0.3)
Threonine	0.5	22.1(0.05)	25.3(0.3)	11.5(1.0)	−3.2(0.4)

[a] Activation free energy ($\Delta G_{diss}^{\ddagger}$) and entropy changes ($-T\Delta S_{diss}^{\ddagger}$) are at 25ºC.
*The uncertainties (std. error) in $\Delta G_{diss}^{\ddagger}$, $\Delta H_{diss}^{\ddagger}$, $\Delta S_{diss}^{\ddagger}$ and $-T\Delta S_{diss}^{\ddagger}$ are indicated in parenthesis.

Table 3. The effects of L-amino acids on the activation thermodynamic parameters of CO-displacement reaction of MbCO by hexacyanoferrate ions at pH 7.0*

L-amino acids	[amino acids] (M)	$\Delta G_{off}^{a\ddagger}$ (kcal mol^{-1})	$\Delta H_{off}^{\ddagger}$ (kcal mol^{-1})	$\Delta S_{off}^{\ddagger}$ (cal mol^{-1} K^{-1})	$-T\Delta S_{off}^{a\ddagger}$ (kcal mol^{-1} K^{-1})
Control	0.0	19.4 (0.04)	19.1 (0.6)	−1.0 (0.1)	0.3 (0.1)

Alanine	0.5	19.4 (0.07)	19.6 (0.4)	0.5 (0.2)	−0.2 (0.4)
Arginine	0.5	19.6 (0.02)	22.7 (0.5)	10.5 (1.1)	−3.1 (0.5)
Glycine	0.5	19.5 (0.09)	19.7 (0.3)	0.7 (1.0)	−0.2 (0.3)
Proline	0.5	19.5 (0.08)	20.1 (0.5)	1.8 (1.1)	−0.5 (0.5)
Serine	0.5	19.5 (0.06)	19.7 (0.3)	1.0 (1.0)	−0.3 (0.3)
Threonine	0.5	19.4 (0.06)	19.5 (0.3)	0.3 (0.3)	−0.1 (0.3)

[a] Activation free energy ($\Delta G_{off}^{\ddagger}$) and entropy changes ($-T\Delta S_{off}^{\ddagger}$) are at 25ºC.

*The uncertainties (std. error) in $\Delta G_{off}^{\ddagger}$, $\Delta H_{off}^{\ddagger}$, $\Delta S_{off}^{\ddagger}$ and $-T\Delta S_{off}^{\ddagger}$ are indicated in parenthesis.

Data from Table 2 and Table 3 provide some important information (i) the presence of amino acids in the reaction medium increase the $\Delta H_{diss/off}^{\ddagger}$ for CO-dissociation reaction of NCO and CO-replacement reaction of MbCO at pH 7.0 and which is more increased for arginine and least for threonine (arginine> proline > serine > glycine> alanine >threonine), confirming that the amino acid-mediated restricted dynamics of NCO and MbCO are more for arginine and least for threonine, and (ii) the amino acids-mediated increase in $\Delta H_{diss/off}^{\ddagger}$ is accompanied by a decrease in enthalpy change ($-T\Delta S_{diss/off}$) at pH 7.0.

5.2.3 Effect of amino acids on the thermodynamic stability of Ferrocyt c and Mb

Fig. 4a and 4b present the GdnHCl-induced equilibrium unfolding transitions of Ferrocyt *c* and Mb, respectively in the absence and presence of 0.5 M of amino acids (alanine, arginine, glycine, proline, serine and threonine) at pH 7.0, 25ºC. Data in Fig. 4a and 4b clearly indicate that the GdnHCl-induced unfolded curves of Ferrocyt *c* and Mb shifts toward the higher concentrations of GdnHCl in the presence of 0.5 M of alanine, glycine, proline, serine and threonine and shifts toward the lower concentration of GdnHCl in the presence of 0.5 M. arginine. These unfolding curves were analyzed by two state transitions between the folded (N) and unfolded (U) conformations of proteins [74]. The resulting free energy of denaturation (ΔG_D), surface area exposed by solvent (m_g), and denaturant midpoint concentration (C_m) for unfolding of Ferrocyt *c* and Mb in the presence of different amino acids (alanine, arginine, glycine, proline, serine and threonine), monitored by Trp fluorescence (ex: 280 nm) are listed in Table 4. Data in Table 4 clearly suggests that among the alanine, glycine, proline, serine and threonine, the C_m and ΔG_D for Ferrocyt *c* and Mb at pH 7.0 are increased more for serine and least for proline (C_m for Ferrocyt *c*: serine > glycine > alanine > threonine ~ proline, C_m for Mb: serine > glycine ~ alanine > threonine > proline, ΔG_D for Ferrocyt *c* and Mb: serine > glycine ~ alanine > threonine > proline), which suggests that amino acid-mediated increase in thermodynamic stability of

Ferrocyt *c* and Mb is more pronounced for serine and least for proline (serine > glycine ~ alanine > threonine > proline).

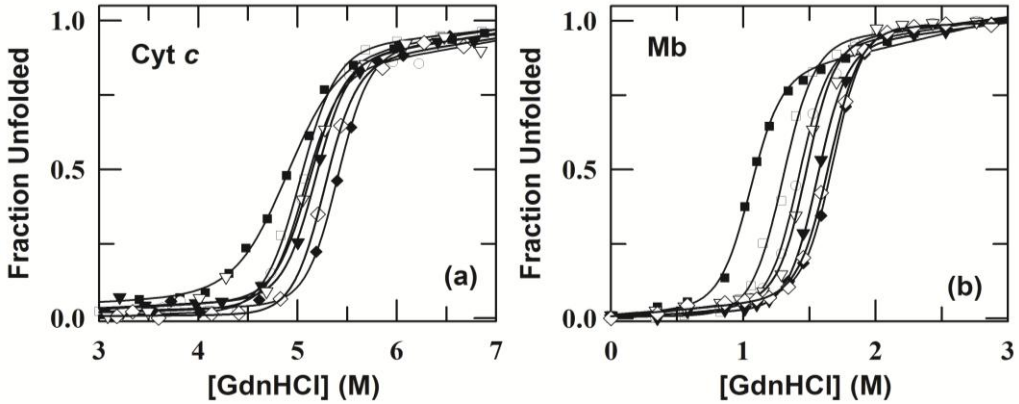

Fig.4. Effect of amino acids on the thermodynamic stability of Ferrocyt *c* and Mb at pH 7.0. Panels (a) and (b) show the GdnHCl-induced equilibrium unfolding curves of Ferrocyt *c* and Mb respectively, in the absence (□) and in the presence of 0.5 M amino acid (alanine (▼), arginine (■), glycine (◊), proline (○), serine (◆) and threonine (▽)) at 25°C, pH ~7.0. The solid curves represent nonlinear least-squares fits to two-state equation (Equation (7), chapter 2) [74].

Table 4. G_D, m_g, and C_m values for GdnHCl-induced unfolding curves of Ferrocyt *c* and Mb in the presence of L-amino acids at pH 7.0, monitored by Trp fluorescence (ex: 280 nm)*.

	Ferrocyt *c*			Mb		
L-amino acids	ΔG_D (kcal mol^{-1})	m_g (kcal mol^{-1}M^{-1})	C_m (M)	ΔG_D (kcal mol^{-1})	m_g (kcal mol^{-1}M^{-1})	C_m (M)
Control	16.2	3.2	5.0	6.4	4.9	1.3
0.5 M Alanine	18.6	3.6	5.2	8.2	5.3	1.6
0.5 M Arginine	10.9	2.2	4.9	5.3	5.1	1.0
0.5 M Glycine	19.3	3.7	5.3	8.3	5.0	1.6
0.5 M Proline	17.2	3.4	5.1	7.6	5.4	1.4
0.5 M Serine	20.0	3.7	5.4	8.9	5.3	1.7
0.5 M Threonine	17.4	3.4	5.1	8.1	5.5	1.5

*The uncertainties of m_g and ΔG_D values reported here are ± 0.3kcal mol^{-1}M^{-1} and ±0.5kcal mol^{-1}, respectively. The uncertainty of C_m values reported here is ±0.3 M.

However, arginine decreases the C_m and ΔG_D for Ferrocyt *c* and Mb at pH 7.0, which suggests that arginine decreases the thermodynamic stability of Ferrocyt *c* and Mb. Due to the preferential excluding and preferential hydration effects [24], alanine, glycine, proline, serine and threonine increase the thermodynamic stability of proteins. Due to presence of guanidium (Gdn^+) group, arginine interacts with aromatic amino acids by cation-π interaction [65], which in results decreases the thermodynamic stability of proteins at pH 7, 25ºC.

5.2.4 Effects of amino acids on the thermal stability of Ferrocyt c and Mb

To verify the effect of amino acids on the thermal stability of Ferrocyt *c* and Mb, the absorbance (Ferrocyt *c* (550 nm) and Mb (409 nm)) and near UV CD (Ferrocyt *c* and Mb (282 nm)) monitored thermal unfolding curves of Ferrocyt *c* and Mb were collected in the absence and presence of varying concentrations of amino acids (alanine, arginine, glycine, proline, serine and threonine) at pH 7.0. The α-band (550 nm) is main characteristics of Fe^{2+}-M80 bond of Ferrocyt *c* (Fig. 5a) at 25ºC, pH 7.0 The soret band (409 nm) is the main characteristics of heme electronic absorption spectrum of Ferricyt *c* and Mb (Fig. 5b) at 25ºC, pH 7.0. As temperature is increased from 25 and 110°C, intensity of α-bands (550 nm) is decreased significantly (Fig. 5a), indicating significant disruption of Fe^{2+}-M80 bond and thermal denaturation of Ferrocyt *c* at 110°C. As temperature is increased from 25 and 90°C, the intensity of soret-band (409 nm) of Mb is also decreased significantly (Fig. 5b), indicating thermal denaturation of Mb at 90°C.

Figs. 5c and 5d present representative thermal unfolding curves as change in excitation coefficient of Ferrocyt *c* (at 550nm) and Mb (at 409 nm), respectively in the absence and presence of 0.5 M amino acid (alanine, arginine, glycine, proline, serine and threonine) at pH 7.0. Fig. 5c and Fig. 5d clearly indicate that the presence of alanine, glycine, proline, serine and threonine shift the thermal unfolding curves of Ferrocyt *c* and Mb to higher temperatures, while the presence of arginine shift the thermal unfolding curves Ferrocyt *c* and Mb to lower temperatures. The absorbance monitored thermal unfolding curves of Ferrocyt *c* and Mb measured under various concentrations of amino acids (alanine, arginine, glycine, proline, serine and threonine) at pH 7.0 were analyzed by van't Hoff equation (Equation (5), chapter 2) [75]. The resulting thermal denaturation midpoint (T_m) and enthalpy change (ΔH_m) are summarized in Table 5. Figs. 6a and 6b present the [Amino acids] dependence thermal denaturation midpoint temperature (T_m) of Ferrocyt *c* (550 nm) and Mb (409 nm) at neutral pH, respectively. Fig. 7a shows the near-UV CD spectra of Ferrocyt *c* collected at 25°C and 106ºC, pH 7.0. Fig. 7b shows the near-UV CD spectra of Mb collected at 25°C and 95ºC, pH 7.0.

Table 5. L-amino acids dependence of the T_m, and ΔH_m for thermal unfolding of Ferrocyt *c* (absorbance 550 nm) and Mb (absorbance 409nm) at pH 7.0*.

		Ferrocyt *c*		Mb	
L-amino acids	[amino acids] (M)	T_m (K)	ΔH_m (kcal mol^{-1})	T_m (K)	ΔH_m (kcal mol^{-1})
Control	0.0	373.9	122.4	356.7	124.4
Alanine	0.25	374.8	147.5	358.4	125.9

	0.5	375.5	149.5	358.8	122.6
	0.75	376.4	112.9	359.3	125.6
Arginine	0.25	372.7	136.2	353.6	111.7
	0.5	371.3	124.6	351.2	107.7
	0.75	370.4	127.0	348.8	103.5
Glycine	0.25	375.1	134.4	358.2	113.6
	0.5	376.1	139.2	358.9	117.6
	0.75	376.9	146.3	359.7	121.4
	1.0	377.8	141.7	360.1	123.0
Proline	0.25	373.7	147.8	357.1	123.4
	0.5	373.7	133.8	356.8	124.2
	0.75	373.0	143.9	356.7	119.0
	1.0	373.1	146.5	356.3	119.3
Serine	0.25	375.8	128.9	358.3	116.5
	0.5	376.7	139.9	359.4	114.8
	0.75	377.5	128.7	360.0	111.6
	1.0	378.1	136.2	360.3	107.9
Threonine	0.25	374.5	135.0	358.3	119.2
	0.5	375.2	142.0	358.8	130.7

*The uncertainties for T_m, and ΔH_m values reported here are ±0.5 ºC and ±5.0 kcal mol^{-1}, respectively.

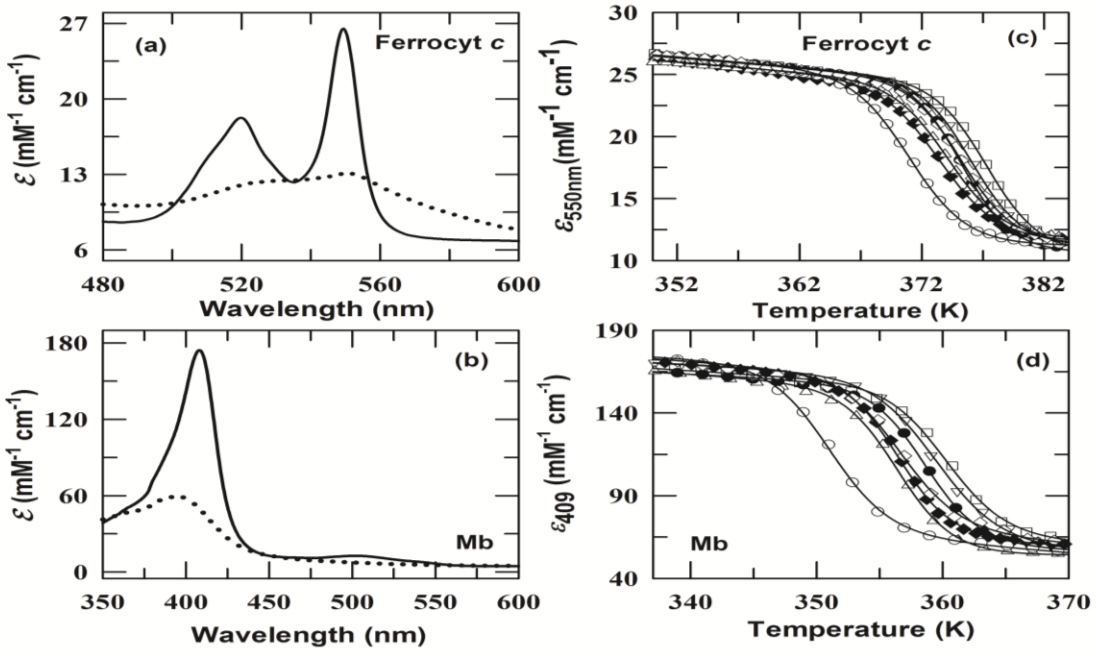

Fig.5. Effects of amino acids on the thermal stability of Ferrocyt *c* and Mb at pH 7.0. Panel (a) shows the visible absorption spectra of Ferrocyt *c* collected at 25ºC (solid line) and 110ºC (dotted line) in the absence of additive at pH 7.0. Panel (b) shows the visible absorption spectra of Mb collected at 25ºC (solid line) and 90ºC (dotted line) in the absence of additive at pH 7.0. Panel (c) presents the thermally-induced unfolding curves of Ferrocyt *c* monitored at 550 nm as the change in excitation coefficient at pH 7.0. Panel (d) presents the thermally induced unfolding curves of Mb monitored at 409 nm as the change in excitation coefficient at pH 7.0. In panels (c) and (d) symbol correspond to: in the absence (◆) and presence of 0.5 M amino acid (alanine (•), arginine (○), glycine (∇), proline (Δ), serine (□) and threonine (◊)). The solid curves in panels (c) and (d) represent the nonlinear least-squares fits of the data to van't Hoff equation (Equation (5), chapter 2) [75].

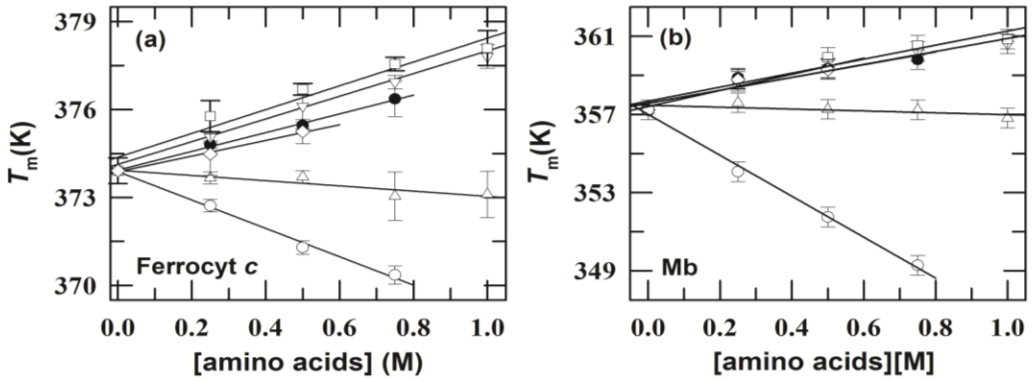

Fig.6. Effects of amino acids on the thermal stability of Ferrocyt *c* and Mb at pH 7.0. Panels (a) and (b) show the variation in T_m as a [Amino acids] for Ferrocyt *c* (550 nm) and Mb (409), respectively at pH 7.0 (alanine (•), arginine (○), glycine (∇), proline (Δ), serine (□) and threonine (◊) The solid lines in panels (a) and (b) are linear least-squares fits to the data.

At higher temperatures, the ellipticity was eliminated and goes towards zeroth ellipticity (Fig. 7a and Fig. 7b), indicating that the tertiary structure was significantly disrupted. Fig.7c and 7d represent the near-UV CD-(282 nm) monitored normalized thermal denaturation curves of Ferrocyt *c* and Mb collected in the absence and presence of 0.5 M amino acids (alanine, arginine, glycine, proline, serine and threonine) at pH 7.0, respectively.

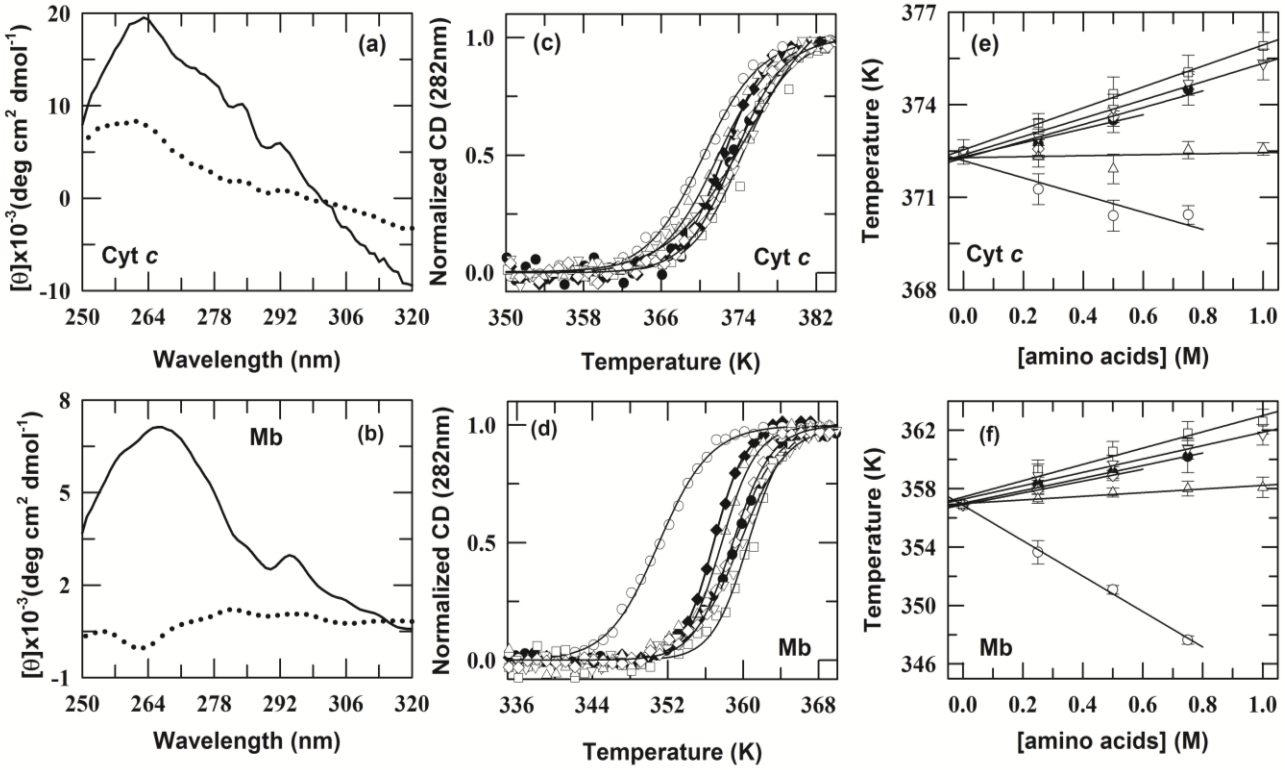

Fig.7. Effects of amino acids on the thermal stability of Ferrocyt *c* and Mb at pH 7.0. Panel (a) shows the near-UV CD spectra of Ferrocyt *c* (~85 µM) collected at 25ºC (solid line) and 106 ºC (dotted line). Panel (b) shows the near-UV CD spectra of Mb (~65 µM) collected at 25ºC (solid line) and 95 ºC (dotted line). Panels (c) and (d) present the

normalized near-UV CD (282 nm) monitored thermal unfolding curves of Ferrocyt *c* and Mb, respectively collected in the absence (◆) and presence of 0.5 M amino acids (alanine (•), arginine (○), glycine (∇), proline (Δ), serine (□) and threonine (◊)). The solid curves in panels (c) and (d) represent the nonlinear least-squares fit of the data to van't Hoff equation (Equation (5), chapter 2) [75]. Panels (e) and (f) present the variation in T_m with [Amino Acids] for Ferrocyt *c* and Mb, respectively (alanine (•), arginine (○), glycine (∇), proline (Δ), serine (□) and threonine (◊)) at pH 7.0. The solid lines in (e) and (f) are the linear least-squares fits to the data.

Fig. 7c and Fig. 7d clearly indicate that the presence of alanine, glycine, proline, serine and threonine shift the thermal unfolding curves of Ferrocyt *c* and Mb to higher temperatures, while the presence of arginine shift the thermal unfolding curves of Ferrocyt *c* and Mb to lower temperatures. The near-UV CD-monitored (282 nm) thermal unfolding curves were analyzed for thermal denaturation midpoint (T_m) and enthalpy change (ΔH_m) by two-state model N$\rightleftharpoons$U using van't Hoff equation (Equation (5), chapter 2) [75]. The resulting T_m and ΔH_m were summarized in Table 6. Fig.7e and Fig.7f present the variation of T_m with [Amino acids] of Ferrocyt *c* and Mb, respectively at pH 7.0.

Figs. 6a, 6b, 7e and 7f reveal that the (i) with increasing the concentration of serine, glycine, alanine and threonine, the T_m for Ferrocyt *c* and Mb are increased linearly, (ii) the amino acid-mediated increase in T_m for Ferrocyt *c* and Mb are more pronounced for serine and least for threonine (serine > glycine > alanine > threonine) (iii) with increasing the [proline], the T_m of Ferrocyt *c* and Mb are not greatly changed (iii) as the [arginine] increase, the T_m of Ferrocyt *c* and Mb are decreased linearly. These results thus suggest that (i) amino acid-mediated increase in thermal stability of Ferrocyt *c* and Mb are more pronounced for serine and least for threonine (serine > glycine > alanine > threonine > proline), (ii) proline presence in the reaction medium not greatly alters the thermal stability of Ferrocyt *c* and Mb, and (iii) arginine presence in the reaction medium decrease the thermal stability of Ferrocyt *c* and Mb.

Table 6. L-amino acids dependence of the T_m, and ΔH_m for thermal unfolding of Ferrocyt *c* and Mb monitored by near-UV CD (282nm) at pH 7.0*.

		Ferrocyt *c*		Mb	
L-amino acids	[amino acids] (M)	T_m (K)	ΔH_m (kcal mol^{-1})	T_m (K)	ΔH_m (kcal mol^{-1})
control	0.0	372.5	122.3	356.9	120.1
Alanine	0.25	372.7	100.2	358.3	93.4
	0.5	373.5	110.7	359.1	111.6
	0.75	374.5	103.0	360.2	96.5
Arginine	0.25	371.3	109.8	353.6	54.4
	0.5	370.4	93.3	351.1	90.3
	0.75	370.4	100.4	347.6	94.4

Glycine	0.25	372.9	68.4	358.9	76.1
	0.5	373.9	73.4	359.7	103.7
	0.75	374.7	80.2	360.7	138.5
	1.0	375.3	73.8	361.7	134.5
Proline	0.25	372.3	117.2	357.3	122.5
	0.5	371.9	95.3	357.7	135.6
	0.75	372.5	95.6	358.0	136.6
	1.0	372.6	107.5	358.1	100.0
Serine	0.25	373.4	120.7	359.3	112.6
	0.5	374.4	106.2	360.5	134.4
	0.75	375.0	85.3	361.8	137.6
	1.0	375.9	105.6	362.6	131.1
Threonine	0.25	372.6	107.3	357.9	133.5
	0.5	373.6	109.7	358.9	123.8

*The uncertainties for T_m, and ΔH_m values reported here are ±0.5 ºC and ±6.0 kcal mol^{-1}, respectively.

The cosolute which raises the surface tension of water generally stabilizes the protein structure and induces the preferential hydration of macromolecules [21]. In view of these amino acids, alanine, glycine and serine increase the surface tension of water [24, 76], so by preferential interaction of these amino acids with proteins [76] or by preferential hydration of proteins [24] increase the thermal stability of Ferrocyt *c* and Mb. Some previous report revealed that the guanidino group present in arginine molecule directly interacts with the aromatic and charged side chains surface residues of proteins. [77-79]. In general, the destabilizers were characterized by their preferential binding to the proteins [78-79] and arginine binds to proteins though cation-π interaction. These types of interaction of arginine to proteins are responsible for the destabilization of native protein [65].

5.2.5 Effect of amino acids on the tertiary structure of Ferricyt c and Mb

Due to high absorbance of L-alanine, L-arginine, L-glycine, L-proline, L-serine and L-threonine in the far-UV CD region, it is not possible to investigate the effect of these amino acids on the secondary structure of Ferricyt *c* and Mb. Traditionally, the near-UV CD spectrum (250-350 nm) is very sensitive to certain aspects of tertiary structure of protein. Signals from 250-270 nm, 270-290 nm and 280-300 nm are attributable due to phenylalanine residues, tyrosine and the tryptophan, respectively. Throughout the near-UVCD spectrum, the broad weak signals are due to the disulfide bonds present in native state of proteins [80]. The near-UV CD spectrum is very sensitive to small changes in tertiary structure due to interactions of protein-ligands and/or changes in solvent conditions.

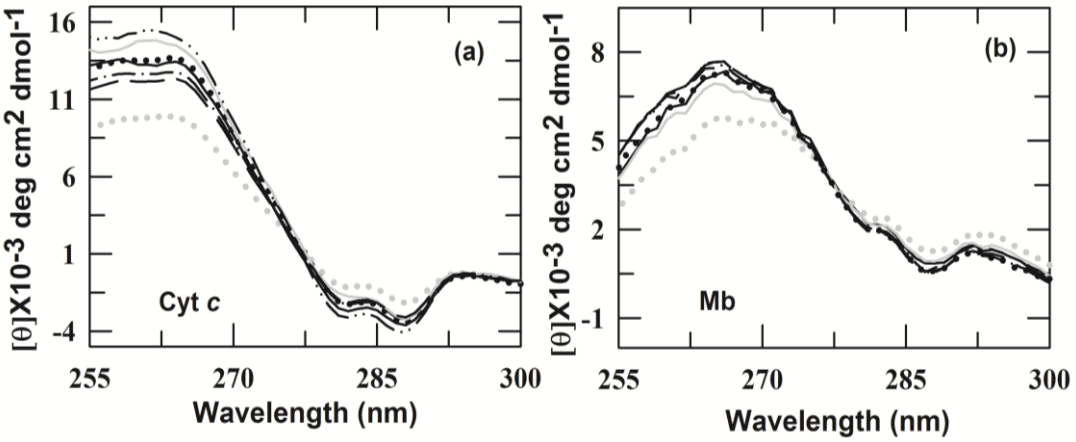

Fig.8. Effects of amino acids on the tertiary structures of Ferrocyt *c* and Mb at pH 7.0**.** Panels (a) and (b) show the near-UV CD spectra of Ferricyt *c* and Mb collected in the absence (solid black line) and in the presence of ~ 0.5 M alanine (black dash-dot line(—·—)), arginine (gray dotted line(·····)), glycine (gray solid line (——)), proline (long dash line (— —)), serine (black dotted line (·····)) and threonine (dash double dotted line(— ·· —)), respectively at 25 °C. The final concentrations of Mb and Ferricyt *c* are 60 and 65μM, respectively.

Figs. 8a and 8b show the near-UV CD spectra of Ferricyt *c* and Mb collected in the absence and presence of 0.5 M of alanine, arginine, glycine, proline, serine and threonine at pH 7.0. Figs.8a and 8b clearly show that the presence of alanine, glycine, proline, serine and threonine in reaction medium not greatly alter the tertiary structure signals of Ferricyt *c* and Mb but the presence of arginine in reaction medium show significant changes in tertiary structure signals of Ferricyt *c* and Mb, which is probably due it forms cation-π interaction with aromatic amino acids residue present in protein.

5.3 Conclusion

L-amino acids (alanine, arginine, glycine, proline, serine, and threonine) significantly alter the internal dynamics of native-like compact state (NCO) and native MbCO at pH 7.0. The kinetic and thermodynamic parameters for CO-dissociation from NCO (NCO→N+CO) and CO-replacement from MbCO by hexacyanoferrate ion were measured at varying concentrations of L-amino acids (alanine, arginine, glycine, proline, serine, and threonine) at pH 7.0. As [amino acids] is increased, the CO−dissociation reaction of NCO and CO−replacement reaction of MbCO are decelerated, indicating that the amino acids presence in the reaction medium reduce the structural fluctuations responsible for CO dissociation from NCO and CO replacement from MbCO. The amino acid−mediated reduction in structural fluctuations of NCO and MbCO typically follow the

order: arginine> serine> proline> glycine> alanine >threonine. Two-state thermodynamic analysis of GdnHCl and thermal unfolding transitions of native Ferrocyt *c* (N-state) and Mb carried out in the presence of various concentrations of amino acids (alanine, arginine, glycine, proline, serine, and threonine) reveals that alanine, glycine, proline, serine, and threonine presence in reaction medium increase the thermodynamic stability of Ferrocyt *c* and Mb but arginine presence in reaction medium decreases the thermodynamic stability of these proteins. The amino acid-mediated increase in thermodynamic stability for Ferrocyt *c* and Mb typically follow the order: serine> glycine> alanine >threonine>proline. The decrease in thermodynamic stability of Ferrocyt *c* and Mb in the presence of arginine is presumably because of the presence of guanidium group (Gdn^+) in the arginine.

5.4 References:

1. A. B. Fulton, *Cell* **30** (1982) 345–347.
2. S. B. Zimmerman, S.O.J. Trach, *J. Mol. Biol.* **222** (1991) 599–620.
3. H. X. Zhou, G. N. Rivas, A. P. Minton, *Annul. Rev. Biophys.* **37** (2008) 375–397.
4. A. P. Minton, *J. Pharm. Sci.* **94** (2005) 1668–1675.
5. A. P. Minton, *J. Biol. Chem.* **276** (2001) 10577–10580.
6. A. P. Minton, *Biophys. J.* **78** (2000) 101–109.
7. G. N. Somero, *Am. J. Physiol.* **251** (1986) R197–R213.
8. P. H. Yancey, M. E. Clark, S. C. Hand, R. D. Bowlus, G. N. Somero, *Science* **217** (1982) 1214–1222.
9. S. Taneja, F. Ahmad, *Biochem. J.* **303** (1994) 147–153.
10. T. Arakawa, S. N. Timasheff, *Biochemistry* **21** (1982) 6536–6545.
11. C. D. Ball, C. R. Hardt, W. J. Duddles, *J. Biol. Chem.* **151** (1943) 163–169.
12. S. L. Bradburg, W. B. Jakoby, *Proc. Natl. Acad. Sci. U.S.A.* **69** (1972) 2373–2376.
13. R. P. Frigon, J. C. Lee, *Arch. Biochem. Biophys.* **153** (1972) 587–589.
14. J. B. Kirkpatrick, L. Hyano, V. L. Thomas, P. M. Howley, *J. Cell Biol.* **47** (1970) 384–394.
15. R. E. Kane, *J. Cell. Biol.* (suppl.) **25** (1965) 137–144.
16. C. Tanford, *J. Am. Chem. Soc.* **84** (1962) 4240–4247.
17. L. G. Paleg, T. J. Douglas, A. V. Daal, D. B. Keech, *Aust. J. Plant Physiol.* **8** (1981) 107–114.
18. M. M. Santoro, Y. Liu, S. M. A. Khan, L. Hou, D. W. Bolen, *Biochemistry* **31** (1992) 5278–5283.

19. G. Parameshwara, L. G. Paleg, D. Aspinall, G. P. Jones, *Proceedings of the International Congress of Plant Physiology*, Society for Plant Physiology and Biochemistry, Water Technology Centre, I.A.R.I., New Delhi (1988).
20. P. H. Yancey, *Transport Processes, lono- and Osmoregulation* (Gilles, R. and Gallen-Baillies, M., eds.), Spinger-Verlag, Berlin (1985) pp. 424–436.
21. T. Arakawa, S.N. Timasheff, *Arch Biochem Biophys.* **224** (1983) 169–177.
22. T. Arakawa, S.N. Timasheff, *Biochemistry* **23** (1984) 5912–5923.
23. T. Arakawa, S.N. Timasheff, *Biochemistry* **23** (1984) 5924–5929.
24. T. Arakawa, S.N. Timasheff, *Biophys J.* **47** (1985) 411–414.
25. J.F. Carpenter, J.H. Crowe, *Cryobiology* **25** (1988) 244–255.
26. J.F. Carpenter, L.M. Crowe, J.H. Crowe, *Biochem. Biophys. Acta* **923** (1987) 109–115.
27. J.F. Carpenter, B. Martin, L.M. Crowe, J.H. Crowe, *Cryobiology* **24** (1987) 455–464.
28. J.F. Carpenter, J.H. Crowe, T. Arakawa, *J. Dairy Sci.* **73** (1990) 3727–3736.
29. J.F. Carpenter, S.J. Prestrelski, T. Arakawa, *Arch. Biochem. Biophys* **303** (1993) 456–464.
30. J.F. Carpenter, S.J. Prestrelski, A. Dong, *Eur. J. Pharm. Biopharm.***45** (1998) 231–238.
31. T. Arakawa, J.F. Carpenter, Y. Kita, J.H. Crowe, *Cryobiology* **27** (1990) 410–415.
32. S.J. Prestrelski, T. Arakawa, J.F. Carpenter, *Arch. Biochem. Biophys.* **303** (1993) 465–473.
33. S.J. Prestrelski, N. Tedeschi, T. Arakawa, J.F. Carpenter, *Biophys. J.* **65** (1993) 661–671.
34. A. Pyne, K. Chatterjee, R. Suryanarayanan, *J. Pharmcol. Sci.* **92** (2003) 2272–2283.
35. G. Bonacci, M.C. Sanchez, M. Gonzalez, D. Ceschin, G. Fidelio, M.A. Vides, G. Chiabrando, *J. Biochem Biophys Methods* **46** (2000) 95–105.
36. X.C. Tang, M.J. Pikal, *Pharmacol Res* **22** (2005) 1167–1175.
37. L.L. Chang, D. Shepherd, J. Sun, X.C. Tang, M.J. Pikal, *J. Pharmacol. Sci.* **94** (2005) 1445–1455.
38. P.H. von Hippel, K.Y. Wong, *Biochemistry* **1** (1962) 664–674.
39. P. H. von Hippel, K.Y. Wong, *J. Biol. Chem.* **240** (1965) 3909–3923.
40. J.F. Back, D. Oakenfull, M.B. Smith, *Biochemistry* **18** (1979) 5191–5196.
41. S.Y. Gerlsma, *J. Biol. Chem.* **243** (1968) 957–961.
42. S.Y. Gerlsma, *Eur. J. Biochem.* **14** (1970) 150–153.
43. S.Y. Patro, E. Freund, B.S. Chang, *Biotechnol. Annu. Rev.* **8** (2002) 55–84.
44. W. Wang, *Int. J Pharmacol* **289** (2005) 1–30.

45. Y. R. Gokarn, A. Kosky, E. Kras, A. McAuley, R. L. Remmele, *Biotechnology, and Drug Delivery Systems*. New York, Taylor & Francis Group, LLC (2006).
46. D. Shah, *Molecular Insights into the Role of Arginine on Protein Stabilization* (Doctoral dissertation) (2011).
47. M. E. Clark, M. Zounes, *Biol. Bull.* (Woods Hole, Mass.) **153** (1977) 468–484.
48. R. D. Bowlus, G. N. Somero, *J. Exp. Zool.* **208** (1979) 137–151.
49. K. Shiraki, M. Kudou, S. Fujiwara, T. Imanaka, T. Takagi, *J. Biochem.* **132** (2002) 591–595.
50. W.A. Jensen, J.M. Armstrong , J. De Giorgio, M.T. Hearn, *Biochim. Biophys. Acta.***1296** (1996) 23–34.
51. M. J. Pikal, Freeze-Drying of Proteins. *Formulation and Delivery of Proteins and Peptides* (Symposium Series #567). Cleland JL, Longer R, Eds. American Chemical Society: Washington, DC, September (1994).
52. T. J. Anchordoquy, J.F. Carpenter, *Arch. Biochem. Biophys.* **332**(1996) 231–238.
53. M. R. Bozorgmehr, H. Monhemi, *J. Solution Chem.* **44** (2015) 45–53.
54. J. Buchner, R. Rudolph, *Biotechnology* **9** (1991)157–162.
55. U. Brinkman, J. Buchner, I. Pastan, *Proc. Natl. Acad. Sci. USA* **89** (1992) 3075–3079.
56. D. Arora, N.J. Khanna, *J. Biotechnol.* **52** (1996) 127–133.
57. K. Tsumoto, K. Shinoki, H. Kondo, M. Uchikawa, T. Juji, I. Kumagai, *J. Immunol. Methds* **219** (1998) 119–129.
58. M. Umentsu, K. Tsumoto, M. Hara, K. S. Ashish, S. Goda, T. Adschiri, I. Kumagai, *J. Biol. Chem.* **279** (2003) 8979–8987.
59. S. Bell, S. Hansen, J. Buchner, *Biophys. Chem.* **96** (2002) 243–257.
60. W.J. Lin, J.A. Traugh, *Protein Expr. Purif.* **4** (1993) 256–264.
61. M.H. Hsih, J.C. Kuo, H.J. Tsai, *Appl. Microbial. Biotechnol.* **48** (1997) 66–72.
62. E.D.B. Clark, E. Schwarz, R. Rudolph, *Methods Enzymol.* **309** (1999) 217–237.
63. D.L. Havehan, E.D.B. Clark, *Biotechnol. Bioeng.* **54** (1997) 221–230.
64. K. Tsumoto, M. Umetsu, I. Kumagai, D. Ejima, T. Arakawa, *Biochem. Biophys. Res. Commun.* **312** (2003) 1383–1386.
65. C. P. Schneider, B. L. Trout, *J. Phys. Chem. B* **113** (2009) 2050−2058.
66. B. M. Baynes, D. I. C. Wang, B. L. Trout, *Biochemistry* **44** (2005) 4919−4925.

67. D. Shukla, B. L. Trout, *J. Phys. Chem. B* **115** (2011) 1243−1253.
68. J.S. Olson, *Methods Enzymol.* **76** (1981) 631–651.
69. http://marlin.bio.umass.edu/biology/kunkel/probe/buffers/aa.html
70. J. Kyte, R. F. Doolittle, *Journal of Molecular Biology* **157** (1982) 105–132.
71. D. Shukla, B. L. Trout, *J. Phys. Chem. B* **114** (2010) 13426–13438.
72. B. M. Baynes and B. L. Trout, *Biophys. J.* **87** (2004) 1631–1639.
73. J. Mikšovská, J.H. Day, R.W. Larsen, *J. Biol. Inorg. Chem.* **8** (2003) 621–625.
74. M. M. Santoro, D. W. Bolen, *Biochemistry* **27** (1988) 8063−8068.
75. M.M. Santoro, D.W. Bolen, *Biochemistry* **31** (1992) 4901–4907.
76. J. R. Pappenheime, M. P. Lepie, J. Wyman, *J. Amer. Chem. Sot.* **58** (1936) 1851–1855.
77. Y. Kita, T. Arakawa, T.Y. Lin, S.N. Timasheff, *Biochemistry* **33** (1994) 15178–15189.
78. T. Arakawa, K. Tsumoto, Y. Kita, B. Chang, D. Ejima, *Amino Acids* **33** (2007) 587─605.
79. T. Arakawa, D. Ejima, K. Tsumoto, N. Obeyama, Y. Tanaka, Y. Kita, et al., *Biophys. Chem.* **127** (2007) 1─8.
80. S. M. Kelly, N. C. Price, *Current Protein and Peptide Science* **1** (2000) 349–384.

Chapter 6

Factor Defining the Effect of Amino Acids on the Thermodynamic Stability and Internal Dynamics of Cytochrome *c* and Myoglobin

6.1 Introduction

Naturally occurring osmolytes are polyols, amino acids, and combinations of methylamines with urea [1-3]. Under protein stabilization environments, several physicochemical approaches have provided extensive evidences for the interaction of osmolytes with proteins [4-14]. However, because of diverse structures of the native proteins, a clear-cut molecular explanation of the interaction of free amino acids with functional groups of proteins is not reported. Amino acids and other compatible osmolytes can interact with the proteins both directly [15-18] and indirectly [12, 18-20]. Some earlier studies have reported that the unfavorable interaction between the hydrated surfaces of proteins and osmolytes stabilizes the native conformation of proteins [21-28]. The stability and dynamics are strongly interrelated to the functional form of protein [29-31]. In general, the stability and dynamics of proteins in solution are strongly depending on the dynamics of the solvents [32-36].

Although several techniques have been used to the study of fast protein dynamics that control the conformational transitions, which are directly associated with the functional form of proteins [37-38], very little studies are available that show relatively slow changes in structural dynamics of proteins across the folding-unfolding transition [39]. Clues to the role of structural dynamics in folding can be obtained by probing the changes in thermal fluctuations at both atomic and large-scale collective level. Although, the effects of denaturants (urea and GdnHCl) on the internal dynamics of native Cyt *c* and Mb have been extensively investigated, [40-45], but the effect of amino acids on the internal dynamics of natively folded carbonmonoxycytochrome *c* (NCO) in the presence of varying concentration denaturants, across the folding-unfolding transition are not explored so far.

Analysis of kinetic and thermodynamic parameters measured for CO-dissociation reaction of NCO at varying concentrations of GdnHCl or urea in the absence and presence of fixed concentrations of L-amino acids (alanine, arginine, glycine, proline, serine, and threonine)

at pH 7.0 reveals that amino acids modulate the denaturant-dependent internal dynamics of NCO. It is observed that (i) in subdenaturing region, L-amino acids (arginine, serine, praline, glycine, alanine, threonine) presence in reaction medium show an additive effect on the denaturant-mediated reduction in structural fluctuations responsible for CO dissociation [40,46], which typically follow the order: arginine> serine> proline> glycine> alanine >threonine, (ii) in denaturing region, these amino acids also counteract the structural fluctuations responsible for unfolding the protein, and (iii) the structural fluctuation that unfolds the protein are found to be more opposed by the larger sized and lesser hydrophobic amino acids (arginine> serine> proline> glycine> alanine >threonine). Thermodynamic analysis of thermal and urea unfolding curves of Cyt *c* and Mb measured at varying concentrations of GdnHCl in the absence and presence of fixed concentration of L-amino acids (alanine, arginine, glycine, proline, serine, and threonine) at pH 7.0 reveals that (i) alanine, glycine, proline, serine and threonine counteract the deleterious effect of denaturants on stability of proteins and they typically follow the order: serine> glycine>alanine>threonine>proline, and (ii) at lower concentrations of GdnHCl, L-arginine show an additive effect on the deleterious effect of denaturant on stability of proteins while at higher concentrations of GdnHCl it counteract the deleterious effect of denaturants.

6.2 Results and Discussion

6.2.1 Effect of amino acids on the denaturant-dependent internal dynamics of NCO

The electronic absorption spectrum of native Ferrocyt *c* shows α-band at 550 nm, which reflects the Fe^{2+}-M80 bond in Ferrocyt *c* [47-48]. If CO is liganded to the native Ferrocyt *c* (NCO), the α-band at 550 nm disappears, while if CO is dissociated from NCO, the α-band (Fe^{2+}-CO+M80→Fe^{2+}-M80+CO) at 550 nm appears (Fig. 1a). Fig. 1b represents the kinetics of CO dissociation from NCO (NCO → N+CO) in the presence of 0.05M GdnHCl at pH 7.0, 25°C. The increase in absorbance intensity at the 550 nm (heme π→π* α-band) in a single exponential is due to slow dissociation of CO (τ=27 min).

To examine the effect of amino acids on the denaturant dependent internal dynamics of NCO, the rate coefficient of CO-dissociation (k_{diss}) form NCO was measured at fixed concentrations of amino acids (alanine, arginine, glycine, proline, serine and threonine) under

variable concentrations of denaturants (urea and GdnHCl) at pH 7.0, 25 °C. Figs. 2a and 2b presents the [Urea] and [GdnHCl]-dependent logarithm of rate coefficient (log k_{diss}) of CO dissociation from NCO, respectively in the absence and presence of 0.5 M of L-amino acids (alanine, arginine, glycine, proline, serine and threonine) at pH 7.0, 25ºC.

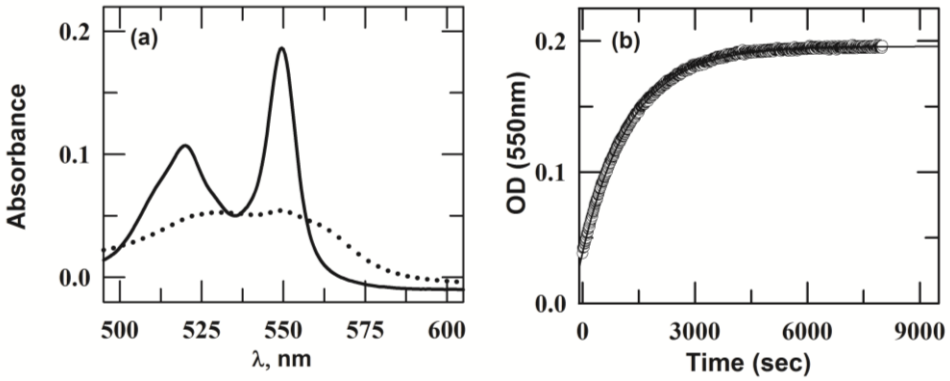

Fig.1. Panel (a) shows the steady-state visible absorption spectra of NCO (dashed line) and N (solid line) states. The spectra were recorded in 50 mM sodium phosphate buffer at pH 7, containing 0.05 M GdnHCl at 25°C. Panel (b) represents the single phase CO dissociation kinetic trace of NCO collected in the presence of 0.05M GdnHCl at pH 7.0, 25°C (τ =27 min).

In the absence of amino acids, as [denaturant] is raised starting from 0.0 to 3.5 M GdnHCl or 8.5 M urea, log k_{diss} initially decreases and then increases, displaying minima at 5.5 M urea (Fig. 2a) or 2.3 M GdnHCl (Fig. 2b). This finding indicates that the subdenaturing concentrations of denaturants constrain the internal dynamics of NCO. Some previous reports also showed that the subdenaturing concentrations of GdnHCl and urea can stabilize proteins by committing $GdnH^+$ and Cl^- ions to screen charge-charge interactions in the native state of the protein [40, 42-43, 49-50]. Since both amino acids and subdenaturing concentrations of denaturant (<2.3 M GdnHCl or <5.5 M urea) individually decrease the rate of CO dissociation reaction (Fig. 2a (chapter 5), Fig. 2a and Fig. 2b), the coexistence of the two in the reaction medium is expected to produce a cumulative effect on the rate of CO dissociation. As [amino acids] is increased from 0 to 0.5 M, the rate-denaturant profile is shifted vertically down to lower k_{diss} (Fig. 2a and Fig. 2b). A slight horizontal shift toward higher concentration of denaturant is also apparent (Fig. 2a and Fig. 2b). The amino acids mediated vertical and slight horizontal shifts in the rate-denaturant profile thus reveal that the amino acids and subdenaturing concentrations of denaturants produce a cumulative effect on the restricted internal dynamics of NCO.

Figs. 2a and 2b show that the denaturant-dependent decrease in logk_{diss} under subdenaturing concentration of denaturant is more pronounced in the presence of arginine and least in the presence of threonine and its typically follows the order as: arginine > serine > proline > glycine > alanine > threonine at pH 7, 25ºC. This finding suggests that the denaturant dependent decrease in logk_{diss} under subdenaturing concentration of denaturant typically follows the size effect (stokes radii: arginine (5.32 Å) > serine (3.12 Å) > glycine (2.56 Å) > alanine (2.28 Å) [51] and hydrophobicity effect (Kyte-Doolittle scale of amino acids hydrophobicity index: arginine (-4.5) > serine (-0.8) > glycine (-0.4) > alanine (1.8) of amino acids at neutral pH [52].

In the denaturing region, the increase in logarithm of k_{diss} (Figs. 2a and 2b) can be interpreted to arise from protein destabilization and structural unfolding action of denaturant that would facilitate the CO dissociation from NCO. In the denaturing region, the log k_{diss} increases to a lesser extent in the presence of amino acids than in the absence (Figs. 2a and 2b), which indicates that the inclusion of amino acids opposes the structural fluctuation that cause unfolding of the protein. Furthermore, the increase in log k_{diss} is more pronounced in the presence of arginine and least in the presence of proline and it typically follows the order as: arginine> >threonine> glycine~ serine ~ proline, at pH 7, 25ºC.

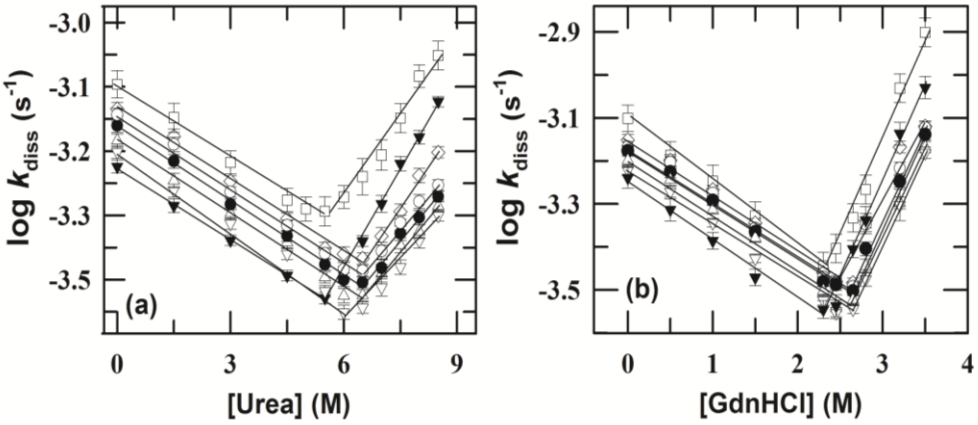

Fig.2. Panels (a) and (b) show [Urea] and [GdnHCl] dependence of logk_{diss}, respectively at 25(±1)°C, pH 7.0 in the absence (□) and presence of 0.5 M amino acids (alanine (o), arginine (▼), glycine (•), proline (▽), serine (Δ) and threonine (◊)). The lines through the data in panels (a) and (b) have been drawn by inspection only.

6.2.2 Effect of amino acids on the denaturant-dependent activation thermodynamic parameter of CO-dissociation reaction of NCO

The cumulative and counteracting effect of amino acid on the denaturant-dependent logk_{diss} warrant a thermodynamic analysis of the CO dissociation reaction of NCO at pH 7.0. Fig. 3 shows the Eyring plots for CO-dissociation reaction from NCO in absence of additive and in the presence of 2.3 and 3.5 M GdnHCl without and with 0.5 M alanine (Fig.3a), 0.5 arginine (Fig.3b), 0.5 M glycine (Fig. 3c), 0.5 M proline (Fig. 3d), 0.5 M serine (Fig.3e) and 0.5M threonine (Fig. 3f) at pH 7.0. Fig. 4 shows the Eyring plots for CO-dissociation reaction from NCO in the presence of 5.5 and 8.5 M urea without and with 0.5 M alanine (Fig.4a), 0.5 arginine (Fig.4b), 0.5 M glycine (Fig. 4c), 0.5 M proline (Fig. 4d), 0.5 M serine (Fig.4e) and 0.5M threonine (Fig. 4f) at pH 7.0. As discussed in the previous chapter, the activation enthalpy ($\Delta H_{diss}^{\ddagger}$) and activation entropy ($\Delta S_{diss}^{\ddagger}$) associated with CO dissociation reaction of NCO was calculated by Eyring equation (Equation (1), chapter 2) [53].

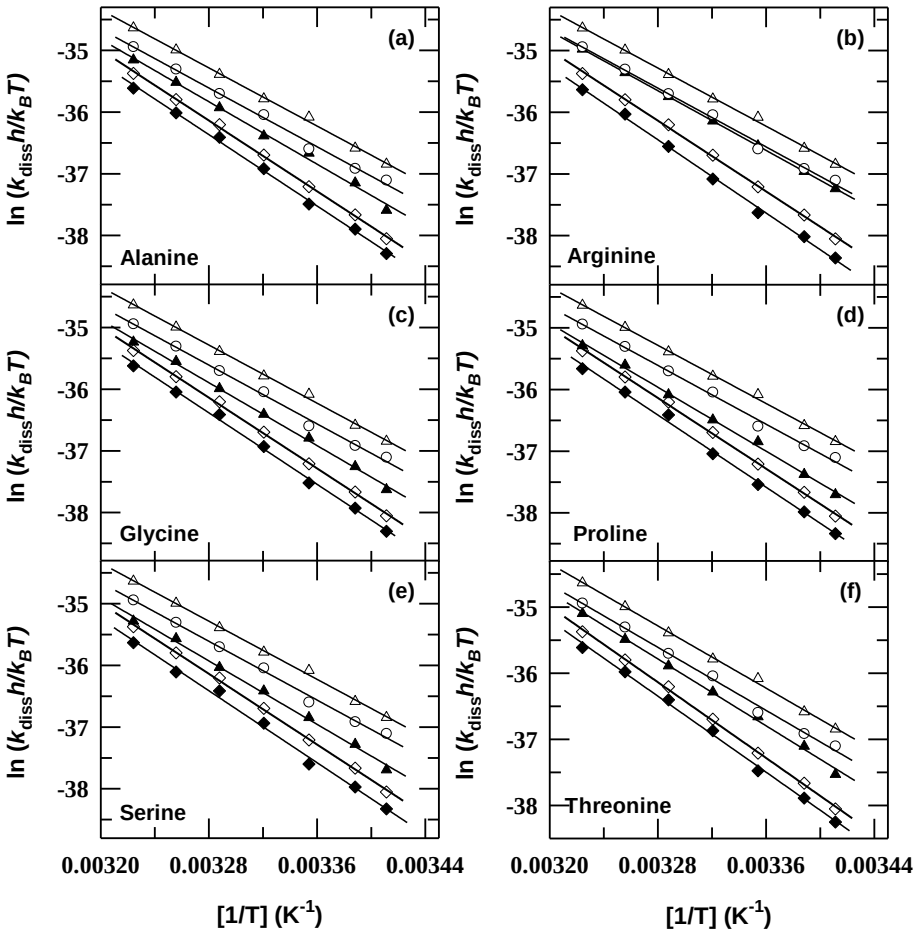

Fig.3. Panel (a) shows the Eyring plots for the CO-dissociation reaction, in the absence of additives (○) and in the presence of 2.3 M GdnHCl (◊); 3.5 M GdnHCl (Δ); 0.5 M alanine with 2.3M GdnHCl (♦) and 0.5 M alanine with 3.5 M GdnHCl (▲) at pH 7.0. Panel (b) shows the Eyring plots for the CO-dissociation reaction in the absence of

additives (○) and in the presence of 2.3 M GdnHCl (◊); 3.5 M GdnHCl (Δ); 0.5 M arginine with 2.3M GdnHCl (♦) and 0.5 M arginine with 3.5 M GdnHCl (▲) at pH 7.0. Panel (c) shows the Eyring plots for the CO-dissociation reaction in the absence of additives (○) and in the presence of 2.3 M GdnHCl (◊); 3.5 M GdnHCl (Δ); 0.5 M glycine with 2.3 M GdnHCl (♦) and 0.5 M glycine with 3.5 M GdnHCl (▲) at pH 7.0. Panel (d) shows the Eyring plots for the CO-dissociation reaction in the absence of additives (○) and in the presence of 2.3 M GdnHCl (◊); 3.5 M GdnHCl (Δ); 0.5 M proline with 2.3M GdnHCl (♦) and 0.5 M proline with 3.5 M GdnHCl (▲) at pH 7.0. Panel (e) shows the Eyring plots for the CO-dissociation reaction in the absence of additives (○) and in the presence of 2.3 M GdnHCl (◊); 3.5 M GdnHCl (Δ); 0.5 M serine with 2.3 M GdnHCl (♦) and 0.5 M serine with 3.5 M GdnHCl (▲) at pH 7.0. Panel (f) shows the Eyring plots for the CO-dissociation reaction in the absence of additives (○) and in the presence of 2.3 M GdnHCl (◊); 3.5 M GdnHCl (Δ); 0.5 M threonine with 2.3M GdnHCl (♦) and 0.5 M threonine with 3.5 M GdnHCl (▲) at pH 7.0. The solid lines in panel (a) to (f) are fitted according to Eyring equation [53].

The values of $\Delta H_{diss}^{\ddagger}$ and $\Delta S_{diss}^{\ddagger}$ for the CO dissociation reaction of NCO at different concentrations of denaturants (GdnHCl and urea) were calculated in the absence and presence of 0.5 M amino acids (alanine, arginine, glycine, proline, serine and threonine). The resulting $\Delta H_{diss}^{\ddagger}$ and $\Delta S_{diss}^{\ddagger}$ are summarized in Table 1.

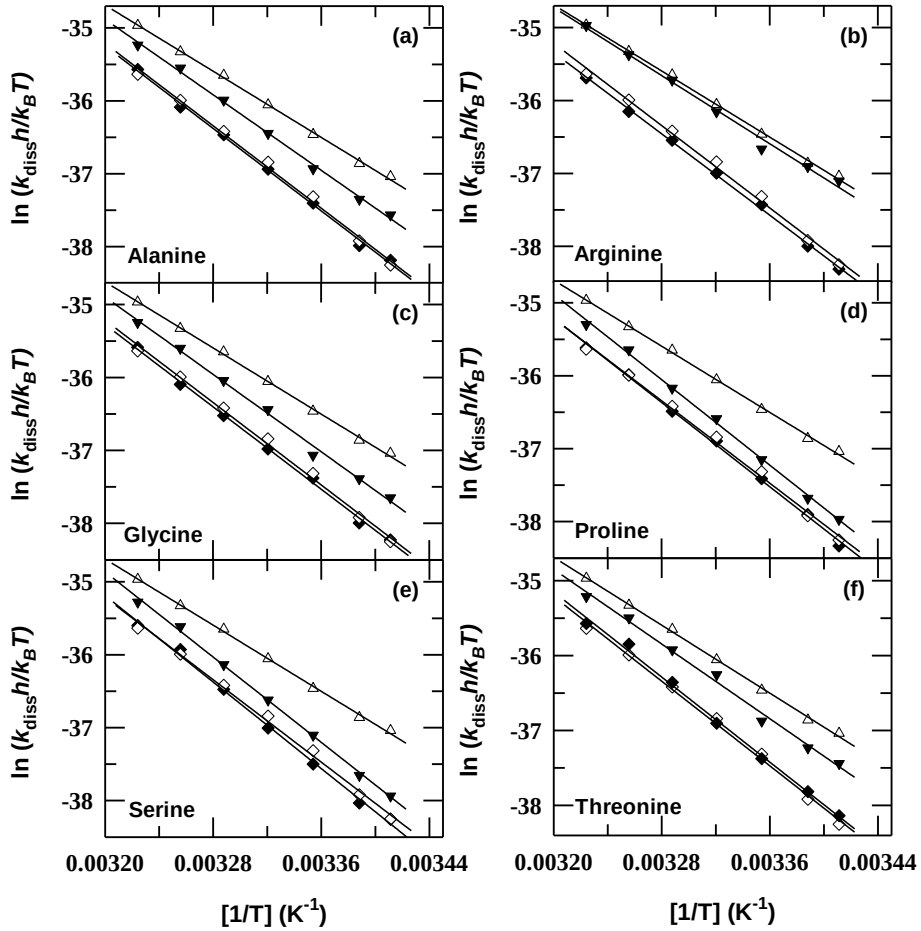

Fig.4. Panel (a) shows the Eyring plots for the CO-dissociation reaction in the presence of 5.5 M urea (◊); 8.5 M urea (Δ); 0.5 M alanine with 5.5 M urea (♦) and 0.5 M alanine with 8.5 M urea (▼) at pH 7.0. Panel (b) shows the Eyring plots for the CO-dissociation reaction in the presence of 5.5 M urea (◊); 8.5 M urea (Δ); 0.5 M arginine with 5.5 M urea (♦) and 0.5 M arginine with 8.5 M urea (▼) at pH 7.0. Panel (c) shows the Eyring plots for the CO-dissociation reaction in the presence of 5.5 M urea (◊); 8.5 M urea (Δ); 0.5 M glycine with 5.5 M urea (♦) and 0.5 M glycine with

8.5 M urea (▼) at pH 7.0. Panel (d) shows the Eyring plots for the CO-dissociation reaction in the presence of 5.5 M urea (◊); 8.5 M urea (Δ); 0.5 M proline with 5.5M urea (♦) and 0.5 M proline with 8.5 M urea (▼) at pH 7.0. Panel (e) shows the Eyring plots for the CO-dissociation reaction in the presence of 5.5 M urea (◊); 8.5 M urea (Δ); 0.5 M serine with 5.5M urea (♦) and 0.5 M serine with 8.5 M urea (▼) at pH 7.0. Panel (f) shows the Eyring plots for the CO-dissociation reaction in the presence of 5.5 M urea (◊); 8.5 M urea (Δ); 0.5 M threonine with 5.5M urea (♦) and 0.5 M threonine with 8.5 M urea (▼) at pH 7.0. The solid lines in panel (a) to (f) are fitted according to Eyring equation [53].

Table 1. Effect of amino acids on the denaturants (GdnHCl and urea) dependence activation parameters for CO-dissociation from NCO in the presence at pH 7.0*.

	Without amino acids				0.5 M Alanine			
[GdnHCl](M)	$\Delta G_{diss}^{a\ddagger}$	$\Delta H_{diss}^{\ddagger}$	$\Delta S_{diss}^{\ddagger}$	$-T\Delta S_{diss}^{a\ddagger}$	$\Delta G_{diss}^{a\ddagger}$	$\Delta H_{diss}^{\ddagger}$	$\Delta S_{diss}^{\ddagger}$	$-T\Delta S_{diss}^{a\ddagger}$
0.0	21.8	23.8	6.9	−2.1	22.1	25.5	12.4	−3.4
2.3	22.2	28.6	21.7	−6.5	22.3	28.9	22.1	−6.6
3.5	21.6	23.6	6.7	−2.0	21.9	25.3	11.3	−3.4
[urea](M)								
5.5	22.3	28.2	19.9	−5.9	22.3	28.6	21.1	−6.3
8.5	21.7	22.7	3.2	−0.9	21.9	25.9	13.1	−3.9
	0.5 M Arginine				0.5 M Glycine			
[GdnHCl](M)	$\Delta G_{diss}^{a\ddagger}$	$\Delta H_{diss}^{\ddagger}$	$\Delta S_{diss}^{\ddagger}$	$-T\Delta S_{diss}^{a\ddagger}$	$\Delta G_{diss}^{a\ddagger}$	$\Delta H_{diss}^{\ddagger}$	$\Delta S_{diss}^{\ddagger}$	$-T\Delta S_{diss}^{a\ddagger}$
0.0	22.5	27.9	19.7	−5.5	22.1	25.8	13.1	−3.6
2.3	22.4	29.7	24.4	−7.3	22.3	29.0	22.2	−6.6
3.5	21.8	24.2	8.0	−2.4	21.9	25.5	11.8	−3.5
[urea](M)								
5.5	22.3	28.9	22.3	−6.7	22.3	28.7	21.4	−6.4
8.5	21.8	23.4	5.4	−1.6	22.0	26.5	15.1	−4.5
	0.5 M Proline				0.5 M Serine			
[GdnHCl](M)	$\Delta G_{diss}^{a\ddagger}$	$\Delta H_{diss}^{\ddagger}$	$\Delta S_{diss}^{\ddagger}$	$-T\Delta S_{diss}^{a\ddagger}$	$\Delta G_{diss}^{a\ddagger}$	$\Delta H_{diss}^{\ddagger}$	$\Delta S_{diss}^{\ddagger}$	$-T\Delta S_{diss}^{a\ddagger}$
0.0	22.3	26.7	16.0	−4.5	22.2	26.4	15.0	−4.2
2.3	22.4	29.2	23.1	−6.9	22.3	29.2	22.8	−6.8
3.5	22.0	25.9	13.0	−3.9	22.0	25.7	12.4	−3.7
[urea](M)								
5.5	22.3	29.3	24.0	−7.2	22.3	29.2	23.8	−7.1
8.5	22.1	28.9	22.0	−6.5	22.2	28.9	22.0	−6.6
	0.5 M Threonine							
[GdnHCl](M)	$\Delta G_{diss}^{a\ddagger}$	$\Delta H_{diss}^{\ddagger}$	$\Delta S_{diss}^{\ddagger}$	$-T\Delta S_{diss}^{a\ddagger}$				
0.0	22.1	25.3	11.5	−3.2				
2.3	22.3	28.7	21.6	−6.4				
3.5	21.9	25.3	11.4	−3.4				
[urea](M)								
5.5	22.3	28.4	20.6	−6.1				
8.5	21.9	24.9	10.1	−3.0				

*$\Delta G_{diss}^{\ddagger}$, $\Delta H^{\ddagger}_{diss}$, $\Delta S_{diss}^{\ddagger}$ and $-T\Delta S_{diss}^{\ddagger}$ are reported as kcal mol^{-1}, kcal mol^{-1}, cal mol^{-1} K^{-1} and kcal mol^{-1} K^{-1}, respectively. The uncertainties associated with $\Delta G_{diss}^{\ddagger}$, $\Delta H^{\ddagger}_{diss}$, $\Delta S_{diss}^{\ddagger}$ and $-T\Delta S_{diss}^{\ddagger}$ are ± 0.1 kcal mol^{-1}, ±0.5 kcal mol^{-1}, ± 3 cal mol^{-1}K^{-1} and ±0.4 kcal mol^{-1} K^{-1}, respectively.

[a]Activation free energy ($\Delta G_{diss}^{\ddagger}$) and entropy changes ($-T\Delta S_{diss}^{\ddagger}$) are given at 25 °C.

The corresponding free energy of activation ($\Delta G_{diss}^{\ddagger}$) and entropy change ($-T\Delta S_{diss}^{\ddagger}$) were also calculated from Gibb free energy equation ($\Delta G_{diss}^{\ddagger} = \Delta H_{diss}^{\ddagger} - T\Delta S_{diss}^{\ddagger}$) at 25 °C. The resulting

$\Delta G_{diss}^{\ddagger}$ and $-T\Delta S_{diss}^{\ddagger}$ are also summarized in Table 1. Data in Table 1 provide some important information (i) subdenaturing concentrations of denaturant (2.3 M GdnHCl or 5.5 M urea) increase the $\Delta H_{diss}^{\ddagger}$ for CO dissociation reaction and which is more increased in the presence of amino acids then in its absence and this increase in $\Delta H_{diss}^{\ddagger}$ typically follows the order: arginine > serine> proline> glycine> alanine >threonine, (ii) the denaturing concentrations of denaturant (3.5 M GdnHCl or 8.5 M urea) decrease the $\Delta H_{diss}^{\ddagger}$ for CO dissociation reaction and which is less decreased in the presence of amino acids then in its absence and this decrease in $\Delta H_{diss}^{\ddagger}$ typically follows the order: proline ~ serine > glycine > alanine > threonine > arginine, (iii) both in the absence and presence of amino acids, the denaturant-mediated increase in $\Delta H_{diss}^{\ddagger}$ within subdenaturing region is accompanied by a decrease in the entropy change, $-T\Delta S_{diss}^{\ddagger}$, and (iv) both in the absence and presence of amino acids, the denaturant-mediated decrease in $\Delta H_{diss}^{\ddagger}$ within denaturing region is accompanied by a increase in the entropy change, $-T\Delta S_{diss}^{\ddagger}$.

6.2.3 Effect of amino acids on the denaturant-dependent thermal unfolding of Ferrocyt c and Mb

Figs. 5a presents the representative thermal denaturation curves of Ferrocyt *c* as change in excitation coefficient at 550 nm in the absence and presence 1.0 M GdnHCl with 0.5 M amino acid (alanine, arginine, glycine, proline, serine, threonine) at pH 7.0. Figs. 5b and 5c present the normalized thermal denaturation curves of Ferrocyt *c* and Mb, respectively collected in the absence and presence of GdnHCl (1M GdnHCl for Ferrocyt *c* (Fig. 5b) or 0.8 M GdnHCl for Mb (Fig. 5c)) with 0.5 M amino acid (alanine, arginine, glycine, proline, serine, and threonine) at pH 7.0. The absorbance-monitored thermal unfolding curves were analyzed for thermal denaturation midpoint (T_m) and enthalpy change, (ΔH_m) using van't Hoff equation as two-state model $N \rightleftharpoons U$ (chapter 2 equation (5)) [54]. The resulting T_m and ΔH_m values for Ferrocyt *c* and Mb at pH 7.0 under various [GdnHCl] both in the absence and presence of 0.5 M of alanine, arginine, glycine, proline, serine and threonine are provided in Table 2 (Ferrocyt *c*) and Table 3 (Mb).

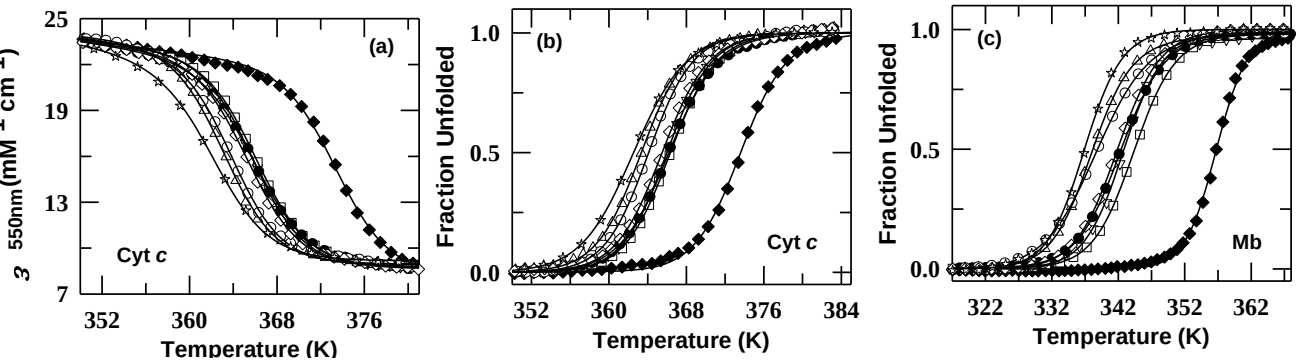

Fig.5. Panel (a) shows thermal denaturation curves of Ferrocyt *c* monitored at 550 nm as the change in excitation coefficient in the absence (◆) and presence of 1 M GdnHCl (☆) and 1 M GdnHCl with 0.5 M amino acid (alanine (●), arginine (○), glycine (▽), proline (Δ), serine (□) and threonine (◊)) at pH 7.0. Panel (b) shows the normalized thermal denaturation curves of Ferrocyt *c* (monitored at 550 nm) in the absence (◆) and presence of 1 M GdnHCl (☆) and 1 M GdnHCl with 0.5 M amino acid (alanine (●), arginine (○), glycine (▽), proline (Δ), serine (□) and threonine (◊)) at pH 7.0. Panel (c) shows absorbance monitored (409 nm) normalized thermal denaturation curves of Mb in the absence (◆) and presence of 0.8M GdnHCl (☆) and 0.8M GdnHCl with 0.5 M amino acid (alanine (●), arginine (○), glycine (▽), proline (Δ), serine (□) and threonine (◊)), pH 7.0. The solid curves represent nonlinear least-squares fits of the data to van't Hoff equation [54] (chapter 2, equation (5)).

Figs. 6a and 6b present T_m vs [GdnHCl] and ΔH_m vs [GdnHCl] plots, respectively for Ferrocyt *c* in the absence and presence of 0.5 M amino acids (alanine, arginine, glycine, proline, serine and threonine) at pH 7.0. Figs. 7a and 7b show the T_m vs [GdnHCl] and ΔH_m vs [GdnHCl] plots, respectively for Mb in the absence and presence of 0.5 M of amino acids (alanine, arginine, glycine, proline, serine and threonine) at pH 7.0.

For calculating the thermal denaturation free energy (ΔG_T), one of the most reliable methods for obtaining an accurate value of heat capacity (ΔC_p) is to measure the T_m dependence of ΔH_m of the transition at different denaturant concentrations [55].

$$\Delta H_m = \Delta C_p T_m + b \qquad (2)$$

where b is the y-intercept. Figs. 6c and 7c show the ΔH_m vs T_m plots for Ferrocyt *c* and Mb, respectively, in the absence and presence of amino acids (alanine, arginine, glycine, proline, serine and threonine). The ΔC_p values for Ferrocyt *c* and Mb in the absence and presence of amino acids (alanine, arginine, glycine, proline, serine and threonine) were calculated (Table 2 and Table 3) by linear least-squares fit of the data to equation 2 [56]. By using the values of T_m, ΔH_m and ΔC_p, the ΔG_T values for Ferrocyt *c* and Mb at 25°C were determined from equation (3) as a function of [GdnHCl] both in the absence and presence of amino acids (alanine, arginine, glycine, proline, serine and threonine).

$$\Delta G_T = \Delta H_m \left(\frac{T}{T_m} - 1 \right) + \Delta C_p \left((T_m - T) + T \ln(T / T_m) \right) \qquad (3)$$

Figs. 6d and 7d present the variation of ΔG_T as a function of [GdnHCl] for Ferrocyt *c* and Mb, respectively at pH 7.0, 25ºC in the absence and presence of amino acids (alanine, arginine, glycine, proline, serine and threonine). The T_m, ΔH_m and ΔG_T values were found to be decreased linearly with [GdnHCl] for Ferrocyt *c* (Figs.6a, 6b and 6d) and Mb (Mb, Figs.7a, 7b and 7d). However, the decrease in T_m, ΔH_m and ΔG_T with [GdnHCl] are less pronounced in the presence of amino acids (alanine, glycine, proline, serine and threonine) then in its absence (Figs.6a, 6b, 6d, Figs.7a, 7b, 7d, Table 1 and Table 2), indicating that these amino acids counteract the destabilization effect of denaturant on thermal stability of Ferrocyt *c* and Mb at pH 7.0.

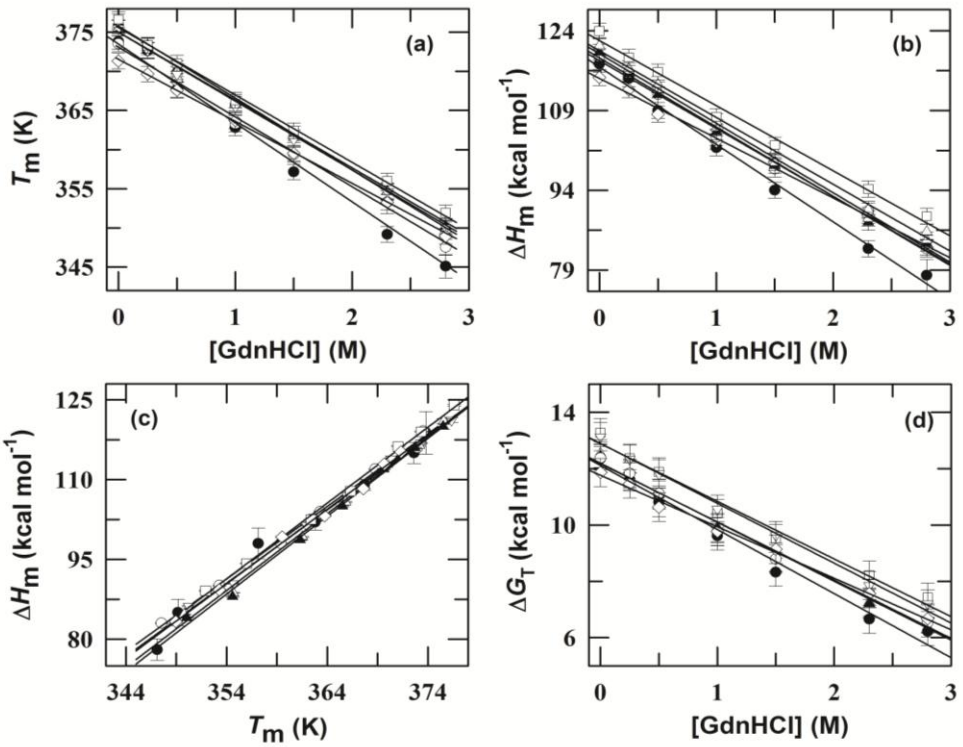

Fig.6. Panels (a) and (b) show the variation in T_m and ΔH_m with [GdnHCl] in the absence (●) and presence 0.5 M alanine (Δ), arginine (◊), glycine (▽), proline (○), serine (□) and threonine (▲) at pH 7.0 in 50 mM sodium phosphate buffer. Panel (c) presents the variation of ΔH_m as a function of T_m for Ferrocyt *c* (absorbance 550 nm) at pH 7.0 obtained at different GdnHCl concentrations in the absence (●) and presence 0.5 M alanine (Δ), arginine (◊), glycine (▽), proline (○), serine (□) and threonine (▲) at pH 7.0. Panel (d) presents the variation in ΔG_T with [GdnHCl] at 25 °C in the absence (●) and presence 0.5 M alanine (Δ), arginine (◊), glycine (▽), proline (○), serine (□) and threonine (▲) at pH 7.0. Solid lines are linear least-squares fits to the data.

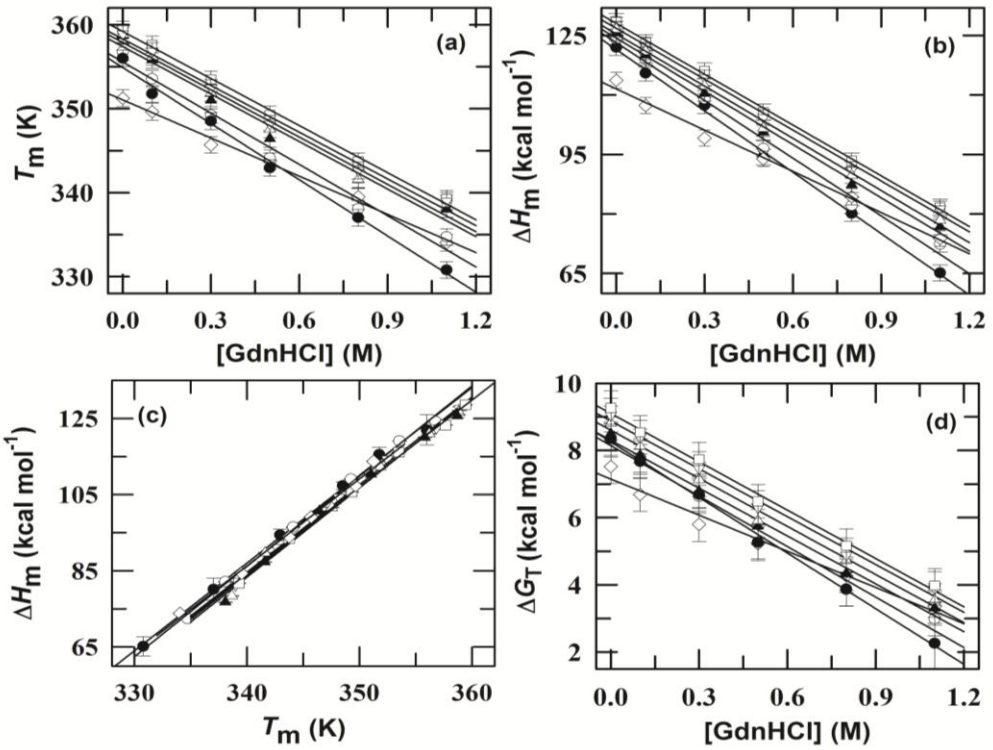

Fig.7. Panels (a) and (b) present the GdnHCl-dependent variation in T_m and ΔH_m for Mb (absorbance 409 nm) at pH 7.0 in the absence (●) and presence 0.5 M alanine (Δ), arginine (◊), glycine (▽), proline (○), serine (□) and threonine (▲) at pH 7.0. Panel (c) presents the variation of ΔH_m as a function of T_m for Mb (absorbance 409 nm) at pH 7.0 obtained at different GdnHCl concentrations in the absence (●) and presence 0.5 M alanine (Δ), arginine (◊), glycine (▽), proline (○), serine (□) and threonine (▲) at pH 7.0. Panel (d) presents the GdnHCl-dependent variation in ΔG_T for Mb (absorbance 409 nm) at pH 7.0 in the absence (●) and presence 0.5 M alanine (Δ), arginine (◊), glycine (▽), proline (○), serine (□) and threonine (▲) at pH 7.0. Solid lines are linear least-squares fits to the data.

Table 2. [GdnHCl] dependence of the T_m, ΔH_m, ΔG_T and ΔC_p for thermal unfolding of Ferrocyt *c* (absorbance 550 nm) both in the absence and presence of 0.5 M L-amino acids at pH 7.0*.

		Control				L-alanine			
Additive	Conc.(M)	T_m	ΔH_m	ΔG_T	ΔC_p	T_m	ΔH_m	ΔG_T	ΔC_p
GdnHCl	0.0	373.8	117.8	12.4	1.39	375.6	121.0	12.5	1.44
	0.25	372.6	115.0	11.8		373.1	116.4	11.7	
	0.5	367.7	109.0	10.8		370.0	112.9	11.1	
	1.0	362.8	102.0	9.6		365.8	105.7	9.9	
	1.5	357.1	94.0	8.3		361.5	99.2	8.9	
	2.3	349.2	83.0	6.6		354.6	88.7	7.3	
	2.8	345.1	78.0	6.2		349.8	84.6	6.7	
		L-arginine				L-glycine			
GdnHCl	0.0	371.3	115.2	11.9	1.40	376.3	121.2	13.1	1.38
	0.25	369.7	112.9	11.5		373.3	116.9	12.3	
	0.5	367.6	108.3	10.6		370.3	113.9	11.8	
	1.0	363.7	103.2	9.8		366.0	106.9	10.6	
	1.5	359.5	99.2	9.1		361.9	101.4	9.6	
	2.3	353.3	89.3	7.6		354.7	90.4	7.8	

	2.8	348.9	83.3	6.7		350.2	86.2	7.2	
			L-proline				L-serine		
GdnHCl	0.0	373.5	119.1	12.4	1.43	376.6	124.0	13.3	1.43
	0.25	373.0	116.0	11.8		373.3	119.0	12.4	
	0.5	368.8	112.0	11.1		371.0	116.2	11.9	
	1.0	363.3	104.0	9.8		366.3	107.8	10.4	
	1.5	359.4	98.0	8.8		362.4	102.5	9.5	
	2.3	353.3	90.1	7.6		356.0	94.2	8.2	
	2.8	347.5	83.0	6.5		351.9	89.1	7.4	
			L-threonine						
GdnHCl	0.0	375.5	120.0	12.5	1.43				
	0.25	372.7	116.0	11.8					
	0.5	369.6	112.0	11.1					
	1.0	365.5	105.0	9.9					
	1.5	361.3	98.7	8.9					
	2.3	354.6	88.0	7.2					
	2.8	350.0	84.0	6.7					

*ΔH_m, T_m,ΔG_T (25 °C) and ΔC_p are reported as kcal mol^{-1}, K, kcal mol^{-1}and kcal mol^{-1} K^{-1} respectively. The standard errors for T_m, ΔH_m, ΔG_T and ΔC_p values reported here are ±0.5 ºC, ±2.0 kcal mol^{-1} , ± 0.5 kcal mol^{-1}, and ± 0.1 kcal mol^{-1} K^{-1} respectively.

Furthermore, the extents of decrease in T_m, ΔH_m and ΔG_T values with [GdnHCl] are lesser for serine and typically follow the order: serine> glycine> alanine >threonine>proline (Figs.6a, 6b, 6d, Figs.7a, 7b, 7d, Table 1 and Table 2). As compared to other amino acids used in this study, arginine has different effect on T_m, ΔH_m and ΔG_T at lower concentrations of GdnHCl, first it decrease the thermal stability of proteins (1.0 M for Ferrocyt *c* and 0.5 M for Mb of GdnHCl) while at higher concentrations of GdnHCl (above 1M or 0.5M GdnHCl) it protects the deleterious effect of denaturants (Figs.6a, 6b, 6d, Figs.7a, 7b, 7d, Tables 1-2).

Amino acids, including alanine, glycine, proline, serine and threonine are naturally occurring osmolytes and they affect the stability of protein molecules by (i) preferential exclusion of osmolytes from the folded protein domain, and (ii) preferential interaction of osmolytes with the unfolded protein [57]. Due to the preferential exclusion or preferential hydration of the protein, surface tension of water increases and this tends to oppose denaturation forces which results in an increase in surface area of the protein. Traditionally, the preferential interaction of osmolytes with unfolded protein tends to favors denaturation, which depends on the hydrophobicity of osmolytes and with increasing hydrophobicity of osmolytes, denaturation of protein increases because denaturation means the exposure of buried hydrophobic side chains in the protein. Thus the observed effects of amino acids on denaturant-dependent thermodynamic stability of Ferrocyt *c* and Mb depends on hydrophobicity of amino acids, which means that the

least hydrophobic amino acids counteract more efficiently on deleterious effect of denaturants on thermodynamic stability of proteins. However, arginine shows different effect on the denaturant-dependent thermodynamic stability of Ferrocyt *c* and Mb at pH 7.0. As [GdnHCl] is increased from 0 M to 2.8 M for Ferrocyt *c* (Figs. 6a, 6b, 6d) or 1.1 M for Mb (Figs. 7a, 7b, 7d) in the presence of 0.5 M arginine, the T_m, ΔH_m and ΔG_T values are approaching toward the control (in the absence of arginine) and these finally crosses at 1.0 M GdnHCl for Ferrocyt *c* (Figs. 6a, 6b, 6d) and 0.5 M GdnHCl for Mb (Figs. 7a, 7b, 7d). These finding suggest that 0.5 M arginine and GdnHCl get associated to each other by head-to-tail hydrogen bonding [58] which as a result affects the slope of the plot of T_m, ΔH_m and ΔG_T versus denaturant concentration. The guanidinium group (Gdn^+) and carboxyl groups of arginine play a crucial role in the interactions between arginine and other molecules. The interactions of Gdn^+ and carboxyl groups alter the self association of arginine molecules under aqueous medium by head-to-tail hydrogen bonding [59]. Some previous reports revealed that the association of arginine with GdnHCl molecules form the cluster with denaturants and thus behaves as a neutral crowder [58-61]. These reports further suggested that the arginine clusters act as a neutral crowder and exert the solvent exclusion effect, results in the stabilization of the protein molecules at neutral pH [58-61]. Therefore, it is expected that ≥ 1.0 M GdnHCl for Ferrocyt *c* and ≥0.5 M GdnHCl for Mb, the arginine clusters, which act as a neutral crowder and exert the solvent exclusion effect counteract the deleterious effect of denaturants on thermodynamic stability of proteins (Figs. 6a, 6b, 6d and Figs. 7a, 7b, 7d). According to Schneider and Trout the [arginine]<0.5 M is neither strongly bound nor excluded from protein surface, but above 0.5 M arginine becomes increasingly excluded and exhibits the crowding effect [59].

Table 3. GdnHCl dependence of the T_m, ΔH_m, ΔG_T and ΔC_p for thermal unfolding of Mb (absorbance 409 nm) in the absence and presence of 0.5 M L-amino acids at pH 7.0*.

		Control				L-alanine			
Additive	Conc.(M)	T_m	ΔH_m	ΔG_T	ΔC_p	T_m	ΔH_m	ΔG_T	ΔC_p
GdnHCl	0.0	355.9	122.0	8.4	2.31	358.8	126.6	8.8	2.31
	0.1	351.7	115.5	7.7		356.2	120.9	8.1	
	0.3	348.5	107.3	6.7		351.8	112.3	7.1	
	0.5	342.9	94.4	5.3		347.5	101.6	5.9	
	0.8	337.0	80.1	3.9		341.6	89.7	4.7	
	1.1	330.8	65.1	2.2		338.6	78.4	3.5	
		L-arginine				L-glycine			
GdnHCl	0.0	351.2	113.7	7.5	2.28	358.9	127.6	9.0	2.3
	0.1	349.6	107.3	6.7		356.8	122.5	8.4	

	0.3	345.7	99.1	5.8		352.5	114.3	7.5	
	0.5	343.7	93.9	5.2		348.2	104.3	6.3	
	0.8	339.5	84.3	4.3		342.6	91.1	4.9	
	1.1	334.0	73.8	3.4		339.0	81.2	3.9	
			L-proline				L-serine		
GdnHCl	0.0	356.8	124.2	8.3	2.37	359.4	128.6	9.3	2.29
	0.1	353.5	119.1	7.8		357.6	123.3	8.5	
	0.3	349.2	109.1	6.6		353.5	116.1	7.8	
	0.5	344.1	96.5	5.3		349.3	105.7	6.5	
	0.8	338.1	82.1	3.9		343.7	93.4	5.2	
	1.1	334.7	72.4	3.0		339.3	81.7	4.0	
			L-threonine						
GdnHCl	0.0	358.7	125.7	8.5	2.35				
	0.1	355.8	120.0	7.9					
	0.3	351.1	110.4	6.8					
	0.5	346.4	100.7	5.7					
	0.8	341.6	87.3	4.3					
	1.1	338.1	76.8	3.3					

*ΔH_m, T_m, ΔG_T (25 °C) and ΔC_p are reported as kcal mol^{-1}, K, kcal mol^{-1}and kcal mol^{-1} K^{-1} respectively. The std. errs. for T_m, ΔH_m, ΔG_T and ΔC_p values reported here are ±0.5 ºC, ±3.0 kcal mol^{-1} , ± 0.4 kcal mol^{-1}, and ± 0.1 kcal mol^{-1} K^{-1} respectively.

6.2.4 Effect of amino acids on the denaturant-dependent thermodynamic stability of Ferricyt c and Mb

Fig. 8a shows the representative normalized urea-induced unfolding curves of Ferricyt *c* collected in the absence and presence of 1.0 M GdnHCl and 1.0 M GdnHCl with 0.25 M of amino acids (alanine, arginine, glycine, proline, serine and threonine) at pH 7.0, 25ºC. Fig. 8b shows the representative normalized urea-induced unfolding curves for Mb collected in the absence and presence of 0.5 M GdnHCl and 0.5 M GdnHCl with 0.25 M of amino acids (alanine, arginine, glycine, proline, serine and threonine) at pH 7.0, 25 ºC. Figs. 8a and 8b show that the inclusion of GdnHCl shifts the urea-induced unfolding curves of Ferricyt *c* and Mb to lower urea concentrations. However, in the presence of 0.25 M of alanine, glycine, proline, serine and threonine, the GdnHCl-triggered shift in the urea-induced unfolding curves of Ferricyt *c* and Mb are less pronounced (Fig. 7b and Fig. 8a) but are more pronounced in the presence of 0.25M of arginine (Fig. 7b and Fig. 8a) at pH 7.0, 25ºC. This finding indicates that the alanine, glycine, proline, serine and threonine counteract the deleterious effect of GdnHCl on thermodynamic stability of Ferricyt *c* and Mb but arginine exhibits an additive effect on the deleterious effect of GdnHCl on thermodynamic stability of these proteins at pH 7.0.

The urea-induced unfolding transitions curves of Ferricyt *c* and Mb collected at different concentrations of GdnHCl in the absence and presence of 0.25M of alanine, arginine, glycine, proline, serine and threonine at pH 7.0, 25 °C were analyzed by assuming a two state transition between the folded (N) and unfolded (U) conformations by using the procedure of Santoro and Bolen (Equation (7), chapter 2) [62]. The calculated values of ΔG_D and m_g for Ferricyt *c* and Mb are summarized in Table 4 and Table 5, respectively. The corresponding values of urea unfolding midpoints, C_m (=$\Delta G_D/m_g$) were also calculated for Ferricyt *c* and Mb and are also summarized in Table 4 and Table 5.

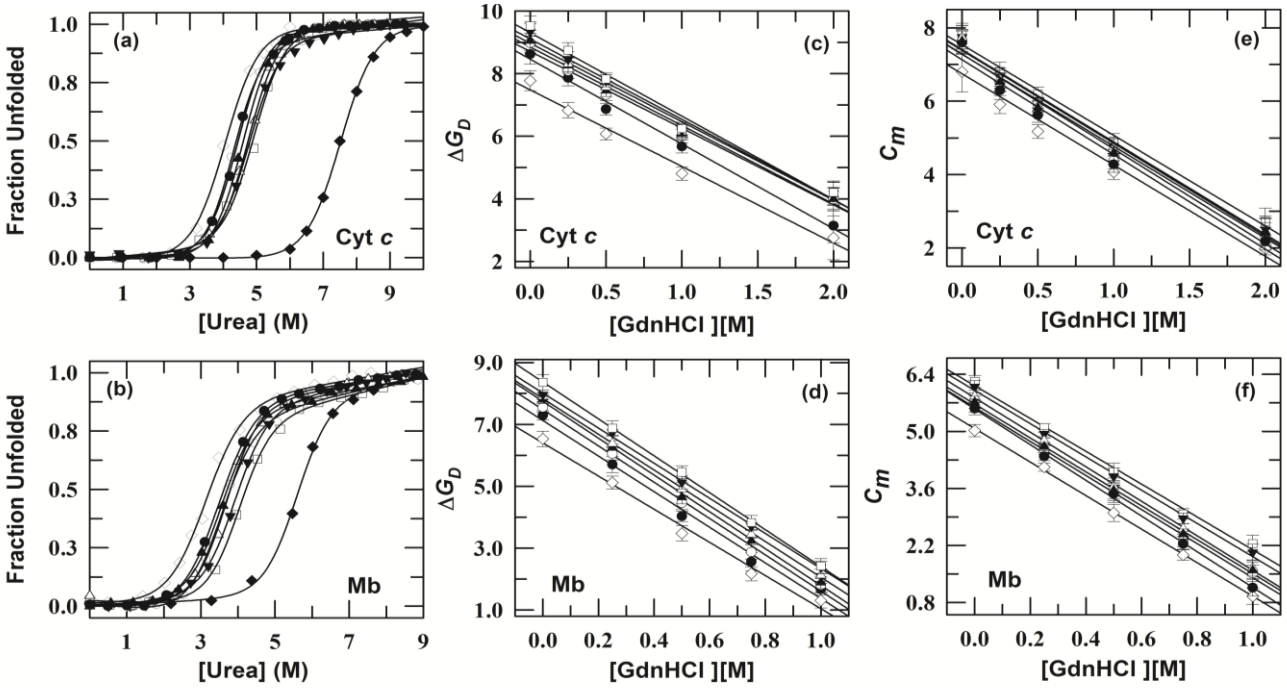

Fig.8. Panel (a) shows the fluorescence-monitored normalized equilibrium urea-induced unfolding curves of Ferricyt *c* in the absence (♦) and presence of 1 M GdnHCl (●) and 1 M GdnHCl with 0.25 M amino acid (alanine (Δ), arginine (◊), glycine (▼), proline (○), serine (□) and threonine (▲)) at pH 7.0 and 25°C. Panel (b) presents the fluorescence-monitored normalized equilibrium urea-induced unfolding curves of Mb in the absence (♦) and presence of 0.5M GdnHCl (●) and 0.5 M GdnHCl with 0.25M amino acid (alanine (Δ), arginine (◊), glycine (▼), proline (○), serine (□) and threonine (▲)) at pH 7.0 and 25°C. The solid curves represent nonlinear least-squares fits according to the standard two-state equation [62] (Equation (7), chapter 2). Panels (c) and (d) show the GdnHCl-dependence variation of the change in unfolding free energy, ΔG_D, for Ferricyt *c* and Mb, respectively in the absence (●) and in the presence of 0.25M alanine (Δ), arginine (◊), glycine (▼), proline (○), serine (□) and threonine (▲) at pH 7.0 and 25 °C. Panels (e) and (f) shows the GdnHCl-dependence variation of the urea unfolding midpoint, C_m, for Ferricyt *c* and Mb, respectively in the absence (●) and in the presence of 0.25M alanine (Δ), arginine (◊), glycine (▼), proline (○), serine (□) and threonine (▲) at pH 7.0 and 25 °C. The thermodynamic parameters are listed in Table 4 (Ferricyt *c*) and Table 5 (Mb). The solid lines in panels (c), (d), (e) and (f) represent linear least-squares fit of the data.

Table 4. Dependence of the ΔG_D, m_g and C_m of Ferricyt *c* on GdnHCl concentration in the absence and presence of 0.25 M amino acids at pH 7.0 as monitored by Trp fluorescence (ex: 280; em: 365 nm)*.

Additive	Conc. (M)	Control ΔG_D (kcal mol^{-1})	Control m_g (kcal mol^{-1}M^{-1})	Control C_m (M)	Conc. (M)	L-alanine ΔG_D (kcal mol^{-1})	L-alanine m_g (kcal mol^{-1}M^{-1})	L-alanine C_m (M)
GdnHCl	0.0	8.6	1.1	7.6	0.0	9.3	1.2	7.7
	0.25	7.9	1.2	6.3	0.25	8.3	1.3	6.6
	0.5	6.9	1.2	5.6	0.5	7.6	1.3	5.9
	1.0	5.7	1.3	4.3	1.0	6.1	1.3	4.7
	2.0	3.7	1.7	2.2	2.0	4.2	1.7	2.4
		L-arginine				L-glycine		
GdnHCl	0.0	7.8	1.1	7.3	0.0	9.3	1.2	7.7
	0.25	6.8	1.2	5.9	0.25	8.4	1.3	6.6
	0.5	6.1	1.2	5.2	0.5	7.8	1.3	5.9
	1.0	4.8	1.2	4.1	1.0	6.2	1.3	4.8
	2.0	2.0	1.0	2.1	2.0	4.2	1.7	2.5
		L-proline				L-serine		
GdnHCl	0.0	9.0	1.2	7.6	0.0	9.5	1.2	7.8
	0.25	8.1	1.2	6.5	0.25	8.7	1.3	6.8
	0.5	7.3	1.2	5.9	0.5	7.8	1.3	6.2
	1.0	6.0	1.4	4.4	1.0	6.2	1.3	4.9
	2.0	4.0	1.7	2.3	2.0	4.2	1.5	2.7
		L-threonine						
GdnHCl	0.0	9.1	1.2	7.6				
	0.25	8.3	1.3	6.5				
	0.5	7.4	1.3	5.8				
	1.0	6.1	1.3	4.6				
	2.0	4.0	1.6	2.4				

*The std. errs. for ΔG_D, m_g, and C_m are ±0.5 (kcal mol^{-1}), ±0.2 (kcal mol^{-1} M^{-1}), and ±0.2 (M), respectively.

Figs.8c and 8d show the [GdnHCl]-dependence of ΔG_D for Ferricyt *c* and Mb, respectively calculated in the absence and in the presence of 0.25 M alanine, arginine, glycine, proline, serine and threonine at pH 7.0 and 25 °C. Figs.8e and 8f show the [GdnHCl]-dependence C_m for Ferricyt *c* and Mb, respectively, calculated in the absence and in the presence of 0.25 M alanine, arginine, glycine, proline, serine and threonine at pH 7.0 and 25 °C.

Table 5. Dependence of the ΔG_D, m_g and C_m of Mb on GdnHCl concentration in the absence and presence of 0.25 M amino acids at pH 7.0 as monitored by Trp fluorescence (ex: 280; em: 365 nm)*.

Additive	Conc. (M)	Control ΔG_D (kcal mol^{-1})	Control m_g (kcal mol^{-1}M^{-1})	Control C_m (M)	Conc. (M)	L-alanine ΔG_D (kcal mol^{-1})	L-alanine m_g (kcal mol^{-1}M^{-1})	L-alanine C_m (M)
GdnHCl	0.0	7.3	1.3	5.6	0.0	7.9	1.3	5.9
	0.25	5.7	1.3	4.4	0.25	6.4	1.3	4.8
	0.5	4.0	1.2	3.5	0.5	4.9	1.3	3.6
	0.75	2.6	1.1	2.2	0.75	3.4	1.3	2.6
	1.0	1.7	1.4	1.2	1.0	2.1	1.3	1.7
		L-arginine				L-glycine		
GdnHCl	0.0	6.5	1.3	5.0	0.0	8.0	1.3	6.1

	0.25	5.1	1.2	4.1	0.25	6.7	1.4	4.9
	0.5	3.5	1.2	3.0	0.5	5.1	1.3	4.0
	0.75	2.2	1.1	2.0	0.75	3.7	1.3	3.0
	1.0	1.3	1.4	0.9	1.0	2.4	1.2	2.0
			L-proline				L-serine	
GdnHCl	0.0	7.5	1.3	5.6	0.0	8.4	1.3	6.2
	0.25	6.0	1.3	4.5	0.25	6.9	1.3	5.1
	0.5	4.5	1.3	3.5	0.5	5.5	1.4	4.0
	0.75	3.0	1.2	2.3	0.75	3.8	1.3	3.0
	1.0	1.8	1.2	1.5	1.0	2.4	1.1	2.2
			L-threonine					
GdnHCl	0.0	7.8	1.4	5.7				
	0.25	6.3	1.4	4.6				
	0.5	4.6	1.3	3.5				
	0.75	3.2	1.3	2.5				
	1.0	1.9	1.2	1.6				

*The std. errs. for ΔG_D, m_g, and C_m are ±0.5 (kcal mol^{-1}), ±0.2 (kcal mol^{-1} M^{-1}), and ±0.2 (M), respectively.

The ΔG_D and C_m decrease linearly with [GdnHCl] (Figs. 8c, 8d, 8e and 8f). However, as compared to in the absence of amino acids, the decrease in ΔG_D and C_m with [GdnHCl] are less pronounced in the presence of 0.25 M of alanine, glycine, proline, serine and threonine, while these are more pronounced in the presence of 0.25 M arginine (Figs. 8c, 8d, 8e and 8f). These results thus suggest that alanine, glycine, proline, serine and threonine counteract the denaturing action of GdnHCl for Ferricyt *c* and Mb. The counteracting effect of amino acids is more for serine and less for proline at pH 7.0 (serine> glycine> alanine >threonine>proline) (Figs. 8c, 8d, 8e, 8f and Tables-4-5). As compared to in the absence of amino acids, the ΔG_D and C_m values were found to be slightly decreased the presence of 0.25 M arginine (Figs. 8c, 8d, 8e, 8f and Tables-4-5), which is due to presence of guanidinium group (Gdn^+) in arginine. Arginine forms some specific type of interactions via aromatic and negatively charged surface amino acid residues of protein, termed as cation-π interaction through guanidium group [59, 63-66]. Earlier reports revealed that arginine interacts both with the protein backbone and also with the side chains of protein [67]. This properties of arginine helps in the destabilizing action on proteins. Since destabilizing cosolutes are described by their preferential binding to the proteins [68-69]. Therefore at lower concentration, arginine decreases the thermodynamic stability of proteins. The arginine shows the two different types of behaviors in aqueous medium from the view-point of dual behaviour of arginine, functioning both like an osmolyte and as a protein denaturant [70].

6.2.5 Effect of amino acids on the denaturant dependent tertiary structure of Ferricyt c and Mb at pH 7.0

Near-UV CD spectra or aromatic CD spectra, in the region 320–250 nm are generally used to probe the asymmetry of aromatic amino acids and regions of disulphide bonds. Native Ferricyt *c* in aqueous solution displays two distinct minima at 282 and 289 nm in the near-UV CD spectrum, which reflect the tertiary structural packing of Trp59 [71]. Signals from 250-270 nm are attributable to phenylalanine residues, signals from 270-290 nm are due to tyrosine, and the regions from 280-300 nm are attributable to tryptophan. Broad weak signals throughout the near-UV CD spectrum are due to the disulfide bonds present in native structure of proteins [71]. Fig.9a and Fig. 9b show the near-UV CD spectra of native Ferricyt *c* and Mb, respectively, in the absence and presence of 3.0 and 9.0 M urea with 0.5 M alanine, arginine, glycine, proline, serine and threonine at pH 7.0, 25ºC. The urea denatured protein (9.0 M urea) has not shown any aromatic band in the presence of 0.5 M of these amino acids at pH 7.0, which indicates that the amino acid (alanine, arginine, glycine, proline, serine and threonine) presences in reaction medium does not induce any structural component of denaturant-induced unfolded Ferricyt *c* and Mb. Due to high absorbance of L-alanine, arginine, glycine, proline, serine and threonine in the far-UV CD region, it is not possible to test the effect of these amino acids on the secondary structure of Ferricyt *c* and Mb.

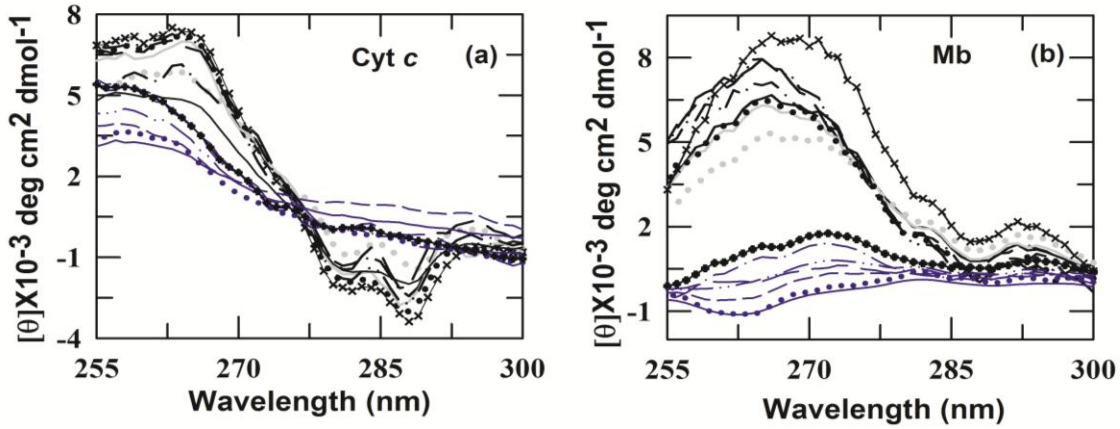

Fig.9. Panel (a) shows the near-UV CD spectra of Ferricyt *c* in the absence (~~××××~~) and in the presence of 3.0 M urea (solid black line), 9.0 M urea (solid blue line), 0.5 M alanine with 3.0 M urea (black dash-dot line) and 9.0 M urea (blue dash dot line); 0.5 M arginine with 3 M urea (gray dotted line) and 9 M urea (blue dotted line); 0.5 M glycine with 3 M urea (gray solid line) and 9 M urea (blue short dash line); 0.5 M proline with 3.0 M urea (long dash line) and 9.0 M urea (blue long dash line); 0.5 M serine with 3.0 M urea (black dotted line) and 9.0 M urea(++++) and 0.5 M threonine with 3.0 M urea (black dash double dotted line) and 9.0 M urea (blue dash double dotted line) at 25 °C. Panel (b) shows the near-UV CD spectra of Mb in the absence (~~××××~~) and in the presence of 1.5 M urea (solid black line), 9.0 M urea (solid blue line), 0.5 M alanine with 1.5 M urea (black dash-dot line) and 9.0 M urea (blue dash dot

line); 0.5 M arginine with 1.5 M urea (gray dotted line) and 9 M urea (blue dotted line); 0.5 M glycine with 1.5 M urea (gray solid line) and 9.0 M urea (blue short dash line); 0.5 M proline with 1.5 M urea (long dash line) and 9.0 M urea (blue long dash line); 0.5 M serine with 1.5 M urea (black dotted line) and 9.0 M urea (++++) and 0.5 M threonine with 1.5 M urea (black dash double dotted line) and 9.0 M urea (blue dash double dotted line) at 25 °C. Protein are used 55μM (Mb) and 60 μM (Ferricyt *c*) concentration, respectively.

6.3 Conclusion

Kinetic and thermodynamic parameters measured for CO-dissociation reaction of natively folded carbonmonoxycytochrome *c* (NCO) at varying concentrations of GdnHCl or urea in the absence and presence of 0.5 M amino acids (alanine, arginine, glycine, proline, serine, and threonine) revealed that (i) the rates of CO-dissociation for NCO (k_{diss}) initially decrease in subdenaturing region and then increase as denaturant concentration is increased from subdenaturing to denaturing milieu, which indicates that the low concentrations of denaturants restrict the internal dynamics of NCO, (ii) within the subdenaturing region, the inclusion of amino acids shifted the rate-denaturant profile vertically down to a lower log k_{diss}, which suggests that the amino acids show an additive effect with the denaturant-mediated constrained dynamics of NCO, (iii) from subdenaturing to denaturing region, the log k_{diss} increases due to structural unfolding of protein (iv) within subdenaturing region, log k_{diss} increase to a lesser extent in the presence of amino acids than in its absence, indicating that amino acids counteract the structural fluctuation that cause unfolding of protein, and (v) the structural fluctuation that unfolds the protein are found to be more opposed by the larger sized and lesser hydrophobic amino acids (arginine> serine> proline> glycine> alanine >threonine). Thermodynamic analysis of thermal and urea unfolding curves of Cyt *c* and Mb measured at varying concentrations of GdnHCl in the absence and presence of fixed concentration of amino acids (alanine, arginine, glycine, proline, serine, and threonine) reveals that (i) alanine, glycine, proline, serine and threonine counteract the deleterious effect of denaturants and they typically follow the this order: serine> glycine> alanine >threonine>proline, and (ii) at lower concentrations of GdnHCl, arginine shows an additive effect on the deleterious effect of denaturant while at higher concentrations of GdnHCl it counteracts the deleterious effect of GdnHCl.

6.4 References:

1. P.W. Hochachka, G.N. Somero, *Biochemical Adaptation: Mechanism and Process in Physiological Evolution*. Oxford University Press, New York, (2002).
2. P.H. Yancey, M.E. Clark, S.C. Hand, R.D. Bowlus, G.N. Somero, *Science* **217** (1982) 1214–1222.
3. P. H. Yancey, *The Journal of Experimental Biology* **208** (2005) 2819–2830.
4. S.N. Timasheff, *Proc. Natl. Acad. Sci. USA* **99** (2002) 9721–9726.
5. D.W. Bolen, I.V. Baskakov, *J. Mol. Biol.* **310** (2001) 955–963.
6. M. Niebuhr, M.H.J. Koch, *Biophys. J.* **89** (2005) 1978–1983.
7. B.J. Bennion, V. Daggett, *Proc. Natl. Acad. Sci. USA* **100** (2003) 5142–5147.
8. P.H. Yancey, J.F. Siebenaller, *J. Exp. Biol.* **202** (1999) 3597–3603.
9. T.Y. Lin, S.N. Timasheff, *Biochemistry* **33** (1994) 12695–12701.
10. I. Baskakov, D.W. Bolen, *Biophys. J.* **74** (1998) 2658–2665.
11. I. Baskakov, A.J. Wang, D.W. Bolen, *Biophys. J.* **74** (1998) 2666–2673.
12. A. J. Wang, D.W. Bolen, *Biochemistry* **36** (1997) 9101–9108.
13. H.C. Tseng, D.J. Graves, *Biochem. Biophys. Res. Commun.* **250** (1998) 726–730.
14. J. Tatzelt, S.B. Prusiner, W.J. Welch, *EMBO J.* **15** (1996) 6363–6373.
15. G.F. Xie, S.N. Timasheff, *Protein Sci.* **6** (1997) 222–232.
16. G.F. Xie, S.N. Timasheff, *Protein Sci.* **6** (1997) 211–221.
17. G.F. Xie, S.N. Timasheff, *Biophys. Chem.* **64** (1997) 25–43.
18. T.Y. Lin, S.N. Timasheff, *Protein Sci.* **5** (1996) 372–381.
19. Q. Zou, B.J. Bennion, V. Daggett, K. Murphy, *J. Am. Chem. Soc.* **124** (2002)1192–1202.
20. A.J. Wang, D.W. Bolen, *Biophys. J.* **71** (1996) 2117–2122.
21. T.O. Street, D.W. Bolen, G.D. Rose, *Proc. Natl. Acad. Sci. USA* **103** (2006) 13997–14002
22. D.W. Bolen, *Methods* **34** (2004) 312–322.
23. P. Attri, P. Venkatesu, M. J. Lee, *J. Phys. Chem. B* **114** (2010) 1471–1478.
24. P. Venkatesu, M. J. Lee, H. M. Lin, *Biochem. Eng. J.* **38** (2008) 326–340.
25. S. Ortiz–Costa, M. M. Sorenson, M. Sola–Penna, *FEBS J.* **275** (2008) 3388–3396.
26. P. Venkatesu, M. J. Lee, H. M. Lin, *J. Phys. Chem. B* **111** (2007) 9045–9056.
27. P. Venkatesu, M. J. Lee, H. M. Lin, *Arch. Biochem. Biophys.* **466** (2007)106–115.

28. P. Venkatesu, M. J. Lee, H. M. Lin, *J. Phys. Chem. B* **113** (2009) 5327–5338.
29. I. J. Finkelstein, A. M. Massari, M. D. Fayer, *Biophys J.* **92** (2007) 3652–3662.
30. C. Viappiani, S. Bettati, S. Bruno, L. Ronda, S. Abbruzzetti, A. Mozzarelli, W. A. Eaton, *Proc. Natl. Acad. Sci. USA.* **101** (2004) 14414–14419.
31. A. Ansari, M. J. Colleen, E. R. Henry, J. Hofrichter, W. A. Eaton, *Biochemistry* **33** (1994) 5128–5145.
32. H. Frauenfelder, B.H. McMahon, R.H. Austin, K. Chu, J.T. Groves, *Proc. Natl. Acad. Sci. U. S. A.* **98** (2001) 2370–2374.
33. P.W. Fenimore, H. Frauenfelder, B.H. McMahon, F.G. Parak, *Proc. Natl. Acad. Sci. U. S. A.* **99** (2002) 16047–16051.
34. P.W. Fenimore, H. Frauenfelder, B.H. McMahon, R.D. Young, *Proc. Natl. Acad. Sci. U. S. A.* **101** (2004) 14408–14413.
35. A. Ansari, C. M. Jones, E. R. Henry, J. Hofrichter, W. A. Eaton, *Science* **256** (1992) 1796–1798.
36. D. Beece, L. Eisenstein, H. Frauenfelder, D.Good, M.C. Marden, L. Reinisch, A. H. Reynolds, L.B. Sorensen, K.T. Yue, *Biochemistry* **19** (1980) 5147–5157.
37. H. Frauenfelder, F. Parak, R. D. Young, *Ann. Rev. Biophys. Biophys. Chem.* **17** (1988) 451–479.
38. I. Schlichting, J. Berendzen, G. N. Phillips, R. M. Sweet, *Nature* **371** (1994) 808– 812.
39. Y. Bai, T. R. Sosnick, L. Mayne, S.W. Englander, *Science* **269** (1995)192–197.
40. A. K. Bhuyan, *Biochemistry* **41** (2002) 13386–13394.
41. R. Varhac, *Biochem. Biophys. Acta* **183** (2013) 739–744.
42. R. Kumar, N. P. Prabhu, M. Yadaiah, A.K. Bhuyan, *Biophys. J.* **87** (2004) 2656–2662.
43. R. Kumar, A. K. Bhuyan, *J. Biol. Inorg. Chem.* **14** (2009)11–21.
44. R. Jain, S. Kaur, R. Kumar, *J. Biochem.* **153** (2013) 161–177.
45. S. Kumar, D. Sharma, R. Kumar, *Biochim. Biophys. Acta.* **1844** (2014) 641–655.
46. R. Jain, D. Sharma, R. Kumar, *J. Biochem* **154** (2013) 341–354.
47. E. Margoliash, N. Frohwirt, *Biochem. J.* **71** (1959) 570–572.
48. R. Varhac, M. Antalik, M. Bano, *J. Biol. Inorg. Chem.* **9** (2004)12–22.

49. G. I. Makhatadze, M. M. Lopez, J. M. Richardson, S. T. Thomas, *Protein Sci.* **7** (1998) 689–697.
50. B. Iberra-Molero, V. V. Loladze, G. I. Makhatadze, J. M. Sanchez-Ruiz, *Biochemistry*. **38** (1999) 8138–8149.
51. http://marlin.bio.umass.edu/biology/kunkel/probe/buffers/aa.html
52. J. Kyte, R. F. Doolittle, *J. Mol. Biol.* **157** (1982) 105–32.
53. J. Mikšovská, J.H. Day, R.W. Larsen, *J. Biol. Inorg. Chem.* **8** (2003) 621–625.
54. M. M. Santoro, D.W. Bolen, *Biochemistry* **31** (1992) 4901–4907.
55. A. K. Bhuyan, D. K. Rao, N. P. Prabhu, *Biochemistry* **44** (2005) 3034−3040.
56. S. N. Timasheff, *Water and Life* (G. N. Somero, C. B. Osmond, and L. Bolis, eds) Springer-Verlag, Berlin and Heidelberg (1992) pp. 69–77.
57. V. Vagenende, A. X. Han, M. Mueller, B. L. Trout, *ACS Chem. Biol.* **8** (2013) 416−422.
58. D. Shukla, B. L. Trout, *J. Phys. Chem. B* **114** (2010)13426−13438.
59. B. M. Baynes, D. I. C. Wang, B. L. Trout, *Biochemistry* **44** (2005) 4919−4925.
60. D. Shukla, C. P. Schneider, B. L. Trout, *Adv. Drug Delivery Rev.* **63** (2011) 1074−1085.
61. S. Sharma, S. Sarkar, S.S. Paul, S. Roy, K. Chattopadhyay, *Sci. Rep.* **3** (2013) 3525.
62. M. M. Santoro, D. W. Bolen, *Biochemistry* **27**(1988) 8063−8068.
63. P. B. Crowley, A. Golovin, *Proteins: Structure, Function, and Bioinformatics* **59** (2005) 231–239.
64. J. P. Gallivan, D. A. Dougherty, *Proc. Natl. Acad. Sci. U. S. A.* **96** (1999) 9459–9464.
65. D. A. Dougherty, *Acc Chem. Res.* **46** (2013) 885–893.
66. H. Minoux, C. Chipot, *J. Am. Chem. Soc.* **121**(1999)10366–10372.
67. T. Arakawa, K. Tsumoto, Y. Kita, B. Chang, D. Ejima, *Amino Acids* **33** (2007) 587─605.
68. T. Arakawa, D. Ejima, K. Tsumoto, N. Obeyama, Y. Tanaka, Y. Kita, et al., *Biophys. Chem.* **127** (2007) 1─8.
69. T. B. Eronina, N. A. Chebotareva, N. N. Sluchanko, V. V. Mikhaylova, V. F. Makeeva, S. G. Roman, S. Y. Kleymenov, B. I. Kurganov, *Int J Biol Macromol.* **68** (2014) 225–232.
70. A.M. Davies, J.G. Guillemette, M. Smith, C. Greenwood, A. G. P. Thurgood, A. G. Mauk, G.R. Moore, *Biochemistry* **32** (1993)5431–5435.
71. S. M. Kelly, N. C. Price, *Current Protein and Peptide Science* **1** (2000) 349–384.

Chapter 7

Structural, Kinetic and Thermodynamic Characterizations of the Macromolecular Crowding-Induced Molten Globule States of the Alkali pH-Denatured Proteins

7.1 Introduction

The fundamental route in protein folding is the compaction of linear chain of amino acid residues into its biologically active three-dimensional structure. It is believed that one or more distinct, populated intermediates are involved during the course of the protein folding process [1]. Such intermediates have compact structures with native like secondary structure content, but disordered or fluctuating tertiary structure [2-8]. These intermediate structures are termed as molten globule (MG)-state. The term "molten globule" has been given by Ohgushi & Wada [4]. The MG-state is typically populates at the late stages of folding [6-7,9-14] but it has also been detected at the early stages of folding of several proteins [15-17]. It is assumed that the MG state, as well as other non-native states of proteins, can be involved for protein insertion and translocation processes through organelles membranes [18-21]. Some previous studies revealed that the intrinsically disordered native like proteins that resemble MG-state [22-26] involved in cell signaling and worked as a regulator, by interactions with DNA and other proteins [27-31]. A previous report revealed that the pH-dependent MG transition is required for the activity of steroidogenic acute regulatory protein that stimulates steroid synthesis [32].

Due to their short-lived, the MG-states are difficult to study at neutral pH. At the extremes of pH, the MG-state is typically stabilized and populated in the presence of salt [9, 33-35]. Few earlier reports suggest that the sugars, polyols, and low concentrations of guanidine hydrochloride (GdnHCl) stabilize and refold the acid-denatured state of proteins to MG states [36-39]. Few recent studies suggest that high concentration of crowding agents also increases the stability and structural contents of folded and partially folded proteins [41-48]. Some previous studies revealed that high concentrations of crowding agents also transform the acid-denatured proteins to MG-states [49-50]. The excluded volume effects are predicted to favor the adoption of

compact conformation as opposed to expanded macromolecular conformations, which are the results of decrease in the total excluded volume. The crowding-induced collapse is important because it can cause aggregations [40, 50-55], which are linked with numerous neurodegenerative disorders [56].

Although, crowding agents usually favor refolding [49, 57-59], but in some cases they appear to be ineffective [60-61]. According to excluded volume theory, a non-specific force between the crowding agents and macromolecules (proteins) that promotes the reduction of total excluded volume which results an adoption of compact conformation, as opposed to expanded macromolecular conformations [62-68]. While the crowding-induced MG-state of acid-denatured protein is studied earlier [49], the crowding-induced MG-state of base-denatured protein is not explored so far. This is the first study that shows the high concentration of crowding agents (dextran 70 and ficoll 70) transform the base-denatured cytochrome *c* (Cyt *c*), apomyoglobin (apoMb) and lysozyme (Lyz) to MG-states *i.e.* C_B-states (crowding agents induced MG-states) at pH 12.9 (±0.1). The C_B-states meet the generic properties of MG-state, *i.e.*, molecular compact state with native-like secondary structure but lacks tertiary structure. The base-denatured Cyt *c* and apoMb (pH 12.9 (±0.1)) also show cold denaturation in the absence of crowding agent. With increase in crowding agent's concentrations, the thermal denaturation temperature increase and the cold denaturation temperature decrease. Alkali-denatured Lyz doesn't show cold denaturation but increase the thermal denaturation temperature in the presence of high concentration of crowding agents. Analysis of kinetic and thermodynamic parameters measured for CO-association reactions of alkaline Ferrocytochrome *c* (Ferrocyt *c*) at pH 12.9 (±0.1) in the absence and presence of different concentrations of crowding agent (dextran 70 and ficoll 70) reveal that the crowding agent presence in reaction medium restrict the internal dynamics of base-denatured protein.

7.2 Results and Discussion

7.2.1 pH-induced denaturation of Ferricyt c, apoMb and Lyz

Figs. 1a, 1b and 1c show the normalized fluorescence-monitored pH-unfolding curves of Cyt *c*, apoMb and Lyz, respectively at 25ºC. Fig. 1a, 1b and 1c also present the far-UV CD (222

nm) monitored pH-unfolding curves of Cyt *c*, apoMb and Lyz, respectively at 25ºC. Data in Fig. 1 provide two important informations (i) the far-UV CD-monitored pH unfolding curves of Cyt *c* and Lyz shift to higher pH than fluorescence monitored unfolding, and (ii) the fluorescence and Far-UV CD-monitored unfolding curves of apoMb are superimposable to each other.

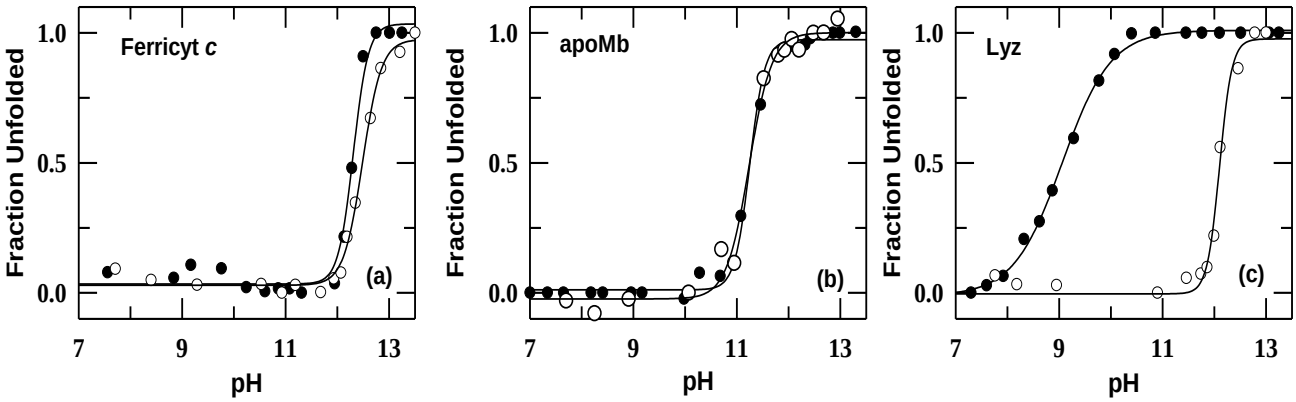

Fig.1. Panels (a), (b) and (c) present the normalized fluorescence monitored (●) pH-unfolding curves of Cyt *c*, apoMb and Lyz, respectively at 25ºC. Panels (a), (b) and (c) also present the far-UV CD (222 nm) monitored (○) alkaline pH-induced unfolding curves for Cyt *c*, apoMb and Lyz, respectively at 25ºC. Solid lines in panel (a) to (c) are fit according to Handerson-Hasalbalch equation (Chapter 2) [9], at 25 °C.

The pH titration curves of Cyt *c*, apoMb and Lyz were analyzed by using the modified Handerson-Hasalbalch equation (chapter 2 equation (8)) [9] which provide the pH-midpoint, (c_m) and the number of OH^- titrated (*n*) (Table 1).

Table1. Fluorescence (exitation.280; emission 365) and far-UV CD (222nm) monitored pH-induced denaturation midpoint, (c_m) for Ferricyt *c* and apoMb and Lyz

	fluorescence monitored		far-UV CD (222nm) monitored	
	pH-midpoint (*C*m)	Number of OH^- titrated (*n*)	pH-midpoint (*C*m)	Number of OH^- titrated (*n*)
Ferricyt *c*	12.3	3.0	12.4	3.2
apoMb	11.2	3.0	11.2	2.0
Lyz	9.1	1.0	12.1	3.6

The single tryptophan W59 of Cyt *c* is typically buried in the hydrophobic core and almost no fluorescence is observed (fluorescence-silent) at native state [69]. However, upon denaturation of protein, a dramatic increase in fluorescence intensity occurs [69-70]. Thus the fluorescence intensity can be used as reliable indicator for molecular expansion and compaction of Cyt *c*. ApoMb has two tryptophans and after unfolding of protein, the fluorescence intensity gets quenched because of exposure of tryptophan residues to the polar solvent [71-73]. Similarly,

unfolding of Lyz (contain 6 aromatic amino acids) to alkaline pH caused rapid decrease in fluorescence intensity with red shift presumably because of exposure of tryptophan residues to the polar solvent and ionization of certain tyrosine groups [74-75]. It is clear from fluorescence-monitored pH titration curves that the Ferricyt *c* (Fig. 1a), apoMb (Fig. 1b) and Lyz (Fig. 1c) get unfolded at extreme alkaline conditions (pH 12.9 (±0.1)). The non-coincidence of the pH transitions of Ferricyt *c* and Lyz monitored by far-UV CD and fluorescence are due to the presence of an equilibrium intermediate in the native to denatured state transition [9,71-72,75]. An earlier report by Nakamura et al have also shown the presence of an equilibrium intermediate in the native to denatured state transition of Ferricyt *c* at pH ~4.1 [33].

7.2.2 Effect of crowding agents on the fluorescence emission spectrum of base-denatured Ferricyt c, apoMb and Lyz

Figs. 2a, 2b and 2c show the effects of crowding agents (dextran 70 and ficoll 70) on the fluorescence emission spectrum of base-denatured Ferricyt *c*, apoMb and Lyz at pH 12.9 (±0.1) (U_B-state). For comparison, Figs. 2a, 2b and 2c also present fluorescence emission spectrum of native proteins at pH 7.0. Fig. 2 clearly shows that the emission observed for the U_B-states of Ferricyt *c* (Fig. 2a, spectrum 2), apoMb (Fig. 2b, spectrum 2) and Lyz (Fig. 2c, spectrum 2) decrease in the presence of ~300 mg ml^{-1} of dextran 70 (Fig. 2a, b, c spectrum 4) and ficoll 70 (Fig. 2a, b, c spectrum 3) which suggests that the base-denatured proteins get compact in the presence of crowding agents.

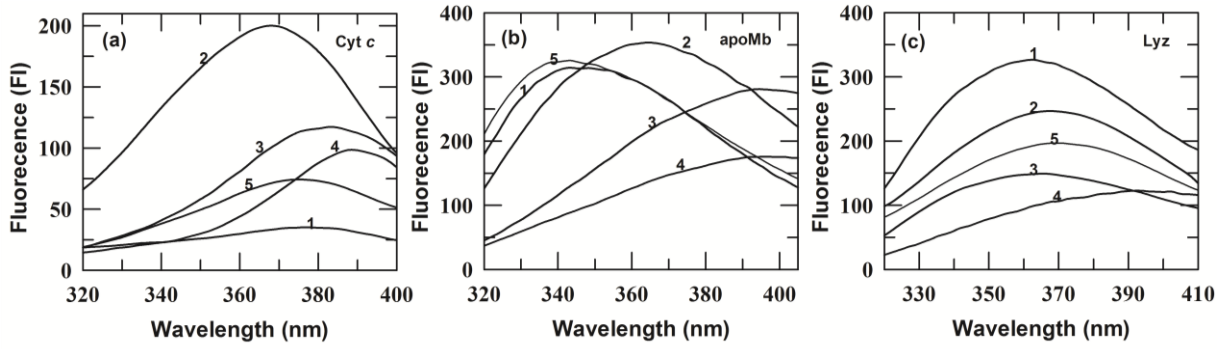

Fig.2. Panels (a), (b) and (c) presents the different state fluorescence emission spectra for Cyt *c*, apoMb and Lyz, respectively at 25ºC indicating the molecular compaction of base denatured protein in the presence of different crowding agents; 1, pH 7.0, native state; 2, pH 12.9(± 0.1) unfolded state; 3, pH 12.9 (±0.1) with 300 mg ml^{-1} ficoll 70; 4, pH 12.9 (±0.1) with 300 mg ml^{-1} dextran 70; 5, pH 12.9 (±0.1) with 2.0 M salt (2.0 M NaCl in panel (a) and (b) and in panel (c) with 2.0 M KCl), respectively.

It was reported that NaCl also compacts the base-denatured proteins to MG-states [9, 35]. Fig. 2 shows that the base-denatured Ferricyt *c*, apoMb and Lyz become compact in the presence of 2.0 M NaCl/ 2.0 M KCl (Fig.2a, b, c spectrum 5) at 25 °C.

7.2.3 Effect of crowding agents on the secondary structure of base-denatured Ferricyt c, apoMb and Lyz

Figs. 3a, 3b and 3c show the far-UV CD spectrum of Ferricyt *c*, apoMb, and Lyz, respectively, in the absence and presence of 5.0 M GdnHCl at pH 7.0, 25 °C. The far-UV CD spectrum of native Ferricyt *c*, apoMb and Lyz at pH 7.0 exhibit two negative bands at 208 nm and 222 nm (Fig. 3a, 3b, 3c), which reflect the well defined as α-helical secondary structure [76]. Figs. 3a, 3b, 3c also show the far-UV CD spectrum of base-denatured Ferricyt *c*, apoMb, and Lyz, respectively in the absence and presence 400 mg ml^{-1} of crowding agents at pH 12.9 (±0.1).

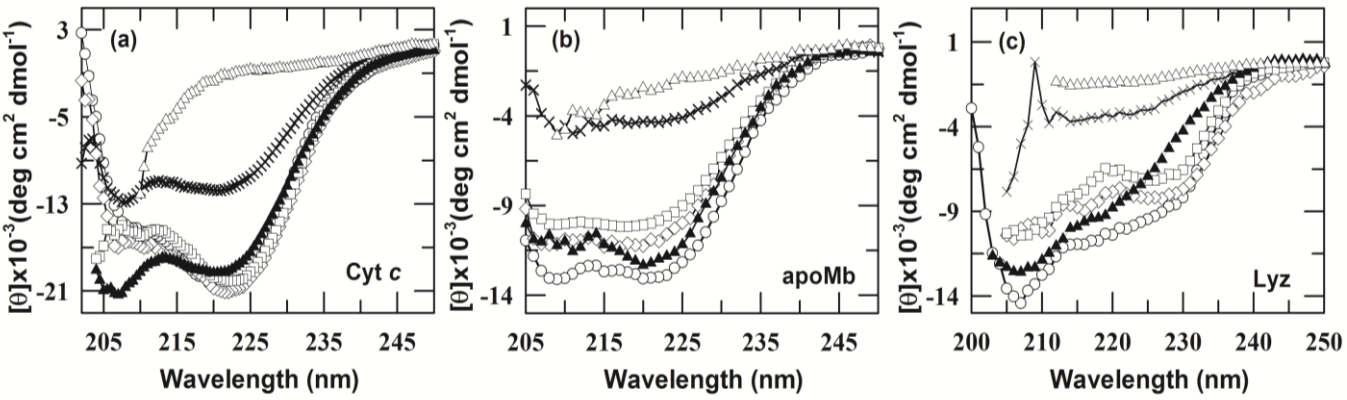

Fig.3. Effect of crowding agents on the secondary structure of base-denatured Ferricyt *c*, apoMb and Lyz at 25 °C. Panel (a), (b) and (c) presents far-UV CD spectra for different states of Ferricyt *c*, apoMb and Lyz at 25°C: pH 7.0, native state (○○○○); pH 12.9 (±0.1), U_B-state (××××); pH 12.9 (±0.1), 400mg ml^{-1} dextran 70 (△△△△); pH 12.9(±0.1), 400 mg ml^{-1} ficoll 70 (□□□□); pH 12.9 (±0.1), 1.5 M salt (▲▲▲▲) (NaCl in panel (a) and (b) and KCl in panel (c)); and pH 7, 5 M GdnHCl (AAAA), respectively.

The peptide bands in the far-UV CD spectrum of Ferricyt *c*, apoMb, and Lyz at pH 7.0 are significantly disrupted in the presence of 5.0 M GdnHCl at pH 7.0, (Figs. 3a, 3b, 3c). The peptide bands in the far-UV CD spectrum of Ferricyt *c*, apoMb, and Lyz are also significantly disrupted in the absence of denaturant at pH 12.9 (±0.1) at 25 °C. These finding indicate that the secondary structures of Ferricyt *c*, apoMb, and Lyz are significantly lost in the absence of denaturant at pH 12.9 (±0.1) and in the presence of 5.0 M GdnHCl at pH 7. When ~ 400 mg ml^{-1} crowding agent (dextran 70 and ficoll 70) is included in the base-denatured Ferricyt *c*, apoMb,

and Lyz at pH 12.9 (±0.1), the base-denatured proteins acquired the native-like peptide bands (Figs. 3a, 3b, 3c), which reveal that the high concentrations of crowding agent induce the native like secondary structures in the base denatured proteins. Dextran and ficoll are inert and non-reactive to protein but occupying the large space in the reaction medium along with protein of interest. So, inert dextran and ficoll decreases the volume available to other macromolecules such as proteins, thus favoring the more compact state over the more expanded base-unfolded state. Therefore the dextran and ficoll-induced molecular compaction in the base-denatured Ferricyt *c*, apoMb and Lyz is attributed to the excluded volume effect.

7.2.4 Crowding agents-induced refolding in the base-denatured Ferricyt c, apoMb and Lyz

Figs. 4a, 4c and 4e show the change in the far-UV CD ellipticity at 222 nm for the base-denatured Ferricyt *c*, apoMb and Lyz, respectively as a function of [Crowding agents] at pH 12.9 (±0.1), 25 °C. Figs. 4a, 4c and 4e clearly revel that the crowding agents transform the base-denatured Ferricyt *c*, apoMb and Lyz (U_B-state) to C_B-states at 25ºC. The Gibbs free energy change, ΔG, for the two-state transition, $U_B \rightarrow C_B$ can be calculated by the equation (1):

$$\Delta G = -RT \ln K = -RT \ln\left[(Y_{obs} - Y_{U_B}) / (Y_{C_B} - Y_{obs}) \right] \qquad (1)$$

where Y_{obs} is the observed value of the CD signal, Y_{UB} and Y_{CB} are the corresponding values for the U_B and C_B-states, respectively. Figs. 4b, 4d and 4f show the ΔG *vs.* [Crowding agents] plots for refolding of Ferricyt *c*, apoMb and Lyz, respectively.

On the assumption of a linear dependence of ΔG on [Crowding agents] [77], the least-squares fit of the data to equation (2), provides the values of ΔG^o and *m* (slop reflecting the cooperatively of the transition) (Table 2.)

$$\Delta G = \Delta G^0 - m[Crowding\ agents] \qquad (2)$$

Table 2 Thermodynamic parameters, free energy (ΔG^o) and *m* (slop) for the refolding (CD 222 nm) of base-denatured proteins (Ferricyt *c*, apoMb and Lyz) in the presence of crowding agents at pH 12.9 (±0.1), 25ºC.

Crowding agents	ΔG^o (kcal mol^{-1})	*m* (kcal mol^{-1} M^{-1})
Ferricyt *c*		
dextran 70	1.81 (0.1)	0.0094
ficoll 70	1.73 (0.1)	0.0086
apoMb		
dextran 70	0.98 (0.1)	0.013

ficoll 70	0.90 (0.1)	0.0074
Lyz		
dextran 70	1.61 (0.1)	0.012
ficoll 70	1.59 (0.1)	0.011

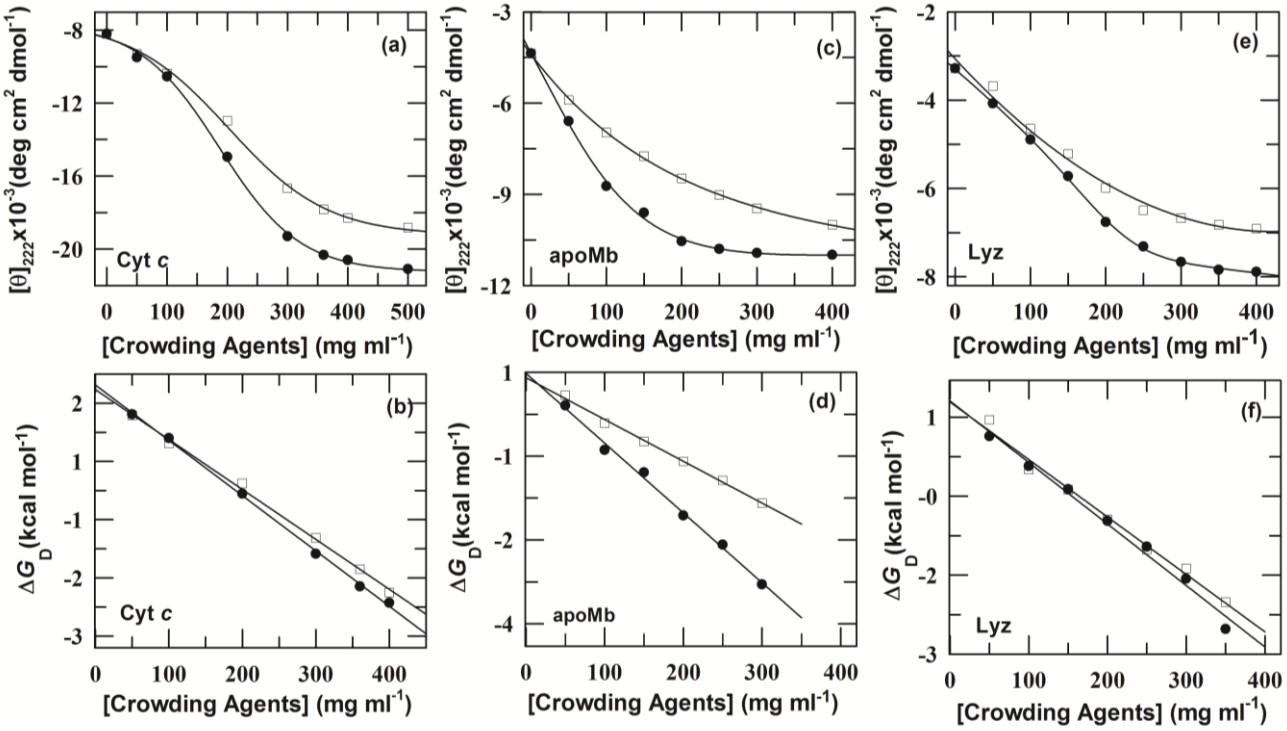

Fig.4. Panels (a), (c) and (e) present the change of mean residue ellipticity of Cyt *c*, apoMb and Lyz, respectively estimated at 222 nm as a function of dextran 70 (●) and ficoll 70(□) concentration at pH 12.9 (±0.1). The continuous lines are just guide to the eye. Panel (b), (d) and (f) presents the plots of Δ*G*, as the function of dextran 70 (●) and ficoll 70 (□) concentration for refolding of base denatured Cyt *c*, apoMb and Lyz , respectively at pH 12.9 (±0.1). The continuous line represents Δ*G* values and was obtained from the best fit to the experimental data according to equation (2).

For a given protein, the ΔG^o values for dextran 70 and ficoll 70 are within error identical (Table 2), suggesting that ΔG^o is independent of the nature of the crowding agent and thus it is a property of the protein alone. Although, the physical importance of the factor *m* is not fully understood, but some earlier reports revealed that it reflects the difference between the accessibility of surface areas of native and denatured states of the polypeptide chain for a given denaturant [77-80]. The high *m* value for dextran 70 (Table 2) than ficoll 70 (Table 2) suggests high effectiveness of dextran 70 towards refolding of base-denatured proteins to MG-states as compared to Ficoll 70.

7.2.5 Effect of crowding agents on the tertiary structures of base-denatured Ferricyt c, apoMb and Lyz

Near-UV CD (aromatic CD spectrum) in the region 250–320 nm is generally used to probe the tertiary structures of the proteins [82-83]. The Near-UV CD ellipticity of proteins is mainly because of aromatic amino acids residues viz; tryptophan, tyrosine and phenylalanine with peaks at 291, 277 and 256 nm, respectively [82-83]. Conventionally, the MGs are generally identified by a dramatic loss of near-UV CD signal [84-85]. Figs. 5a, 5b and 5c present the relevant aromatic CD spectra of different states of Ferricyt *c*, Lyz and apoMb, respectively.

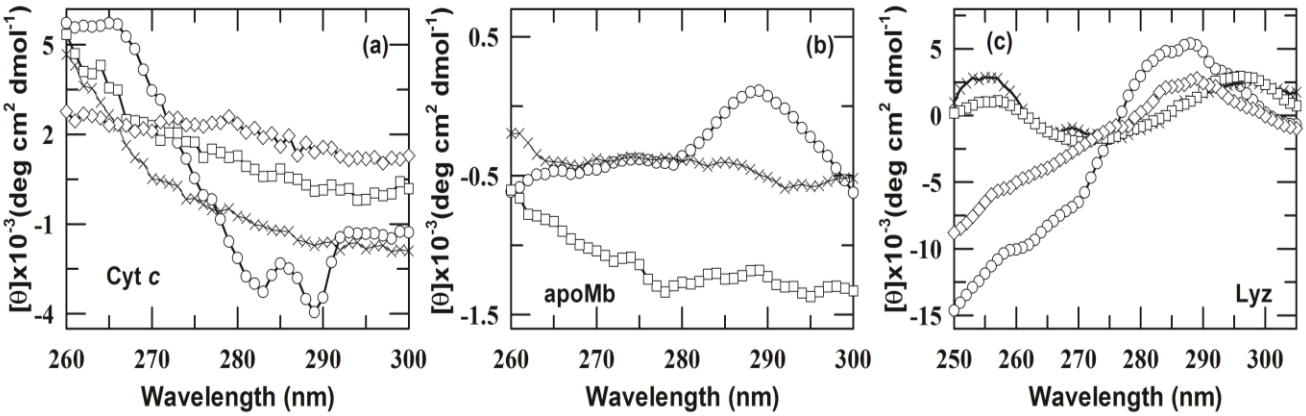

Fig.5. Panels (a), (b) and (c) present the near-UV CD spectra for different states of Ferricyt *c*, apoMb and Lyz at 25°C: pH 7.0, native state (○○○○); pH 12.9(±0.1), U_B-state (××××); pH 12.9(±0.1), 400 mg ml^{-1} dextran 70 (◊◊◊◊) and pH 12.9(±0.1), 400 mg ml^{-1} ficoll 70 (□□□□), respectively.

Conventionally, the MGs are generally identified by a dramatic loss of near-UV CD signal [84-85]. Figs. 5a, 5b and 5c present the relevant aromatic CD spectra of different states of Ferricyt *c*, Lyz and apoMb, respectively. The aromatic CD band responsible for tertiary structure is significantly lost at pH 12.9 (±0.1) (Figs. 5a, 5b and 5c). When ~ 400 mg ml^{-1} crowding agent (dextran 70 and ficoll 70) is included in the base-denatured Ferricyt *c* and Lyz at pH 12.9 (±0.1) the base-denatured Ferricyt *c* and Lyz not acquired the aromatic band (Figs. 5a, 5b, 5c). The base-denatured apoMb at pH 12.9 (±0.1) also not acquired the aromatic band with inclusion of 400 mg ml^{-1} ficoll 70. These finding indicate that the inclusion of high concentrations of crowding agents does not induces the tertiary structures in the base denatured Ferricyt *c*, apoMb and Lyz.

7.2.6 ANS binding to different states of Ferricyt c, apoMb and Lyz

Traditionally, ANS, an extrinsic fluorescent probe which binds to exposed hydrophobic clusters of folding intermediates is widely used to detect the MG-states of proteins [84, 86-90]. The binding of ANS to different states of protein generally increases the ANS fluorescence intensity of MG-state more than the native and unfolded states [84, 86-90]. ANS has much stronger affinity to MG-state as compared with the native or the fully unfolded states. The stronger affinity to MGs is because of the absence of rigid packing of hydrophobic clusters in MGs and hence, due to a greater accessibility of the protein hydrophobic core for a solvent. Figs. 6a, 6b and 6c show the ANS fluorescence spectra of native Ferricyt *c*, apoMb and Lyz, respectively at 25 °C, pH 7.0. Figs. 6a, 6b and 6c also show the ANS fluorescence spectra of base-denatured Ferricyt *c*, apoMb and Lyz, respectively in the absence and presence of ~400 mg ml^{-1} crowding agent (dextran 70 and ficoll 70) at 25 °C. Clearly, the ANS fluorescence intensity of base-denatured Ferricyt *c*, apoMb and Lyz is increased more in the presence of ~400 mg ml^{-1} crowding agent (spectra 3 and 4 of Figs. 6a, 6b and 6c) than in its absence (spectrum 2 of Figs. 6a, 6b and.6c). This finding provide an evidence that the high concentration of crowding agents transform base-denatured Ferricyt *c*, apoMb and Lyz to MG-states at pH 12.9 (±0.1), 25 ºC.

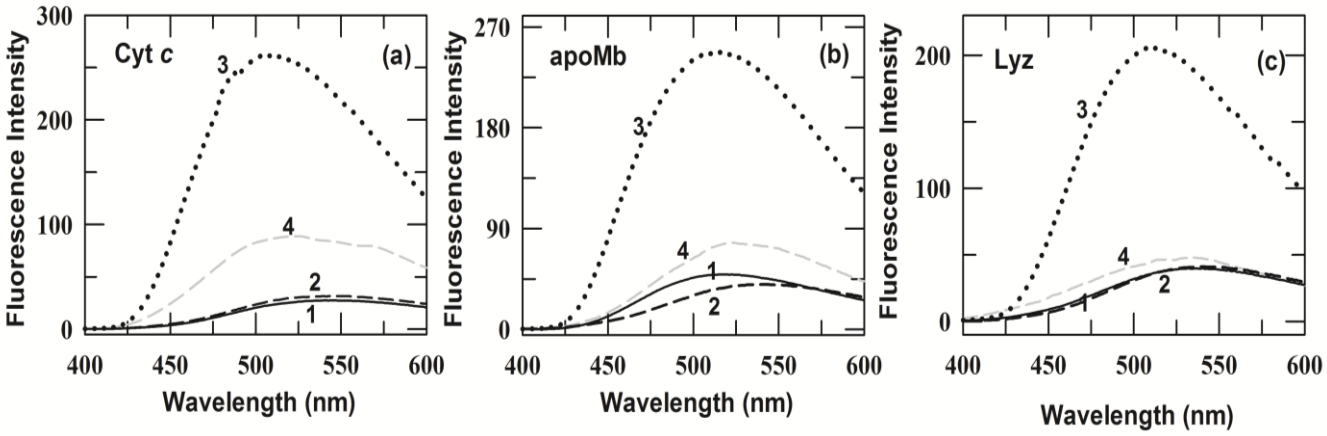

Fig.6. Panels (a), (b) and (c) present the different states fluorescence emission spectra of ANS-protein complex for Cyt *c*, apoMb and Lyz as: native protein pH 7 (spectrum 1; solid black line), pH-12.9 (±0.1) unfolded state (spectrum 2, black short dash line), pH 12.9 (±0.1) with 400 mg ml^{-1} ficoll 70 (spectrum 3; black dotted line), pH 12.9 (±0.1) with 400 mg ml^{-1} dextran 70 (spectrum 4; gray short-dash line), respectively at 25ºC.

Because of the rigid and tightly packed conformations interior of native protein molecule with a low accessibility of protein hydrophobic clusters to a solvent leads to decrease ANS affinity for the native protein (spectrum 1 of Figs. 6a, 6b and.6c). The solvent accessible hydrophobic core

are completely absent in the denatured or unfolded proteins (spectrum 2 of Figs. 6a, 6b and 6c) [90]. Therefore it shows least binding affinity to unfolded proteins.

7.2.7 Effects of crowding-agents on thermal denaturations of base-denatured proteins

To evaluate the role of hydrophobic interactions and to determine the effects of crowding agents on thermal denaturations of base-denatured Ferricyt *c*, apoMb and Lyz, the far-UV CD monitored (222 nm) thermal denaturation curves of Ferricyt *c*, apoMb and Lyz were collected at pH 12.9 (±0.1), respectively in the absence and presence of ~ 300 mg ml^{-1} of dextran 70 and ficoll 70. Figs. 7a, 7b and 7c present the far-UV CD monitored normalized thermal denaturation curves of Ferricyt *c*, apoMb and Lyz at pH 12.9 (±0.1), respectively in the absence and presence of ~ 300 mg ml^{-1} of dextran 70 and ficoll 70. Earlier studies show that the pH-denatured Ferricyt *c* and apoMb can undergoes cold denaturation process in the presence of low concentrations of salt [9, 91-92]. Data in Figs. 7a and 7b show that of the base-denatured Ferricyt *c* and apoMb also show cold denaturation in the presence of 0.01 M NaCl at pH 12.9 (±0.1). Since the low temperature ellipticity values are dependent on crowding agent concentration while the high-temperature ones are not (Figs. 7a and 7b), so, the thermal denaturation data for base-denatured Ferricyt *c*, apoMb and Lyz were normalized using equation (3)

$$\theta = \frac{\theta_{obs} - (m_1 T + \theta_1)}{(m_2 T + \theta_2) - (m_1 T + \theta_1)} \qquad (3)$$

where, θ_{obs} is the observed ellipticity, T is the temperature, m_1 and θ_1 are the slope and intercept, respectively, of the pre transition baseline for the 300 mg ml^{-1} dextran 70 curve, and m_2 and θ_2 are the slope and intercept of the post-transition baseline in the presence of a given concentration of dextran 70 and ficoll 70. The normalized thermal unfolding curves in Figs. 7a, 7b and 7c were analyzed by the Gibbs-Helmholtz equation (chapter 2 equation (6)) [9]. Table 3 listed the T_m, ΔH_m and ΔC_p values for base-denatured Ferricyt c, apoMb and Lyz obtained in the absence and presence of 300 mg ml^{-1} of dextran70 and ficoll 70. The T_m value for the thermal unfolding of base denatured Ferricyt *c*, apoMb and Lyz increase with increasing concentration of dextran 70 and ficoll 70 (Table 3), and which is more increased for dextran 70 than ficoll 70. This finding indicates that the macromolecular crowding effect alters the thermal stability of base-denatured

proteins. Some earlier reports revealed that the crowding agents increase the thermal stability of acid-denatured protein [49, 93].

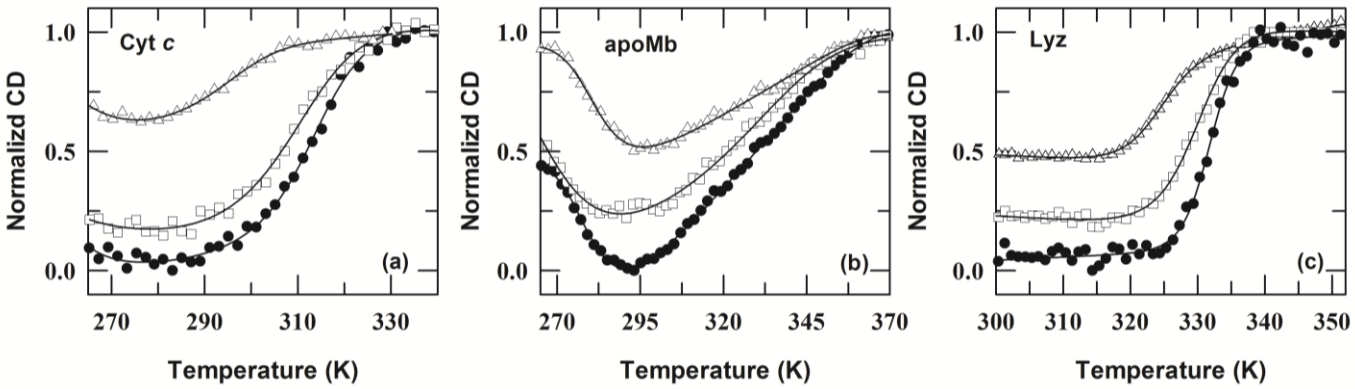

Fig.7. Panels (a) (b) and (c) present the normalized far-UV CD (222nm) monitored thermal melting curves of alkali-denatured Ferricyt *c*, apoMb and Lyz at pH 12.9 in the presence of 0.001 M NaCl (Δ), 300 mg ml^{-1} dextran 70, (•) and 300 mg ml^{-1} ficoll 70 (□), respectively. The continuous lines are fits according to Gibbs-Helmholtz equation (chapter 2 equation (6)). Table 3 listed the thermodynamic parameters extracted from the 222 nm data set.

Table 3 Effect of crowding agents on thermodynamic parameters (midpoint temperature (T_m), enthalpy (ΔH_m), and heat capacity (ΔC_p)) for thermal unfolding (CD 222 nm) of base-denatured Ferricyt *c*, apoMb and Lyz at pH 12.9 (±0.1).

Crowding agents	Concentration (crowder) (mg ml^{-1})	T_m (K)	ΔH_m (kcal mol^{-1})	ΔC_p (kcal mol^{-1} $K^{-1)}$
Ferricyt *c*				
Control	0.0	292.1	30.0	1.2
dextran 70	300	311.8	31.9	1.1
ficoll 70	300	308.1	26.4	1.0
apoMb				
Control	0.0	333.0	8.2	0.4
dextran 70	300	338.1	21.0	0.7
ficoll 70	300	335.0	19.3	0.6
Lyz				
Control	0.0	323.9	70.5	1.2
dextran 70	300	331.4	80.0	1.4
ficoll 70	300	329.2	72.1	1.3

* The uncertainty in the values of T_m, ΔH_m and ΔC_p are ±1.0 K, ±5.0 kcal mol^{-1} and ±0.5 kcal $mol^{-1}K^{-1}$, respectively.

The base-denatured Ferricyt *c* and apoMb in the absences of crowding agent undergoes cold denaturation (Figs. 7a and 7b). With increasing crowding agent concentration, the low temperature unfolding transition becomes less obvious (Figs. 7a and 7b). However, the base-denatured Lyz at pH 12.9 (±0.1) in the absence of crowding agent does not show cold denaturation process (Fig. 7c). Cold denaturation phenomenon is typically based on the

thermodynamic principles of protein stability [94-96] and generally arises due to decrease of hydrophobic interactions in proteins as temperature is lowered [97]. However, few previous reports reveal that both hydrophobic and hydrophilic interactions are accountable for cold denaturation [98-99].

7.2.8 Effects of dextran 70 and ficoll 70 on the internal dynamics of base-denatured Cyt c

Some previous studies on the internal mobility of different states of protein reveal that the MG-state exhibits increased side chains fluctuations relative to that of in the native-state [3, 5]. Although, overall motional freedom of MG-state is restricted relative to the dynamic of the denatured state. Few earlier reports have shown that the salt-induced MG-state of base-denatured protein was stiff and dynamically constrained at pH ~13 [35, 100]. To examine how dynamic the interior of the crowding induced MG-state of base-denatured proteins, the experiments were conducted for the kinetics of association of CO with Ferrocyt *c* at pH 12.9 (± 0.1) in the absence and presence of different concentrations of crowding agents (dextran 70 and ficoll 70) at 25 °C. Since destabilized Ferrocyt *c* binds CO when the CO was used in saturating concentration (~1.0 mM) [35, 101-102]. The intramolecular thermal collisions provide the energy for barrier crossing in the CO-association reaction, Ferrocyt *c* + CO → Ferrocyt *c*-CO, the rate coefficient for the CO association reaction (k_{ass}) is expected to decrease if the amplitudes of thermal fluctuations are reduced as a result of constraints on the collective modes of intramolecular motion [35,101-102]. The association kinetics were monitored by the absorbance at 550 nm, following the addition of a small volume of CO-saturated aqueous alkaline solution (pH 12.9 (±0.1)) containing different concentration of dextran 70 and ficoll 70 at 25ºC. The α-band (550 nm) of Ferrocyt *c* was lost after the formation of Ferrocyt-CO (Fe^{2+}-M80 + CO → Fe^{2+}-CO + M80), complex (Fig.8a) [103]. Fig. 8b shows the representative kinetic trace of CO-association to alkaline Ferrocyt *c* at pH 12.9 (±0.1) in the absence of crowding agents, monitoring by the decrease in absorbance at 550 nm, 25°C. The kinetics of CO-association was well described by a single exponential rate expression with a time constant, τ_{ass} of ~ 2 min. at pH 12.9 (±0.1), 25 °C. Fig. 8c shows the logarithm of k_{ass} for alkaline Ferrocyt *c* as a function of different concentration of dextran70 and ficoll 70 at pH 12.9 (±0.1), 25 °C. These data provide an opportunity to analyze the dynamical behavior of the crowding induced MG-state of base-denatured protein. As [Crowding agent] is increased from 0.0

to 300 mg ml^{-1}, the log k_{ass} decreases monoexponentially, and which is more decreased for dextran 70 than ficoll 70 (Fig. 8c).

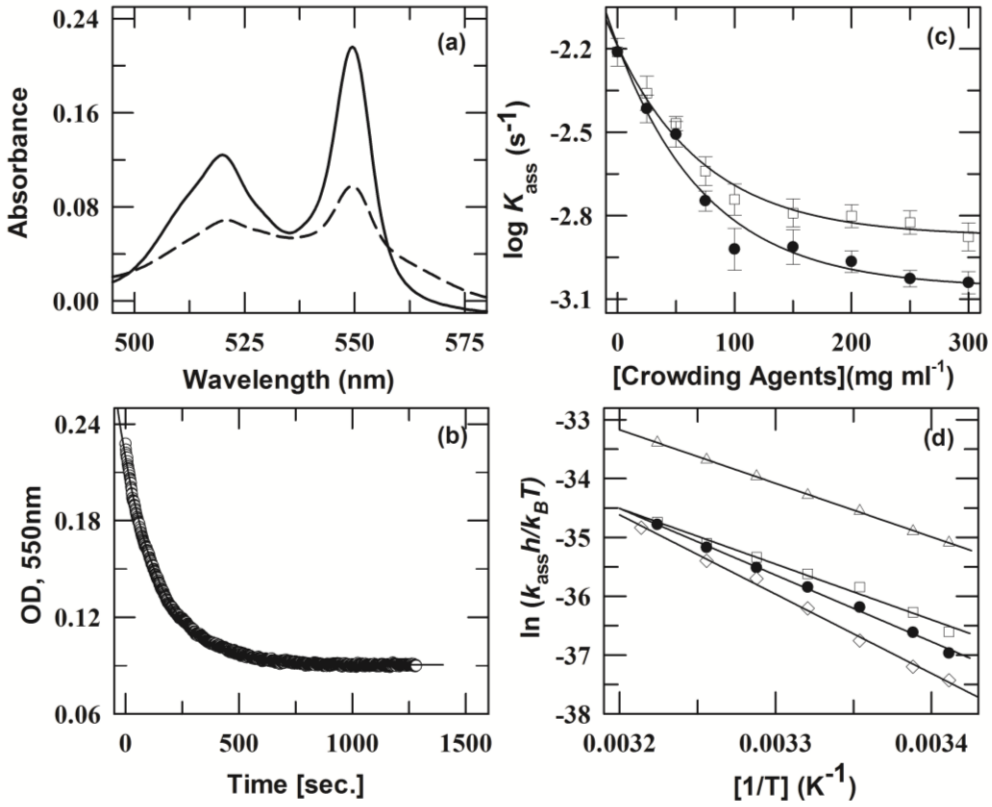

Fig.8. Panel (a) shows the steady- state visible absorption spectra of Ferrocyt *c* (solid line) and Ferrocyt *c*-CO (dash line) at 25ºC, pH 12.9 (±0.1) in 2mM CAPS-buffer. (b) The slow single-phase CO-association kinetic trace of alkaline Ferrocyt *c* (τ =2.0 min in the absence of crowding agent at pH 12.9(±0.1), 25°C). Panel (c) shows dependence of the rate of CO association of alkaline Ferrocyt *c* (pH 12.9) with dextran 70 (●), ficoll 70 (□) at 25 °C. The lines through the data have been drawn by inspection only. (d) Eyring plot for the CO association reaction of alkaline Ferrocyt *c* at pH 12.9(±0.1); in the absence (Δ) and in the presence of 200 mg ml^{-1} dextran 70 (●), 200 mg ml^{-1} ficoll 70 (□) and at pH 7 in the absence of crowding agents (◊). Eyring plots were analyzed by linear least-squares analysis (Fig.8d) (equation (1) chapter 2) [104] and the thermodynamic parameters are listed in Table 4.

This finding suggests that (i) the motional freedoms and internal motions of alkali-denatured protein were reduced in the presence of crowding agents that tend to retard the CO-association to protein and constrains the internal dynamics of alkali-denatured protein, and (ii) the crowding-mediated restricted dynamic of CO association reaction of alkaline Ferrocyt *c* is more pronounced for dextran 70 than that of ficoll 70.

To further investigate the effect of crowding agents on the internal dynamics of base-denatured protein, the crowding agents dependence of the activation thermodynamic parameters

viz; activation free energy ($\Delta G^{\ddagger}_{ass}$), activation enthalpy ($\Delta H^{\ddagger}_{ass}$), activation entropy ($\Delta S^{\ddagger}_{ass}$) and entropy change ($-T\Delta S^{\ddagger}_{ass}$) for the CO-association reaction of alkaline Ferrocyt *c* was determined. If the internal dynamics of base-denatured protein is constrained, then $\Delta H^{\ddagger}_{ass}$ for CO association reaction will be increased. Fig. 8d shows the Eyring plots for the CO association reaction of alkaline Ferrocyt *c* in the absence and presence of ~200 mg ml^{-1} of dextran70 and ficoll 70. Fig. 8d also shows the Eyring plots for the CO association to native Ferrocyt *c* in the absence of crowding agents at pH 7.0. Eyring plots were analyzed by linear least-squares analysis (Equation (1), chapter 2) [104] of the temperature dependent k_{ass}. Table 4 summarizes the values of $\Delta G^{\ddagger}_{ass}$, $\Delta H^{\ddagger}_{ass}$, $\Delta S^{\ddagger}_{ass}$ and $-T\Delta S^{\ddagger}_{ass}$ for alkaline Ferrocyt *c* in the absence and presence of ~200 mg ml^{-1} of dextran 70 and ficoll 70. Clearly, the value of $\Delta H^{\ddagger}_{ass}$ for base-denatured protein is found to be higher in the presence of crowding agent than in its absence (Table 4). The value of $\Delta H^{\ddagger}_{ass}$ for base-denatured protein in the presence of crowding agents (dextran 70 and ficoll 70) is found to be lower than the native protein at pH 7.0 (Table 4). These results clearly indicate that the internal dynamics of base-denatured protein in the presence of crowding agent is more constrained relative to that in the absence of crowding agents but is relatively less constrained than the native state (Table 4).

Table 4 The effect of crowding agents on activation thermodynamic parameters for CO-association reaction of Ferrocyt *c* at pH 12.9 (±0.1).*

Additives	Concentration (mg ml^{-1})	$\Delta G_{ass}{}^{a\ddagger}$ (kcal mol^{-1})	$\Delta H_{ass}{}^{\ddagger}$ (kcal mol^{-1})	$\Delta S_{ass}{}^{\ddagger}$ (cal mol^{-1} K^{-1})	$-T\Delta S_{ass}{}^{a\ddagger}$ (kcal mol^{-1} K^{-1})
Control	0.0	20.6 (0.05)	18.2 (0.2)	−8.1 (0.6)	2.4 (0.2)
Dextran 70	200	21.6 (0.05)	22.6 (0.6)	3.4 (1.8)	−1.0 (0.5)
Ficoll 70	200	21.4 (0.08)	18.9 (0.9)	−8.5 (3.0)	2.5 (0.9)
Control (pH 7)	0.0	22.0 (0.1)	26.0 (0.1)	12.4 (0.8)	−3.7 (0.2)

[a] Activation free energy ($\Delta G_{ass}{}^{\ddagger}$) and entropy changes ($-T\Delta S_{ass}{}^{\ddagger}$) are given at 25ºC.
*The uncertainties (standard error) in $\Delta G_{ass}{}^{\ddagger}$, $\Delta H_{ass}{}^{\ddagger}$, $-T\Delta S_{ass}{}^{a\ddagger}$ and $\Delta S_{ass}{}^{\ddagger}$ are indicated in parenthesis.

The data in Table 4 also suggests that the increase of $\Delta H_{ass}{}^{\ddagger}$ due to crowding agents (dextran 70 and ficoll 70) is accompanied by a decrease in the entropy change $-T\Delta S_{ass}{}^{\ddagger}$. The entropy-enthalpy plots could be used to describe the entropic and enthalpic contributions of crowders on stability and folding of proteins [105]. In entropy-enthalpy plots, sectors 1 and 2 correspond to stabilizing cosolutes while sectors 3 and 4 correspond to destabilizing cosolutes. Furthermore, sector 1 and sector 3 represent the enthalpically dominated effect while sector 2 and sector 4 represent

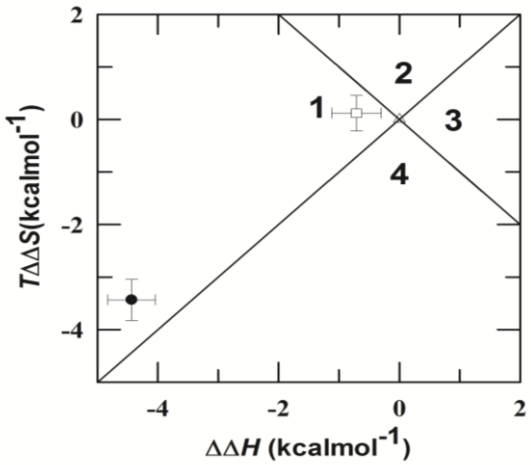

entropically dominated effect [105]. Fig. 9 presents the $T\Delta\Delta S$ *vs* $\Delta\Delta H$ plots for alkaline Ferrocyt *c* in the presence of dextran 70 and ficoll 70 at pH 12.9 (±0.1). Clearly, the data points for crowders lie in sector 1 (Fig. 9), which is in general agreement with the models that describes enthalpically dominated stabilization [105-106].

Fig.9. The $T\Delta\Delta S$ and $\Delta\Delta H$ plot for different crowders. Data points correspond to in the absence (Δ) and presence of 200 mg ml^{-1} of dextran 70 (●) and ficoll 70(□) for Ferrocyt *c* at pH 12.9 (±0.1).

7.3 Conclusion

The high concentrations of crowding agents (dextran 70 and ficoll 70) transform the base-denatured Ferricyt *c*, apoMb and Lyz at pH 12.9 (±0.1) to MG-states. The formation of MG-states of base-denatured Ferricyt *c*, apoMb and Lyz in the presence of crowding agents is found to be dependent on the concentration and shape of crowding agents. The crowding agent-induced MG-states of base-denatured denatured Ferricyt *c*, apoMb and Lyz resemble the generic properties of MG-states (*i.e.*, molecular compact state with native-like secondary structure and disordered or lost tertiary structure). ANS binding experiments also confirmed that the crowding agents presence in reaction medium transforms the base-denatured denatured Ferricyt *c*, apoMb and Lyz to MG-states. Analysis of the thermal denaturation curves of base-denatured Ferricyt *c*, apoMb and Lyz in the absence and presence of crowding agents (dextran 70 and ficoll 70) revealed that (i) the base-denatured Ferricyt *c* and apoMb exhibit cold denaturation, (ii) crowding agent presence in the reaction medium increases the thermal stability of base-denatured proteins and which is found to be increased more for dextran 70 than that of ficoll 70. Analysis of kinetic and thermodynamic parameters measured for CO association reaction of alkaline Ferrocyt *c* at pH 12.9 (±0.1) in the absence and presence of different concentrations of crowding agents (dextran 70 and ficoll 70) revealed substantially restricted overall motion and stiffness of the polypeptide chain in crowding agent induced MG-state of base-denatured Ferricyt *c*.

7.4 References:

1. P. G. Wolynes, J. N. Onuchic, D. Thirumalai, *Science* **267** (1995) 1619–1620.
2. O. B. Ptitsyn, *TIBS* **20** (1995) 376–379.
3. D. A. Dolgikh, R. I. Gilmanshin, E.V. Brazhnikov, V. E. Bychkova, G.V. Semisotnov, S.Y. Venyaminov, O. B. Ptitsyn, *FEBS Lett.* **136** (1981) 311–315.
4. M. Ohgushi, A. Wada, *FEBS Lett.* **164** (1983) 21–24.
5. D. A. Dolgikh, L.V. Abaturov, I. A. Bolotina, E.V. Brazhnikov, V. E. Bychkova, R. I. Gilmanshin, Y.O. Lebedev, G.V. Semisotnov, E. I. Tiktopulo, O.B. Ptitsyn, *Eur. Biophys. J.* **13** (1985) 109–121.
6. K. Kuwajima, M. Arai, in *Mechanisms of Protein Folding* (Pain, R. H., Ed.) 2nd ed. Oxford University Press, New York, (2000) pp 138–174.
7. M. Arai, K. Kuwajima, *Adv. Protein Chem.* **53** (2000) 209–282.
8. O. B. Ptitsyn, *J. Protein Chem.* **6** (1987) 213–293.
9. R. Kumar, N.P. Prabhu, D.K. Rao, A.K. Bhuyan, *J. Mol. Biol.* **364** (2006) 483–495.
10. A. K. Bhuyan, *Biochemistry* **49** (2010) 7774–7782.
11. T. K. Das, S. Mazumdar, S. Mitra, *Eur. J. Biochem.* **254** (1998) 662–670.
12. A. Naeem, R. H. Khan, *Int. J. Biochem. Cell Biol.* **36** (2004) 2281–2292.
13. A. L. Shapiro, E.Vinuela, J. V. Maizel, *Biochem. Biophys. Res. Commun.* **28** (1967) 815–820.
14. K. Weber, M. Osborn, *J. Biol. Chem.* **244** (1969) 4406–4412.
15. Y.V. Griko, P.L. Privalov, *J. Mol. Biol*. **235** (1994) 1318–1325.
16. K. Shirahama, K. Tsujii, T. Takagi, *J. Biochem.* **75** (1974) 309–319.
17. N. Robinson, C. Tanford, *Biochemistry* **14** (1975) 369–378.
18. V. E. Bychkova, R. H. Pain, O. B. Ptitsyn, *FEBS Letters* **238** (1988) 231–234.
19. F. G. Van-der Goot, J. H. Lakey, F. Pattus, *Trends Cell Biol.* **2** (1992) 343–348.
20. S. Bañuelos, A. Muga, *J. Biol. Chem.* **270** (1995) 29910–29915.
21. E. A. Bryson, S. E. Rankin, M. Carey, A. Watts, T. J. T. Pinheiro, *Biochemistry* **38** (1999) 9758–9767.
22. A. L. Fink, *Curr. Opin. Struct. Biol.* **15** (2005) 35–41.
23. P. Tompa, *Bioassays* **25** (2003) 847–855.

24. H. J. Dyson, P. E. Wright, *Curr. Opin. Struct. Biol.* **12** (2002) 54–60.
25. P. Tompa, *Trends Biochem. Sci.* **27** (2002) 527–533.
26. V. N. Uversky, *Eur. J. Biochem.* **269** (2002) 2–12.
27. K. I. Nakayama, S. Hatakeyama, K. Nakayama, *Biochem. Biophys. Res. Commun.* **282** (2001) 853–860.
28. A. K. Dunker, M. S. Cortese, P. Romero, L. M. Iakoucheva, V. N. Uversky, *FEBS J.* **272** (2005) 5129–5148.
29. E. Kokai, A. Tantos, E.Vissi, B. Szoor, P. Tompa, J. Gausz, L. Alphey, P. Friedrich, V. Dombradi, *Arch. Biochem. Biophys.* **451** (2006) 59–67.
30. P. Radivojac, S. Vucetic, T.R. O'Connor, V.N. Uversky, Z. Obradovic, A. Dunker, *Proteins: Struct. Funct. Genet.* **63** (2006) 398–410.
31. P. Tompa, P. Banki, M. Bokor, P. Kamasa, D. Kovacs, G. Lasanda, K.Tompa, *Biophys. J.* **91** (2006) 2243–2249.
32. B.Y. Baker, D.C. Yaworsky, W.L. Miller, *J. Biol. Chem.* **280** (2005) 41753–41760.
33. S. Nakamura, T. Baba, S. Kidokoro, *Biophys. Chem.* **127** (2007) 103–112.
34. S. Nakamura, S. Kidokoro, *Biophys. Chem.* **113** (2005) 161–168.
35. D. K. Rao, R. Kumar, M. Yadaiah, A. K. Bhuyan, *Biochemistry* **45** (2006) 3412–3420.
36. P. R. Davis-Searles, A.S. Morar, A. J. Saunderes, D. A. Erie, G. J. Pielak, *Biochemistry* **37** (1998) 17048–17053.
37. A.J. Saunderes, P.R. Davis-Searles, D.L. Allen, G.J. Pielak. D.A. Erie *Biopolymers* **53** (2000) 293–307.
38. T. Kamiyama, Y. Sadahide, Y. Nogusa, K. Gekko, *Biochim. Biophys. Acta* **1434** (1999) 44–57.
39. S. Nakamura, Y. Seki, E. Katoh, S. Kidokoro, *Biochemistry* **50** (2011) 3116–3126.
40. B. V. Berg, R. J. Ellis, C.M. Dobson, *EMBO J.* **18** (1999) 6927–6933.
41. L. Stagg, S. Zhang, M.S. Cheung, P. Wittung-Stafshede, *Proc. Nat. Acad. Sci. USA* **48** (2007) 18976–18981.
42. M. S. Cheung, D. Klimov, D. Thirumalai, *Proc. Nat. Acad. Sci. USA* **13** (2005) 4753–4758.
43. Y. Wang, M. Sarkar, A.E. Smith, A.S. Krois, G.J. Pielak, *J. Am. Chem. Soc.* **134** (2012) 16614─166118.

44. M. Erlkamp, S. Grobelny, R. Winter, *Phys. Chem. Chem. Phys.* **16** (2014) 5965─5976.
45. M. S. Cheung, D. Thirumalai, *J. Phys. Chem. B* **111** (2007) 8250–8257.
46. Y. Zhai, R. Winter, *ChemPhysChem* **14** (2013) 386─393.
47. A. Christiansen, P. Wittung-Stafshede, *FEBS Lett.* **588** (2014) 811–814.
48. D. L. Pincus, C. Hyeon, D. Thirumalai, *J. Am. Chem. Soc.* **130** (2008) 7364–7372.
49. K. Sasahara, P. McPhie, A.P. Minton, *J. Mol. Biol.* **326** (2003) 1227–1237.
50. D. M. Hatters, A. P. Minton, G. J. Howlett, *J. Biol. Chem.* **277** (2002) 7824–7830.
51. R. Engel, A. H. Westphal, D. H. Huberts, S. M. Nabuurs, S. Lindhoud, A. J. Visser, C. P. van Mierlo, *J. Biol. Chem.* **283** (2008) 27383–27394.
52. J. Li, S. Zhang, C. Wang, *J. Biol. Chem.* **276** (2001) 34396–34401.
53. R. J. Ellis, A. P. Minton, *Biol. Chem.* **387** (2006) 485–497.
54. S. Mittal, L. R. Singh, *J. Biochem.* **156** (2014) 273–282.
55. L. Breydo, K. D. Reddy, A. Piai, I. C. Felli, R. Pierattelli, V. N. Uversky, *Biochim. Biophys. Acta* **1844** (2014) 346–357.
56. E. E. Wanker, *Mol. Med. Today* **6** (2000) 387–391.
57. Y. Qu, D.W. Bolen, *Biophys. Chem.* **101–102** (2002) 155–165.
58. A. P. Minton, *Curr. Opin. Struct. Biol.* **10** (2000) 34–39.
59. B. Van den Berg, R. Wain, C. M. Dobson, R. J. Ellis, *EMBO J.* **19** (2000) 3870–3875.
60. S. L. Flaugh, K. J. Lumb, *Biomacromolecules* **2** (2001) 538–540.
61. M. M. Dedmon, C. N. Patel, G. B. Young, G. J. Pielak, *Proc. Natl. Acad. Sci. USA.* **99** (2002) 12681–12684.
62. A. P. Minton, J. Wilf, *Biochemistry* **20** (1981) 4821–4826.
63. A. P. Minton, *Mol. Cell. Biochem.* **55** (1983) 119–140.
64. G. B. Ralston, *J. Chem. Edu.* **10** (1990) 857–860.
65. S. B. Zimmerman, A. P. Minton, *Annu. Rev. Biophys. Biomol. Struct.* **22** (1993) 27–65.
66. A. P. Minton, *Methods Enzymol.* **295** (1998) 127–149.
67. A. P. Minton, *Biophys. J.* **78** (2000) 101–109.
68. A. P. Minton, *J. Biol.Chem.* **276** (2001) 10577–10580.
69. J. M. Vanderkooi, M. Erecinska, *Eur. J. Biochem.* **60** (1975) 199–207.
70. T.Y. Tsong, *J. Biol. Chem.* **249** (1974) 1988–1990.

71. R. A. Staniforth, M. G. Bigotti, F. Cutruzzolà, C. T. Allocatelli, M. Brunori, *J. Mol. Biol.* **275** (1998) 133–148.
72. E. P. Kirby, R. F. Steiner, *J. Biol. Chem.* **245** (1970) 6300–6306.
73. G. B. Postnikova, E. M. Yumakova, *Eur. J. Biochem.* **198** (1991) 241–246.
74. S. S. Lehrer G. D. Fasman, *J. Bio. Chem.* **242** (1967) 4644–4651.
75. M. A. Ansari, S. Zubair, S. M. Atif, M. Kashif, N. Khan, M. Rehan, T. Anwar, A. Iqbal, M. Owais, *Protein Pept. Lett.* **17** (2010) 11–17.
76. S. Y. Venyaminov, J. T. Yang, Determination of protein secondary structure, in Circular Dichroism and the Conformational Analysis of Biomolecules (Fasman, G. D., ed.), Plenum, New York, (1996) pp. 69–107.
77. C.N. Pace, *CRC Crit. Rev. Biochem.* **3** (1975) 1–43.
78. J. A. Schellman, *Biopolymers* **26** (1987) 549–559.
79. D. O. Alonso, K. A. Dill, *Biochemistry* **30** (1991) 5974–5985.
80. S. L. Mayo, R. L. Baldwin, *Science* **262** (1993) 873–876.
81. J. A. Knapp, C. N. Pace, *Biochemistry* **13** (1974) 1289–1294.
82. K. Kuwajima, E.P. Garvey, B.E. Finn, C.R. Mathews, S. Sugai, *Biochemistry* **30** (1991) 7693–7703.
83. A. Arroyo-Reyna, A. Hernandez-Arana, R. Arreguin-Espinosa, *Biochem. J.* **300** (1994) 107–110.
84. O. B. Ptitsyn, *Adv. Protein Chem.* **47** (1995) 83–229.
85. Y. Goto, L. J. Calciano, A. L. Fink. *Proc. Natl. Acad. Sci. USA* **87** (1990) 573–577.
86. O. B. Ptitsyn, G. V. Semisotnov, The mechanism of protein folding. In: B. T. Nall, K. A. Dill, editors. *Conformations and forces in protein folding*. AAAS; Washington, DC. (1991) pp. 155–168.
87. M. Engelhard, P. A. Evans, *Protein Sci*. **4** (1995)1553–1562.
88. V. N. Uversky, S. Winter, G. Löber, *Biophys. Chem.* **60** (1996) 79–88.
89. E. Schonbrunn, S. Eschenburg, K. Luger, W. Kabsch, N. Amrhein, *Proc. Natl. Acad. Sci. USA* **97** (2000) 6345–6349.
90. G. V. Semisotonov, N. A. Rodionova, O. I. Razgulyaev, V. N. Uversky, A. F. Gripas, R. I. Gilmanshin, *Biopolymers* **31** (1991) 119–128.

91. P. L. Privalov, *Crit. Rev. Biochem. Mol. Biol.* **25** (1990) 281–305.
92. I. Nishii, M. Kataoka, F. Tokunaga, Y. Goto, *Biochemistry* **33** (1994) 4903–4909.
93. D.L. Zhang, L.J. Wu, J. Chen, Y. Liang, *Acta Biochim Biophys Sin (Shanghai)* **44** (2012) 703–711.
94. P.L. Privalov, *Adv. Protein Chem.* **33** (1979) 167–241.
95. W.J. Becktel, J.A. Schellman, *Biopolymers* **26** (1987) 1859–1877.
96. K.P. Murphy, E. Freire, *Adv. Protein Chem.* **43** (1992) 313–361.
97. G. I. Makhatadze, P. L. Privalov, *Adv. Protein Chem.* **47** (1995) 307–425.
98. R. S. Spolar, J. R. Livingstone, M.T. Record, *Biochemistry* **31** (1992) 3947–3955.
99. R.S. Spolar, M.T. Record, *Science* **263** (1994) 777–784.
100. R. Jain, S. Kaur, R. Kumar, *J. Biochem.* **153** (2013)161–177.
101. A. K. Bhuyan, R. Kumar, *Biochemistry* **41** (2002) 12821–12834.
102. H. Theorell, A. Åkesson, *J. Am. Chem. Soc.* **63** (1941) 1812–1827.
103. R. Jain, D. Sharma, R. Kumar, *J. Biochem.* **154** (2013) 341–354.
104. J. Mikšovská, J.H. Day, R.W. Larsen, *J. Biol. Inorg. Chem.* **8** (2003) 621–625.
105. S. Sukenik, L. Sapir, D. Harries, *Colloid Interface Sci.* **18** (2013) 495–501.
106. L. Sapir, D. Harries, *Curr. Opin. Colloid Interface Sci.* **20** (2015) 3–10.

Chapter 8

Structural, Kinetic and Thermodynamic Characterizations of the Alcohol and Cation-induced Molten Globule States of the Base-Denatured Proteins

8.1 Introduction

Protein folding is a physical process in which a newly synthesized polypeptides chain folds to a three dimensional native conformation. In determining the stability of native proteins, the roles of electrostatic [1-5], hydrophobic [6-7] and hydrogen bonding [8-9] interactions are well recognized. After synthesis of protein in cytoplasm they undergoes through a specific set of folding pathway in order to fold into biologically active form [10]. The intermediate state of protein folding has become an essential part for protein folding studies [11-12]. Such intermediates are generally termed as "molten globule" (MG-state) [13-15]. MG-state is considered to be an intermediate in the folding pathway of proteins [13-15]. The main characteristic features of MG-state are (i) abundant secondary structure, (ii) largely flexible side chains and a compact dimension, (iii) the absence of the specific tertiary structure produced by the tight packing of side chains, and (iv) presence of loosely packed hydrophobic core that increases the hydrophobic surface area that accessible to the solvent [14-17]. The MG conformations are usually assumed to be important for initiating the folding process, so its characterization is crucial to understand the protein folding process. Structural characterization of protein under different solvents conditions would provide information: (i) about the structure of protein molecule, and (ii) the roles of different stabilizing and destabilizing forces [18]. Increasing evidence indicates that the MGs are also involved in several biological processes such as cell signaling, steroid synthesis and many more [19-24]. Mild denaturing conditions, alcohols and salt are generally used for the MGs characterizations [25-29]. Alcohol is the best studied cosolvents which alters the protein structure, because it weakening the nonlocal hydrophobic interactions and at the same time promoting the local polar interactions and hydrogen bonds in proteins [30-31]. Alcohols induce extensively higher helical structure in a partially or completely unfolded protein as

compared to folded protein [32]. 2,2,2-trifluoroethanol (TFE) is the simplest alcohol and its derivatives are generally used as anesthetics. Because of the presence of three fluorine atoms in TFE, it has extraordinary ability to interact and affect the structures of proteins. It is toxic to blood, male reproductive system, brain, upper respiratory tract and eyes [33]. The effects of TFE on proteins were reported previously on stabilization of helical, β-turn and β-hairpin structures, and disruption of the native tertiary structure and quaternary structures of intact proteins leading to aggregates [34-37]

Salt influences the protein stability directly by preferential binding to the native or unfolded state or indirectly by changing the properties of solvent [38-41]. The indirect effects of salt are similar for different proteins and are usually acts as additive. Conventionally, the effects of salt on protein stability are normally attributed to several factors, including, (i) electrostatic (Debye-Hückel) screening of Coulombic interactions, which operates at low to intermediate salt concentration [42-43], (ii) specific ion binding [44-45] or increased surface tension of water [46-50] that alter hydrophobic interactions (the Hofmeister effect) at very high salt concentration. The grading of monoatomic cations correlates with surface charge density, but for complex polyatomic cations, the underlying mechanism of the Hofmeister ordering is not fully recognized [38, 42-43]. While the correlations between anionic effects on protein structure and enzyme activity and anion position in the Hofmeister series are extensively explored [38-39,43,48,51-54], correlations between the effects of cations on protein properties and the Hofmeister series are less explored [38, 55-59]. This is presumably because the anions are more proficient than cations in disturbing the properties of polypeptide chains. Some previous reports revealed that the anion–water interaction is stronger than the cation–water interaction due to the asymmetry of the dipoles in water [38, 40, 60], therefore, the anions have a greater effect on water ordering than cations. In fact, the interactions between ions and proteins generally depend on the electrostatics of the protein surface, so the cation–protein interactions will be more pronounced if the net charge of the protein is negative [38]. A drastic reduction of the electrostatic free energy can disrupt the electrostatic balance of protein charges. Such conditions also discourage the hydrogen-bonded local interactions because the solution pH fairly approaches the pKa values of peptide amide hydrogen [61].

The present chapter analyzed the effect of cations and TFE on the highly negatively charged base-denatured (U_B-states) cytochrome *c* (Cyt *c*), apomyoglobin (apoMb) and hen egg white lysozyme (Lyz) at pH 12.9 (±0.1). Cyt *c* is a single-domain, helical globular protein containing 104 amino acids and one covalently attached heme group [62]. ApoMb is a natural intermediate in biosynthesis of Mb, and has some structural features in common with the heme-containing native Mb [63]. Lyz is a glycoside hydrolases enzyme which also known as N-acetylmuramide glycanhydrolase. Lyz hydrolyzes the glycosidic bond of peptidoglycans (found in the cell walls of bacteria, especially Gram-positive bacteria) that connects *N*-acetylmuramic acid with the fourth carbon atom of N-acetylglucosamine [64-65].

The MG-state is typically stabilized and populated at extremes of pH in the presence of salt [66-71]. Pioneering work by Goto and coworkers has shown that the net charge of salt anion is the main determinant for anion-induced stabilization of MG-state of acid-denatured proteins [72]. The MG state is the third thermodynamic state of proteins [73]. The temperature function studies of the protein provides important information regarding the thermodynamic stability of proteins because the pH destabilized states in the presence of salt are amenable to cold denaturation in the experimentally available low temperatures [69, 74]. Thus, the study of the MG state continues to be a thrust area in the biophysical research of proteins.

While the effects of salt and TFE on the structural and thermodynamic properties of native and acid pH-denatured proteins are extensively studied [66-69, 70-72, 75-80], the effects of these additives on structural, kinetics and thermodynamic properties of base-denatured proteins are not explored so far. Keeping this in view, this chapter evaluated the effect of cations of chloride salt (*i.e.,* CsCl, NaCl and KCl) and alcohol (TFE) on the structural, kinetics and thermodynamic properties of base-denatured Ferricyt *c*, apoMb and Lyz at 12.9 (±0.1). The results from CD, Trp-fluorescence and 1-anilino-8-napthalene sulfonate (ANS) binding experiments suggest that cations of chloride salt (*i.e.,* CsCl, NaCl and KCl) and TFE transform the base-denatured Ferricyt *c*, apoMb and Lyz (pH 12.9 (±0.1)) to generic MG-states. The choice of extreme alkaline environment, for these experiments was driven by available information about the thermodynamic and structural properties, and the folding−unfolding behavior of the Ferricyt *c* and Lyz, at this pH [81-86]. Kinetic and thermodynamic experiments involving the measurement of the CO-association to the base−denatured Ferrocyt *c* (pH 12.9 (±0.1)) in the absence and presence of

different concentrations of TFE and salt (NaCl, KCl and CsCl) indicate that the cations of chloride salt (CsCl, NaCl and KCl) and TFE presence in the reaction medium constrain the internal dynamics of base−denatured Ferrocyt *c*. Thermodynamic analysis of the far UV−CD (222 nm)-monitored thermal denaturation curves of base-denatured Ferricyt *c*, apoMb and Lyz (pH 12.9 (±0.1)) measured in the absence and presence of cations of chloride salt (CsCl, NaCl and KCl) suggests that the cations (Na^+, K^+ and Cs^+) presence in the reaction medium increases the thermal stability of base-denatured protein.

8.2 Results and Discussion

8.2.1 Effect of cations on the base-denatured Ferricyt c, apoMb and Lyz

To find out the effect of different cations on the base-denatured proteins, the far-UV CD (222 nm) monitored pH-induced unfolding curves of Ferricyt *c*, apoMb and Lyz were measured in the absence and presence of different cations of chloride salt (NaCl, KCl and CsCl) at 25 °C. Figs. 1a, 1b and 1c show the far-UV CD (222 nm) monitored pH-induced unfolding curves of Ferricyt *c*, apoMb and Lyz collected in the absence and presence of 1.0 M NaCl, KCl and CsCl, respectively. The MRE observed for the native protein at 222 nm decreases at extreme basic pH (Figs. 1a, 1b and 1c), which suggests pH-induced unfolding of these proteins. The pH-titration curve of Ferricyt *c* (Fig. 1a), apoMb (Fig. 1b) and Lyz (Fig. 1c) shifts to higher pH in the presence of 1.0 M NaCl, KCl and CsCl, which suggests that the cations presence in reaction medium increase the stability of Ferricyt *c*, apoMb and Lyz against alkaline pH. The pH-titration curves for Ferricyt *c*, apoMb and Lyz were analyzed by using the modified Handerson-Hasalbalch equation (chapter 2 equation (8)) [81], which provide the pH midpoint (C_m) (Table 1).

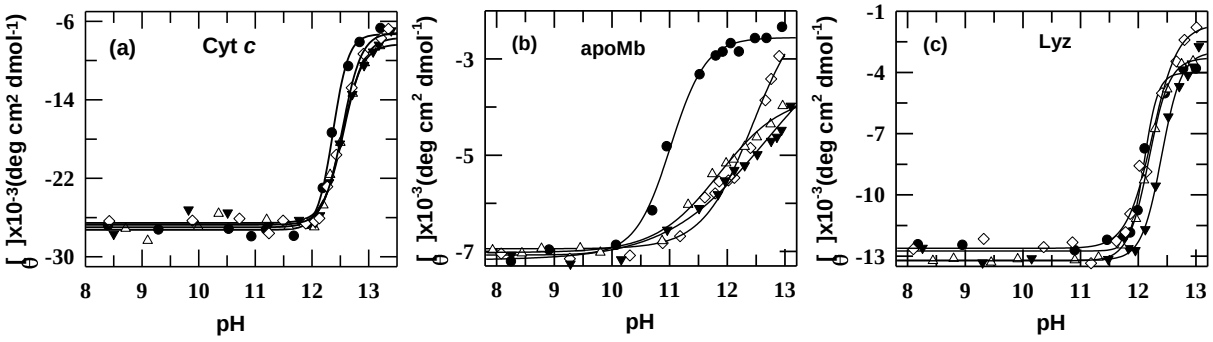

Fig.1. Panel (a) presents far-UV CD (222nm) monitored alkaline pH-induced unfolding of Ferricyt *c* (26 μM) in the

absence (•) and presence of 1.0 M NaCl (◊); KCl (▼) and CsCl (Δ) at 25 ºC. Panel (b) presents the far-UV CD (222 nm) monitored alkaline pH-induced unfolding of apoMb (8 µM) in the absence (•) and presence of 1 M chloride salt of 1.0 M NaCl (◊); KCl (▼) and CsCl (Δ) at 25 ºC. Panel (c) shows the far-UV CD (222 nm) monitored alkaline pH-induced unfolding of Lyz (13 µM) in the absence (•) and presence of 1 M 1.0 M NaCl (◊); KCl (▼) and CsCl (Δ) at 25 ºC. Solid lines in panel (a), (b) and (c) are fits according to equation (8) from chapter 2 [81], at 25 °C.

The increase in C_m in the presence of salt (NaCl, KCl and CsCl) indicates that presence of cations in reaction medium opposes the pH-induced denaturation of proteins. Ion-stabilized denatured states were generally categorized as MG states [15, 20].

Table1. pH-midpoint, (c_m) of Ferricyt *c*, apoMb and Lyz in the absence and presence of 1.0 M (NaCl, KCl and CsCl) at 25 °C.

	Ferricyt *c*	apoMb
	Far-UV CD (222 nm)	Far-UV CD (222 nm)
Cation	pH-midpoint (*C*m)	pH-midpoint (*C*m)
Control	12.37	11.02
Na^+	12.54	12.43
K^+	12.56	12.29
Cs^+	12.53	11.86
	Lyz (Far-UV CD (222 nm))	
Control	12.10	
Na^+	12.22	
K^+	12.40	
Cs^+	12.18	

8.2.2 Cations-induced molecular compaction of base-denatured Ferricyt c, apoMb and Lyz

Fig. 2a, 2b, and 2c present the florescence emission spectra of different states of Ferricyt *c*, apoMb and Lyz, respectively at 25ºC. Native state of Ferricyt *c* (N-state) at pH 7.0 is fluorescence-silent while the base-denatured state of Ferricyt *c* (U_B-state) at pH 12.9 (±0.1) is fluorescent (Fig. 2a). Previous reports also revealed that fluorescence intensity of Ferricyt *c* increases at alkaline pH environment [34-37]. Unfolding of Ferricyt *c* results in an increase in the heme-Trp distance due to molecular expansion [52-53] and its molecular compaction occurs in presence of 2.0 M NaCl, KCl and CsCl (Fig. 2a).

Native apoMb at pH 7 shows good fluorescence emission (Spectrum 1 of Fig. 2b) while the base-denatured apoMb also shows fluorescence emission with a red shift in emission maxima (spectrum 2 of Fig 2b) but after the addition of 2.0 M KCl (spectrum 3 of Fig 2b) or 2.0 M CsCl (spectrum 4 of Fig 2b) in base-denatured apoMb, the intensity of emission spectra decrease with a blue shift in emission maxima (Fig 2b), suggesting that the cations cause molecular compaction of U_B-state to B-state of apoMb [87].

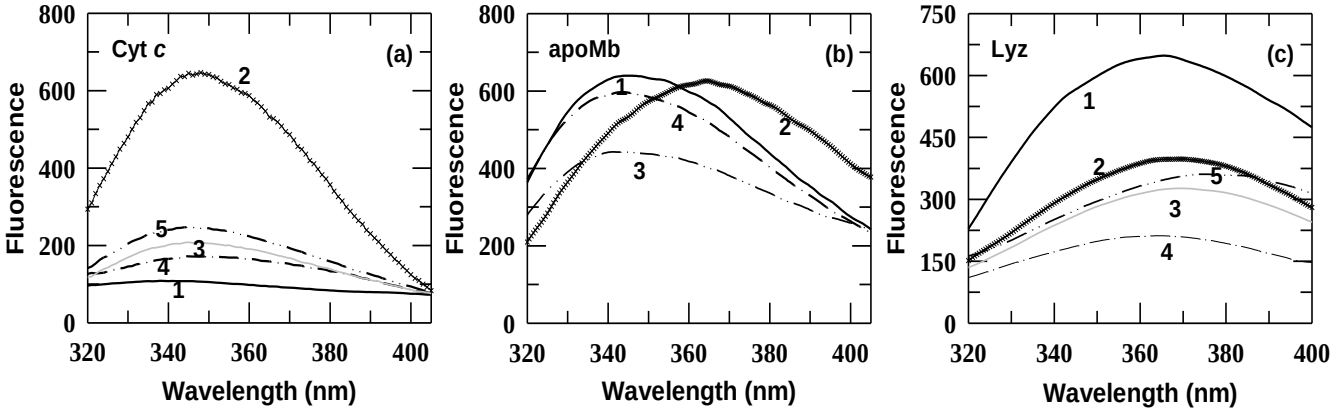

Fig.2. Panel (a) presents the fluorescence emission spectra of different states of Ferricyt *c* (6.0 μM) at 25ºC (spectrum 1: pH 7.0, native state (solid-line); spectrum 2: pH 12.9 (±0.1), unfolded state (thin cross line); spectrum 3, pH 12.9 (±0.1) with 2 M NaCl (gray solid line); spectrum 4, pH 12.9 (±0.1) with 2 M KCl (dash-dot line) and spectrum 5, pH 12.9 (±0.1) with 2 M CsCl (double-dot-dash line). Panel (b) presents the fluorescence emission spectra of different states of apoMb (6.0 μM) at 25ºC (spectrum 1: pH 7.0, native state (solid-line); spectrum 2: pH 12.9 (±0.1), unfolded state (thin cross line); spectrum 3, pH 12.9 (±0.1) with 2 M KCl (dash-dot line) and spectrum 4, pH 12.9 (±0.1) with 2 M CsCl (double-dot-dash line). Panel (c) presents the fluorescence emission spectra of different states of Lyz (6.0 μM) at 25ºC (spectrum 1: pH 7.0, native state (solid-line); spectrum 2: pH 12.9 (±0.1), unfolded state (thin cross line); spectrum 3, pH 12.9 (±0.1) with 2 M NaCl (gray solid line); spectrum 4, pH 12.9 (±0.1) with 2 M KCl (dash-dot line) and spectrum 5, pH 12.9 (±0.1) with 2 M CsCl (double-dot-dash line).

Unfolding of Lyz at alkaline pH result in a rapid decrease in fluorescence intensity with a red shift in emission maxima presumably because of exposure of Trp residues to the polar solvent and ionization of certain tyrosine groups [88-89]. Fig. 2c presents florescence emission spectra of different states of Lyz. The native Lyz at pH 7.0 shows good fluorescence emission (spectrum 1 of Fig. 2c). However, the fluorescence emission intensity of base-denatured Lyz at pH 12.9 (±0.1) decreases with a red shift in emission maxima (spectrum 2 of Fig. 2c). The addition of 2.0 M of salt (NaCl, KCl and CsCl) in the base-denatured Lyz further decrease the intensity of fluorescence emission because of cation induced molecular compaction of U_B-state to B-state (spectra 3,4,5 of Fig, 2c).

8.2.3 Cations and TFE induce the native-like secondary structures in the base-denatured Ferricyt c, apoMb and Lyz

Traditionally, the MG-states have native-like secondary structural contents [14-15]. Figs. 3a, 3b and 3c present the far-UV CD spectra for Ferricyt *c* apoMb and Lyz, respectively at pH 7.0 and at pH 12.9 (±0.1) in the absence and presence of 2.0 M of salt (NaCl, KCl and CsCl) at 25 °C. Figs. 3a, 3b and 3c show that as pH is increased from 7.0 to 12.9 (±0.1), the negative cotton effect

for Ferricyt *c* apoMb and Lyz at 222 nm is significantly lost, which suggests that these proteins significantly lost their secondary structural components at pH ~12.9 (±0.1). When 2.0 M salt (NaCl, KCl and CsCl) is included in the base pH-denatured Ferricyt *c* and apoMb (pH 12.9 (±0.1), the base-denatured Ferricyt *c* and apoMb acquired the native-like negative cotton effect at 222 nm (Figs. 3a and 3b), which indicates that the cations induce the native-like secondary structure in the base denatured Ferricyt *c* and apoMb at pH ~12.9 (±0.1). However, the base-denatured Lyz (pH ~12.9 (±0.1)) only acquired the native-like secondary structures in the presence of 2.0 M of KCl (Fig. 3c).

Figs. 3d, 3e and 3f present the far-UV CD spectra for Ferricyt *c* apoMb and Lyz, respectively at pH 7.0 and at pH 12.9 (±0.1) in the absence and presence of 45% (v/v) TFE at 25 °C. Clearly, the base-denatured Ferricyt *c* apoMb and Lyz also acquired the native-like secondary structure in the presence of ~ 45% (v/v) TFE at pH ~12.9 (±0.1) (Figs. 3d, 3e and 3f).

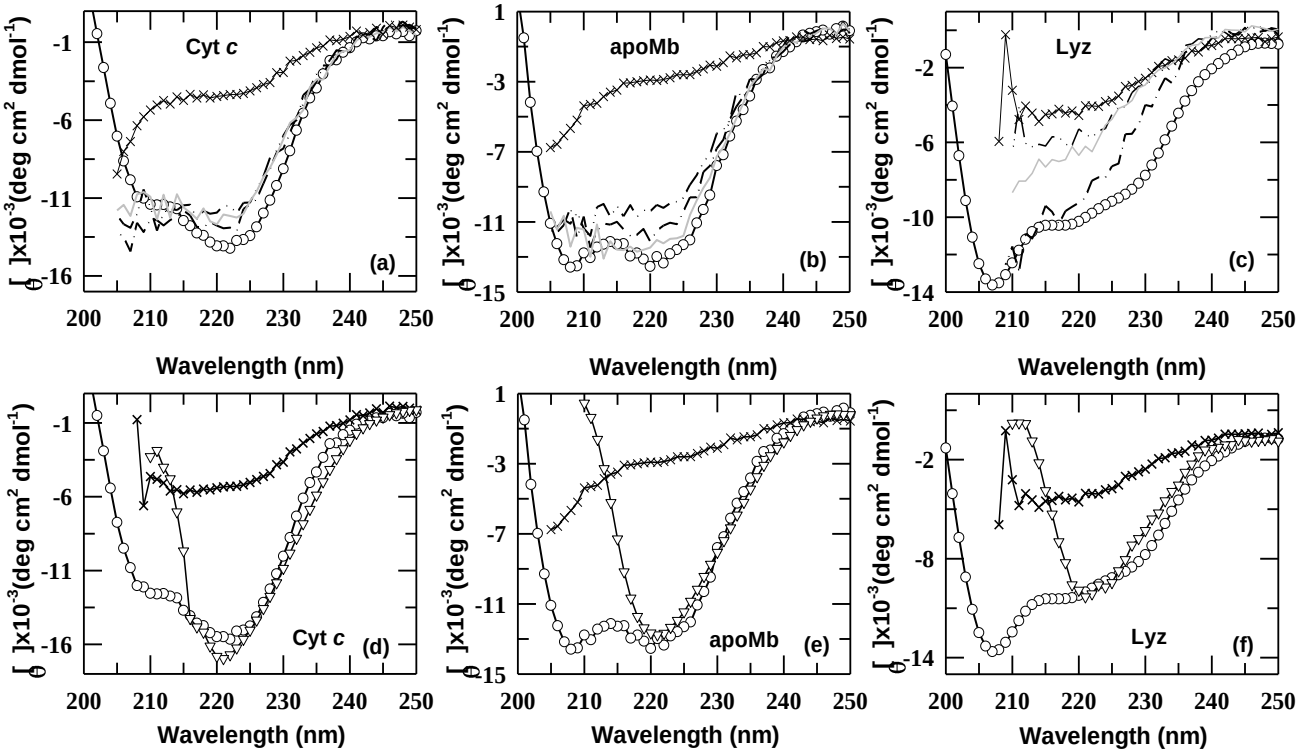

Fig.3. Panel (a) presents the far-UV CD spectra for different states of Ferricyt *c* (16 µM), (pH 7.0, native state (○○○); pH 12.9 (±0.1) unfolded state (××××××) ; pH 12.9 (±0.1) with 2.0 M NaCl (gray solid line); pH 12.9 (±0.1) with 2 M KCl (dash-dot line) and pH 12.9 (±0.1) with 2 M CsCl (double-dot-dash line) at 25ºC. Panels (b) present the far-UV CD spectra for different states of apoMb (15 µM), (pH 7.0, native state (○○○); pH 12.9 ± (0.1) unfolded state (××××××) ; pH 12.9 (±0.1) with 2 M NaCl (gray solid line); pH 12.9 (±0.1) with 2 M KCl (dash-dot line) and pH 12.9 (±0.1) with 2 M CsCl (double-dot-dash line) at 25ºC. Panel (c) presents the far-UV CD spectra for different states of Lyz (12 µM), (pH 7.0, native state (○○○); pH 12.9 ± (0.1) unfolded state (××××××) ; pH 12.9 (±0.1) with 2 M NaCl

(gray solid line) ; pH 12.9 (±0.1) with 2 M KCl (dash-dot line) and pH 12.9 (±0.1) with 2 M CsCl (double-dot-dash line) at 25ºC. Panels (d), (e) and (f) present the far-UV CD spectra for Ferricyt *c* (16 µM), apoMb (15µM) and Lyz (12 µM), respectively (pH 7.0, native state (○○○); pH 12.9 (±0.1) unfolded state (×××); pH 12.9 (±0.1) with 45% (v/v) TFE (▽▽▽)).

Figs. 4a, 4b and 4c present the far-UV CD (222 nm) monitored cations (Cs^+, Na^+ and K^+) induced $U_B \rightarrow$ B transitions for the Ferricyt *c*, apoMb and Lyz, respectively. Clearly, the base-denatured U_B-states of Ferricyt *c* and apoMb acquire secondary structure with the increment of cations (Cs^+, Na^+ and K^+) concentrations (Figs. 4a, 4b and 4c). However, in case of base-denatured Lyz (pH ~12.9 (±0.1)), the base-denatured Lyz only acquired the significant amount of secondary structure with the increment of K^+ concentrations (Fig. 4c). Figs. 4d, 4e and 4f show the normalized far-UV CD monitored cations (Cs^+, Na^+ and K^+) induced refolding transition of U_B-state to B-state for the Ferricyt *c*, apoMb and Lyz, respectively at pH 12.9 (±0.1), 25° C. The Gibbs free energy change, ΔG, for the salt-induced two-state transitions, $U_B \rightarrow$B of Ferricyt *c* apoMb and Lyz was calculated by the equation (1):

$$\Delta G = -RT \ln K = -RT \ln\left[(Y_{obs} - Y_{UB}) / (Y_B - Y_{obs})\right] \quad (1)$$

where, Y_{obs} is the observed value of the CD signal, Y_{UB} and Y_B are the CD signal intensities for the U_B and B-states, respectively. By assuming a linear dependence of ΔG on [Cation] [57], the least-squares fit of the data to equation (2),

$$\Delta G = \Delta G^0 + m[\text{Cation}] \quad (2)$$

provides, ΔG^o and m for different cations-induced $U_B \rightarrow$B transition (Figs. 4g, 4h and 4i), respectively (Table 2).

Table 2 Thermodynamic parameters, free energy change (ΔG^o) and slop (m) for the refolding (CD 222 nm) of base-denatured Ferricyt *c*, apoMb and Lyz in the presence of cations (Cs^+, Na^+ and K^+) at pH 12.9 (±0.1), 25 ºC.

Salt	ΔG^o (kcal mol^{-1})	m(kcal mol^{-1} M^{-1})
Ferricyt *c*		
NaCl	1.22 (0.05)	1.98 (0.05)
KCl	1.22 (0.05)	2.03 (0.05)
CsCl	1.21 (0.07)	1.66 (0.07)
apoMb		
NaCl	0.69 (0.03)	2.26 (0.04)
KCl	0.62 (0.05)	1.90 (0.05)
CsCl	0.34 (0.06)	1.45 (0.1)
Lyz		
NaCl	-	-
KCl	1.52 (0.01)	1.26 (0.1)
CsCl	1.52 (0.2)	1.42 (0.2)

The ΔG^o values of Cs^+, Na^+ and K^+ for each base-denatured Ferricyt *c* and apoMb are within error identical (Table 2), suggesting that ΔG^o is independent of the physical properties of cations. Although, the physical importance of the factor *m* is not fully understood, but some earlier reports revealed that it reflects the difference between the accessibility of surface areas of native and denatured states of the polypeptide chain for a given denaturant [90-93].

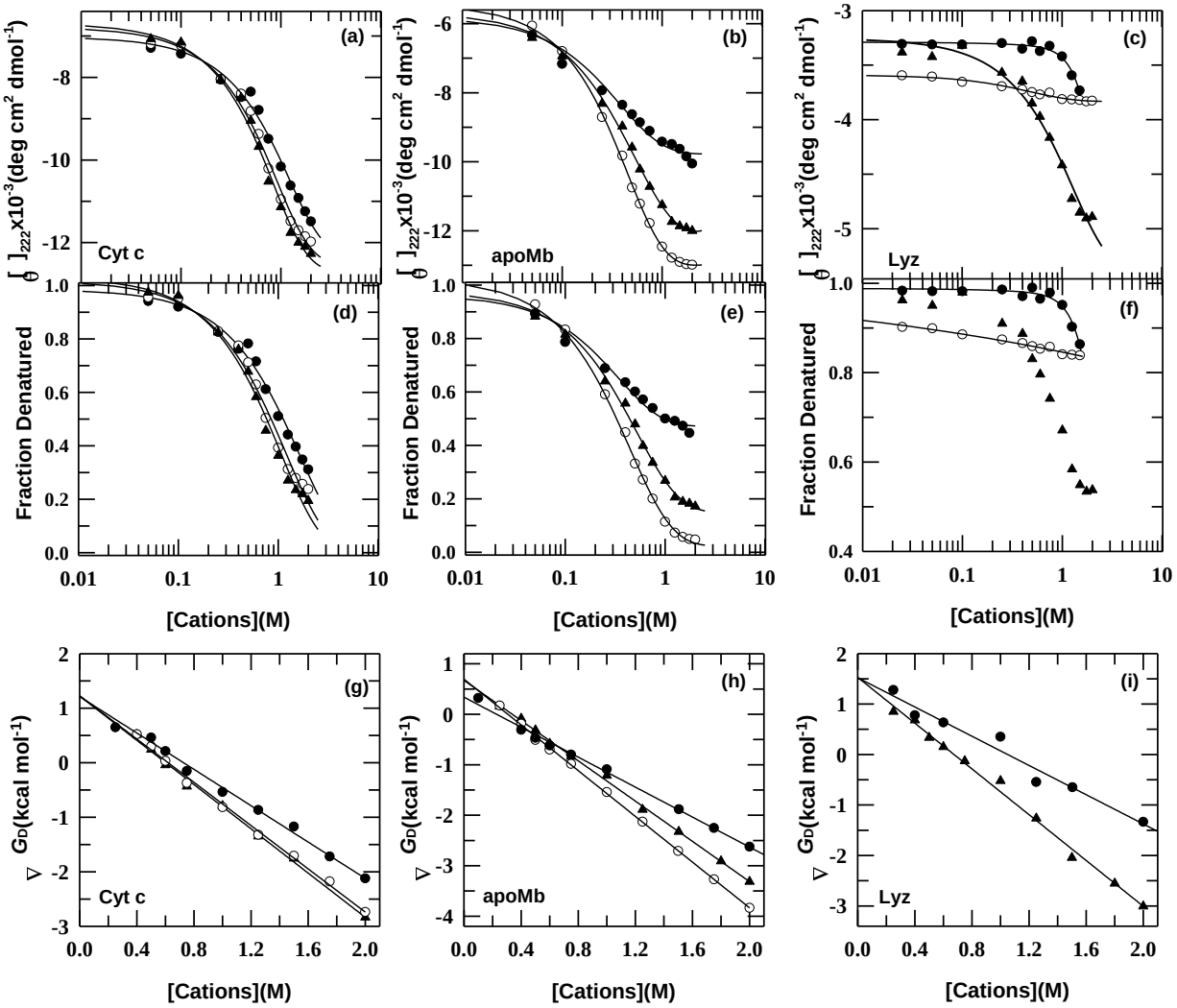

Fig.4. Panels (a), (b) and (c) show the variation of the far-UV CD at 222 nm values of base denatured Ferricyt *c* (14 µM), apoMb (14 µM) and Lyz (7 µM), respectively as a function of chloride salt of Cs^+ (●), Na^+(○) and K^+ (▲) at pH 12.9 (±0.1). Panels (d), (e) and (f) show normalized cation-induced (chloride salt of Cs^+ (●), Na^+ (○) and K^+ (▲)) refolding transition (CD 222 nm) of base denatured Ferricyt *c*, apoMb and Lyz, respectively at pH 12.9 (±0.1). The solid lines in panel (a) to (f) are just guide the eye. Panels (g) and (h) present the plots of ΔG, as the function of chloride salt of Cs^+ (●), Na^+ (○) and K^+(▲) concentration for refolding of base denatured Ferricyt *c* and apoMb, respectively at pH 12.9 (±0.1). Panel (i) presents the plots of ΔG, as the function of chloride salt of Cs^+ (●) and K^+(▲) concentration for refolding of base denatured Lyz at pH 12.9 (±0.1). The linear least-squares best fit of the data to equation (2) [57] provided, ΔG^o and *m* values (Table 2)

Figs. 5a, 5b and 5c present the far-UV CD (222 nm) monitored TFE induced $U_B \rightarrow H_B$ transitions for Ferricyt *c*, apoMb and Lyz, respectively at 25 °C. Figs. 5d, 5e and 5f present the normalized far-UV CD monitored TFE induced refolding transition of U_B-state to H_B-state for Ferricyt *c*, apoMb and Lyz, respectively at pH 12.9 (±0.1), 25° C. Clearly, the base-denatured U_B-states of Ferricyt *c*, apoMb and Lyz acquired the secondary structure with the increment of [TFE] (Figs. 5d, 5e and 5f). The Gibbs free energy change, ΔG, for TFE-induced two-state transitions, $U_B \rightarrow H_B$ of Ferricyt *c* apoMb and Lyz was calculated by the eq (1). By assuming a linear dependence of ΔG on [TFE] [57], the least-squares fit of the data to eq (3),

$$\Delta G = \Delta G^0 + m[TFE] \qquad (3)$$

provides, ΔG^o and *m* for TFE-induced $U_B \rightarrow H_B$ transition of Ferricyt *c* (Insets of Fig. 5d), apoMb (Insets of Fig. 5e) and Lyz (Insets of Fig. 5f), respectively (Table 3).

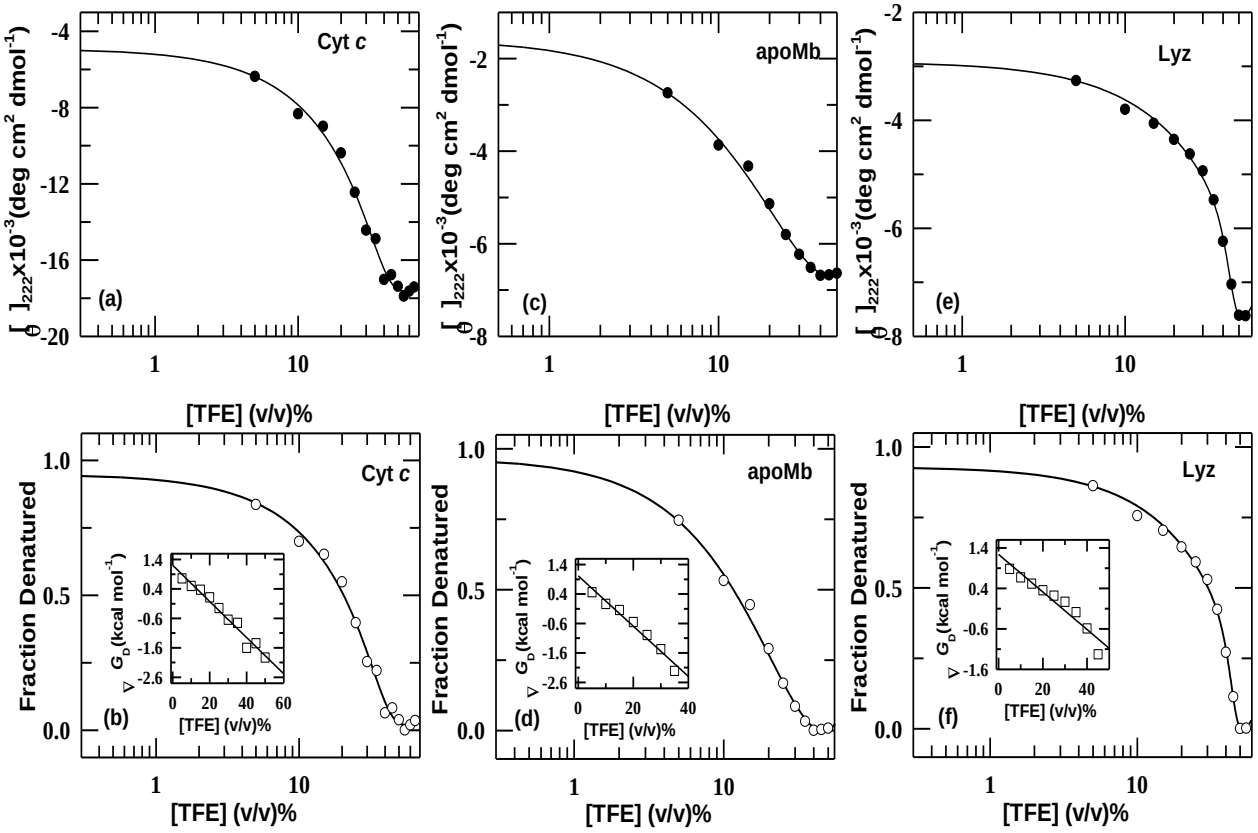

Fig.5. Panels (a), (b) and (c) shows the normalized TFE-induced (●) refolding transition (CD 222 nm) of base denatured Ferricyt *c* (16 µM), apoMb(16 µM) and Lyz (16 µM), respectively, at pH 12.9 (±0.1). Panels (d), (e) and (f) show normalized TFE-induced (○) refolding transition (CD 222 nm) of base denatured Ferricyt *c*, apoMb and Lyz, respectively at pH 12.9 (±0.1). The solid line through the data in panels (a) to (f) has been drawn by inspection only. Inset of the panel (d), (e) and (f) shows unfolding free energy changes in the transition region calculated from the equilibrium curve. The solid lines are the linear least-squares best fit of the data to equation (3).

Table 3 Thermodynamic parameters, free energy change (ΔG^o) and slop (m) for the refolding (CD 222 nm) of base-denatured Ferricyt *c*, apoMb and Lyz in the presence of TFE at pH 12.9 (±0.1), 25 ºC.

	ΔG^o (kcal mol^{-1})	m (kcal mol^{-1} M^{-1})
Ferricyt *c*	1.2	0.6
apoMb	1.0	0.8
Lyz	1.0	0.3

8.2.4 B-and H_B–states of Ferricyt c, apoMb and Lyz do not acquire tertiary structure

Fig. 6a, 6b and 6c present the near-UV CD spectra for Ferricyt *c*, apoMb and Lyz, respectively for native state at pH 7.0 (N-state), base-denatured state at pH 12.9 (±0.1) (U_B-state) and base-denatured state at pH 12.9 (±0.1) in the presence of 2.0 M of cations of chloride salt (CsCl, NaCl and KCl) (B-state) at 25 °C. Fig. 6a, 6b and 6c also present the near-UV CD spectra for Ferricyt *c*, apoMb and Lyz, respectively for base-denatured state at pH 12.9 (±0.1) in the presence of 45% (v/v) TFE at 25 °C. Figs. 6a, 6b and 6c clearly suggest that the tertiary structures of base-denatured Ferricyt *c*, apoMb and Lyz are significantly disrupted at pH 12.9 (±0.1). The inclusion of 2.0 M salt (NaCl, KCl and CsCl) or % (v/v) TFE does not induce the tertiary structures in the base denatured Ferricyt *c* (Fig. 6a), apoMb (Fig. 6b) and Lyz (Fig. 6c). This finding provides evidence that the cations (Cs^+, Na^+ and K^+) and alcohol (TFE) transform the base-denatured Ferricyt *c*, apoMb and Lyz to MG-states.

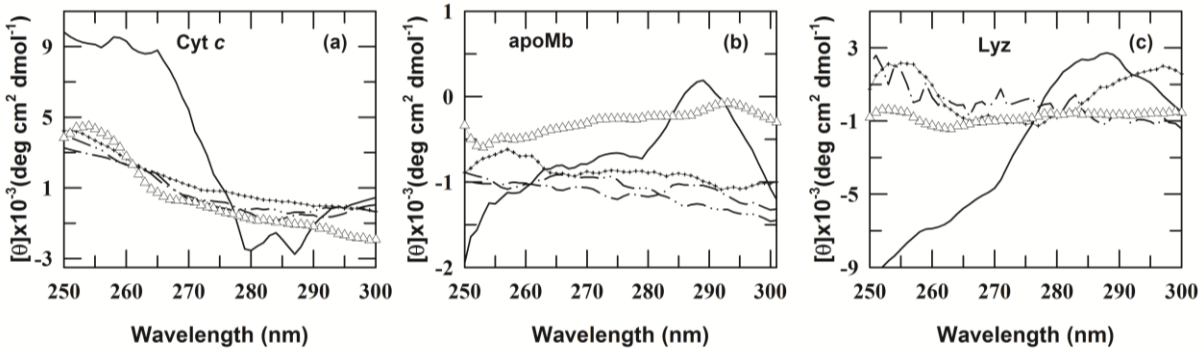

Fig.6. Panels (a), (b) and (c) present the near-UV CD spectra for different states of Ferricyt *c* (70 µM), apoMb (60 µM) and Lyz (60 µM), respectively (pH 7.0, native state (solid-line); pH 12.9 (± 0.1) unfolded state (××××××); pH 12.9 (±0.1) with 2.0 M NaCl (gray solid line); pH 12.9 (± 0.1) with 2.0 M KCl (dash-dot line): pH 12.9 (± 0.1) with 2.0 M CsCl (double-dot-dash line) and pH 12.9 (±0.1) with 45% (v/v) TFE (ΔΔΔΔ), at 25ºC.

8.2.5 ANS binding to native, base-denatured and cations and alcohol-induced MG states of Ferricyt c, apoMb and Lyz

Traditionally, 1-anilino-8-naphthalene sulfonate (ANS), which binds to exposed hydrophobic clusters of folding intermediates are used as a fluorescence probe for determining the non-polar character of proteins and membranes [94-95]. Upon binding to the apolar surfaces or in a less polar environment, its fluorescence intensity is enhanced and the emission maximum is shifted to lower wavelengths. As compared to the native or the fully unfolded states, the ANS has much stronger affinity to the MG-state of proteins [94]. This is presumably because of (i) the deficiency of rigid packing of hydrophobic clusters in MGs, and (ii) due to a greater accessibility of the protein hydrophobic core for a solvent. The rigid and tightly packed conformations interior of native protein molecule with a low accessibility of protein hydrophobic clusters to a solvent results in decrease of ANS affinity for the native protein [94]. The solvent accessible hydrophobic core are completely absent in the denatured or unfolded proteins [94]. Therefore it shows least binding affinity to unfolded proteins.

Figs. 7a, 7b and 7c present the ANS fluorescence emission spectra for Ferricyt *c*, apoMb and Lyz, respectively for native state at pH 7.0 (N-state), base-denatured state at pH 12.9 (U_B-state) and base-denatured state at pH 12.9 in the presence of 2.0 M of cations of chloride salt (Cs^+, Na^+ and K^+) (B-state) at 25 °C. Fig. 8a, 8b and 8c present the ANS fluorescence emission spectra for Ferricyt *c*, apoMb and Lyz, respectively for native state at pH 7.0 (N-states), base-denatured state at pH 12.9 (U_B-states) and base-denatured state at pH 12.9 in the presence of 45% (v/v) TFE at 25 °C.

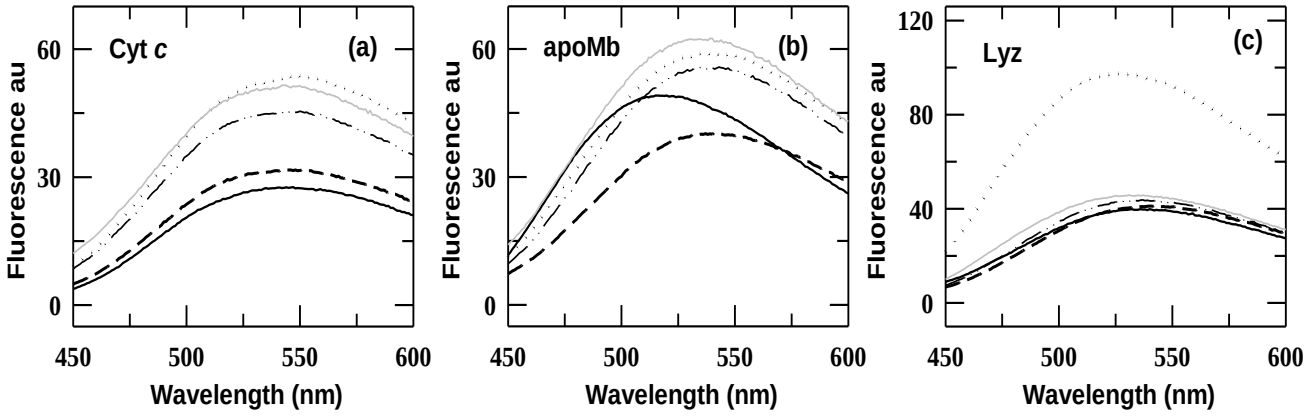

Fig.7. Panels (a), (b) and (c) present the ANS fluorescence emission spectra of different state for Ferricyt *c* (8 µM), apoMb (8 µM) and Lyz (8 µM), respectively (native state pH 7 (solid black line), pH 12.9 (± 0.1) unfolded state (long dash line); pH 12.9 (± 0.1) with 2.0 M KCl (dotted black line); pH 12.9 (± 0.1) with 2.0 M NaCl (solid gray line) and pH 12.9 (± 0.1) with 2.0 M CsCl (double-dot-dash line) at 25 ºC.

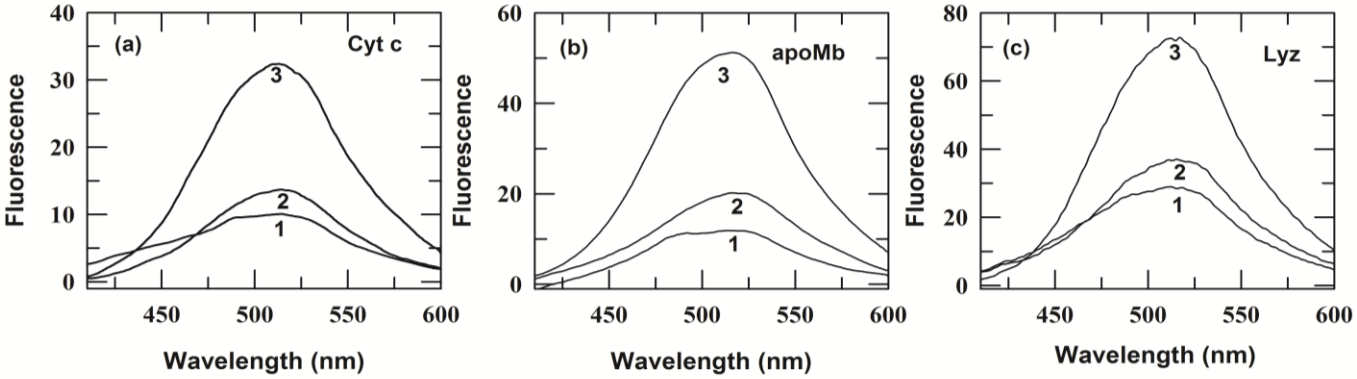

Fig.8. Panel (a), (b) and (c) present the ANS fluorescence emission spectra for different states of Ferricyt *c* (8 µM), apoMb (8 µM) and Lyz (8 µM), respectively (native protein pH 7 (spectrum 1); pH-12.9 (±0.1) unfolded state (spectrum 2); pH 12.9 (± 0.1) with 45% TFE (spectrum 3).

Clearly, the binding of ANS to B-state (Figs. 7a, 7b and 7c) and H_B-state (Figs. 8a, 8b and 8c) have maximum fluorescence intensity than the native and U_B-states (Figs. 7a, 7b, 7c and Figs. 8a, 8b, 8c), which suggests that in the B-state and H_B-state of proteins, the hydrophobic clusters which were originally buried inside are now solvent exposed.

8.2.6 Effect of cations on thermal denaturation of base-denatured Ferricyt c, apoMb and Lyz at pH 12.9

To test the effect of cations of chloride salt (CsCl, NaCl and KCl) on thermal denaturation of base-denatured proteins, the far-UV CD (222 nm) monitored thermal denaturation curves of base-denatured Ferricyt *c*, apoMb and Lyz were recorded in the presence different concentrations of NaCl, KCl and CsCl at pH 12.9 (±0.1). The thermal denaturation data were normalized according to equation (4):

$$\theta = \frac{\theta_{obs} - (m_1 T + \theta_1)}{(m_2 T + \theta_2) - (m_1 T + \theta_1)} \qquad (4)$$

where, θ_{obs} is the observed ellipticity, T is the temperature, m_1 and θ_1 are slope and intercept, respectively, of the pretransition baseline, and m_2 and θ_2 are slope and intercept of the post-transition baseline. Fig. 9a, 9b and 9c present the normalized far-UV CD (222 nm) monitored thermal denaturation curves of base-denatured Ferricyt *c*, apoMb and Lyz, respectively in the presence of different concentrations of NaCl, KCl and CsCl at pH 12.9 (±0.1). At very low salt concentration (0.001 M NaCl), the base-denatured Ferricyt *c* and apoMb exhibit two temperature transitions, the first correspond to cold denaturation and the second correspond to heat denaturation (Figs. 9a and 9b). However, at very low salt concentration (0.001 M NaCl), the base-

denatured Lyz at pH 12.9 (±0.1) does not exhibit cold denaturation (Fig. 9c). The normalized thermal denaturation curves were analyzed by the Gibbs-Helmholtz equation (chapter 2 equation (4)) [70]. The thermal denaturation parameters are listed in Table 4. Clearly, as salt concentration is increased, the T_m and ΔH_m values are also increased, which suggests that the cations presence in the reaction medium increase the thermal stability of base-denatured Ferricyt *c*, apoMb and Lyz at pH 12.9 (±0.1).

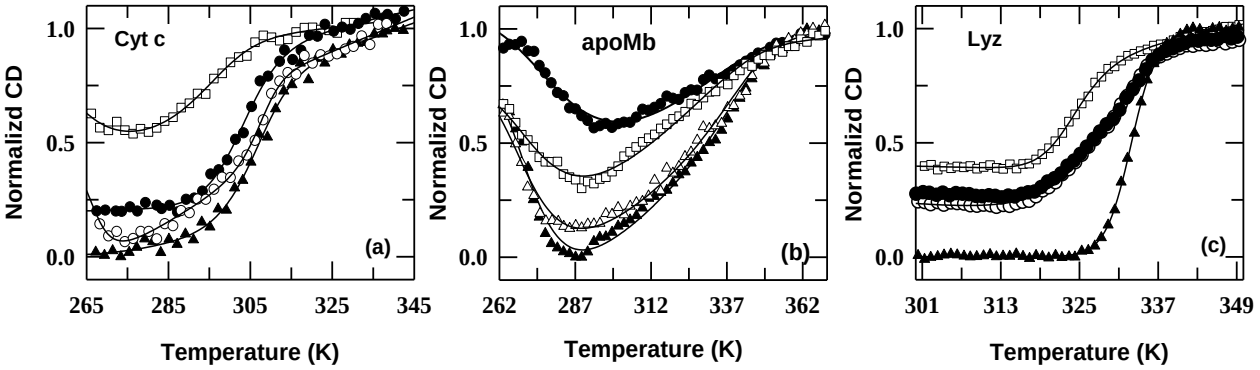

Fig.9. Panel (a) presents the normalized far-UV CD (222 nm)-monitored thermal melting curves of base-denatured Ferricyt *c* (16 µM) at pH 12.9 (± 0.1) in the presence of 0.001 M NaCl (□), 1.0 M NaCl (○), 1.0 M KCl (▲) and 1.0 M CsCl (●). Panel (b) presents the normalized far-UV CD (222 nm) monitored thermal melting curves of alkali-denatured apoMb (20 Mµ) at pH 12.9 (±0.1) in the presence of 0.001 M NaCl (●), 1.0 M NaCl (▲) 1.0 M KCl (Δ) and 1.0 M CsCl (□). Panel (c) presents the normalized far-UV CD (222nm) thermal melting curves of Lyz (25 µM) in the absence (□) and presence of 2.0 M KCl (▲), 2.0 M NaCl (●) and 2.0 M CsCl (○) at pH 12.9 (±0.1). The continuous lines are fits according to Gibbs-Helmholtz equation (chapter 2 equation (6)). Table 4 listed the thermodynamic parameters extracted from the 222 nm data set.

Table 4. Thermodynamic parameter for unfolding (CD 222 nm) of the base-denatured Ferricyt *c*, apoMb and Lyz (pH 12.9(±0.1)) in the absence and presence of NaCl, KCl and CsCl at pH 12.9 (±0.1)*.

	Ferricyt *c*			
Additives	Concentration (M)	T_m (K)	ΔH_m(kcal mol^{-1})	ΔC_P (kcal mol^{-1})
Control	0.001NaCl	292.1	30.0	1.2
NaCl	1.00	303.4	34.8	1.1
KCl	1.00	305.2	37.0	1.09
CsCl	1.00	302.2	35.3	1.16
	apoMb			
Control	0.001NaCl	333.4	8.0	0.4
NaCl	1.0	340.7	25.0	0.7
KCl	1.0	338.9	21.0	0.6
CsCl	1.0	336.1	15.0	0.5
	Lyz			
Control	0.0	323.9	70.5	1.2
NaCl	2.0	329.4	48.62	1.02
KCl	2.0	332.9	110.9	2.17
CsCl	2.0	328.04	46.9	1.4

* The uncertainty in the values of T_m, ΔH_m and ΔC_p are ±1.0 K, ±5.0 kcal mol^{-1} and ±0.5 kcal mol^{-1}K^{-1}, respectively.

8.2.7 Effect of cations and alcohol on the kinetics of CO association to alkaline **Ferrocyt *c***

Under the mild destabilizing conditions, Ferrocyt *c* can be driven to bind CO when CO is used in saturating concentration (~1mM) [96-98]. Intramolecular thermal collisions provide the energy for barrier crossing in the CO association reaction (i.e. Ferrocyt *c* +CO→ Ferrocyt *c*-CO) of Ferrocyt *c*. The rate coefficient for CO association reaction, k_{ass} is expected to decrease if the amplitudes of thermal fluctuations are reduced as a result of constraints on the collective modes of intramolecular motion [99]. Fig. 10a typifies the kinetics of CO-association to alkaline Ferrocyt *c* (pH 12.9 (±0.1) (550 nm), following the addition of a small volume of the protein solution to a CO-saturated aqueous alkaline solution (pH 12.9 (±0.1)) at 25ºC. The CO-association kinetics of alkaline Ferrocyt *c* is described by a monoexponential decay function (Fig. 10a). Fig 10b shows the logarithm of k_{ass} for alkaline Ferrocyt *c* (pH 12.9 (±0.1)) as a function of salt (CsCl, NaCl and KCl) concentrations at 25 ºC. With the increment in NaCl and KCl concentrations, log k_{ass} decreases mono exponentially and saturates at around 0.5 M salt (Fig 10b). With the increment in CsCl concentration, the log k_{ass} decreases at low concentration and then increases at higher salt concentration (≥0.25 M CsCl) (Fig 10b). At low salt concentrations, the decrease in log k_{ass} is more observed in the presence of CsCl and least in the presence of NaCl (CsCl > KCl > NaCl), which suggests that the value of log k_{ass} is more decreased for the larger cations and least for the smaller cation ($Cs^+ > K^+ > Na^+$) (cesium (1.67 Å), potassium (1.52 Å), sodium (1.16 Å) (chloride salt)) [100-101]. At higher salt concentration, the log k_{ass} is more observed for the CsCl and least in the presence of KCl (CsCl > NaCl> KCl). The increase in log k_{ass} in the presence of higher concentrations CsCl (≥0.25 M CsCl) can be interpreted to arise from protein destabilization that would facilitate CO association process. Fig. 10c presents the log k_{ass} for alkaline Ferrocyt *c* (pH 12.9 (± 0.1)) as a function of [TFE] at 25ºC. As [TFE] is increased from 0 to 20 % (v/v), the log k_{ass} initially decreases and shows a minima at 5% (v/v) and then increases, which suggests that the low concentrations of TFE may form some extra internal H-bonds and which in results constrain the internal dynamics of protein but at higher concentrations, the destabilizing effect of TFE due to hydrophobicity increase the structural fluctuations responsible for unfolding the protein.

To further investigate the effects of cations (Cs^+, Na^+ and K^+) and alcohol (TFE) on internal dynamics of base-denatured proteins, the activation thermodynamic parameters for CO

association reaction of alkaline Ferrocyt *c* were calculated in the presence of different concentrations of NaCl, KCl, CsCl and TFE at pH 12.9 (±0.1).

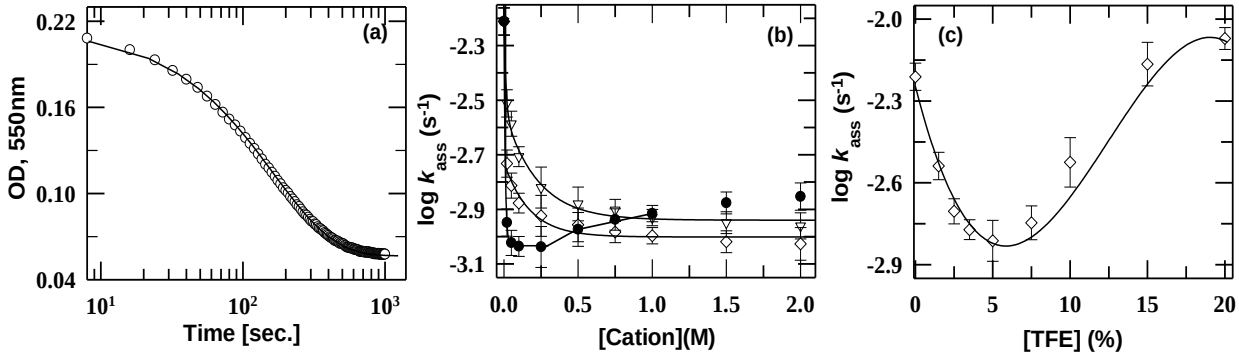

Fig.10. Panel (a) represents the slow single-phase CO-association kinetic trace of alkaline Ferrocyt *c* (τ= 2 min, pH 12.9 (±0.1), 298.15 K) (b) Dependence of log k_{ass} for alkaline Ferrocyt *c* on NaCl (▽), KCl (◊) and CsCl (●) concentration at pH 12.9 (±0.1), 298.15 K. Panel (c) presents the dependence of log k_{ass} for alkaline Ferrocyt *c* on TFE (◊) concentration at pH 12.9 (±0.1), 298.15 K. Solid lines in panel (b) and (c) are just guide to the eye.

Fig. 11a shows the Eyring plots for the CO association reaction of alkaline Ferrocyt *c* in the absence and presence of 1.0 M salt (NaCl, KCl, CsCl) at pH 12.9 (±0.1). Fig.11b shows the Eyring plots for the CO-association reaction of alkaline Ferrocyt *c* in the absence and presence of 5% (v/v) TFE at pH 12.9 (±0.1). Eyring plots were analyzed by linear least-squares analysis (Equation (1), chapter 2) [100, 102] of the temperature dependent k_{ass} in the absence and presence of different cations and TFE. Table 5 summarized the resulted activation enthalpy ($\Delta H_{ass}^{\ddagger}$) and activation entropy ($\Delta S_{ass}^{\ddagger}$).

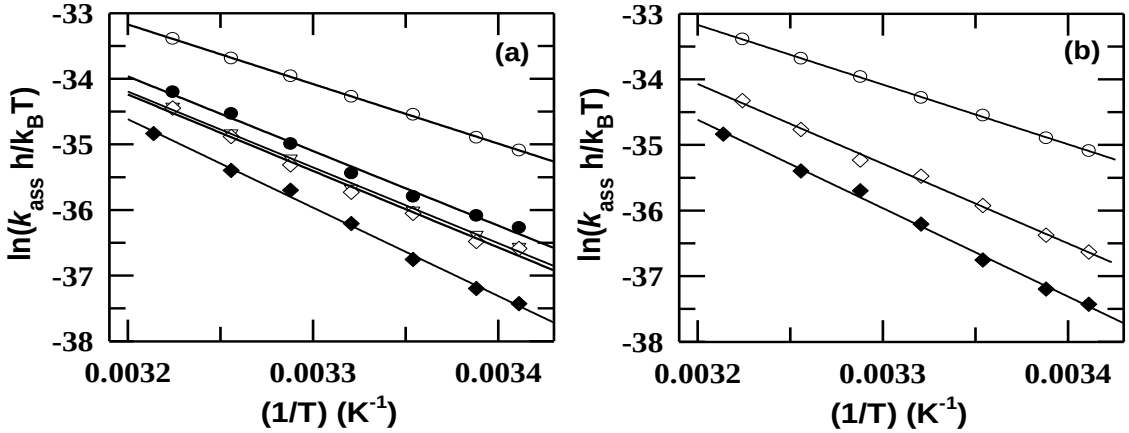

Fig.11. Panels (a) and (b) show the Eyring plots for the CO-association reaction in the absence (○) of additives at pH 12.9 (± 0.1). Panel (a) shows the Eyring plots for 1.0 M NaCl (▽); 1.0 M KCl (◊) and 1.0 M CsCl (●) at pH 12.9 (±0.1). Panel (b) shows the Eyring plots for CO-association reaction of alkaline Ferrocyt *c* (pH 12.9 (± 0.1)) in the presence of 5% TFE (◊). Panel (a) and (b) also show the Eyring plots for CO-association in the absence of additives

at pH 7.0 (♦) and pH 12.9 (○). The solid lines are fit to the data according to Eyring equation [102]. All reactions were carried out is in 2 mM CAPS buffer at pH 12.9 (± 0.1).The thermodynamic parameters are listed in Table 5.

Table 5 The effect of cations and TFE on activation thermodynamic parameters for CO-association of Ferrocyt *c* at pH 12.9 (±0.1)*

Additives	Concentration	$\Delta G_{ass}^{a\ddagger}$ (kcal mol^{-1})	$\Delta H_{ass}^{\ddagger}$ (kcal mol^{-1})	$\Delta S_{ass}^{\ddagger}$ (cal mol^{-1} K^{-1})	$-T\Delta S_{ass}^{a\ddagger}$ (kcal mol^{-1} K^{-1})
Control	0.0	20.6 (0.05)	18.2 (0.2)	−8.2 (0.6)	2.4 (0.2)
NaCl	1M	21.4 (0.07)	23.1 (0.7)	5.6 (2.3)	−1.6 (0.6)
KCl	1M	21.5 (0.1)	23.3 (0.9)	6.1 (3.0)	−1.8 (0.9)
CsCl	1M	21.3 (0.1)	22.7 (1.0)	4.8 (3.2)	−1.4 (1.0)
TFE	5% (V/V)	21.4 (0.06)	24.3 (0.6)	9.7 (0.6)	−2.9 (0.6)
Control pH 7.0	0.0	22.0 (0.01)	26.0 (0.1)	12.4 (0.8)	−3.7 (0.2)

[a] Activation free energy ($\Delta G_{ass}^{\ddagger}$) and entropy changes ($-T\Delta S_{ass}^{\ddagger}$) are given at 25ºC.
*The uncertainties (standard error) in $\Delta G_{ass}^{\ddagger}$, $\Delta H_{ass}^{\ddagger}$, $-T\Delta S_{ass}^{a\ddagger}$ and $\Delta S_{ass}^{\ddagger}$ are indicated in parenthesis.

If the internal dynamics of alkali-denatured protein is indeed constrained at some concentration of CsCl, NaCl and KCl or TFE, then the $\Delta H_{ass}^{\ddagger}$ for CO-association at that salt or TFE concentration will be relatively higher. The data in Table 5 clearly indicate that the $\Delta H_{ass}^{\ddagger}$ for CO-association reaction of alkaline Ferrocyt *c* is larger in the presence of cations (Cs^+, Na^+ and K^+) or alcohol (TFE) then in its absence. However, the $\Delta H_{ass}^{\ddagger}$ for CO-association reaction of alkaline Ferrocyt *c* (pH 12.9 (±0.1)) is lower than the native Ferrocyt *c* (pH 7.0).

8.2.8 Mechanism of Cations and TFE-induced protein stabilization

The extreme basic pH unfolded Ferricyt *c*, apoMb and Lyz carries highly negative charge. Previous reports revealed that the net charge of salt anion is the main determinant for anion-induced stabilization of MG-state of acid-denatured proteins [72]. Previous reports also revealed that the size of anions also plays an important role in the anion-induced stabilization of MG-state of acid-denatured proteins [103]. A previous report for a protein carrying net negative charge at pH 7.0 revealed that the effect of cations on protein stability is largest for NH_4^+ and decreases as a function of increased charge density ($NH_4^+ > K^+ \sim Cs^+ \sim Na^+ > Li$) [38]. Present study presents a monovalent cations-induced stabilization of MG-state of base-denatured Cyt *c*, apoMb and Lyz. The effect of cation-induced refolding (secondary structure) and increase in thermal stability of base denatured Ferricyt *c* and Lyz is more observed in the presence of K^+ and least in the presence of Cs^+ ($K^+ > Na^+ > Cs^+$) (Fig 4a, Fig 9a for Ferricyt *c* ; Figs. 4c, 9c for Lyz and Table 3). However, the effect of cation-induced refolding (secondary structure) and increase in thermal stability of base denatured apoMb is more observed in the presence of Na^+ and least in the Cs^+

($Na^+ > K^+ > Cs^+$) (Figs. 4b, 9b). These results suggest that the charge density plays an important role in the cation-induced stabilization of base denatured proteins. CO-association reaction of alkaline Ferrocyt *c* showed that the internal dynamics of protein is more constrained in the presence of Cs^+ and least in the presence of Na^+ ($Cs^+ > K^+ > Na^+$) (up to ~ 0.35 M) (Fig. 10b). These results thus suggests that the size of monoatomic cations ($Cs^+ > K^+ > Na^+$) plays an important role in constraining the internal dynamics of protein.

The base-denatured Ferricyt *c*, apoMb and Lyz in the presence of 45% (v/v) of TFE acquired the native like secondary helical structure (Fig. 3d, 3e and 3f)), but does not acquired tertiary structure (Fig. 6a, 6b and 6c). According to Thomas & Dill (1993), TFE can weaken the nonlocal interactions of proteins but favoring local interactions [104]. Some previous studies also suggested that TFE favoring the internal H-bonds and which are large enough to account for the increase in helicity or helical content of proteins [105-108]. Extensive helix formation in the presence of TFE is the formation of non-native helical structure which results the disruption of the specific native tertiary structure of proteins [109]. Therefore, the alkali-denatured proteins acquired the native-like secondary structure but did not acquired any tertiary structural signals in the presence of TFE and these are the basic properties of the intermediates state of protein, *i.e.* the TFE-induced molten globule state.

8.3. Conclusion

TFE and cations (Na^+, K^+ and Cs^+) transformed the alkali pH-denatured Ferricyt *c*, apoMb and Lyz (U_B-states) to MG-states at pH 12.9 (±0.1). Near-UV CD, far-UV CD, tryptophan fluorescence and ANS binding experiments of base-denatured Ferricyt *c*, apoMb and Lyz carried out in the absence and presence of different concentrations of TFE and salt (NaCl, KCl and CsCl) revealed that the TFE and cations (Na^+, K^+ and Cs^+) induced fully populated conformations are molecular compact states containing native-like secondary structural contents but disordered tertiary interactions. Kinetic and thermodynamic experiments involving the measurement of the CO-association to the alkali Ferrocyt *c* (pH 12.9 (±0.1)) in the absence and presence of different concentrations of TFE and salt (NaCl, KCl, and CsCl) indicate that the TFE and cations (Na^+, K^+ and Cs^+) presence in the reaction medium constrained the internal dynamics of alkali Ferrocyt *c*. Thermodynamic analysis of CD (222 nm)-monitored thermal denaturation curves of base-

denatured Ferricyt *c*, apoMb and Lyz (pH 12.9 (±0.1) measured in the absence and presence of different concentrations of salt (NaCl, KCl and CsCl) suggests that the cations (Na^+, K^+ and Cs^+) presence in the reaction medium increase the thermal stability of base-denatured proteins.

8.4. References:

1. A. Karshikoff, R. Ladenstein, The Role of Electrostatic Interactions in the Stabilization of Proteins from Thermophiles. In *Methods in Protein Structure and Stability Analysis: Conformational Stability, Size, Shape and Surface of Protein Molecules*; Uversky, V. N., Permyakov, E., Eds., Nova Biomedical Books, New York, (2007) pp 71.
2. D. Perl, G. Holtermann, F. X. Schmid, *Biochemistry* **40** (2001) 15501–15511.
3. S. Jayaraman, D. L. Gantz, O. Gursky, *Biochemistry* **45** (2006) 4620–4628.
4. S. Benjwal, S. Jayaraman, O. Gursky, *Biochemistry* **44** (2005) 10218–10226.
5. B. N. Dominy, D. Perl, F. X. Schmid, C. L. Brooks, *J. Mol. Biol.* **319** (2002) 541–544.
6. R. Jaenicke, G. Bohm, *Curr. Opin. Struct. Biol.* **8** (1998) 738–748.
7. C. N. Pace, *Methods Enzymol.* **259** (1995) 538–554.
8. G. Vogt, S. Woell, P. Argos, *J. Mol. Biol.* **269** (1997) 631–643.
9. A. H. Elcock, J. A. McCammon, *J. Mol. Biol.* **280** (1998) 731–748
10. K. A. Dill, H.S. Chan, *Nat. Struct. Biol.* **4** (1997) 10–19.
11. P. S. Kim, R.L. Baldwin, *Annu. Rev. Biochem.* **59** (1990) 631– 660.
12. C. Redfield, R.A. Smith, C.M. Dobson, *Nat. Struct. Biol.* **1** (1994) 23–29.
13. O.B. Ptitsyn, R.H. Pain, G.V. Semisotnov, E. Zerovnik, O.I. Razgulyaev, *FEBS Lett.* **262** (1990) 20–24.
14. K. Kuwajima, *Proteins: Struct. Funct. Genet.* **6** (1989) 87–103.
15. O.B. Ptitsyn, *Adv. Protein Chem.* **47** (1995) 83–229.
16. Y. Kumar, S. Tayyab, S. Muzammil, *Arch. Biochem. Biophy.* **426** (2004) 3–10.
17. O.B. Ptitsyn, *Protein Folding* (Creighton, T.E., Eds.) Freeman, New York, (1992) pp. 243–300.
18. S. N. Timasheff, *Annu. Rev. Biophys. Biomol. Struct.* **22** (1993) 67–97.
19. K.I. Nakayama, S. Hatakeyama, K. Nakayama, *Biochem. Biophys. Res. Commun.* **282** (2001) 853–860.

20. A.K. Dunker, M.S. Cortese, P. Romero, L.M. Iakoucheva, V.N. Uversky, *FEBS J.* **272** (2005) 5129–5148.
21. E. Kokai, A. Tantos, E. Vissi, B. Szoor, P. Tompa, J. Gausz, L. Alphey, P. Friedrich, V. Dombradi, *Arch. Biochem. Biophys.* **451** (2006) 59–67.
22. P. Radivojac, S. Vucetic, T.R. O'Connor, V.N. Uversky, Z. Obradovic, A. Dunker, *Proteins: Struct. Funct. Genet.* **63** (2006) 398–410.
23. P. Tompa, P. Banki, M. Bokor, P. Kamasa, D. Kovacs, G. Lasanda, K. Tompa, *Biophys. J.* **91** (2006) 2243–2249.
24. B.Y. Baker, D.C. Yaworsky, W.L. Miller, *J. Biol. Chem.* **280** (2005) 41753–41760.
25. F. Edwin, Y. V. Sharma, M. V. Jagannadham, *Biochem. Biophys. Res. Commun.* **290** (2002) 1441–1446.
26. Y. O. Kamatari, T. M. Konno, M. Kataoka, K. J. Akasaka, *Mol. Biol.* **259** (1996) 512–523.
27. A. L. Fink, L. J. Calciano, Y. Goto, T. Kurotsu, D. R. Palleros, *Biochemistry* **33** (1994) 12504–12511.
28. P. D. Thomas, K. A. Dill, *Protein Sci.* **2** (1993) 2050–2065.
29. K. Shiraki, K. Nishikawa, Y. Goto, *J. Mol. Biol.* **245** (1995) 180–194.
30. T. Konno, J. Iwashita, K. Nagayama, *Protein science* **9**, (2000) 564–569.
31. F. Rashid, S. Sharma, M.A. Baig, B. Bano, *Biochem. Cell Biol.* **84** (2006) 126–134.
32. Y.O. Kamatari, T. Konno, M. Kataoka, K. Akasaka, *J. Mol. Biol.* **259** (1996) 512–523.
33. E. Zerovnik, M. Skarabot, K. Skerget, S. Giannini, V. Stoka, S. Jenko–Kokalj, R.A. Staniforth, *Amyloid* **14** (2007) 237–247.
34. A. Miranker, S.E. Radford, M. Karplus, C.M. Dobson, *Nature (London)* **349** (1991) 633–636.
35. S.E. Radford, C.M. Dobson, P.A. Evans, *Nature (London)* **358** (1992) 302–307.
36. S. Barker, K.H. Mayo, *J. Am. Chem. Soc*. **113** (1991) 8199– 8205.
37. K. Gast, D. Zirwer, M. Muller–Frohne, G. Damaschun, *Protein Sci.* **8** (1999) 625–634.
38. E. Sedlák, L. Stagg, P. Wittung-Stafshede, *Arch. Biochem. Biophys.* **474** (2008) 128–135.
39. R.L. Baldwin, *Biophys. J.* **71** (1996) 2056–2063.
40. K.D. Collins, *Biophys. J.* **72** (1997) 65–76.
41. Y. Zhang, S. Furyk, D.E. Bergbreiter, P.S. Cremer, *J. Am. Chem. Soc.* **127** (2005) 14505–14510.
42. R. Vogel, *Curr. Opin. Colloid Interface Sci.* **9** (2004) 133–138.

43. Y. Goto, S. Aimoto, *J. Mol. Biol.* **218** (1991) 387–396.
44. C. H. Ramos, R.L. Baldwin, *Protein Sci.* **11** (2002) 1771–1778.
45. G. Zoldák, M. Sprinzl, E. Sedlák, *Eur. J. Biochem.* **271** (2004) 48–57.
46. J.M. Broering, A.S. Bommarius, *J. Phys. Chem. B.* **109** (2005) 20612–20619.
47. M.G. Cacace, E.M. Landau, J.J. Ramsden, *Q. Rev. Biophys.* **30** (1997) 241–277.
48. H. Zhao, *J. Mol. Catal. B Enzym.* **37** (2005) 16–25.
49. C.N. Pace, G.R. Grimsley, *Biochemistry* **27** (1988) 3242–3246.
50. C. Ebel, P. Faou, B. Kernel, G. Zaccai, *Biochemistry* **38** (1999) 9039–9047.
51. Y. Goto, N. Takahashi, A.L. Fink, *Biochemistry* **29** (1990) 3480–3488.
52. C.H. Ramos, R.L. Baldwin, *Protein Sci.* **11** (2002) 1771–1778.
53. G. Zoldák, M. Sprinzl, E. Sedlák, *Eur. J. Biochem.* **271** (2004) 48–57.
54. J.M. Broering, A.S. Bommarius, *J. Phys. Chem. B.* **109** (2005) 20612–20619.
55. M.G. Cacace, E.M. Landau, J.J. Ramsden, *Q. Rev. Biophys.* **30** (1997) 241–277.
56. S.I. Merenbloom, T.G. Flick, M.P. Daly, E. R. Williams, *J. Am. Soc. Mass Spectrom.* **22** (2011) 1978-1990.
57. C. Ebel, P. Faou, B. Kernel, G. Zaccai, *Biochemistry* **38** (1999) 9039–9047.
58. E. Bismuto, et.al, *Eur. Biophys. J.* **33** (2004) 38–49.
59. A.J. Richard, et.al, *Cata. Biochim. Biophys. Acta* **1764** (2006) 1546–1552.
60. B. Hribar, N.T. Southall, V. Vlachy, K.A. Dill, *J. Am. Chem. Soc.* **121** (2002)12302–12311.
61. P. Sashi, U. M. Yasin, A. K. Bhuyan, *Biochemistry* **51** (2012) 3273−3283.
62. G.W. Bushnell, G.V. Louie, G.D. Brayer, *J. Mol. Biol.* **214** (1990) 585– 595.
63. L. Lin, R. J. Pinker, K. Forde, G. D. Rose, N. R. Kallenbach, *Nat. Struc. Biol.* **1** (1994) 447 – 452.
64. I. Kumagai, S. Kojima, Y. Tamaki, K. Miura, *J. Biochem*. **102** (1987) 733−740.
65. B.A. Malcolm, S. Rosenberg, M.J. Corey, J.S. Allen, A. Baetselier, J.F. Kirsch, *Proc. Natl. Acad. Sci. USA* **86** (1989) 133−137.
66. S. Nakamura, Y. Seki, E. Katoh, S. Kidokoro, *Biochemistry* **50** (2011) 3116–3126.
67. S. Nakamura, S. Kidokoro, *J. Phys. Chem. B.* **116** (2012) 1927–1932.
68. S. Nakamura, T. Baba, S. Kidokoro, *Biophys. Chem.* **127** (2007) 103–112.
69. Y. Kuroda, S. Kidokoro, A. Wada, *J. Mol. Biol.* **233** (1992) 1139–1153.

70. R. Kumar, N. P. Prabhu, D. K. Rao, A. K. Bhuyan, *J. Mol. Biol.* **364** (2006) 483−495.
71. D. Hamada, S. Kidokoro, H. Fukada, K. Takahashi, Y. Goto, *Proc. Nat. Acad. Sci. USA* **91** (1994) 10325–10329.
72. Y. Goto, N. Takahashi, A.L. Fink, *Biochemistry* **29** (1990) 3480–3488.
73. O. B. Ptitsyn, V.N. Uversky, *FEBS Letters* **341** (1994) 15–18.
74. I. Nishii, M. Kataoka, F. Tokunaga, Y. Goto, *Biochemistry* **33** (1994) 4903–4909.
75. V. E. Bychkova, A. E. Dujsekina, S. I. Klenin, E. I. Tiktopulo, V. N. Uversky, O. B. Ptitsyn, *Biochemistry* **35** (1996) 6058–6063.
76. T. Konno, J. Iwashita, K. Nagayama, *Protein Science* **9** (2000) 564–569.
77. F. Khan, R. H. Khan, S Muzammil, *Biochim. Biophys. Acta.* **1481** (2000) 229–236.
78. K. Gast, D. Zirwer, M. Müller–Frohne, G. Damaschun, *Protein Science* **8** (1999) 625–634.
79. Y. O. Kamatari, T. Konno, M. Kataoka, K. Akasaka, *J. Mol. Biol.* **259** (1996) 512–523.
80. Y. O. Kamatari, S. Ohji, T. Konno, Y. Seki, K. Soda, M. Kataoka, K. Akasaka, *Protein Sci.* **8** (1999) 873–882.
81. R. Jain, S. Kaur, R. Kumar, *J. Biochem.* **153** (2013) 161–177.
82. R. Kumar, N. P. Prabhu, A. K. Bhuyan, *Biochemistry* **44** (2005) 9359−9367.
83. A. K. Bhuyan, *Biochemistry* **49** (2010) 7764−7773.
84. A. K. Bhuyan, *Biochemistry* **49** (2010) 7774−7782.
85. D.K. Rao, R. Kumar, M.Yadaiah, A.K. Bhuyan, *Biochemistry* **45** (2006) 3412–3420.
86. M. Hameed, B. Ahmad, K. M. Fazili, K. Andrabi, R. H. Khan, *J. Biochem.* **141**(2007) 573–583.
87. R. A. Staniforth, M. G. Bigotti, F. Cutruzzolà, C. T. Allocatelli, M. Brunori, *J. Mol. Biol.* **275** (1998) 133–148.
88. S. S. Lehrer G. D. Fasman, *J. Bio. Chem.* **242** (1967) 4644–4651.
89. M.A. Ansari, S. Zubair, S.M. Atif, M. Kashif, N. Khan, M. Rehan, T. Anwar, A. Iqbal, M. Owais, *Protein Pept. Lett.* **17** (2010) 11–17.
90. C.N. Pace, *CRC Crit. Rev. Biochem.* **3** (1975) 1–43.
91. J. A. Schellman, *Biopolymers* **26** (1987) 549–559.
92. D. O. Alonso, K. A. Dill, *Biochemistry* **30** (1991) 5974–5985.
93. S. L. Mayo, R. L. Baldwin, *Science* **262** (1993) 873–876.

94. G.V. Semisotonov, N.A. Rodionova, O.I. Razgulyaev, V.N. Uversky, A.F. Gripas, R.I. Gilmanshin, *Biopolymers* **31** (1991) 119–128.
95. E. Schonbrunn, S. Eschenburg, K. Luger, W. Kabsch, N. Amrhein, *Proc. Natl. Acad. Sci. USA* **97** (2000) 6345–6349.
96. D.K. Rao, R. Kumar, M.Yadaiah, A.K. Bhuyan, *Biochemistry* **45** (2006) 3412–3420.
97. A. K. Bhuyan, R. Kumar, *Biochemistry* **41** (2002) 12821–12834.
98. H. Theorell, A. Kesson, *J. Am. Chem. Soc.* **63** (1941) 1812–1827.
99. R. Kumar, N.P. Prabhu, M. Yadaiah, A.K. Bhuyan, *Biophys. J.* **87** (2004) 2656–2662.
100. R. Kumar, D. Sharma, R. Jain, S. Kumar, R. Kumar, *Biophy. Chem.* **207** (2015) 61–73.
101. A. F. Wells, *Structural Inorganic Chemistry* (5th ed.) (1984).
102. J. Mikšovská, J.H. Day, R.W. Larsen, *J. Biol. Inorg. Chem.* **8** (2003) 621─625.
103. R. Santucci, C. Bongiovanni, G. Mei, T. Ferri, F. Polizio, A. Desideri, *Biochemistry* **39** (2000) 12632–12638.
104. P.D. Thomas, K. A. Dill, *Protein Sci.* **2** (1993) 2050–2065.
105. P. Luo, R.L. Baldwin, *Biochemistry* **36** (1997) 8413–8421.
106. G .Conio, E. Patrone, S. Brighetti, *J. Biol. Chem.* **245** (1970) 3335–3340.
107. A. Cammers-Goodwin, T.J. Allen, S.L. Oslick, K.F. McClure, J.H. Lee, D.S. Kemp, *J. Am. Chem. Soc.* **118** (1996) 3082–3090.
108. R. Walgers, T.C. Lee, A. Cammers-Goodwin, *J. Am. Chem. Soc.* **120** (1998) 5073–5079.
109. T. Sivaraman, T.K.S. Kumar, C. Yu, *Int. J. Biol. Macromol.* **19** (1996) 235–239.

Chapter 9

Effect of Synergistic Anions on the Stability and Iron Release Kinetics of Transferrins

9.1 Introduction

Transferrins (Tfs) are a family of iron-binding proteins that include serum transferrin (sTf), ovotransferrin (oTf), and lactoferrin (Lf)) [1]. Tfs also have ability to bind several nonferrous metal ions; few of them are of therapeutic and diagnostic interest [2-8]. sTf and oTf can act as an iron transporter to target cells while Lf inhibits bacterial growth. The affinity of Tfs for Fe^{3+} is extremely high (~10^{23} M^{-1}) [2, 9-10]. Tfs are folded into two globular lobes, the *N*-lobe and the *C*-lobe, interconnected with a short peptide chain [1, 11-14]. The iron binding sites are similar in both lobes and each lobe binds one Fe^{3+} ion tightly but reversibly [1, 11-12]. The iron coordination is distorted octahedral with four ligands provided by amino acid residues (two tyrosines, one aspartic acid, and one histidine) and the remaining coordinates is shared by a synergistic anion [1, 11-12]. A defining feature of Tfs is that they do not bind Fe^{3+} at the specific binding site in the absence of synergistic anion [15-18]. The naturally occurring synergistic anion is carbonate but small organic molecules with adjacent electrophilic groups (oxalate, malonate, glycolate, maleate, glycine, *etc*) can function as synergistic anion [16-18].

In the iron free state, the two lobes are in the open conformation [19-23]. Upon complex formation with iron, each lobe undergoes an open to closed conformational transition [19-23] and forms a number of interdomain hydrogen bonds [19-25]. These hydrogen bonds differ among the sTf, oTf and Lf and also between the two lobes of a given protein [25-26]. Since substitution of carbonate anion by other synergistic anions cause the in-equivalency of the metal binding sites, [27-30] so it is possible that these interdomain hydrogen bonds can also differ for different synergistic anion bound protein. The interdomain hydrogen bonds especially when situated at the lips of the iron binding cleft can control the access of water from bulk solvent to the iron binding site and constitute a trigger for the cleft opening [26, 31-33]. Breaking of these weak interdomain hydrogen bonds is necessary for iron release [32-33].

There is a considerable interest in understanding the interaction of synergistic anions with the metal and protein [16-19] because synergistic anion plays crucial role in the uptake and release of iron by Tfs [10, 32-40]. Several previous reports suggest that many non-synergistic anions (sulfate, chloride, nitrate, perchlorate etc.) also bind to the protein [41-47] and play a crucial role in chelator-mediated iron release from Tfs [41, 47, 48-62]. In addition, there are many reports which reveal that both synergistic [10, 32-40] and non-synergistic [51, 55, 63-66] anions requirement are essential for the iron uptake and release by Tfs. An important step during the iron donating interaction of sTf with cells is the proton assist freeing of synergistic anion [67]. In an *in-vitro* model of Fe^{3+} release into cells, decreasing the pH of protein solution in the presence of an iron chelator causes discharge of Fe^{3+} ion from the protein because of the proton assist freeing of synergistic anion [68]. It is apparent that if we are to understand iron release from Tfs in cells and in-vitro, we must understand the interactions of synergistic anions with the metal and protein. Although sTf, oTf, and Lf have identical ligands to the iron, the ability of iron binding differs among them and also between the two lobes of a given protein [14, 69-74]. Such differences were ascribed to the variations in the second shell network made up of amino acid residues which are hydrogen bonded to the primary ligands [74]. In a few earlier studies, the in-equivalency of the metal binding sites has been emphasized by substitution of one synergistic anion by another [27-30]. Particularly, substitution of carbonate by oxalate has been established a reliable probe to distinguish site-specific binding preferences in sTf, oTf, and Lf [27-30].

Everse et al has shown that substitution of oxalate for carbonate enhances the ability of iron binding to sTf and also inhibits the iron release from Fe_NsTf by cells thereby interfering with normal iron metabolism [17]. Two earlier reports revealed that the high plasma oxalate levels and iron deficiency anemia in children with autism spectrum disorders might be mediated *via* oxalate bound sTf [75-76]. While the effect of substitution of oxalate for carbonate on the ability of iron binding to sTf and kinetics of Fe^{3+} release from Fe_NsTf [16-17] was studied earlier, the effects of substitution of oxalate for carbonate on the structural and thermal stability of Fe_2sTf and Fe_2oTf (Tfs) as well as on the thermodynamics parameters (activation enthalpy ($\Delta H^{\ddagger}$), activation entropy ($\Delta S^{\ddagger}$), activation free energy ($\Delta G^{\ddagger}$), and change in entropy ($-T\Delta S^{\ddagger}$)) associated for Fe^{2+} release from Fe_NsTf and Fe_NoTf (Fe_NTfs) are not explored so far. To understand better the manner in which substitution of oxalate for carbonate influences the structural stability of Tfs fold and

stability of iron binding to Tfs, these properties for carbonate and oxalate bound Fe_2Tfs are studied by calorimetric (DSC) and spectroscopic (absorbance at 465 nm, fluorescence emission at 340 nm, far-UV CD at 222 nm and near-UV CD at 282 nm) methods. These techniques provided evidences that substitution of oxalate for carbonate increases the structural stability of Tfs fold and stability of iron binding to Tfs. To gain insight into the synergistic anion-binding linkage to protein and active site stability to the dynamics of iron release, the kinetics and thermodynamic parameters for Fe^{2+} (by reduction with sodium dithionite) release from the carbonate and oxalate bound Fe_NTfs (Fe_NsTf and Fe_NoTf) have been studied at pH 7.4 and 5.6. Kinetic and thermodynamic parameters measured for the Fe^{2+} release for the carbonate and oxalate bound Fe_NTfs at pH 7.4 and 5.6 reveal that the iron release from the oxalate bound Fe_NTfs occur relatively slowly with larger enthalpic barrier than the carbonate bound species.

9.2 Results and Discussion

9.2.1 Effect of pH, urea and temperature on the visible absorption and fluorescence emission spectra of carbonate and oxalate bound Fe_2Tfs

Absorption spectrum of carbonate bound Fe_2Tfs (Fe_2oTf and Fe_2sTf) at pH 7.4 shows the broad visible maximum (the tyrosine phenolate-Fe^{3+}charge transfer band) at around 465 nm (Fig. 1a, b, 1c for sTf and Fig. 2a, 2b for oTf), indicating that metal ions are fully coordinated with Tfs (sTf and oTf).

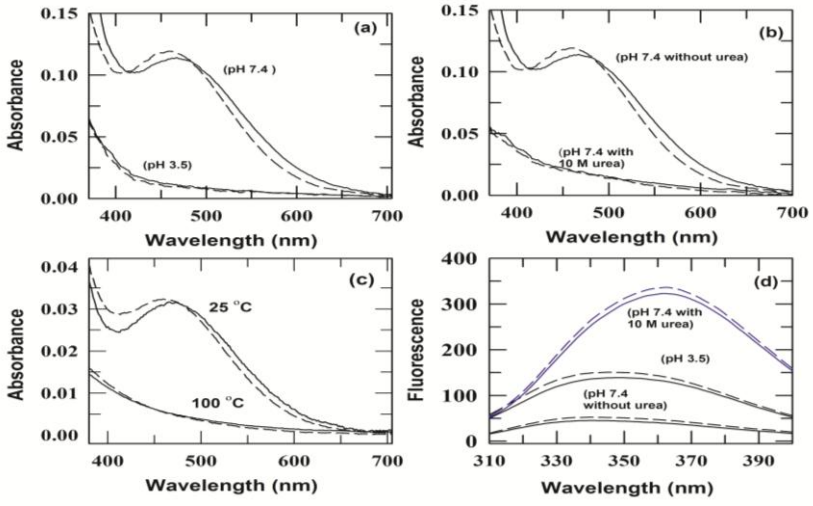

Fig.1. Effect of pH, urea and temperature on the visible absorption and fluorescence emission spectra of oxalate and carbonate bound Fe_2sTf. (a) Effect of pH on the visible absorption spectra of the oxalate (solid line) and carbonate (short dash line) bound Fe_2sTf at 25 ºC. (b) Effect of urea on the visible absorption spectra of the oxalate (solid line) and carbonate

(short dash line) bound Fe_2sTf at 25 ºC. (c) Effect of temperature on the visible absorption spectra of the oxalate (solid line) and carbonate (short dash line) bound Fe_2sTf at pH 7.4. (d) Effect of pH and urea on the fluorescence emission spectra of the oxalate (solid line) and carbonate (short dash line) bound Fe_2sTf at 25 ºC.

Substitution of oxalate for carbonate exhibits only a little effect on the visible absorption band (Fig. 1a, 1b for sTf and Fig. 2a, 2b for oTf). As pH is decreased from 7.4 to 3.5 or urea concentration is increased from 0 to 10 M (pH 7.4), or temperature is increased from 25 to 100 °C, the visible maximums for carbonate and oxalate bound Fe_2Tfs are significantly eliminated (Fig. 1a, 1b, 1c for Fe_2sTf and Fig.2a, b, for Fe_2oTf), indicating that both *N*-and *C*-sites released their bound metal ions. At pH 3.5 or 10 M urea at pH 7.4, the quenching of Trp fluorescence by bound Fe^{3+} is also diminished (Fig. 1d and 2c for Fe_2sTf and Fe_2oTf, respectively), which confirms that metal ions are fully released from *N*-and *C*-sites of proteins.

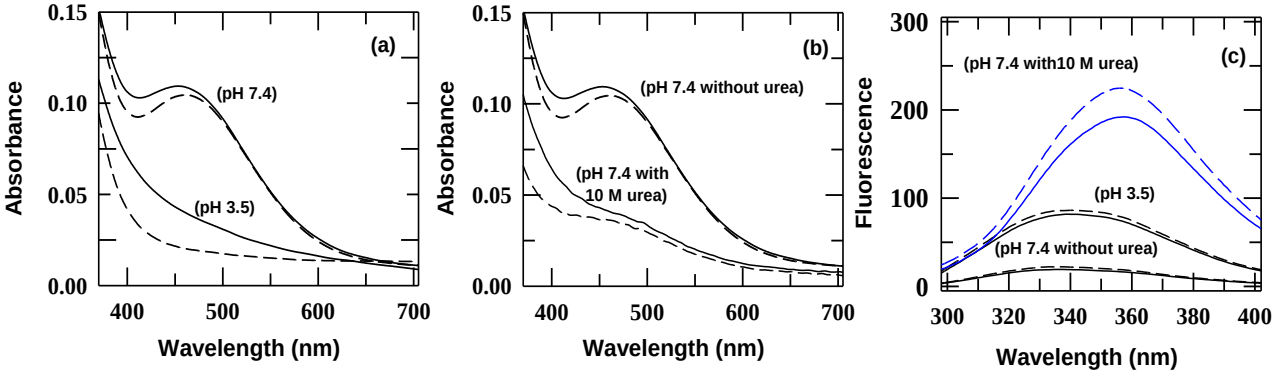

Fig.2. Effect of pH and urea on the visible absorption and fluorescence emission spectra of oxalate and carbonate bound Fe_2oTf. (a) Effect of pH on the visible absorption spectra of the oxalate (solid line) and carbonate (short dash line) bound Fe_2oTf at 25ºC. (b) Effect of urea on the visible absorption spectra of the oxalate (solid line) and carbonate (short dash line) bound Fe_2oTf at 25ºC. (c) Effect of pH and urea on the fluorescence emission spectra of the oxalate (solid line) and carbonate (short dash line) bound Fe_2oTf at 25ºC.

9.2.2 The oxalate effect on the stability of iron centers of Tfs

Equilibrium experiments that measure retention of iron as a function of pH, urea and temperature are useful methods to qualitatively determine the stability of iron centers of Fe_2Tfs [17, 66]. To determine the effect of oxalate substitution for carbonate on the stability of iron centers of Tfs, the percentage of iron remaining (based on absorbance at 465 nm) was measured as a function of pH and [urea] for carbonate and oxalate bound Fe_2Tfs. Fig. 3a and Fig.4a present the normalized pH-titrations of iron release for carbonate and oxalate bound Fe_2Tfs at 25°C. The pH-titrations were analyzed by using the following transformed Henderson-Hasselbalch equation [66]

$$Y_{\text{obs}} = \left[\frac{C_{Fe^{3+}-Tfs} + C_{apo-Tfs}\left[10^{(C_m{}^{*}-pH)}\right]}{1+10^{(C_m{}^{*}-pH)}} \right] \quad (1)$$

where $C_{Fe}{}^{3+}{}_{\text{-}Tfs}$ and $C_{apo\text{-}Tfs}$ are the normalized spectroscopic signals for iron-bound and iron free states, respectively, and $C_{\text{m}}{}^{*}$ is the pH-midpoint where Fe_2Tfs released 50% of bound irons. The resulting $C_{\text{m}}{}^{*}$ values of iron release for carbonate and oxalate bound Fe_2Tfs are provided in Table 1 (Fe_2sTf) and Table 2 (Fe_2oTf).

Fig. 3b presents the normalized thermal denaturation curves of iron release for carbonate and oxalate bound Fe_2sTf (Fig.3b) at pH 7.4. After heating the Fe_2sTf to 100 °C, the 465 nm was not restored on cooling the protein to 25 °C (data not shown). The thermally induced iron release from Fe_2sTf is irreversible [5, 66, 77] and kinetically controlled [66]. Thermal denaturation midpoint (T_{m}) of iron release for carbonate and oxalate bound Fe_2sTf was obtained by differentiation of the fraction of iron released versus temperature (Table 1). The resulting T_{m} of iron release for carbonate and oxalate bound Fe_2sTf are provided in Table 1. Fig. 3c and Fig.3d present the normalized urea denaturation profiles of iron release for carbonate and oxalate bound Fe_2sTf at pH 7.4 and pH 5.6, respectively at 25 °C. Fig. 4b and Fig.4c present the normalized urea denaturation profiles of iron release for carbonate and oxalate bound Fe_2oTf at pH 7.4 and 5.6, respectively at 25 °C. The normalized urea titrations of iron release for the carbonate and oxalate bound Fe_2Tfs were analyzed by using two-state equation (2) [78],

$$A_{obs} = \frac{(c_{pre} + m_{pre}[D]) + (c_{post} + m_{post}[D])\exp\left(\frac{-\Delta G_D{}^{o} + m_g[D]}{RT}\right)}{1+\exp\left(\frac{-\Delta G_D{}^{o} + m_g[D]}{RT}\right)} \quad (2)$$

where A_{obs} is the absorbance signals at given urea concentration, D, $\Delta G_{\text{D}}°$ is the reaction free energy in the absence of denaturant, m_{g} is the surface area exposed by the solvent [79]. The values of $\Delta G_{\text{D}}°$ and m_{g} for the iron release of carbonate and oxalate bound Fe_2sTf and Fe_2oTf are summarized in Table 1 and Table 2, respectively. The values of urea midpoint ($C_{\text{m}}=\Delta G_{\text{D}}°/m_{\text{g}}$) for iron release of carbonate and oxalate bound Fe_2sTf and Fe_2oTf are also summarized in Table 1 and Table 2, respectively. The magnitudes of thermal (T_{m}) and urea (C_{m}) denaturation midpoints for iron release of oxalate bound Fe_2sTf and Fe_2oTf are found to be higher than carbonate bound species (Table 1 and Table 2), indicating that oxalate bound Fe_2Tfs binds iron more tightly and stably than the carbonate bound species. The magnitude of pH-midpoint for iron release ($C_{\text{m}}{}^{*}$) of oxalate bound Fe_2Tfs was found to be lower than carbonate bound species (Table 1 and Table 2),

which further confirms that the stability of iron centers of oxalate bound Fe_2Tfs was higher than carbonate bound Fe_2Tfs.

Table 1. Synergistic anion dependence of pH-, urea, and temperature midpoints for iron release of sTf-Fe^{3+}complex as monitored by absorbance at 465 nm.

	Oxalate			Carbonate		
pH-induced iron release [a]						
pH-midpoint (C_m)	4.1			4.9		
Temperature-induced iron release [b]						
Temperature midpoint (T_m(K)) at pH 7.4	364.2			360.2		
Urea-induced iron release [c]						
	C_m	ΔG_D°	m_g	C_m	ΔG_D°	m_g
pH 7.4	7.4	9.5	1.3	6.8	8.4	1.2
pH 5.6	4.3	4.2	1.0	3.5	3.6	1.0

[a] The uncertainty of C_m values reported here is ±0.1.
[b] The uncertainty of T_m ±0.05K.
[c] C_m, ΔG_D°, and m_g are reported as M, kcal mol^{-1}, and kcal mol^{-1}M^{-1}. The uncertainty of C_m, ΔG_D°, and m_g values reported here is ±0.1 M, ± 0.2kcal mol^{-1}, and 0.02 kcal mol^{-1} M^{-1}.

Table 2 Synergistic anion dependence of pH and urea midpoints for iron release of Fe_2oTf as monitored by absorbance at 465 nm.

	Oxalate			Carbonate		
pH-induced iron release [a]						
pH-midpoint (C_m)	4.6			5.2		
Urea-induced iron release [b]						
	C_m	ΔG_D°	m_g	C_m	ΔG_D°	m_g
pH 7.4	7.6	9.0	1.2	7.2	7.8	1.1
pH 5.6	4.2	3.4	0.8	3.9	3.2	0.8

[a] The uncertainty of C_m values reported here is ±0.2.
[b] C_m, ΔG_D°, and m_g are reported as M, kcal mol^{-1}, and kcal mol^{-1}M^{-1}. The uncertainty of C_m, ΔG_D°, and m_g values reported here is ±0.1 M, ± 0.4kcal mol^{-1}, and 0.02 kcal mol^{-1} M^{-1}.

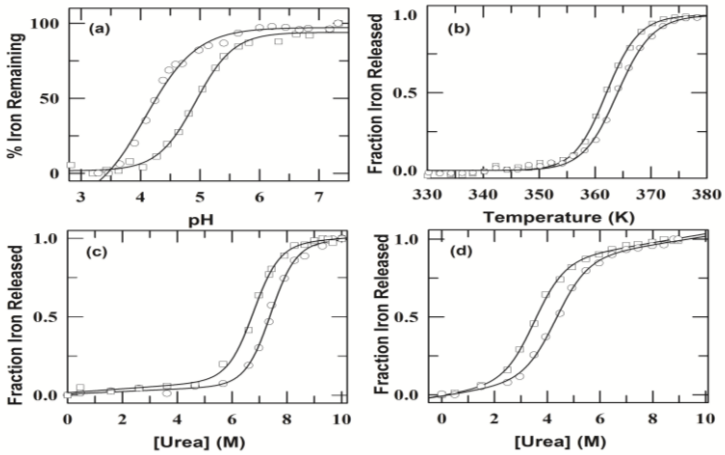

Fig.3. pH, temperature and urea dependence of iron release curves of oxalate and carbonate bound Fe_2sTf. (a) pH-induced absorbance (465 nm)-monitored iron release profiles of oxalate (o) and carbonate (□) bound Fe_2sTf at 25 ºC. (b) Temperature-induced absorbance (465 nm)-monitored iron release profiles of oxalate (o) and carbonate (□) bound Fe_2sTf at pH 7.4. The solid lines in panel (a) fits according to equitation (1) and the solid lines in panel (b) just to guide the eye. The pH-midpoints and temperature-midpoints, at which half of the iron is released from the oxalate and carbonate bound Fe_2sTf are

summarized in Table 1. Panels (c) and (d) show the urea dependence of iron release profiles of oxalate (o) and carbonate (□) bound Fe_2sTf at pH 7.4 and 5.6, respectively (25 ºC). The solid lines in panels (c) and (d), represents a non-linear least squares fit of the data to equation (2). The urea-induced iron release mid-points, C_m ($=\Delta G_D°/m_g$) for the oxalate and carbonate bound Fe_2sTf at pH 7.4 and 5.6 were calculated and summarized in Table 1

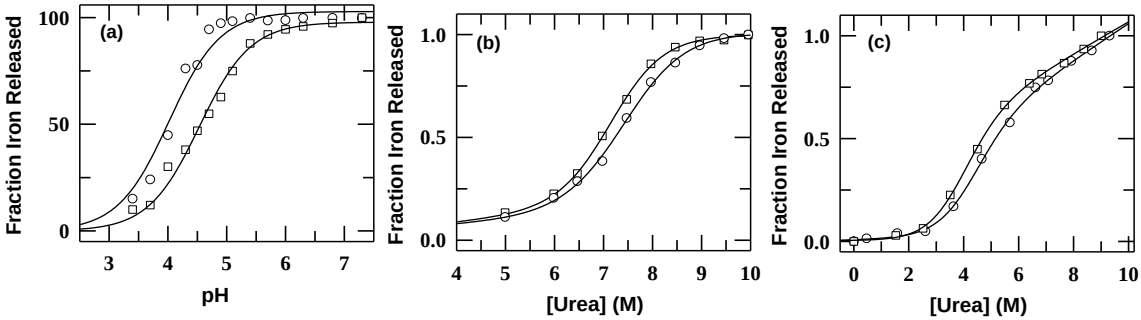

Fig.4. pH and urea dependence of iron release curves of oxalate and carbonate bound Fe_2oTf. (a) pH-induced absorbance (465 nm)-monitored iron release profiles for the oxalate (o) and carbonate (□) bound Fe_2oTf at 25 ºC. The solid line in panel (a) fits according to equitation (1). The pH-midpoint, at which half of the iron is released from the oxalate and carbonate bound Fe_2oTf is summarized in Table 2. Panels (b) and (c) show the urea dependence of iron release profiles of oxalate (o) and carbonate (□) bound Fe_2oTf at pH 7.4 and 5.6, respectively (25 ºC). The solid lines in panels (b) and (c), represents a non-linear least squares fit of the data to equation (2). The urea-induced iron release mid-points, C_m ($=\Delta G_D°/m_g$) for the oxalate and carbonate bound Fe_2oTf at pH 7.4 and 5.6 were calculated and summarized in Table 2.

The oxalate bound Fe_2Tfs binds iron more tightly and stably than the carbonate bound species because (i) oxalate binds iron in a symmetric bidentate fashion [17], (ii) the pK_a value of oxalate is lower than carbonate (pK_a values of oxalate and carbonate are 4.2 and 6.4, respectively) [17,80].

9.2.3 Oxalate effect on the structural stability of Fe_2Tfs

The far-UV CD spectrum of carbonate bound Fe_2Tfs at pH 7.4 exhibits the negative extrema at ~208 nm and a shoulder ~215-225 nm (Fig.5a (Fe_2sTf) and Fig.6a (Fe_2oTf)), which reflects the secondary structure of carbonate bound proteins. Substitution of oxalate for carbonate produces only a very little effect on the peptide bands (Fig. 5a and Fig. 6a). The near-UV CD spectra (250–300 nm) for carbonate and oxalate bound Fe_2Tfs at pH 7.4, 25 °C (Fig. 5b (Fe_2sTf) and Fig. 6b (Fe_2oTf)) show the three aromatic residue bands at 255–270 nm (phenylalanine), 282 nm (tyrosine) and 291 nm (tryptophan), which reflect the tertiary structure of Fe_2Tfs. As [urea] is increased from 0 to 10 M, the peptide and aromatic bands of synergistic anions bound Fe_2Tfs are substantially disrupted (Figs.5a, 5b and Figs.6a, 6b), indicating that the secondary and tertiary structures of proteins are significantly destabilized.

The near-UV CD spectroscopy can also be used to probe the structural changes induced by metal binding to Tfs [86]. The effect of synergistic anions on metal binding ability of Tfs can influence the structural stability of protein. To test this hypothesis, the far-UV (222 nm) and near-UV (282) CD-monitored urea-induced unfolding transitions of carbonate and oxalate bound Fe_2sTf (Figs. 5c-d) and Fe_2oTf (Figs. 6c-d) were collected at pH 7.4, 25 °C. The normalized urea-induced unfolding transitions of carbonate and oxalate bound Fe_2sTf and Fe_2oTf were analyzed by the two-state unfolding procedure (Equation (2)) [78]. The resulting unfolding free energy, $\Delta G_D°$, and surface area exposed by solvent, m_g, for carbonate and oxalate bound Fe_2sTf and Fe_2oTf are summarized in Table 3. The urea mid-point for unfolding of the synergistic anion bound Fe_2sTf and Fe_2oTf was also calculated ($C_m = \Delta G_D°/m_g$) and provided in Table 3. The value of C_m for oxalate bound Fe_2sTf and Fe_2oTf were found to be higher than the carbonate bound species (Figs. 5c, d (Fe_2sTf), Figs. 6c, d (Fe_2oTf) and Table 3), indicating that the oxalate bound Fe_2sTf and Fe_2oTf have relatively more structural stability than the carbonate bound species. Notably, the values of urea-denaturation midpoints for iron release of oxalate bound Fe_2sTf and Fe_2oTf were found relatively more than the carbonate bound species (Table 1 and Table 2), indicating that the effect of synergistic anions on metal binding ability of Tfs also influences the structural stability of the protein.

Inset of Fig. 5e shows the spectra for the oxalate and carbonate bound Fe_2sTf at 25 °C and 100 °C, pH 7.4. Clearly, the secondary structures of oxalate and carbonate bound Fe_2sTf are significantly disrupted at 100°C, pH 7.4 (Inset of Fig. 5e). To test the effect of oxalate substitution for carbonate on thermal stability of Fe_2Tfs, the far-UV (222 nm) CD-monitored thermal unfolding transitions of carbonate and oxalate bound Fe_2sTf (5 μM) were collected in 0.2 M HEPES buffer at pH 7.4 (Fig. 5e). The thermally induced unfolding of Fe_2sTf is irreversible and kinetically controlled [66]. Thermal denaturation midpoint (T_m) for unfolding of carbonate and oxalate bound Fe_2sTf was obtained by differentiation of the fraction unfolded versus temperature. Clearly, the value of T_m for unfolding of oxalate bound Fe_2sTf is found to be higher than carbonate bound species (Table 4), indicating that oxalate bound Fe_2Tfs is thermally more stable than the carbonate bound species.

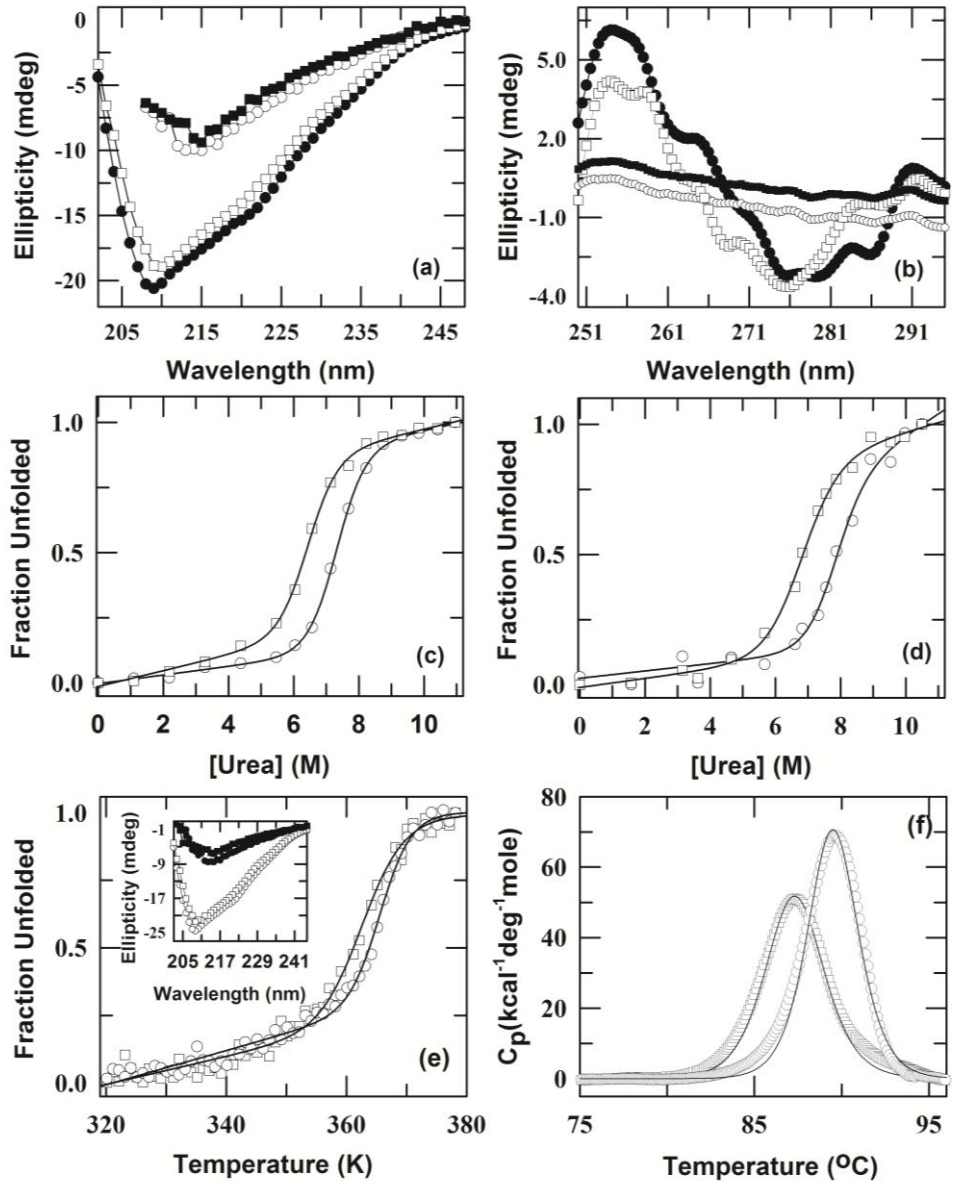

Fig.5. Urea and temperature-induced unfolding of oxalate and carbonate bound Fe_2sTf. Panels (a) and (b) represent the far-UV and near-UV CD spectra at pH 7.4 (25 °C), respectively for the oxalate (in the absence (●●●●) and presence of 10.0 M urea (○○○○)) and carbonate (in the absence (□□□□) and presence of 10.0 M urea (■■■■)) bound Fe_2sTf. Panels (c) and (d) present the far-UV (222 nm) and near-UV (282 nm) CD-monitored normalized urea-induced unfolding curves, respectively (pH 7.4, 25ºC) for oxalate (o) and carbonate (□) bound Fe_2sTf. The solid lines in panels (c) and (d) represent a non-linear least squares fit of the data to equation (2). The urea-induced unfolding midpoints, C_m ($=\Delta G_D°/m_g$) for the oxalate and carbonate bound Fe_2sTf were calculated and summarized in Table 3. Panel (e) presents the thermal unfolding normalized curves of oxalate (o) and carbonate (□) bound Fe_2sTf as evaluated from the change in ellipticity at 222 nm. The inset in panel (e) shows the far-UV CD spectra of oxalate (at 25 °C (○○○○) and 100 °C (●●●●)) and carbonate (at 25 °C (□□□□) and 100 °C (■■■■)) bound Fe_2sTf at pH 7.4. The solid lines are just to guide the eye. The thermal unfolding midpoints (T_m) for oxalate and carbonate bound Fe_2sTf are listed in Table 4. Panel (f) represents the DSC thermogram of oxalate (o) and carbonate (□) bound Fe_2sTf at pH 7.4. The solid lines resulted from fitting the data to the two-state model and the resulting thermodynamic parameters are summarized in Table 5.

Table 3. Synergistic anions dependence of C_m, ΔG_D°, and m_g for urea-induced unfolding of Fe_2Tfs (CD at 222 nm and 282 nm) at pH 7.4.*

	CD 222 nm			CD 282 nm		
Bovine Serum Transferrin (Fe_2sTf)						
Synergistic anions	C_m (M)	ΔG_D° (kcal mol^{-1})	m_g (kcal mol^{-1}M^{-1})	C_m (M)	ΔG_D° (kcal mol^{-1})	m_g (kcal mol^{-1}M^{-1})
Oxalate	7.4	9.4	1.27	8.0	8.0	1.0
Carbonate	6.4	8.3	1.29	6.9	6.4	0.9
Ovotransferrin (oTf)						
Oxalate	6.8	6.2	0.9	6.7	6.6	1.0
Carbonate	6.5	5.4	0.8	6.3	5.2	0.8

* The uncertainty of C_m, ΔG_D°, and m_g values reported here are ±0.05 M, ± 0.2kcal mol^{-1}, and 0.02kcal mol^{-1} M^{-1}.

Table 4. Synergistic anions dependence of T_m for thermally-unfolding of Fe_2sTf (222 nm) at pH 7.4.*

Synergistic anions	Oxalate	Carbonate
Method calculating T_m	T_m (K)	T_m (K)
By differentiation of the fraction of iron released versus temperature	365.8	363.0

* The uncertainty of T_m reported here is ± 0.5K.

To further test the effect of oxalate substitution for carbonate on thermal stability of Fe_2Tfs, the differential scanning calorimetric (DSC) thermogram for oxalate and carbonate bound Fe_2sTf were measured in 0.5 M HEPES buffer at pH 7.4. The DSC thermograms for oxalate and carbonate bound Fe2sTf were analyzed by two-state model, provided by microcal origin software [77]. Thermodynamic parameters obtained from DSC thermograms of oxalate and carbonate bound Fe_2sTf are summarized in Table 5.

Table 5. Thermodynamic parameters obtained from D.S.C. thermogram of oxalate and carbonate bound Fe_2sTf at pH 7.4.

	pH 7.4	
Synergistic anions	T_m (ºC)	ΔH (kcal mol^{-1})
Oxalate	89.5 ±0.06	271.8 ±4.6
Carbonate	87.3 ±0.02	231.2 ±1.1

Clearly the thermal unfolding midpoint (T_m) and calorimetric enthalpy (ΔH) are relatively higher for oxalate bound Fe_2sTf than carbonate bound species, which further confirms that the oxalate bound Fe_2sTf is thermally more stable than the carbonate bound species.

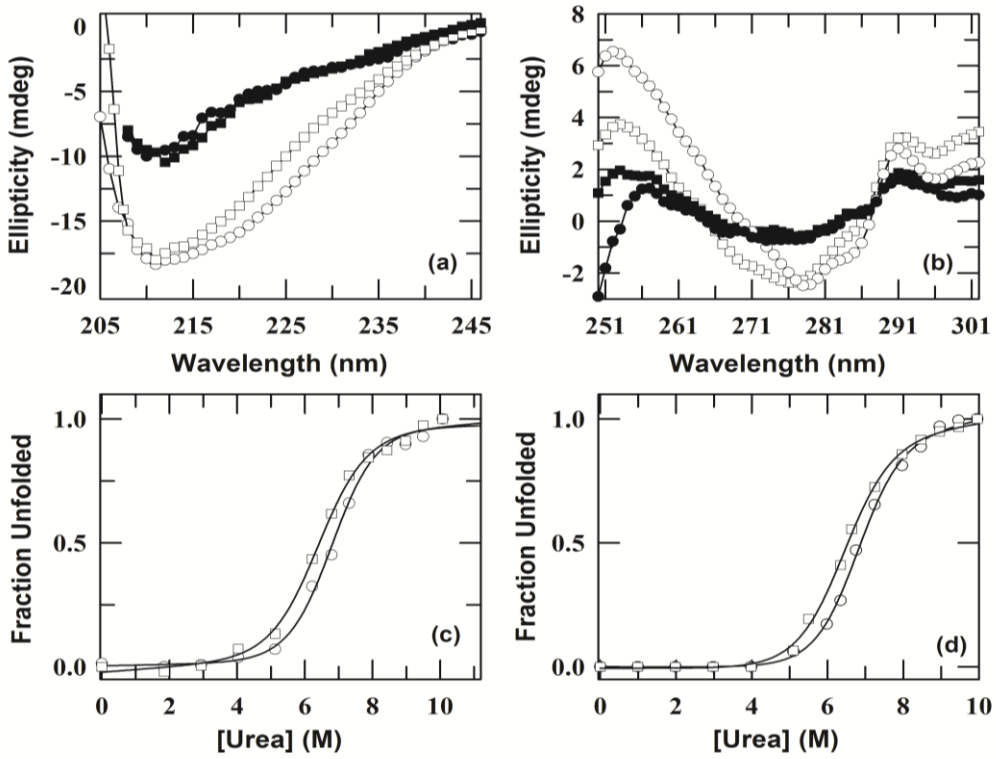

Fig.6. Urea-induced unfolding of oxalate and carbonate bound Fe_2oTf at pH 7.4. Panels (a) and (b) represent the far-UV and near-UV CD spectra at pH 7.4 (25 °C), respectively for the oxalate (in the absence (oooo) and presence of 10.0 M urea (●●●●)), and carbonate (in the absence (□□□□) and presence of 10.0 M urea (■■■■)) bound Fe_2oTf. Panels (c) and (d) show the far-UV (222 nm) and near-UV (282 nm) CD monitored normalized urea-induced unfolding curves, respectively for the oxalate (o) and carbonate (□) bound Fe_2oTf, at pH 7.4, 25ºC. The solid lines in panels (c) and (d) represent a non-linear least squares fit of the data to equation (2). The urea-induced unfolding midpoints, C_m ($=\Delta G_D°/m_g$) for the oxalate and carbonate bound Fe_2oTf were calculated and summarized in Table 3.

9.2.4 Oxalate effect on the dynamics of iron release from Fe_NTfs

To determine the effect of substitution of oxalate for carbonate on the active site stability to the dynamics of iron release from Fe_NTfs, the kinetics and thermodynamic parameters for Fe^{3+} (by urea-denaturation) and Fe^{2+} (by reduction with sodium dithionite in the presence of bathophenanthroline sulfonate (BPS)) release from the carbonate and oxalate bound Fe_NsTf and Fe_NoTf have been measured at pH 7.4 and 5.6. The urea denaturation-induced Fe^{3+} release kinetic traces for the carbonate and oxalate bound Fe_NsTf at pH 7.4 and 5.6 are shown in Figs. 7a and 7b, respectively. Figs. 7c and 7d present the reductive Fe^{2+} release kinetic traces for the carbonate and oxalate bound Fe_NsTf at pH 7.4 and 5.6, respectively at 25°C. The urea denaturation-induced Fe^{3+} release kinetic profiles for the carbonate and oxalate bound Fe_NoTf at pH 7.4 and 5.6 are shown in Figs. 8a and 8b, respectively. Figs. 8c and 8d present the reductive Fe^{2+} release kinetic profiles

for the carbonate and oxalate bound Fe_NsTf at pH 7.4 and 5.6, respectively at 25°C. Both at pH 7.4 and 5.6, the kinetics data for Fe^{3+} and Fe^{2+} release from the carbonate and oxalate bound Fe_NsTf and Fe_NoTf were analyzed by nonlinear least-squares fit to a single-exponential rate expression (Figs. 7a-d and Figs. 8a-d). Table 6 summarizes the observed rate constant (k_{obs}) for Fe^{3+} and Fe^{2+} release from the carbonate and oxalate bound Fe_NsTf and Fe_NoTf at 25 °C. Interestingly, at both pH 7.4 and 5.6, the magnitudes of k_{obs} for Fe^{3+} and Fe^{2+} release from the oxalate bound Fe_NsTf and Fe_NoTf were found to be relatively lower than the carbonate bound species (Figs. 7a-d and Figs. 8a-d; and Table 6), indicating that the substitution of oxalate for carbonate retards the iron release from Fe_NTfs at both physiological and mildly acidic pH conditions.

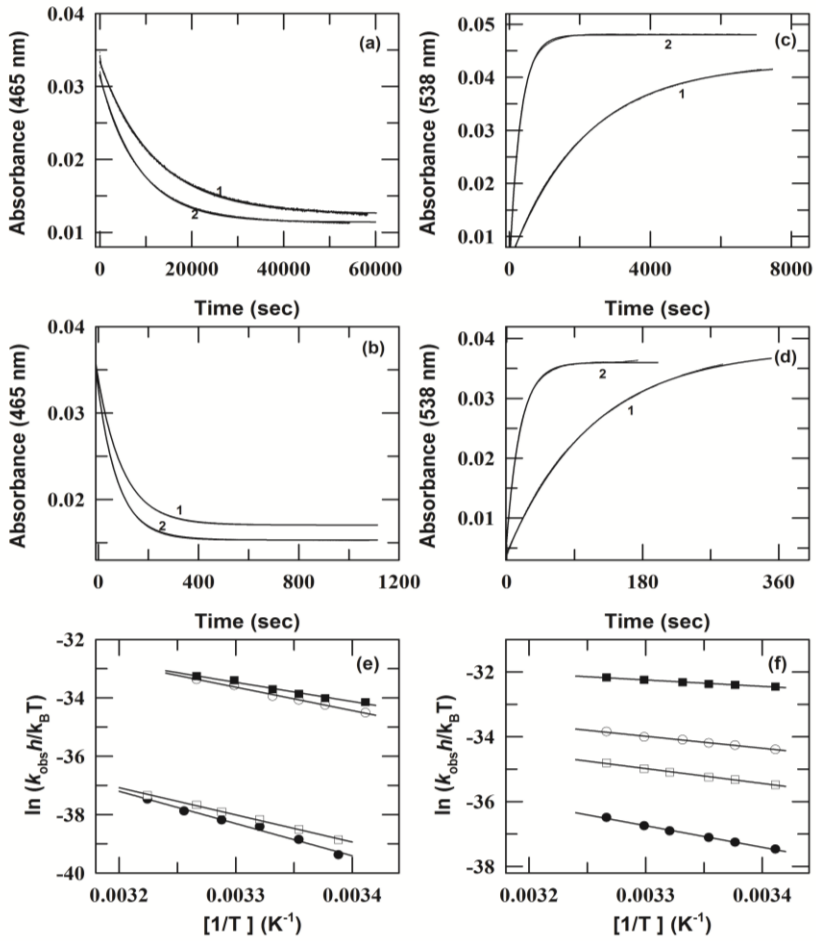

Fig.7. Kinetics of Fe^{3+} and Fe^{2+} release from carbonate and oxalate bound Fe_NsTf at pH 7.4 and 5.6, 25 ºC. Panels (a) and (b) present the single phase urea denaturation-induced Fe^{3+} release kinetic traces of oxalate (trace 1) and carbonate (trace 2) bound Fe_NsTf at pH 7.4 and 5.6, respectively. Panels (c) and (d) present the single phase sodium dithionite (using BPS) induced Fe^{2+} release kinetic traces of oxalate (trace 1) and carbonate (trace 2) bound Fe_NsTf at pH 7.4 and 5.6, respectively. The solid lines in panels (a), (b), (c) and (d) show least-squares fit of the data to a single

exponential function. The resulting rate constants for iron release, k_{obs}, for the oxalate and carbonate bound Fe_NsTf at pH 7.4 and 5.6 are summarized in Table 6. Panel (e) show the Eyring plots for urea- induced iron release from the oxalate (pH 7.4 (o), and pH 5.6 (●)) and carbonate (pH 7.4(□) and pH 5.6 (■)) bound Fe_NsTf. Panel (f) show the Eyring plots for reductive iron release from the oxalate (pH 7.4 (o), and pH 5.6 (●)) and carbonate (pH 7.4(□) and pH 5.6 (■)) bound Fe_NsTf. The solid lines in panels (e) and (f) show linear fit of the data to Eyring equation (Equation (1), chapter 2) [87-88]. The activation parameters are summarizes in Table 7.

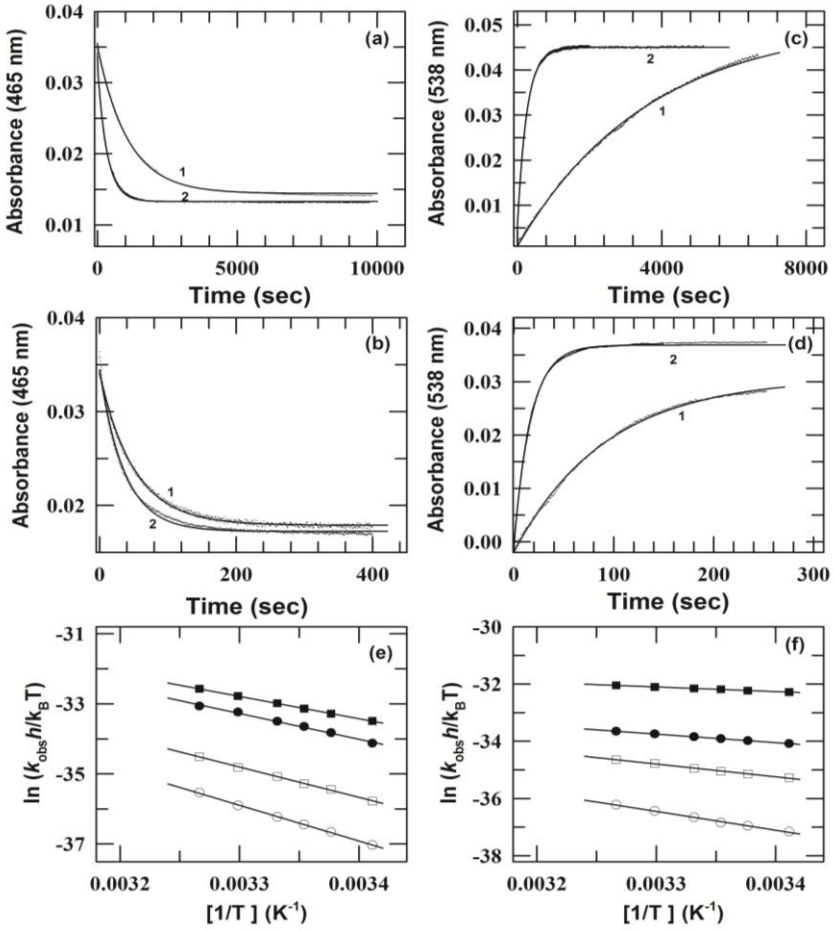

Fig.8. Kinetics of Fe^{3+} and Fe^{2+} release from carbonate and oxalate bound Fe_NoTf at pH 7.4 and 5.6, 25 ºC. Panels (a) and (b) present the single phase urea denaturation-induced Fe^{3+} release kinetic traces of oxalate (trace 1) and carbonate (trace 2) bound Fe_NoTf at pH 7.4 and 5.6, respectively. Panels (c) and (d) present the single phase sodium dithionite (using BPS) induced Fe^{2+} release kinetic traces of oxalate (trace 1) and carbonate (trace 2) bound Fe_NoTf at pH 7.4 and 5.6, respectively. The solid lines in panels (a), (b), (c) and (d) show least-squares fit of the data to a single exponential function. The resulting rate constants for iron release, k_{obs}, for the oxalate and carbonate bound Fe_NsTf at pH 7.4 and 5.6 are summarized in Table 6. Panel (e) presents the Eyring plots for urea-induced iron release for the oxalate (pH 7.4 (o), and pH 5.6 (●)) and carbonate (pH 7.4(□) and pH 5.6 (■)) bound Fe_NoTf. Panel (f) presents the Eyring plots for reductive iron release for the oxalate (pH 7.4 (o), and pH 5.6 (●)) and carbonate (pH 7.4(□) and pH 5.6 (■)) bound Fe_NoTf. The solid lines in panels (e) and (f) show linear fit of the data to Eyring equation (Equation (1), chapter 2) [87-88]. The activation parameters are summarizes in Table 8.

Table 6. Synergistic anions dependence of the k_{obs} (rate constant) for urea-denaturation induced and Sodium dithionite induced Fe^{3+} and Fe^{2+} release kinetics of Fe_NTfs at pH 7.4 and pH 5.6.*

	pH ~7.4		pH ~5.6	
Fe_NsTf	$k_{obs}(sec^{-1})$		$k_{obs}(sec^{-1})$	
Synergistic anions	Urea-denaturation induced Fe^{3+} release	Sodium dithionite induced Fe^{2+} release	U Urea-denaturation induced Fe^{3+} release	Sodium dithionite induced Fe^{2+} release
Oxalate	8.4×10^{-5}	4.7×10^{-4}	9.9×10^{-3}	8.7×10^{-3}
Carbonate	1.2×10^{-4}	3.2×10^{-3}	0.012	0.054
Fe_NoTf	$k_{obs}(sec^{-1})$		$k_{obs}(sec^{-1})$	
Oxalate	4.7×10^{-4}	2.5×10^{-4}	0.020	0.011
Carbonate	3.2×10^{-3}	3.8×10^{-3}	0.027	0.059

*The standard error of k_{obs} is ±5% observed by independent set of experiment.

The substitution of oxalate for carbonate retards the iron release from Fe_NTfs at pH 7.4 and 5.6 because (i) oxalate has lower pKa than carbonate, (ii) due to bulkiness and planner geometry, the oxalate has a special ability to bind to the iron in a symmetric bidentate fashion [17], (iii) the important role of Arg124 in serving as an anchor for the carbonate ion is greatly diminished by the substitution of oxalate [17]. If the dynamics of Fe^{3+} and Fe^{2+} release for the oxalate bound Fe_NsTf and Fe_NoTf are relatively more restricted than the carbonate bound species, the enthalpic energy barriers for Fe^{3+} and Fe^{2+} release reactions of oxalate bound Fe_NsTf and Fe_NoTf should be larger than the carbonate bound species. To test this hypothesis, the activation thermodynamic parameters for Fe^{3+} and Fe^{2+} release reactions of carbonate and oxalate bound Fe_NsTf and Fe_NoTf were determined at pH 7.4 and 5.6. Figs. 7e and 7f present the Eyring plots for Fe^{3+} and Fe^{2+} release reactions, respectively, for carbonate and oxalate bound Fe_NsTf at pH 7.4 and 5.6. Fig. 8e and Fig. 8f present the Eyring plots for Fe^{3+} and Fe^{2+} release reactions, respectively, for carbonate and oxalate bound Fe_NoTf at pH 7.4 and 5.6. Eyring plots for Fe^{3+} and Fe^{2+} release reactions of carbonate and oxalate bound Fe_NsTf and Fe_NoTf at pH 7.4 and 5.6 were analyzed by linear least-squares analysis [87-88]. Table 7 and Table 8 summarizes the values of activation enthalpy ($\Delta H^{\ddagger}$) and activation entropy ($\Delta S^{\ddagger}$) for Fe^{3+} and Fe^{2+} release reactions of carbonate and oxalate bound Fe_NsTf and Fe_NoTf, respectively. By using the $\Delta H^{\ddagger}$ and $\Delta S^{\ddagger}$, the corresponding activation free energy ($\Delta G^{\ddagger} = \Delta H^{\ddagger} - T\Delta S^{\ddagger}$) and entropy change ($-T\Delta S^{\ddagger}$), for Fe^{3+} and Fe^{2+} release reactions were calculated at 25 °C (Table 7 (Fe_NsTf) and Table 8 (Fe_NoTf)).

Table 7. Synergistic anions dependence of the activation thermodynamic parameters of urea-denaturation induced Fe^{3+} release and sodium dithionite-induced Fe^{2+} release reactions of Fe_NsTf.*

	pH ~7.4				pH ~5.6			
Urea-denaturation induced Fe^{3+} release								
Synergistic anions	$\Delta G^{a\ddagger}$	$\Delta H^{\ddagger}$	$\Delta S^{\ddagger}$	$-T\Delta S^{a\ddagger}$	$\Delta G^{a\ddagger}$	$\Delta H^{\ddagger}$	$\Delta S^{\ddagger}$	$-T\Delta S^{a\ddagger}$
Oxalate	23.2	22.1	−0.004	1.1	20.3	16.0	−0.014	4.3
Carbonate	22.9	18.6	−0.015	4.3	20.1	13.2	−0.023	6.9
Sodium dithionite-induced Fe^{2+} release								
Oxalate	22.1	13.3	−0.03	8.8	20.4	7.4	−0.04	13.0
Carbonate	21.0	9.2	−0.04	11.8	19.3	3.9	−0.05	15.3

*The uncertainty of $\Delta G^{\ddagger}$, $\Delta H^{\ddagger}$, $\Delta S^{\ddagger}$, and $-T\Delta S^{\ddagger}$ values reported here are 0.002 kcal mol^{-1}, ±0.4 kcal mol^{-1}, ±0.001 kcal $mol^{-1}K^{-1}$, and ±0.4 kcal mol^{-1} respectively.

[a] Activation free energy ($\Delta G^{\ddagger}$) and entropy changes ($-T\Delta S^{\ddagger}$) are given at 25ºC.

Table 8. Synergistic anions dependence of the activation parameters of urea-denaturation induced Fe^{3+} release and sodium dithionite-induced Fe^{2+} release Fe_NoTf.*

	pH ~7.4				pH ~5.6			
Urea-denaturation induced Fe^{3+} release								
Synergistic anions	$\Delta G^{a\ddagger}$	$\Delta H^{\ddagger}$	$\Delta S^{\ddagger}$	$-T\Delta S^{a\ddagger}$	$\Delta G^{a\ddagger}$	$\Delta H^{\ddagger}$	$\Delta S^{\ddagger}$	$-T\Delta S^{a\ddagger}$
Oxalate	21.9	20.4	−0.005	1.5	20.1	14.7	−0.018	5.4
Carbonate	21.1	17.3	−0.013	3.8	19.7	12.7	−0.024	7.0
Sodium dithionite-induced Fe^{2+} release								
Oxalate	22.0	13.1	−0.030	8.9	20.3	6.0	−0.048	14.3
Carbonate	20.8	8.9	−0.040	11.9	19.4	3.2	−0.054	16.1

*The uncertainty of $\Delta G^{\ddagger}$, $\Delta H^{\ddagger}$, $\Delta S^{\ddagger}$, and $-T\Delta S^{\ddagger}$ values reported here are 0.002 kcal mol^{-1}, ±0.4 kcal mol^{-1}, ±0.001 kcal $mol^{-1}K^{-1}$, and ±0.4 kcal mol^{-1} respectively.

[a] Activation free energy ($\Delta G^{\ddagger}$) and entropy changes ($-T\Delta S^{\ddagger}$) are given at 25ºC.

The data in Table 7 and Table 8 reveals that the substitution of oxalate for carbonate (i) increase the enthalpic barriers ($\Delta H^{\ddagger}$) for Fe^{3+} and Fe^{2+} release reactions, (ii) the increase in $\Delta H^{\ddagger}$ is accompanied by a decrease in the entropy change, $-T\Delta S^{\ddagger}$, and (iii) the enthalpic effect is more dominated then the entropic.

9.3. Conclusion

Carbonate is the main synergistic anion *in-vivo* but in the absence of it, oxalate can function as synergistic anion. This chapter analyzed the effect of oxalate on the stability and iron release dynamics of Fe^{3+}-Tfs complex. Analysis of the pH and denaturations profiles of iron release (based on absorbance (465 nm)) for carbonate and oxalate bound Fe_2sTf and Fe_2oTf reveals that the oxalate bound Fe_2Tfs binds iron more tightly and stably than the carbonate bound species. Analysis of thermal denaturation curves (based on absorbance at 465 nm) for carbonate and oxalate bound Fe_2sTf further confirmed this result. Thermodynamic analysis of the far-UV (222 nm) and near-UV (282nm) CD-monitored urea unfolding curves for carbonate and oxalate bound Fe_2sTf and Fe_2oTf reveals that the oxalate bound Fe_2Tfs has relatively higher structural

stability than the carbonate bound species. Analysis of thermal unfolding curves (CD 222 nm) and DSC scans for carbonate and oxalate bound Fe_2sTf further confirms this result. Kinetic and thermodynamic parameters measured for Fe^{2+} and Fe^{3+} release from carbonate and oxalate bound Fe_NsTf and Fe_NoTf revealed that the substitution of oxalate for carbonate (i) retards the iron release (ii) increase the enthalpic barrier ($\Delta H^{\ddagger}$) for iron release, (iii) the increase in $\Delta H^{\ddagger}$ is accompanied by a decrease in the entropy change, $-T\Delta S^{\ddagger}$, and (iv) the enthalpic effect is more dominated then the entropic.

9.4. References:

1. P. Aisen, I. Listowsky, *Annu. Rev. Biochem.* **49** (1980) 357–393.
2. H. Sun, H. Li, P. J. Sadler, *Chem. Rev.* **99** (1999**)** 2817–2842.
3. M. Guo, H. Sun, H. J. McArdle, L. Gambling, P. J. Sadler, *Biochemistry* **39** (2000) 10023–10033.
4. A. D. Tinoco, A. M. Valentine, *J. Am. Chem. Soc.* **127** (2005) 11218–11219.
5. A. D. Tinoco, C. D. Incarvito, A. M. Valentine, *J. Am. Chem. Soc.* **129** (2007) 3444–3454.
6. M. Hémadi , N.T. Ha-Duong, S. Plantevin, C. Vidaud, J. M. El Hage Chahine, *J. Biol. Inorg. Chem.* **15** (2010) 497–504.
7. Z. Chikh, N.T. Ha-Duong, G. Miquel, J. M. El Hage Chahine, *J. Biol. Inorg. Chem.* **12** (2007) 90–100.
8. W. Zhong, J. A. Parkinson, M. Guo, P. J. Sadler, *J. Biol. Inorg. Chem.* **7** (2002) 589–599.
9. R. Aasa, B. G. Malmstrom, P. Saltman, T. Vanngård, *Biochim. Biophys. Acta* **75** (1963) 203–222.
10. R.T.A. MacGillivray, A. B. Mason, A. B. Transferrins. In Molecular and Cellular Iron Transport. (Templeton, D.M. ed.) Marcel Dekker Inc., New York (2002) pp. 41–69.
11. E. N. Baker, *Adv. Inorg. Chem.* **41** (1994) 389–463.
12. B. F. Anderson, H. M. Baker, G. E. Norris, D. W. Rice, E. N. Baker, *J. Mol. Biol.* **209** (1989) 711–734.
13. E. N. Baker, P. F. Lindley, *J. Inorg. Biochem.* **47** (1992) 147–16.
14. M. Haridas, B. F. Anderson, E. N. Baker, *Acta Crystallogr D Biol Crystallogr* **51** (1995) 629–646.

15. O. Zak, B.Tam, R.T. A. MacGillivray, P. Aisen, *Biochemistry* **36** (1997) 11036–11043.
16. M. R. Schlabach, G. W. Bates, *J. Biol. Chem.* **250** (1975) 2182–2188.
17. P. J. Halbrooks, A. B. Mason, T. A. Adams, S. K. Briggs, S. J. Everse, *J. Mol. Biol.* **339** (2004) 217–226.
18. W. R. Harris, *Biochemistry* **24** (1985) 7412–7418.
19. B. F. Anderson, H. M. Baker, G. E. Norris, S. V. Rumball, E. N. Baker, *Nature* **344** (1990) 784–787.
20. H. Kurokawa, B. Mikami, M. Hirose, *J. Mol. Biol.* **254** (1995) 196–207.
21. H. Kurokawa, J. C. Dewan, B. Mikami, J. C. Sacchettini, M. Hirose, *J. Biol. Chem.* **274** (1999) 28445–28452.
22. A. K. Sharma, K. R. Rajashankar, M. P.Yadav, T. P. Singh, *Acta Crystallogr. D. Biol. Crystallogr*. **55** (1999)1152–1157.
23. P. D. Jeffrey, M. C. Bewley, R. T. A. MacGillivray, A. B. Mason, R. C. Woodworth, E. N. Baker, *Biochemistry* **37** (1998) 13978–13986.
24. T. E. Adams, A. B. Mason, Q.Y. He, P. J. Halbrooks, S. K. Briggs, V. C. Smith, R. T. A. MacGillivray, S. J. Everse, *J. Biol. Chem.* **278** (2003) 6027–33.
25. A. S. Moore, B. F. Anderson, C. R. Groom, M. Haridas, E. N. Baker, *J. Mol. Biol.* **274** (1997) 222–236.
26. J. C. Dewan, B. Mikami, M. Hirose, J. C. Sacchettini, *Biochemistry* **32** (1993) 11963–11968.
27. J. L. Zweier, *J. Biol. Chem.* **253** (1978) 7616–7621.
28. M. Sola, *Eur. J. Biochem.* **194** (1990) 349–353.
29. M. S. Shongwe, C. A. Smith, E. W. Ainscough, H. M. Baker, A. M. Brodie, E. N. Baker, *Biochemistry* **31** (1992) 4451–4458.
30. A. Seidel, E. Bill, L. Häggström, P. Nordblad, F. Kilár, *Arch. Biochem. Biophys.* **308** (1994) 52–63.
31. R. Pakdaman, F. B. Abdallah, J. M. El Hage Chahine, *J. Mol. Biol.* **293** (1999) 1273–1284.
32. F. Bou-Abdallah, J.M. El Hage Chahine, *Eur. J. Biochem.* **258** (1998) 1022−1031.
33. F. Bou-Abdallah, J.M. El Hage Chahine, *Eur. J. Biochem.* **263** (1999) 912−920.
34. A. Dautry-Varsat, A. Ciechanover, H. F. Lodish, *Proc. Natl. Acad. Sci. USA.* **80** (1983) 2258–2262.

35. M. Hemadi, N. T. Ha-Duong, J. M. El Hage Chahine, *J. Mol. Biol.* **358** (2006) 1125–1136.
36. R. F. Campbell, N. D. Chasteen, *J. Biol. Chem.* **252** (1977) 5996–6001.
37. J. L. Zweier, J. B. Wooten, J. S. Cohen, *Biochemistry* **20** (1981) 3505–3510.
38. P. Aisen, A. Leibman, R. A. Pinkowitz, S. Pollack, *Biochemistry* **12** (1973) 3679–3684.
39. P. Aisen, E. B. Brown, *Prog. Hematol.* **9** (1975) 25–56.
40. K. Thorstensen, I. Romslo, *Biochem. J.* **271** (1990) 1–9.
41. Q.Y. He, A. B. Mason, B. M. Tam, R. T. A. MacGillivray, R. C. Woodworth, *Biochemistry* **38** (1999) 9704–9711.
42. D.A. Folajtar, N. D. Chasteen, *J. Am. Chem. Soc.* **104** (1982) 5775–5780.
43. J. D. Bell, J. Brown, D. G. Kubal, P. J. Sadler, *Biochem. Soc. Trans.* **16** (1988) 714–715.
44. J. K. Grady, A. B. Mason, R. C. Woodworth, N. D. Chasteen, *Biochem. J.* **309** (1995) 403–410.
45. W. R. Harris, A. M. Cafferty, S. Abdollahi, K. Trankler, *Biochim. Biophys. Acta* **1383** (1998) 197–221.
46. A. Wishnia, I. Weber, R. C. Warner, *J. Am. Chem. Soc.* **83** (1961) 2071–2080.
47. Q. Y. He, A. B. Mason, V. Nguyen, R. T. A. MacGillivray, R. C. Woodworth, *Biochem. J.* **350** (2000) 909–915.
48. S. L. Byrne, A. N. Steere, N. D. Chasteen, A. B. Mason, *Biochemistry* **49** (2010) 4200–4207.
49. T. J. Egan, D. C. Ross, L. R. Purves, P. A. Adams, *Inorg. Chem.* **31** (1992) 1994–1998.
50. H. M. Marques, D. L. Watson, T. J. Egan, *Inorg. Chem.* **30** (1991) 3758–3762.
51. S. A. Kretchmar, K. N. Raymond, *Inorg. Chem.* **27** (1988) 1436–1441.
52. J. Williams, N. D. Chasteen, K. Moreton, *Biochem. J.* **201** (1982) 527–532.
53. W. R. Harris, P. K. Bali, *Inorg. Chem.* **27** (1988) 2687–2691.
54. D. A. Baldwin, T. J. Egan, H. M. Marques, *Biochim. Biophys. Acta* **1038** (1990) 1–9.
55. T. J. Egan, O. Zak, P. Aisen, *Biochemistry* **32** (1993) 8162–8167.
56. H. M. Marques, T. Walton, T. J. Egan, *J. Inorg. Biochem.* **57** (1995) 11–21.
57. O. Zak, B. Tam, R. T. A. MacGillivray, P. Aisen, *Biochemistry* **36** (1997) 11036–11043.
58. Y. Li, W. R. Harris, *Biochim. Biophys. Acta* **1387** (1998) 89–102.
59. H. M. Marques, T. J. Egan, G. Pattrick, *S. Afr. J. Sci.* **86** (1990) 21–24.
60. B. K. Muralidhara, M. Hirose, *J. Biol. Chem.* **275** (2000) 12463–12469.

61. K. Mizutani, B. K. Muralidhara, H. Yamashita, S. Tabata, B. Mikami, M. Hirose, *J. Biol. Chem.* **276** (2001) 35940–35946.
62. D. H. Hamilton, I. Turcot, A. Stintzi, K. N. Raymond, *J. Biol. Inorg. Chem.* **9** (2004) 936–944.
63. G. N. Ling, The Aqueous Cytoplasm (Keith, A.D. ed.). Marcel Dekker Inc., New York, (1979) pp. 23–60.
64. N. D. Chasteen, *Adv. Inorg. Biochem.* **5 (**1983) 201–233.
65. R. Kumar, A.G. Mauk, *J. Phys. Chem. B* **116** (2012) 3795–3807.
66. R. Kumar, A. G. Mauk, *J. Phys. Chem. B* **113** (2009) 12400–12409.
67. P. Aisen, A. Leibman, *Biochim. Biophys. Acta* **304** (1973) 797–804.
68. J. M. El Hage Chahine, R. Pakdaman, *Eur. J. Biochem*. **230** (1995) 1102−1110.
69. E. N. Baker, S. V. Rumball, B. F. Anderson, *Trends Biochem. Sci*. **12** (1987) 350–353.
70. P. Aisen, A. Leibman, H. A. Reich, *J. Biol. Chem*. (1966) 1666–1670.
71. P. Aisen, A. Leibman, *Biochem. Biophys. Res. Commun*. **3** (1968) 407–413.
72. P. Aisen, A. Leibman, J. Zweier, *J. Biol. Chem.* **253** (1978) 1930–1937.
73. E. H. Morgan, E. Baker, *Biochim. Biophys. Acta* **363** (1974) 240–248.
74. H. M. Baker, B. F. Anderson, A. M. Brodie, M. S. Shongwe, C. A. Smith, E. N. Baker, *Biochemistry* **35** (1996) 9007–9013.
75. A. N. Luck, C. E. Bobst, I. A. Kaltashov, A. B. Mason, *Biochemistry* **52 (**2013) 8333–8341.
76. J. Konstantynowicz, T. Porowski, W. Zoch-Zwierz, J. Wasilewska, H. Kadziela-Olech, W. Kulak, S. C. Owens, J. P. Jastrzebska, M. Kaczmarski, *European Journal of Paediatric Neurology* **16** (2012) 485–491.
77. L. N. Lin, A. B. Mason, R. C. Woodworth, J. F. Brandts, *Biochemistry* **33** (1994) 1881–1888.
78. M. M. Santoro, D.W. Bolen, *Biochemistry* **27** (1988) 8063–8068.
79. C. Tanford, *Adv Protein Chem*. **23** (1968) 121–282.
80. W. R. Harris, *J. Inorg. Biochem.* **27** (1986) 41–52.
81. L. N. Lin, A. B. Mason, R. C. Woodworth, J. F. Brandts, *Biochemistry* **30** (1991) 11660–11669.
82. P. Aisen, A. Leibman, J. Zweier, *J. Biol. Chem.* **253** (1978) 1930–1937**.**
83. J. Brock, *In Metalloproteins* (Harrison, P. M., Ed.), Verlag Chemie, Weinheim, (1985) Part 2, pp 183-262.

84. L. N. Lin, A. B. Mason, R. C. Woodworth, J. F. Brandts, *Biochemistry* **32 (**1993**)** 9398–9406.
85. T. Terpstra, J. McNally, T. H. L. Han, N. T. Ha-Duong., J. M. El Hage Chahine, F. B. Abdallah, *J. Inorg. Biochem.* **136** (2014) 24–32.
86. M. Zhang, D. R. Gumerov, I. A. Kaltashov, A. B. Mason, *J Am. Soc Mass Spectrom* **15** (2004) 1658–1664.
87. J. Miksovská, J.H. Day, R.W. Larsen, *J. Biol. Inorg. Chem.* **8** (2003) 621–625.
88. R. Kumar, D. Sharma, R. Jain, S. Kumar, R. Kumar, *Biophys Chem.* **207** (2015) 61–73.

List of Publications

Papers in SCI/refereed journals

1. **Rajesh Kumar**, Deepak Sharma, Rishu Jain, Sandeep Kumar and Rajesh Kumar, Role of macromolecular crowding and salt ions on the structural-fluctuation of a highly compact configuration of carbonmonoxycytochrome *c*, *Biophysical Chemistry* 207 (2015) 61–73 (Impact Factor = 2.0)

2. Rishu Jain†, **Rajesh Kumar**†, Sandeep Kumar, Ritika Chhabra, Mukesh chand Agarwal and Rajesh Kumar, Analysis of the pH-dependent stability and millisecond folding kinetics of horse cytochrome *c*, *Archive of Biochemistry and Biophysics* 585 (2015) 52–63 (Impact Factor 3.1)

3. Rajesh Kumar, Rishu Jain and **Rajesh Kumar**, Viscosity-dependent structural fluctuation of the M80-containing Ω-loop of horse ferrocytochrome *c*, *Chemical Physics* 418 (2013) 57–64 (Impact Factor 1.7)

4. Sandeep Kumar, Deepak Sharma, **Rajesh Kumar** and Rajesh Kumar, Electrostatic effects controls the stability and iron release kinetics of ovotransferrin, *J. Biol. Inorg. Chem.* 19(6) (2014) 1009-1024. (Impact Factor = 2.54)

5. **Rajesh Kumar**, Deepak Sharma and Rajesh Kumar, The oxalate effect on the stability and iron release dynamics of serum transferrin. (***Manuscript under preparation***)

6. **Rajesh Kumar**, Deepak Sharma and Rajesh Kumar, Factor defining on the effect of macromolecular crowding on stability and dynamics Ferrocytochrome *c* (***Manuscript under preparation***)

7. **Rajesh Kumar**, Deepak Sharma and Rajesh Kumar, Factor Defining the Effects of Arginine on the Stability and Internal Dynamics of Horse cytochrome ***c*****.** (***Manuscript under preparation***)

† These authors are equally contributed.

Papers/ posters in Conferences

1. **Rajesh Kumar** and Rajesh Kumar "The Glycine Effect on Release of Iron from Transferrins" NCIMSF-2013, School of Chemistry and Biochemistry, Thapar University-Patiala
2. **Rajesh Kumar**, Sandeep Kumar, and Rajesh Kumar. "Effect of neutral salts on the stability of acid-denatured hen egg white lysozyme", *Material Research Society of India (23rd Annual meeting 2012)* Thapar University, 143.
3. Sandeep Kumar, **Rajesh Kumar** and Rajesh Kumar "A Typical Effect of Salts on the Stability of Fe^{3+} Ovotransferrin-CO_3^{2-} Complex", *Material Research Society of India (23rd Annual meeting 2012)* Thapar University